5-2007

A Novel Power Supply for Generating a One Atmosphere Uniform Glow Discharge Plasma (OAUGDP®)

Laurent Jose Calvez
University of Tennessee - Knoxville

To the Graduate Council:

I am submitting herewith a thesis written by Laurent Jose Calvez entitled "A Novel Power Supply for Generating a One Atmosphere Uniform Glow Discharge Plasma (OAUGDP®)." I have examined the final electronic copy of this thesis for form and content and recommend that it be accepted in partial fulfillment of the requirements for the degree of Master of Science, with a major in Electrical Engineering.

J. Reece Roth, Major Professor

We have read this thesis and recommend its acceptance:

Leon Tolbert, Marshall Pace

Accepted for the Council:
Carolyn R. Hodges

Vice Provost and Dean of the Graduate School

(Original signatures are on file with official student records.)

To the Graduate Council:

I am submitting herewith a thesis written by Laurent Jose (Jo) Calvez entitled "A Novel Power Supply for Generating a One Atmosphere Uniform Glow Discharge Plasma (OAUGDP®)." I have examined the final electronic copy of this thesis for form and content and recommend that it be accepted in partial fulfillment of the requirements for the degree of Master of Science, with a major in Electrical Engineering.

Dr. J. Reece Roth
Major Professor

We have read this thesis
and recommend its acceptance:

Dr. Leon Tolbert

Dr. Marshall Pace

Accepted for the Council:
Carolyn Hodges
Vice Provost and
Dean of the Graduate School

(Original signatures are on file with official student records.)

A Novel Power Supply for Generating a One Atmosphere Uniform Glow Discharge Plasma (OAUGDP®).

A Thesis Presented for the
Master of Science Degree
University of Tennessee, Knoxville

Laurent Jose (Jo) Calvez
May 2007

Acknowledgements

I dedicate this work to my wife Tami and our son Alexander. I want to thank my father who built the capacitor support structure that I designed. I also want to thank Mrs. Friederike Fritzges, Sales Manager at KOPAFILM Elektrofolien GmbH, for authorizing a generous sample of premium biaxially-oriented polypropylene dielectric film. Thanks to Dr. Leon Tolbert and his doctoral student Faisal Khan for their assistance. Likewise, thanks to Dr. Igor Alexeff for his insight and suggestions. Thank you to Sirous Nourgostar for spending time in the lab so I could gather data, and for his conversation and suggestions. Also, thanks to Texas Instruments for sending free samples of the UC3872 controller. Finally, thank you to my committee members, Dr. Marshall Pace and Dr. Leon Tolbert, and to Dr. Roth for his instruction and guidance.

Abstract

A high voltage transformer connected to an atmospheric plasma generator is driven as a current-fed push-pull parallel resonant system, switched by a resonant lamp controller integrated circuit from Texas Instruments (UC3872) in such a manner as to be automatically maintained at resonance. The frequency range of interest is the audio range, which creates a particularly uniform glow discharge in atmospheric pressure air. Frequency control is achieved by a specially constructed high voltage variable capacitor connected parallel to the secondary, in conjunction with a variable parallel primary inductance. Voltage control is achieved by variation of the input DC current amplitude.

Table of Contents

List of Tables

List of Figures

Nomenclature

kHz	kilohertz
kV	kilovolts
mm	millimeters
cm	centimeters
L	inductance, in henries
H	henries
C	capacitance, in farads
μF	microfarads
mil	one thousandth of an inch
dI/dt	time rate of change of current
dV/dt	time rate of change of voltage
Ω	ohms
kΩ	kilo-ohms
A	amperes
mA	milliamperes
dBm	unit relating power level in decibels to 1 mW reference
mW	milliwatt

Acronyms

IC	integrated circuit
DBD	dielectric barrier discharge
DC	direct current
AC	alternating current
OAUGDP®	one atmosphere uniform glow discharge plasma
BOPP	biaxially-oriented polypropylene
RFI	radio frequency interference
PWM	pulse width modulation
MOSFET	metal oxide semiconductor field-effect transistor

1. Introduction

Atmospheric plasmas are increasingly applied to advantage in various industrial processes. Atmospheric plasma discharges always require high voltage (>500V) to initiate, although operating voltages differ according to the type of discharge, which can occur at very low currents as a corona discharge or at very high currents as an arc discharge. Glow discharges occur between these extreme current regimes, at moderate current values, providing energetic plasma without excess heating. The glow discharge plasma can be used to generate reactive species, including ozone, and is particularly suited for increasing the surface energy of delicate materials, such as thin films. However, in the latter case it is important that plasma filamentation be avoided, a phenomenon in which localized electron avalanching results in non-uniformity of energy distribution and treatment effect. Dr. J. R. Roth at the University of Tennessee has demonstrated that a uniform glow discharge plasma can be formed in air at ambient pressures using frequencies in the audio range. This uniform discharge, referred to as the One Atmosphere Uniform Glow Discharge Plasma (OAUGDP®), generates ion/electron pairs at highest efficiency, resulting in electron kinetic temperatures greater than 10,000 K while ion and ambient neutral gas temperatures remain near room temperature.

The goal of this project was to explore a new manner of generating high voltages at frequencies in the audio range in order to generate the One Atmosphere Uniform Glow Discharge Plasma (OAUGDP®). Specifically, the goal was to produce output voltages varying from 1 kV to 20 kV over a frequency range from 1 kHz to 20 kHz. It was decided that a current-fed push-pull parallel resonant circuit would be employed,

switched by a commercial integrated circuit resonant lamp controller in such a manner as to be automatically maintained at resonance. A high voltage variable capacitor was designed and constructed to act in parallel in the secondary circuit as a manually variable frequency modulator, and a variable inductor was constructed to act in parallel with the transformer primary to provide further frequency control. This power supply is intended to act as a bench-top prototype development system, with which the performance of any transformer and plasma reactor combination can be studied over a range of frequencies and voltages to determine optimum operating parameters, which can later be implemented with off-the-shelf discrete components.

Chapter 2 provides a review of the literature describing the use of resonant switching power supplies to generate atmospheric plasma, and their application in industry. The last section focuses specifically on the current-sourced push-pull parallel resonant inverter circuit upon which the power supply developed for this thesis is based.

Chapter 3 details the resonant system employed for this project, based upon a specific transformer and plasma actuator, and particularly describing the design and construction of the variable capacitor and variable inductor. The switching and control circuits are also discussed.

Chapter 4 provides a summary and discussion of data gathered during preliminary testing and then during plasma generation.

Chapter 5 presents conclusions arrived at during the course of this project, including possible explanations for problems encountered and suggestions for further improvement of the power supply.

2. Literature Review

2.1 Atmospheric Plasma

Atmospheric plasma discharges are used in a variety of industrial applications, including increasing the surface energy of materials [1], generating ozone [2], and generating reactive species [3]. Figure 2.1 illustrates the regimes of a plasma discharge, from corona at very low currents, to the normal glow discharge, to the arc regime at high currents [4]. The dielectric barrier discharge (DBD) is a widely applied method of generating atmospheric plasma, using one or two dielectric barriers placed between high voltage discharge electrodes. The dielectric material suppresses arcing and forces the plasma to remain in the Townsend avalanche regime. A DBD produces a plasma that consists of many short-lived micrometer-scale filaments of relatively high electron density and energy, resulting in an overall non-uniformity of effect on workpieces located in the dielectric barrier discharge. The One Atmosphere Uniform Glow Discharge Plasma

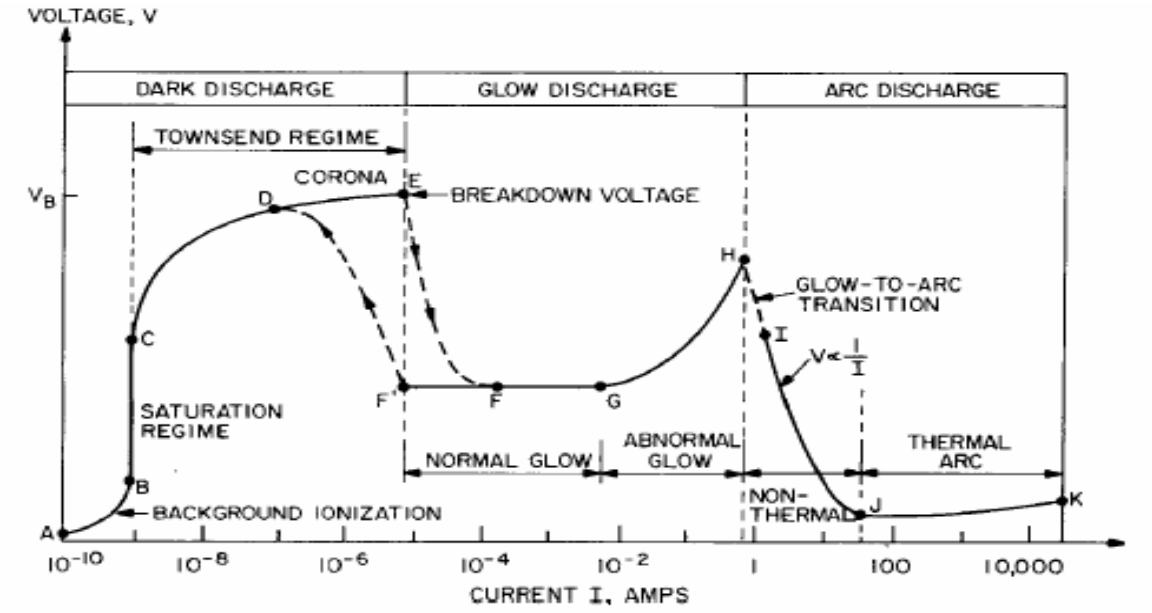

Figure 2.1. Classical DC discharge regimes, from Roth [4].

(OAUGDP®) [5][6] produces a uniform glow plasma in small discharge gaps (<3mm in air) with driving frequencies in the audio midrange that promote ion trapping between the electrodes. The OAUGDP® is well suited for many industrial applications due to its uniformity of effect. The goal of this thesis is to build a small and inexpensive high voltage power supply that can function in the audio range in order to produce an OAUGDP® discharge.

2.2 Resonant Switching Power Supplies

2.2.1 General

Switching power supplies are usually operated at high frequencies to minimize size and cost, but this in turn makes them susceptible to parasitic reactive circuit elements and thus more likely to generate electromagnetic 'noise,' or radio frequency interference (RFI). A resonant circuit can be used to automatically compensate for parasitic elements and can greatly reduce noise generation and switching transients. Resonant mode converters generally input a square pulse of voltage or current to an L-C circuit in a manner timed to match its natural frequency, causing energy to be stored in the resonant circuit. This energy can then be drawn off by the load. A major advantage of a resonant mode topology is 'soft' switching, which can be made to occur at zero voltage or zero current, so that switches experience much lower transients, create less radio frequency interference, and operate more efficiently. High peak currents and increased control complexity are the major drawbacks associated with resonant converters.

There are many system and control approaches to resonant power supplies. The resonant LC circuit can be series or parallel, or a combination of both [7][8]. Switching

control can be accomplished by phase-shifted pulse width modulation (PWM) [9][10], a combination of pulse density and pulse frequency modulation [2], and other methodologies [11][12]. Resonant power supplies have been adapted to drive many kinds of loads, including welders [13], induction heating loads [14], and high voltage loads. High voltage applications include medical X-Ray power supplies [10], plasma jets and general-application discharges [7][12][15], dielectric barrier discharges for degrading toxic organic compounds [3], and ozone generators [2][11][16][17][18].

In most instances a transformer is used to provide high voltage, although there exist a few higher-order resonant circuit designs that do not require them [7][19][20]. A high voltage transformer has inherent parasitic reactances (illustrated in Figure 2.2) due to the manner of its construction. Because of imperfect magnetic coupling of the primary and secondary coils, there arises a leakage inductance, generally identified as a lumped series primary inductance. When the current through the transformer primary is reversed each switching cycle, the leakage inductance causes high voltage spikes which can damage the semiconductor switches. In the secondary coil there is a significant distributed capacitance between the various windings and layers of windings,

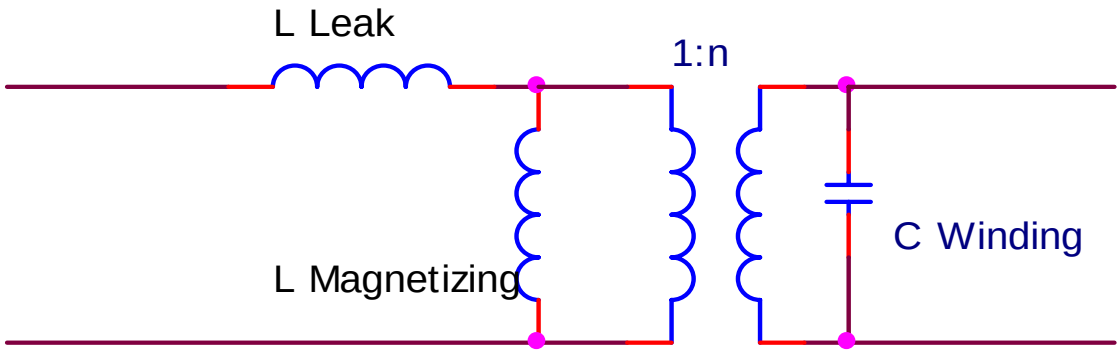

Figure 2.2. Parasitic reactances of a high voltage transformer.

which can result in current spikes and slow voltage rise-times in the secondary. The most efficient high voltage resonant inverters incorporate either or both of these parasitic transformer components into the resonant circuit design [8][10][21][22].

2.2.2 Current-Fed Parallel Topology

Many high voltage resonant circuits described in the literature employ a voltage-sourced series resonant topology, often using frequency variation above resonance for output voltage control [3][9][12][16]. By its nature, a plasma reactor/generator is highly capacitive, adding to the large secondary winding capacitance of the high voltage transformer required to power it. A parallel tank circuit with significant capacitance initially appears as a short circuit to a voltage source, so it is better driven with a current source. The current-fed push-pull parallel resonant inverter is well suited to serve as a power supply for an atmospheric plasma discharge because it assimilates any capacitance in the transformer secondary as part of the resonant circuit. This secondary capacitance is 'reflected' to the primary by a factor of the square of the turns ratio, and it will tend to resonate at some frequency as part of a parallel circuit with the transformer magnetizing inductance.

The main disadvantage of a current-sourced parallel-resonant inverter is that the output voltage gain is lowest at resonance [23]. For this reason, a high voltage transformer with sufficient turns ratio must be selected if operation occurs at resonance. A major advantage of the current-fed parallel resonant inverter is that both (push-pull) transistors are driven with respect to ground, resulting in a simple gate drive circuit [24]. A diode in series with each switch disables the MOSFET intrinsic body diode, resulting

in unidirectional current flow and preventing energy reflection back to the source; an alternating square wave current results, with amplitude equivalent to half the input DC current. When the circuit operates near the resonant frequency, the source can be approximated as a sine wave of the square wave's fundamental frequency with amplitude $(I_{DC}\sqrt{2})/\pi$ amperes [15]. A parallel resonant circuit is more efficient when operated at or below resonance [23], when the resonating tank circuit behaves as an inductive load to the source in terms of the load resistance voltage and the fundamental component of the input current. This allows the series diode to turn off with zero dI/dt and low dV/dt and the MOSFET to turn on with zero current, resulting in higher circuit efficiency [24]. The converse will be true if the circuit is driven above the resonant frequency. Operating a resonant power supply at the circuit resonant frequency results in true zero voltage switching and highest efficiency, but it precludes output voltage control by frequency variation.

The current-fed push-pull parallel resonant inverter circuit described by Alonso et al. [11] uses the resonant lamp ballast controller UC3872 from Unitrode (Texas Instruments) to maintain the system at resonance. This integrated circuit detects zero crossings of the resonant voltage waveform to control switching, so that any system combination of a high voltage transformer and plasma reactor will be driven at its own intrinsic resonant frequency so long as it coincides with a synchronization range determined by timing capacitors associated with the integrated circuit. Figure 2.3 provides a conceptual illustration of the total system, and Figure 2.4 is a comprehensive circuit schematic used to gather the data presented in this document.

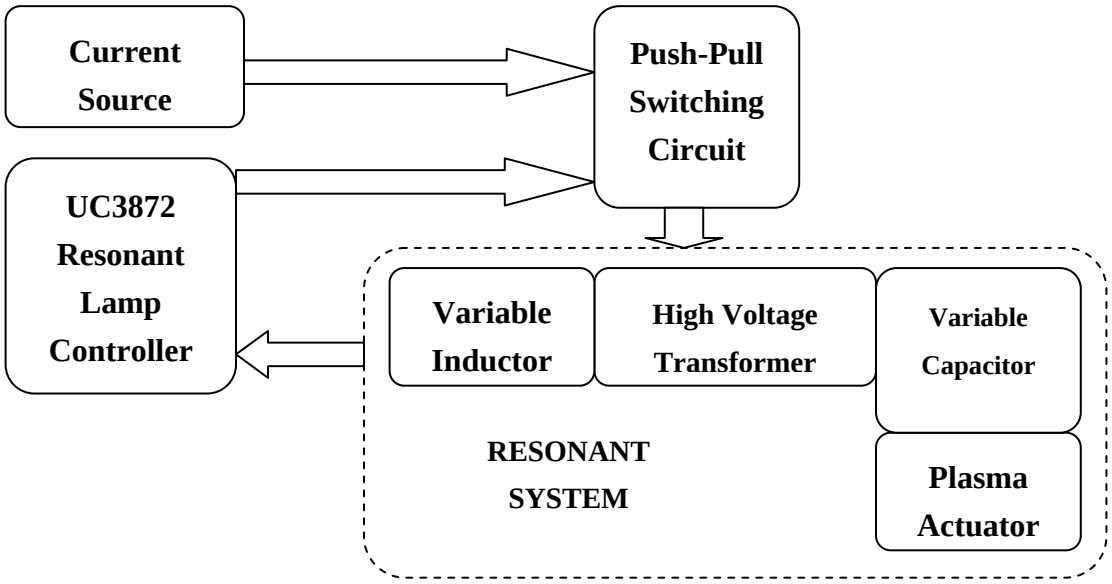

Figure 2.3. Conceptual block diagram.

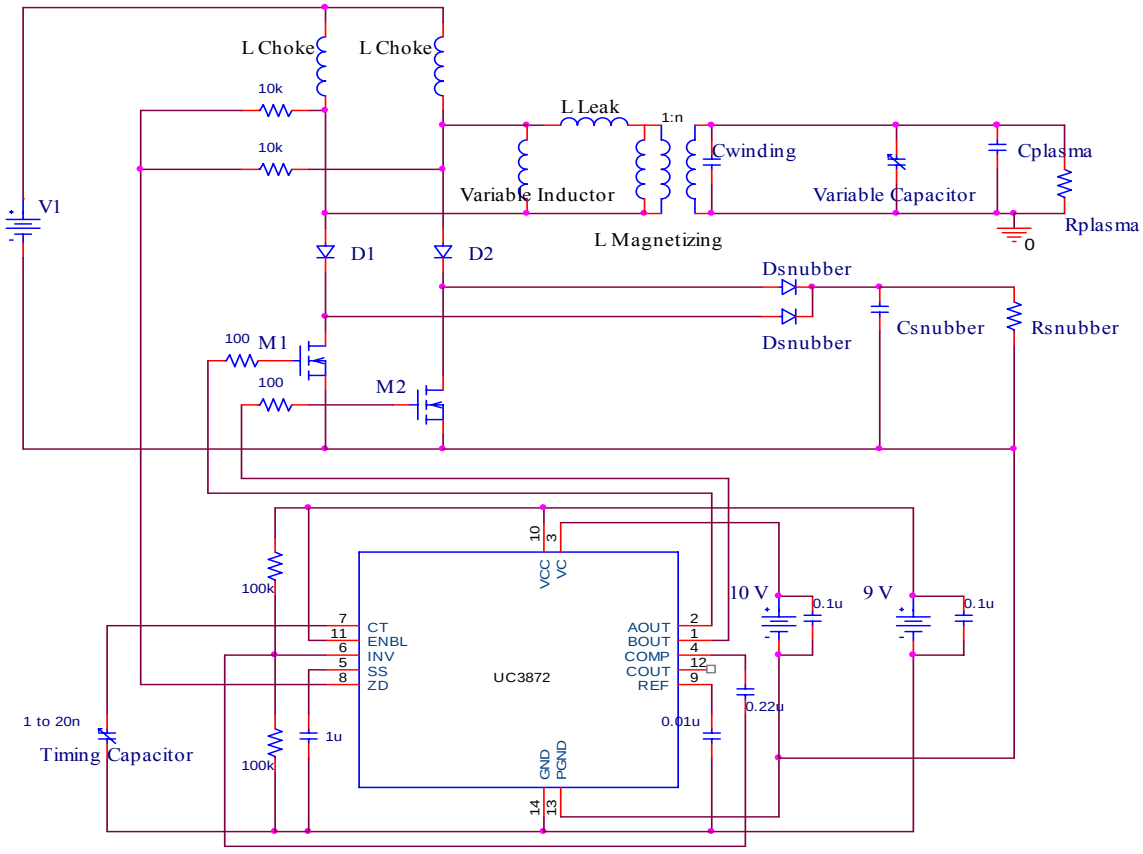

Figure 2.4. Complete circuit, based on Alonso [11].

3. Design and Construction

3.1 Resonant System

The basic resonant system consists of any reasonable combination of high voltage transformer and plasma generator, where "reasonable" refers to proper matching of plasma current draw and transformer volt-ampere capability. Such a combination will tend to oscillate at two frequencies, in a parallel and then series fashion. The lower frequency is normally associated with the larger magnetizing inductance, which oscillates in parallel with the secondary capacitance. The higher frequency is normally associated with the smaller leakage inductance oscillating in series with the secondary capacitance. The difference between these frequencies is a function of the amount of leakage inductance in relation to magnetizing inductance.

The UC3872 resonant controller can be expected to maintain the system at the lower resonant frequency so long as the proper value of timing capacitance is employed to limit the synchronization range [25]. The UC3872 uses voltage feedback to detect zero-crossings of the resonant tank, switching the push-pull MOSFET pair accordingly. A parallel variable capacitor in the secondary will increase total capacitance and thus decrease the system's natural frequency, providing manual frequency control. Past experience demonstrates that a high voltage capacitor on the order of 5 nanofarads can be easily constructed; simulations indicate that such a value would be sufficient to achieve the desired frequency control. However, simulations also reveal that in order to sweep across the entire frequency range desired, in addition to varying the capacitance, a variation of the resonating inductance may also be required. This can be accomplished

by connecting an inductor across the transformer primary, which will have the effect of reducing the total resonating inductance and increasing the oscillation frequency.

Spreadsheets were developed to assist in the design of the capacitor and the inductor. For the capacitor, an effort was made to minimize the required plate area, and to approximate the effect of multiple and varied dielectric separator media, including air gaps. For the inductor, an effort was made to minimize turns and to achieve the desired range of variation by inserting a high permeability core to facilitate varying from a minimum to a maximum inductance value.

3.1.1 Transformer and Plasma Actuators

The transformer used for this project was model SP216 from Plasma Technics, Inc. in Racine, Wisconsin (see Figure 3.1). The SP216 is presented by the manufacturer as a component designed to operate in resonant systems with a frequency range of 5 to 25kHz

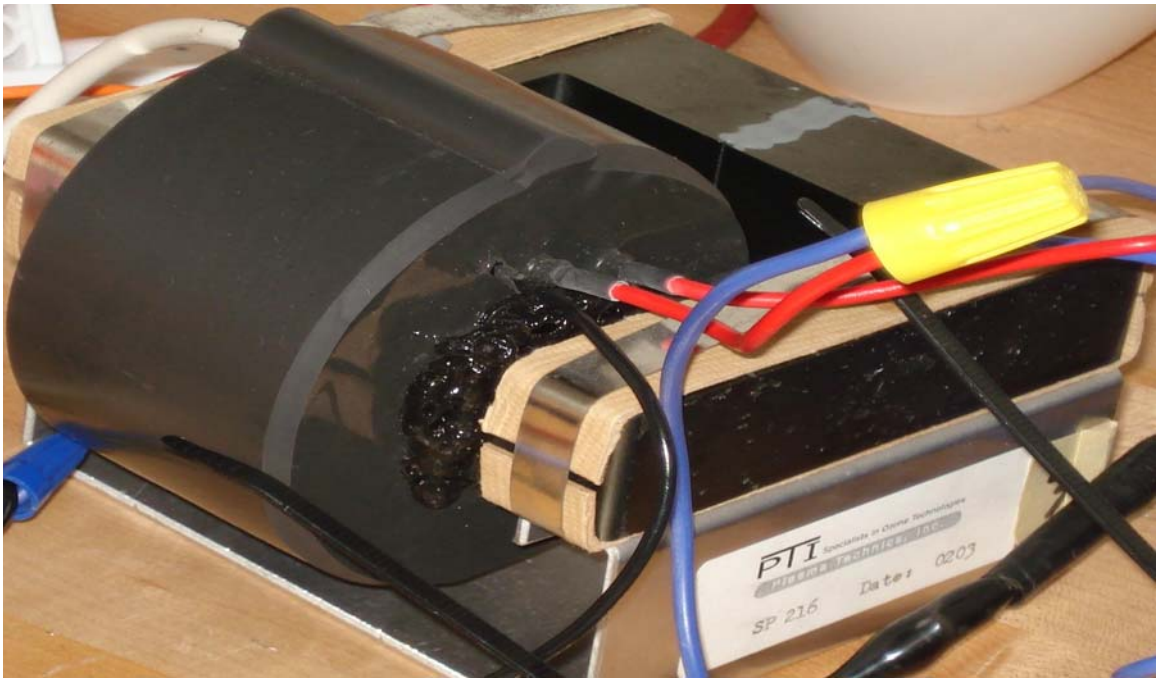

Figure 3.1. SP216 transformer from Plasma Technics, Inc.

and output voltages up to 15 kV [26]. The SP216 is rated for up to 240 VAC inverter input and 1000 VA output. Measurements in the lab indicated that the turns ratio of the SP216 is approximately 1:100.

A small quartz dielectric plasma actuator having a measured capacitance of 15 pF was used as the primary load (see Figure 3.2). The actuator consists of two adhesive copper strips, approximately 5 mm x 80 mm, fixed on opposite sides of the 1 mm thick, 50 mm x 125 mm quartz plate with no gap or overlap between their closest edges. Connecting wires are soldered to the end of each copper strip and routed in opposite directions to prevent high voltage arcing.

A panel plasma actuator with aluminum oxide as the dielectric, having a measured capacitance of 540 pF was used as an intermediate load. The panel is approximately 1 mm thick and 100 mm x 140 mm, with a 90 mm x 125 mm metallic ground plane on one side and a series of end-connected metal strips on the other (see Figures 3.3 and 3.4). The 25 metal strips are approximately 1 mm wide and 80 mm long and spaced apart approximately 4 mm. The panel represents a significantly larger capacitive load than the

Figure 3.2. Quartz plasma actuator.

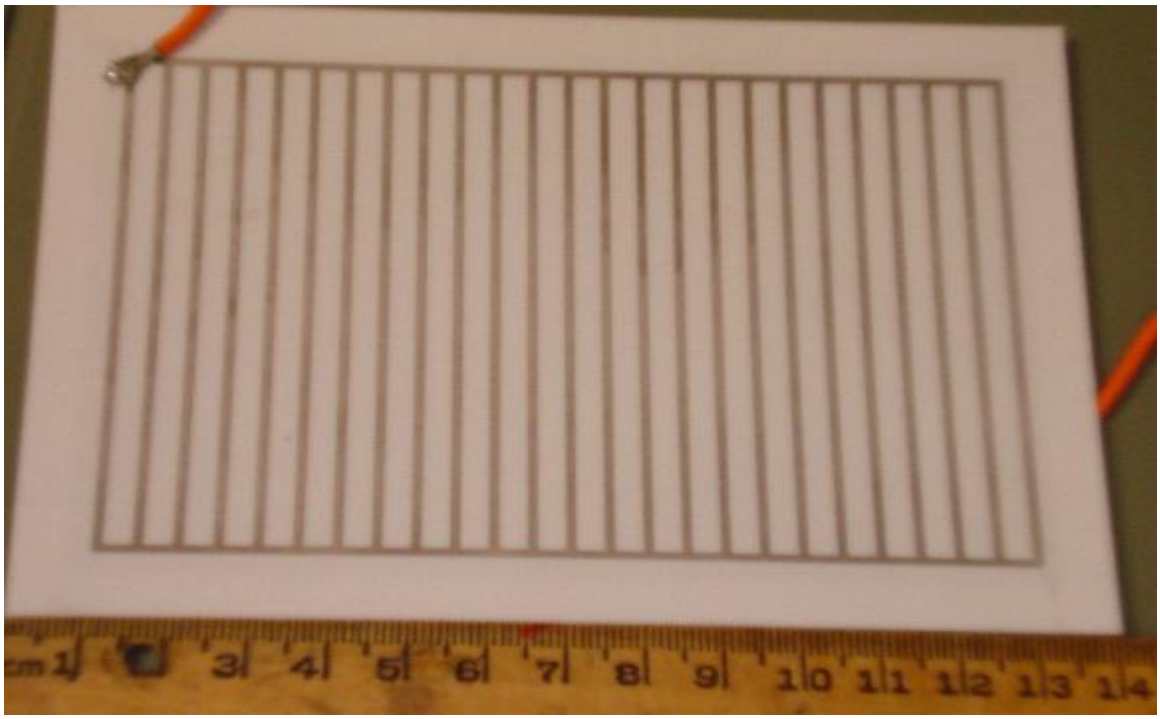

Figure 3.3. Panel plasma actuator, aluminum oxide, metal strips.

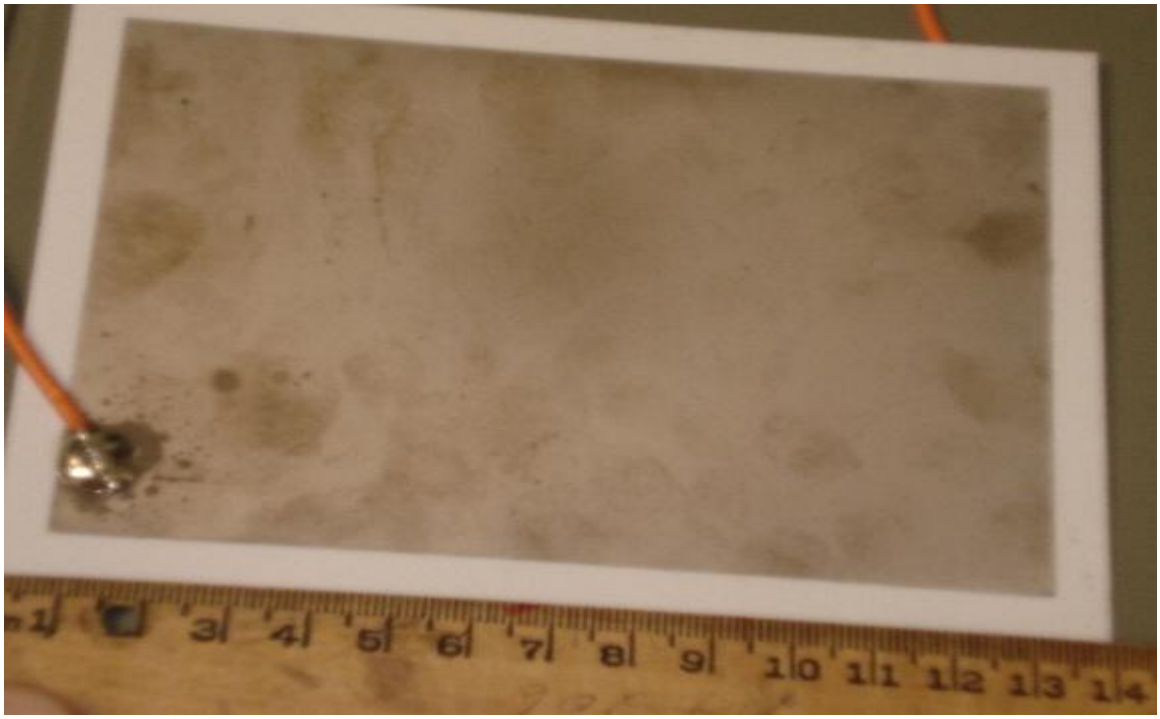

Figure 3.4. Panel plasma actuator, aluminum oxide, ground plane.

smaller quartz actuator, and it consistently operated at lower frequency and output voltage than the smaller actuator during testing. Again, wires are soldered to the electrodes on each side and routed in opposite directions.

3.1.2 Variable Capacitor

The fundamental concept of the variable capacitor is illustrated in Figure 3.5. Preliminary PSpice simulations indicated that a maximum variable capacitance on the order of three nanofarads would provide the desired range of frequency control. Although various dielectrics were considered, it was initially decided to use a commercially available polyethylene or polypropylene film, since these materials are widely available, easy to work with, and in particular have a low loss factor. A preliminary computer program designed to calculate capacitance values indicated that using the standard 6-mil sheets available at the local builders' supply store would require up to twenty 8-inch (.2032 m) by 14-inch (.3556 m) electrodes for a capacitance in the desired range. Further

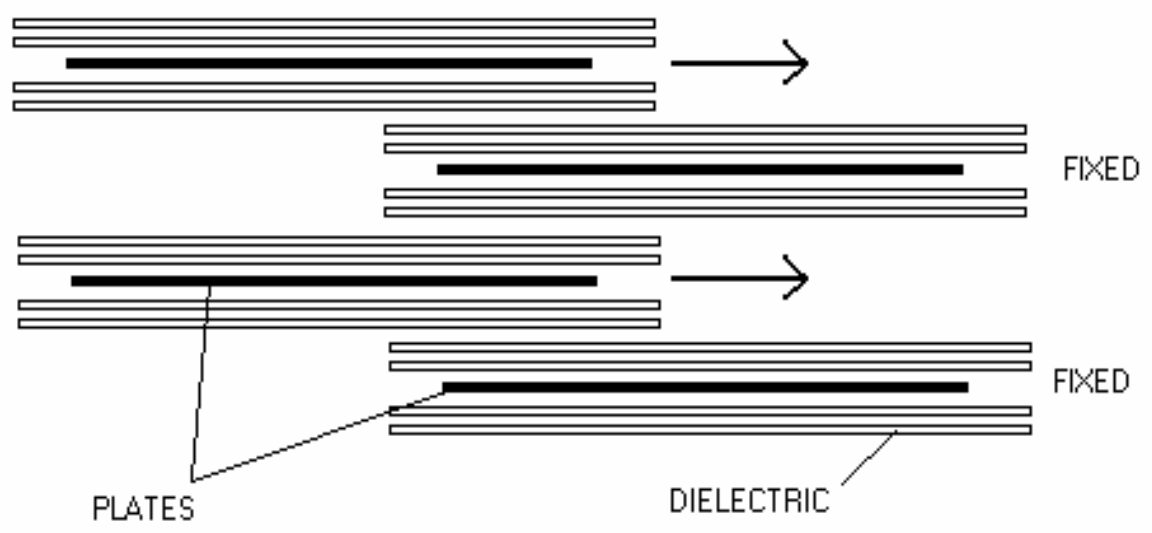

Figure 3.5. Fundamental variable capacitor design.

research led to the identification of a specially manufactured form of polypropylene with much higher dielectric strength than normal polypropylene, allowing for much thinner (and fewer) dielectric sheets, which in turn increases total capacitance. Biaxially oriented polypropylene (BOPP) is manufactured by stretching the film in two directions (machine and transverse directions) as it is formed, which orients the molecules parallel with the plane of the film, enhancing its mechanical and electrical properties. Samples of BOPP were obtained directly from two manufacturers: 6013(RRP) from Jiangmen Enrichment Industrial LTD in Guangdong, China, and Kopafilm MET from Kopafilm Elektrofolien GMBH, of Nidda/Ober-Schmitten, Germany. Also available was a roll of Hostaphan (PET) high voltage dielectric film from Hoechst-Celanese, circa 1993. These films are very thin and require considerable care in their handling, but they allow for improvements in the capacitor size and value. The spreadsheet capacitance calculations indicated that a capacitor of 3 nanofarads could be constructed with the BOPP dielectric film by using as few as 8 electrodes, 4 inches (10.16 cm) wide and with 6 inches (15.24 cm) of overlap, a drastic improvement in comparison to the original design. Only the Kopafilm BOPP was used in the variable capacitors used in data collection.

The capacitors were designed to withstand more than twice the expected maximum voltage. The original intention was to forego the use of any additional liquid dielectric barrier, although such is often recommended for high voltage capacitors. In constructing the capacitor, each individual aluminum foil (heavy gauge) electrode was fixed between two sets of multiple dielectric films, and all was then sandwiched between two sheets of Bristol paper. A group of these electrode sets were mechanically connected at one end, with equivalent spacers between, using vinyl bolts (see Figure 3.6). The same-set plates

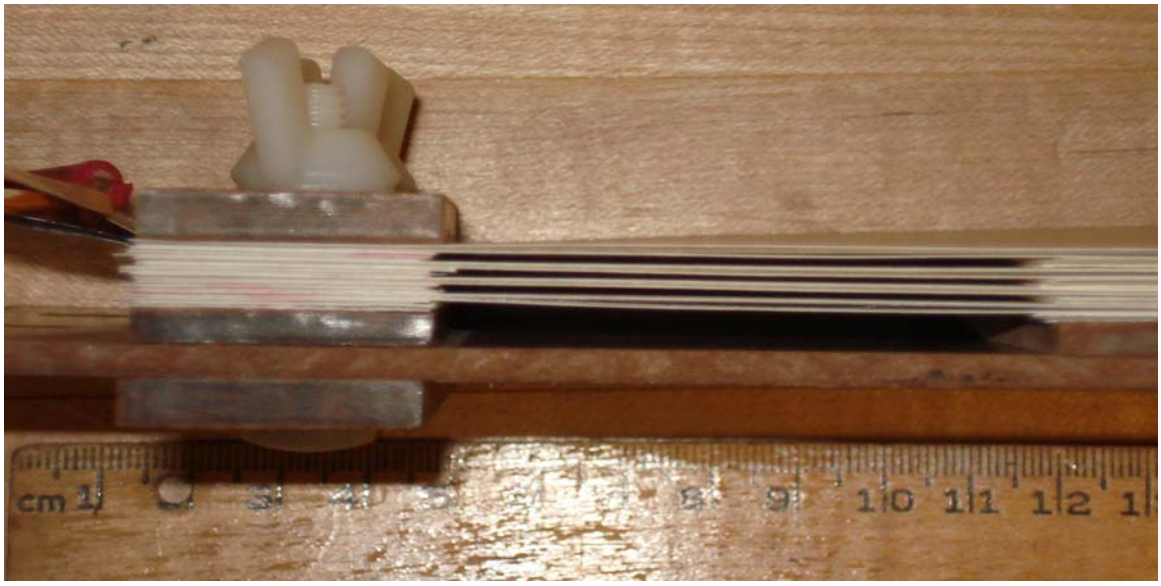

Figure 3.6. Side view of variable capacitor.

were interconnected with one-inch (2.54 cm) wide aluminum foil tabs. A brass tab with soldered wire connection was used to provide electrical connection to the exterior circuit. The capacitor consisted of the interleaving of two oppositely connected groups of these electrodes, sliding from a position of minimal overlap to full overlap of 6 inches (15.24 cm). See Figures 3.7 and 3.8 for illustration of minimum and maximum electrode overlap. A larger electrode width allows for greater maximum capacitance, while a thinner electrode provides a smaller variation of capacitance. An effort was made to minimize the risk of breakdown by rounding all corners of the electrodes and connecting tabs in an effort to reduce electric field intensity, and Kapton tape was used to minimize corona formation at exposed edges.

A capacitor support system was designed consisting of two rectangular wooden plates: a lower plate, fixed to a supporting frame, and a moving plate to slide on top of the fixed plate. At the far ends of each are holes through which vinyl bolts secure the entire assemblage of wooden spacers, paper, dielectric films, and electrodes. The fixed

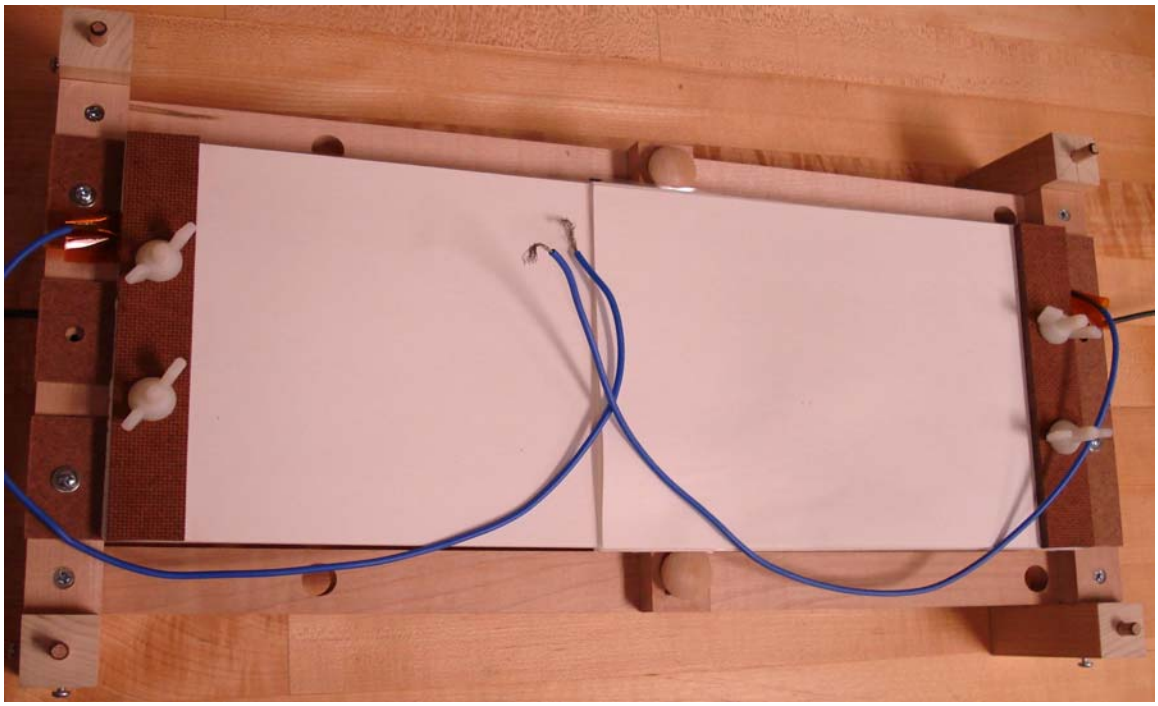

Figure 3.7. Variable capacitor, minimal plate overlap, minimum capacitance.

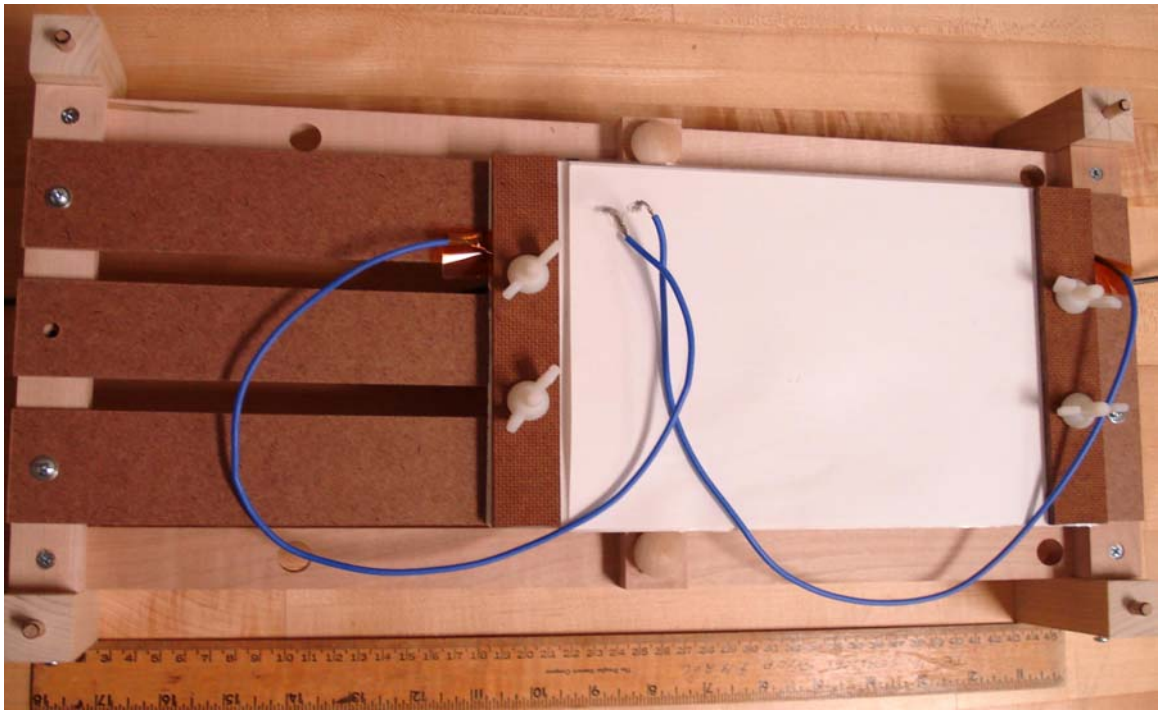

Figure 3.8. Variable capacitor, maximum plate overlap, maximum capacitance.

and moving plates, each securing a set of opposing electrodes, were elevated and secured on a wooden frame. Three stackable capacitor support frames were constructed, identical except for the width of electrode supported, with one frame supporting a large capacitor, another frame a medium capacitor, and another frame supporting two small capacitors with the thinnest electrodes (see Figure 3.9). A wooden board with a brass weight was placed on top of the electrodes to minimize the possibility of electrode vibration.

3.1.3 Variable Inductor

A spreadsheet was developed to aid in the design of a variable inductor to operate in parallel with the transformer primary. Different inductance equations from two sources [27][28] were verified to be equivalent; one was used repeatedly to isolate length, diameter, and turns, and the effect of their variation on total inductance, while the other

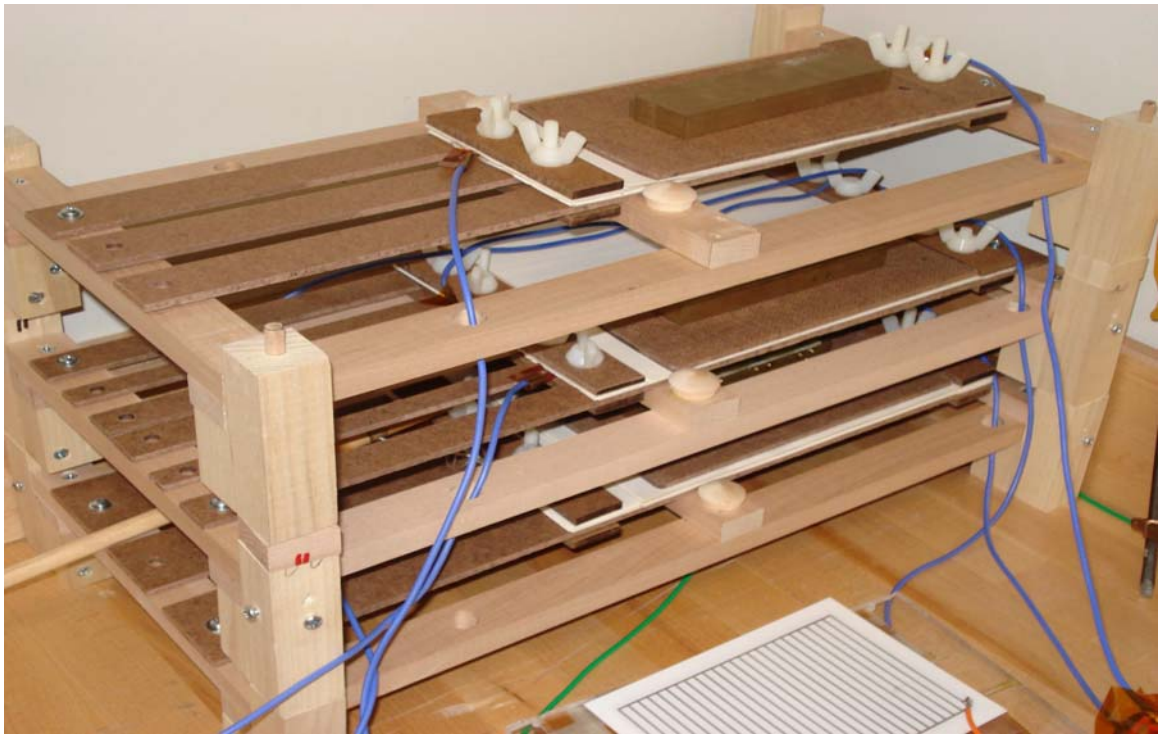

Figure 3.9. Stacked variable capacitor frames.

provided inductance value confirmation and allowed direct calculation in inches instead of meters. Both of these equations operate on the assumption of a value of unity for relative permeability, which is to say air is the transformer core material. A third equation [29] was employed to allow for the variation of relative permeability. The intent was to wind a coil on a standard PVC pipe form, limiting the layers to three, and then to insert a material such as steel within the coil diameter to increase the inductance (see Figure 3.10). A formulation considering the alternating series of inductances due to partial core insertion was developed using an estimation of effective permeability based upon the fraction of cross-sectional area occupied by the core material in comparison with the coil, assuming the core was of significantly smaller diameter. For example, it was determined that a minimal inductance on the order of 0.5 mH could be wound in three layers or less of 14AWG wire on a standard PVC pipe form of 2 inches (5.08 cm) diameter and length less than a foot (30.5 cm), and that the inductance value could then be increased to tens of millihenries by inserting a steel bolt into the coil. Professor Igor Alexeff advised that a

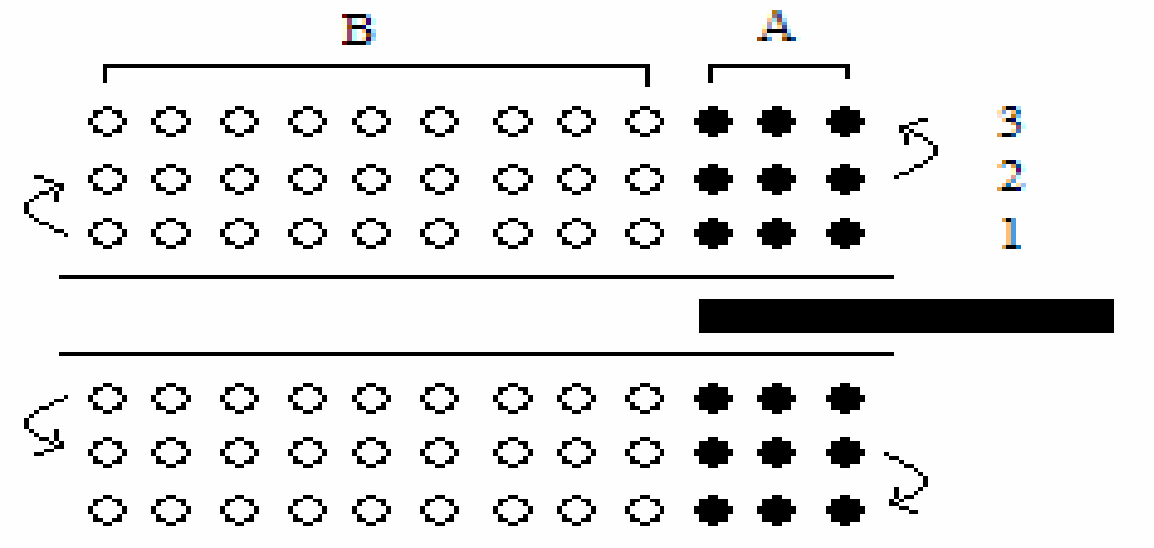

Figure 3.10. Illustration of variable inductor.

Figure 3.11. Variable inductor, with switch.

ferrite core be used in lieu of steel.

Another inductor was constructed using available materials. A coil eight inches (20.32 cm) long was wound in two and a half layers with approximately forty feet (12 m) of 18AWG stranded wire on a plastic tube with diameter 13/16$^{th's}$ of an inch (2.06 cm), resulting in 182 total turns. A series of ferrite beads of similar outside diameter were strung together to provide a core that could be easily adjusted by pulling the string connecting them. The ferrite beads occupy approximately half the core volume, so with an estimate of 1000 for the ferrite permeability value, an effective permeability of 500 was applied in the spreadsheet calculations, which then indicated an approximate maximum inductance value of 22 millihenries. This inductor (shown in Figure 3.11) did have the intended effect on the resonant system when applied across the primary, allowing for operation at and beyond the highest frequencies desired, but the actual

inductance was later found to be smaller by an order of magnitude, probably due to a poor estimate of relative permeability for the beads, the composition of which was unknown.

3.2 Control and Switching Circuits, Power Supplies

The control circuit consisted of the UC3872 resonant lamp ballast controller integrated circuit and associated discrete components, including 100 Ω resistors from the gate drive signal pins, 10 kΩ resistors to limit current flow into the zero-detect pin, and various filter capacitors as recommended by the manufacturer. The most important component associated with the UC 3872 was the timing capacitor, the size of which sets the frequency range. The synchronization frequency range is approximately 1.5:1, which means that if the capacitor in the timing circuit sets a minimum frequency of 4 kHz, then the maximum frequency for which the UC3872 will provide synchronization will be approximately 6 kHz. For this reason, several dip switches were used to add a variety of capacitor values to the timing circuit. As the resonant circuit capacitance was varied, causing the system resonant frequency to change, it was often necessary to change the value of the timing capacitance so the controller IC could synchronize with the new frequency. Initially the controller circuit was constructed on a breadboard in order to allow for changes and troubleshooting. Later, the entire control circuit was soldered onto a modular circuit board (see Figure 3.12).

The switching circuit was soldered directly onto a modular circuit board with secured connection leads (see Figure 3.13). Early PSpice simulations indicated that an input current on the order of 3 A would be required to attain the maximum desired output

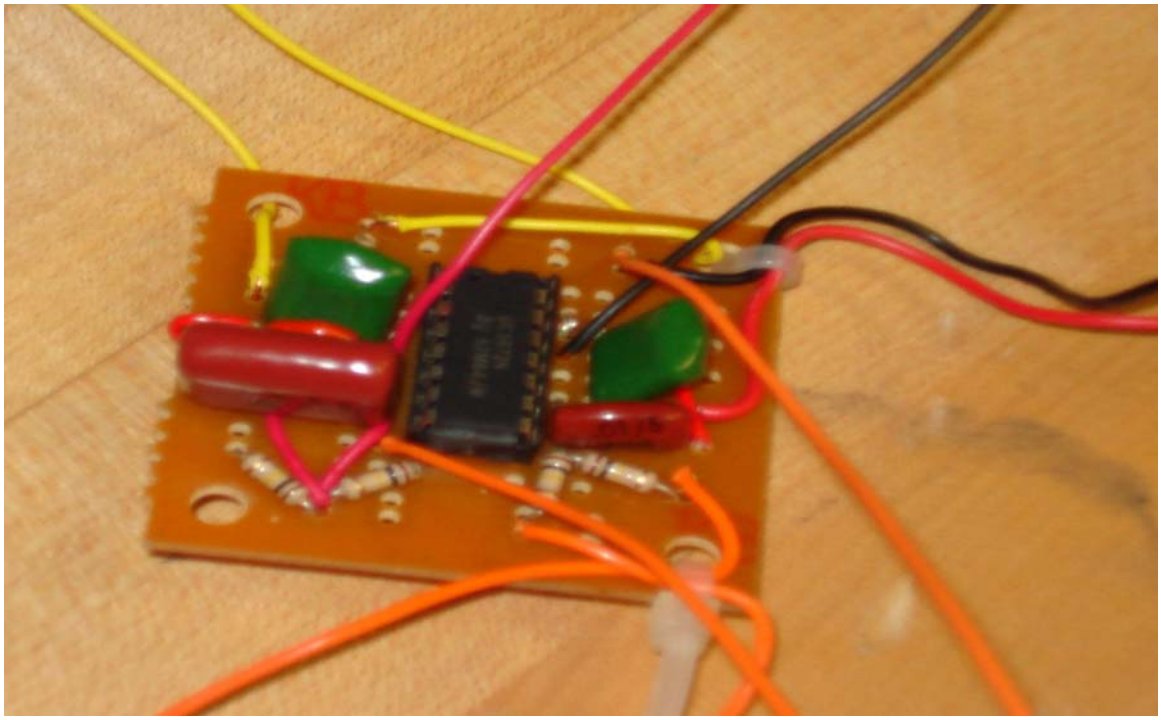

Figure 3.12. Control Module.

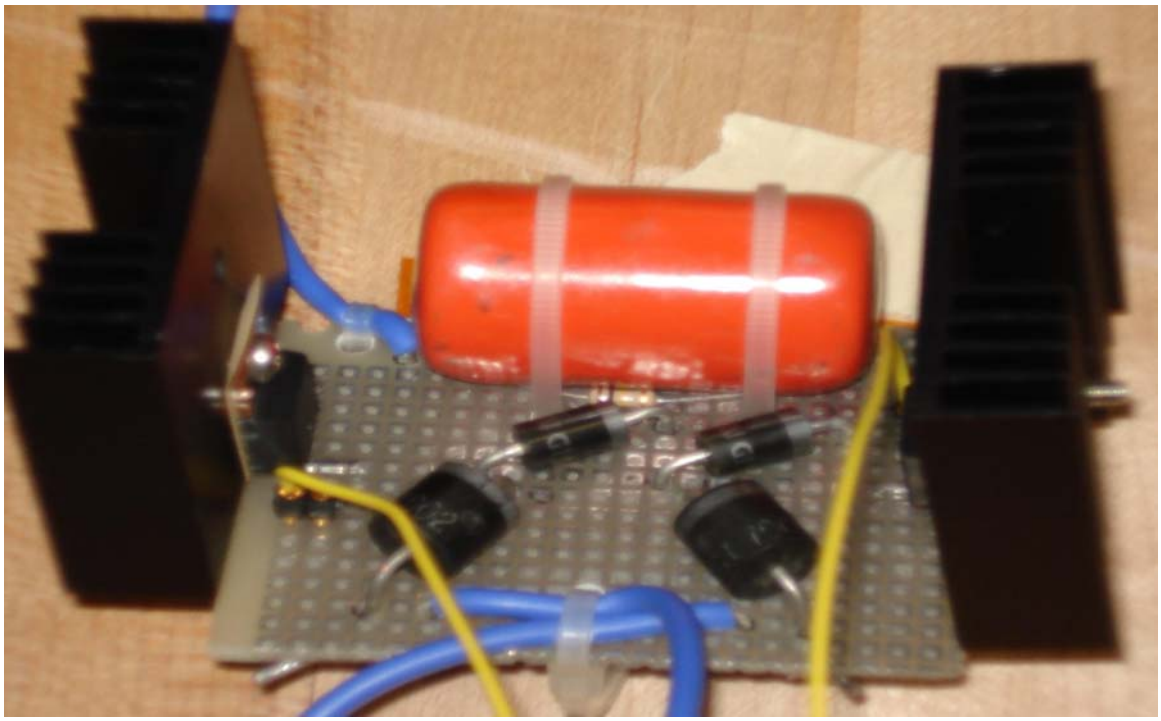

Figure 3.13. Switching Module.

20 kV, so components were selected with this value as a benchmark. However, in some cases components that exceeded the necessary ratings were used, since these were available at no cost. A P600G diode, rated for 6 A of average forward current and 400 V recurrent peak reverse voltage, was connected in series with each of two IRF640 MOSFET switches, mounted on heat sinks and rated to deliver a continuous drain current of 18 A and to withstand a drain-source voltage of 200 V. Together, the P600G diode and the IRF640 formed the unidirectional switch.

In order to protect the MOSFETs from voltage spikes generated at each switching event by the leakage inductance of the transformer, a voltage-clamping snubber was included. The snubber consisted of two FR304 fast-recovery diodes, rated to conduct 3 A average current and to withstand 400 V of peak repetitive reverse voltage, a 0.1 μF Sprague capacitor, rated for 1000 VDC, and a 1/4 W, 100 kΩ resistor. The main concern in selecting the snubber components is that the time constant of the RC combination be significantly larger than the switching period, so voltage rise in the snubber capacitor is very slow during the period when the MOSFET is not conducting. The modular control circuit, associated timing capacitor bank, and the switching module are pictured in Figure 3.14.

Initially, two toroidal cores wrapped with approximately 70 turns of # 18AWG served as choke inductors to ensure a uniform DC current to the switching circuit. It became evident during testing that these choke coils were insufficient (they were later measured to be 0.75 mH each), and so they were replaced with two large choke inductors of nominal 40mH each.

Three separate power sources were required to operate the system: a 9 VDC battery

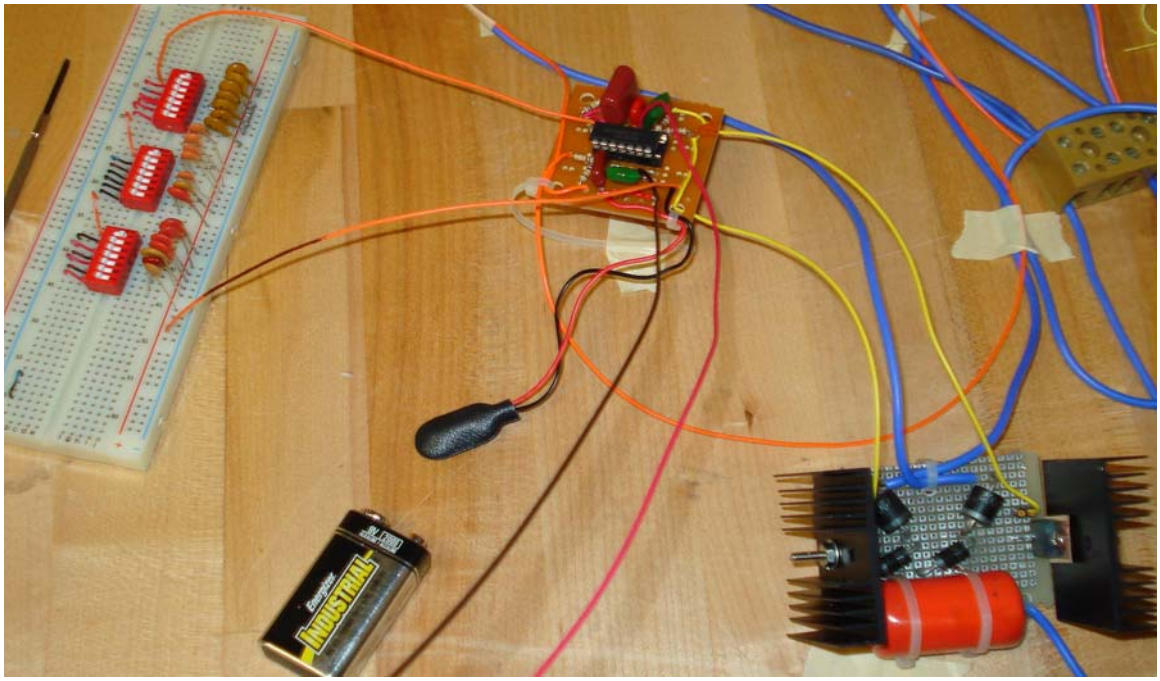

Figure 3.14. Switching module, control module, and timing capacitors.

powered the electronic circuitry of the UC3872 controller IC, a separate power source of approximately 10 VDC supplied the gate drive circuitry within the UC3872, and a current supply was required to power the resonant circuit. A Hewlett Packard Harrison 6102A DC power supply rated for 50 V and 500 mA was employed for initial testing. This power supply was capable of operating in the current mode, so it was able to provide a steady voltage for the gate drive circuit while simultaneously delivering a steady current for the switched tank circuit. Data gathered during initial testing, using the HP Harrison 6102A, are labeled with specific input current values. Later, two other power supplies were used to replace the damaged HP Harrison 6102A. The Kepco CK40-0.8M DC power supply, rated for 40 VDC and 0.8 A, was used to power the gate drive circuit, and a Sorenson Q Nobatron QRC40-8, rated for 40 VDC and 8 A, provided the main current to the tank circuit. Both of these supplies operated only in the voltage mode.

4. Results

4.1 Low frequency network analyzer data

Three high voltage transformers were immediately available: an old flyback transformer from a black and white television, an automotive High Energy Ignition coil with the laminated core removed, and the 1000VA SP216 high voltage transformer from Plasma Technics, Inc. of Racine, Wisconsin. The Hewlett-Packard 3577A network analyzer was used to measure the frequency signatures of each of these transformers due to their internal inductance and capacitance values. The flyback transformer was found to oscillate at a low frequency of approximately 16 kHz and an upper frequency of 50 kHz (see Figure 4.1). The core-less automotive induction coil, an autotransformer, resonated at 10 kHz only (see Figure 4.2). The PTI SP216 transformer demonstrated

Figure 4.1. Flyback transformer frequency signature.
(Ordinate measures relative impedance (dBm), abscissa measures frequency (Hz).)

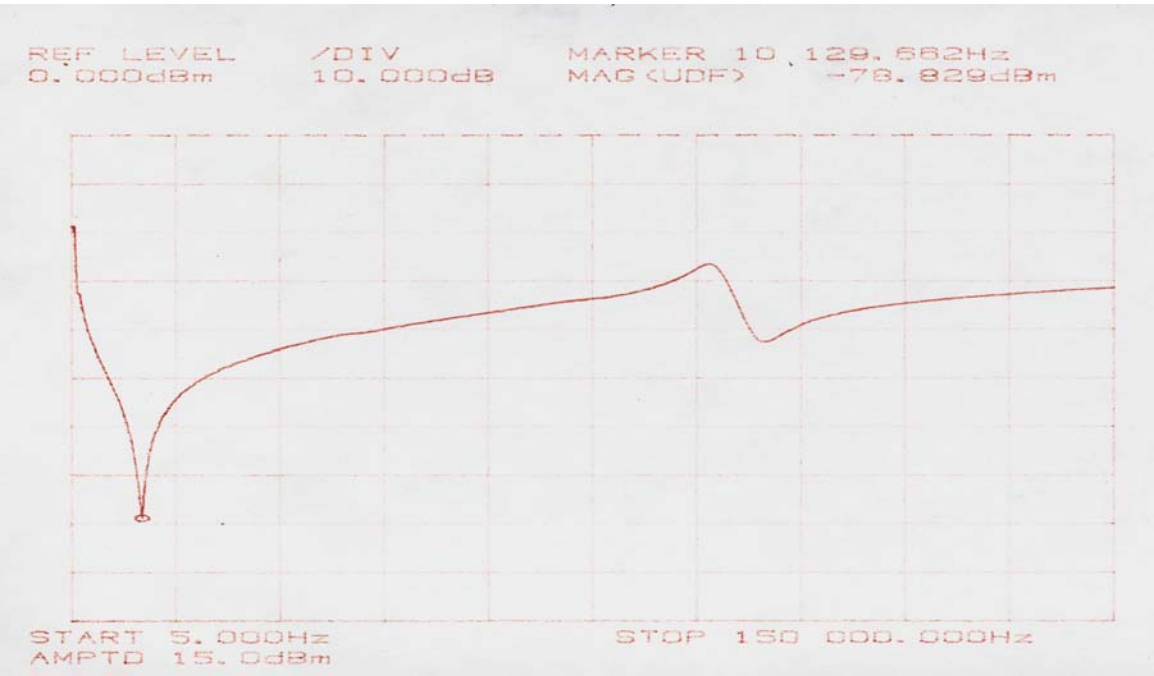

Figure 4.2. No-core automotive transformer frequency signature.
(Ordinate measures relative impedance (dBm), abscissa measures frequency (Hz).)

resonance at a low frequency of 7.7 kHz and a high frequency of 14.5 kHz (see Figure 4.3). Since it is advertised as being capable of operating over a range from 5 to 25 kHz, and up to 15 kV, the PTI SP216 was selected to be the system transformer upon which the power supply would be based. Two different loads were connected to the SP216 secondary and the resulting frequency response characterized using the network analyzer: the medium-sized aluminum oxide panel (see Figure 4.4), and the Mod IV reactor, a fairly large parallel plate reactor in the plasma lab (see Figure 4.5). Adding these plasma actuators in the secondary of the transformer represented an increase in capacitance, and a corresponding reduction in resonant frequency response was noted in the network analyzer data.

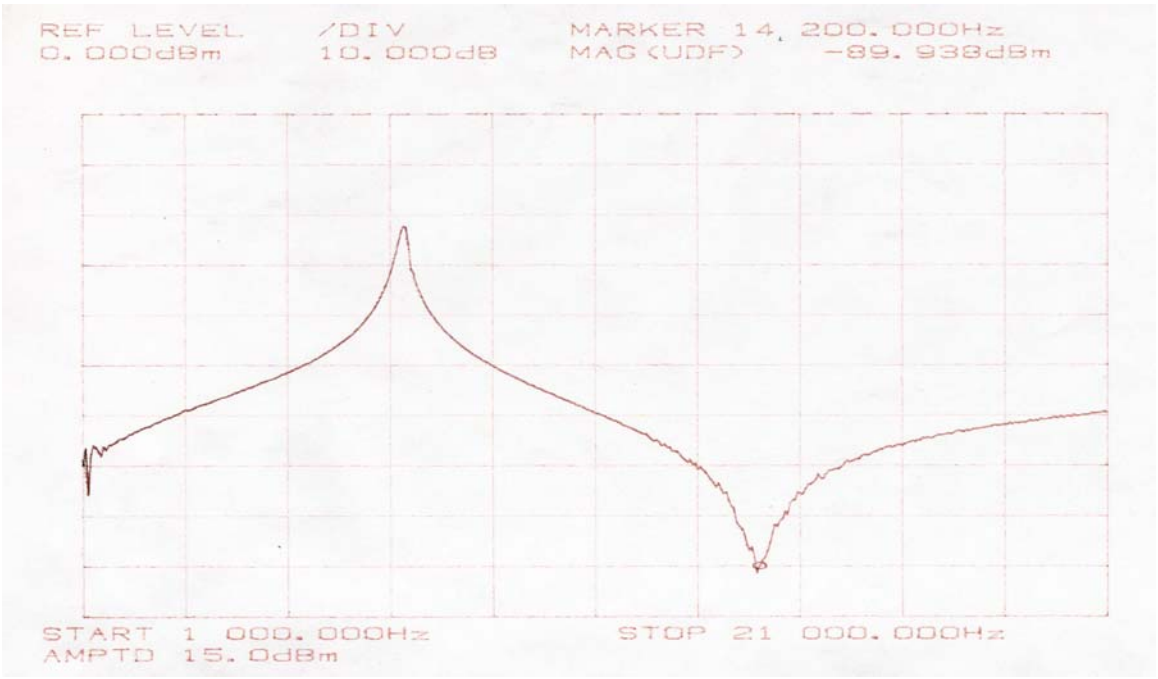

Figure 4.3. PTI SP216 transformer frequency signature.
(Ordinate measures relative impedance (dBm), abscissa measures frequency (Hz).)

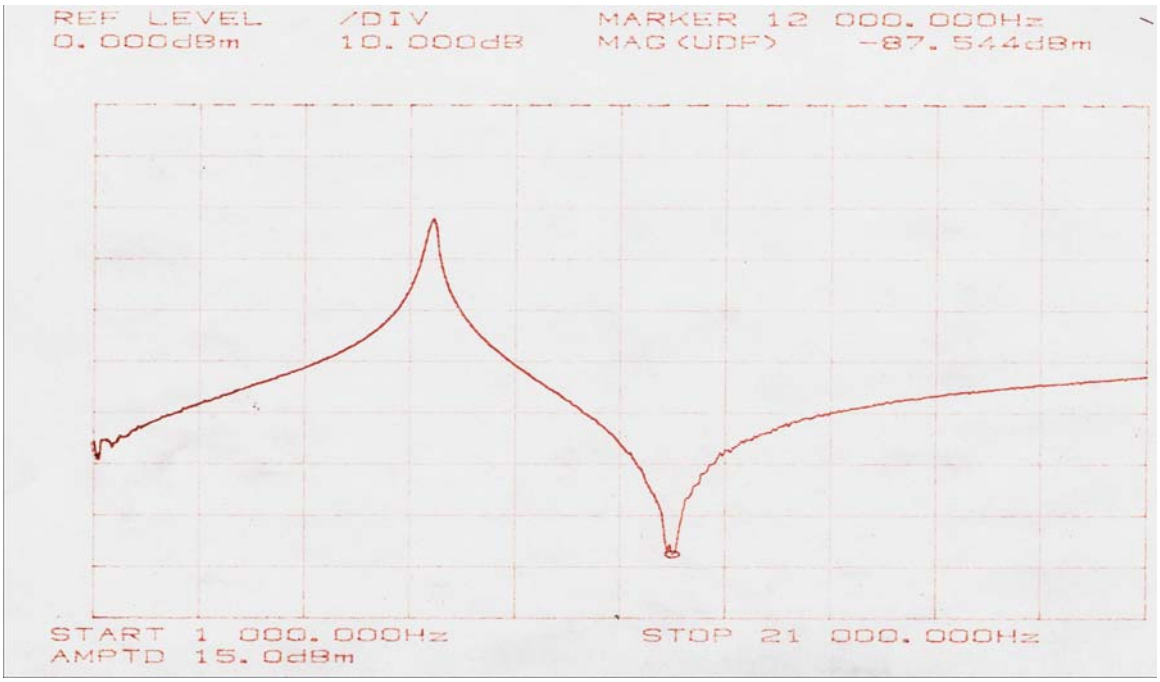

Figure 4.4. PTI SP216 + panel frequency signature.
(Ordinate measures relative impedance (dBm), abscissa measures frequency (Hz).)

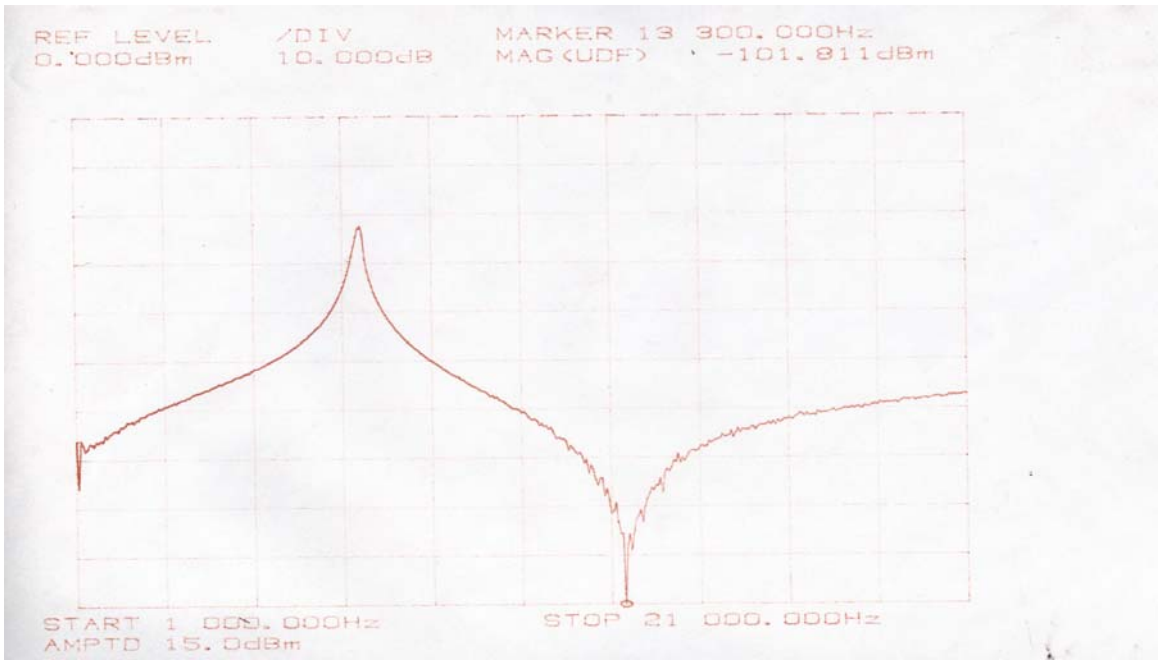

Figure 4.5. PTI SP216 + Mod IV parallel-plate reactor frequency signature.
(Ordinate measures relative impedance (dBm), abscissa measures frequency (Hz).)

4.2 Component Measurements

Three different sizes of variable capacitor were designed and built to provide different increments of variation while together summing to the desired total value of at least 3 nF. A variable inductor was constructed to allow for additional adjustment of the system resonant frequency. Tables 4.1 through 4.5 list the parameters for these components, along with their calculated and measured values. All measurements of capacitance and inductance were made using a Hewlett Packard 4332A LCR meter (s/n 1544J01297). The values provided for the KOPAFILM MET dielectric are from the product specification document published by KOPAFILM Elektrofolien [30]. The thickness of Bristol paper was found in a paper thickness chart published by Case Paper Company, Inc. [31], and the paper dielectric values were found in a dielectric list at RFCafe.com on the internet [32].

Table 4.1: Large Variable Capacitor Calculations and Measurements

Parameter	Data
Electrode Width	.1016 m
Maximum Electrode Overlap	.1524 m
Number of Electrodes	8
Primary Dielectric Material	KOPAFILM MET
Primary Dielectric Thickness	20 μm
Primary Dielectric Breakdown	650 kV/mm
Primary Relative Permittivity	2.2
Sheets of Primary Dielectric	8
Secondary Dielectric Material	Bristol Paper (67#)
Secondary Dielectric Thickness	2.3e-4 m
Secondary Dielectric Breakdown	7.8 kV/mm
Secondary Relative Permittivity	3
Sheets of Secondary Dielectric	2
Estimated Total Air Gap	2.54 e-4 m
Estimated Total Breakdown Voltage	107 kV
Calculated Maximum Capacitance	2.57 nF
Maximum Measured Capacitance	
With no additional weight	3.05 nF
With Board + added weight (.592 kg total)	3.75 nF
Minimum Measured Capacitance	
With no additional weight	58.0 pF
With board only (.103 kg)	60.0 pF
With Board + added weight (.592 kg total)	62.5 pF

Table 4.2: Medium Variable Capacitor Calculations and Measurements

Parameter	Data
Electrode Width	.0508 m
Maximum Electrode Overlap	.1524 m
Number of Electrodes	4
Primary Dielectric Material	KOPAFILM MET
Primary Dielectric Thickness	20 μm
Primary Dielectric Breakdown	650 kV/mm
Primary Relative Permittivity	2.2
Sheets of Primary Dielectric	8
Secondary Dielectric Material	Bristol Paper (67#)
Secondary Dielectric Thickness	2.3e-4 m
Secondary Dielectric Breakdown	7.8 kV/mm
Secondary Relative Permittivity	3
Sheets of Secondary Dielectric	2
Estimated Total Air Gap	2.54 e-4 m
Estimated Total Breakdown Voltage	107 kV
Calculated Maximum Capacitance	550 pF
Maximum Measured Capacitance	
With no additional weight	570 pF
With Board + added weight (.525 kg total)	665 pF
Minimum Measured Capacitance	
With no additional weight	26.5 pF
With board only (.064 kg)	28.0 pF
With Board + added weight (.525 kg total)	28.5 pF

Table 4.3: Small Variable Capacitor Calculations and Measurements

Parameter	Data
Electrode Width	.0254 m
Maximum Electrode Overlap	.1524 m
Number of Electrodes	2
Primary Dielectric Material	KOPAFILM MET
Primary Dielectric Thickness	20 μm
Primary Dielectric Breakdown	650 kV/mm
Primary Relative Permittivity	2.2
Sheets of Primary Dielectric	4
Secondary Dielectric Material	Bristol Paper (67#)
Secondary Dielectric Thickness	2.3e-4 m
Secondary Dielectric Breakdown	7.8 kV/mm
Secondary Relative Permittivity	3
Sheets of Secondary Dielectric	2
Estimated Total Air Gap	2.54 e-4 m
Estimated Total Breakdown Voltage	55 kV
Calculated Maximum Capacitance	102 pF
Maximum Measured Capacitance	
With no additional weight	125 pF
With Board + added weight (.301 kg total)	155 pF
Minimum Measured Capacitance	
With no additional weight	25.0 pF
With board only (.051 kg)	26.0 pF
With Board + added weight (.301 kg total)	26.5 pF

Table 4.4: Variable Inductor Calculations and Measurements

Parameter	Data
Coil Diameter	.0206 m
Coil Length	.2032 m
Number of Turns	182
Number of Layers	2.5
Removable Core Material	ferrite beads
Length of Core Material	.0254 m x 8 beads
Estimated Relative Permeability	500
Calculated Inductances	
No Core Material	0.07 mH
One Bead	3.39 mH
Two Beads	6.74 mH
Three Beads	10.1 mH
Four Beads	13.4 mH
Five Beads	14.8 mH
Six Beads	15.7 mH
Seven Beads	16.8 mH
Eight Beads	24.3 mH
Measured Inductances	
No Core Material	90 μH
One Bead, Centered	120 μH
Two Beads, Centered	240 μH
Three Beads, Centered	420 μH
Four Beads, Centered	710 μH
Five Beads, Centered	1.05 mH
Six Beads, Centered	1.50 mH
Seven Beads, Centered	1.85 mH
Eight Beads, Centered	2.15 mH

Table 4.5: Other Measurements

Parameter	Data
Hand-Wound Toroidal Choke Inductances	
Choke I	0.75 mH
Choke II	0.75 mH
Chokes I & II in series	1.50 mH
Commercial Toroidal Choke Inductances	
AMVECO I (40 mH nominal)	44 mH
AMVECO II (40 mH nominal)	44 mH
AMVECO I & II in series	87 mH
PTI SP216 Transformer	
Primary Coil Inductance	6.1 mH
Secondary Winding Capacitance	40 pF
Quartz Actuator	
Capacitance (no plasma)	15 pF
Panel Actuator	
Capacitance (no plasma)	540 pF
Large Orange Polypropylene Variable HV Capacitor	
2 electrodes	470 pF
4 electrodes	1.3 nF
6 electrodes	2.2 nF

A permeability value for the ferrite beads was estimated to be approximately 1000, based on manufacturer FerroxCube's Soft Ferrites and Accessories Application and Information Document [33], and this value was halved since the bead only occupied about half of the volume of the core when inserted. This estimation was obviously erroneous, since the measured inductor values were less than the predicted values by an order of magnitude. There are many different types of ferrite materials, and the ones in hand have no identifying marks, so a very rough estimation could not be avoided. Another factor leading to error was the calculating assumption that the core is one continuous piece of material, whereas in reality there are air gaps between the eight beads, which decrease the inductance. Note, however, that the inductance calculated for the winding with no core inserted was reasonably accurate, with a twenty percent error attributable to a failure to account for an average winding radius based on multiple layers of wire.

4.3 Initial Testing: 140 mA Input Current, No Plasma

Once construction and assembly of the various components was completed, a series of low power tests were run to measure the overall performance of the system. A Tektronix P6015A 1000x high voltage probe was used to measure the output voltage, a Pearson Current Monitor Model 2100 was used to measure current (ignored in low power testing), and data were collected using a Tektronix TDS3014B oscilloscope. The lowest current setting at which the control circuit could synchronize was 140 mA. It is important to note that 140 mA was what the Hewlett Packard Harrison 6102A DC power supply delivered to the entire circuit, and that only half of that current passed through the

transformer primary at any given instant, or even less than half if the auxiliary inductor was included in the circuit. Data were collected separately for the quartz actuator and the aluminum oxide panel actuator, each tested with and without the variable inductor at its maximum value of 2.15 mH connected in parallel with the transformer primary. This variable inductor is referred to in the data as the Auxiliary Inductor, with its inductance specified according to whether the full ferrite core was inserted (2.15 mH), only half the ferrite core was inserted (0.71 mH), or there was no ferrite core at all (0.09 mH). The data for each configuration are presented in Appendices A through D. Figures 4.6 and 4.7 summarize the resonant frequency and output voltage data for the two different actuators with 140 mA total input current. No plasma was formed at the resulting output voltages, all of which are reported as root-mean-square (RMS) values. The highest frequencies were attained when the variable secondary capacitor was set to its minimum

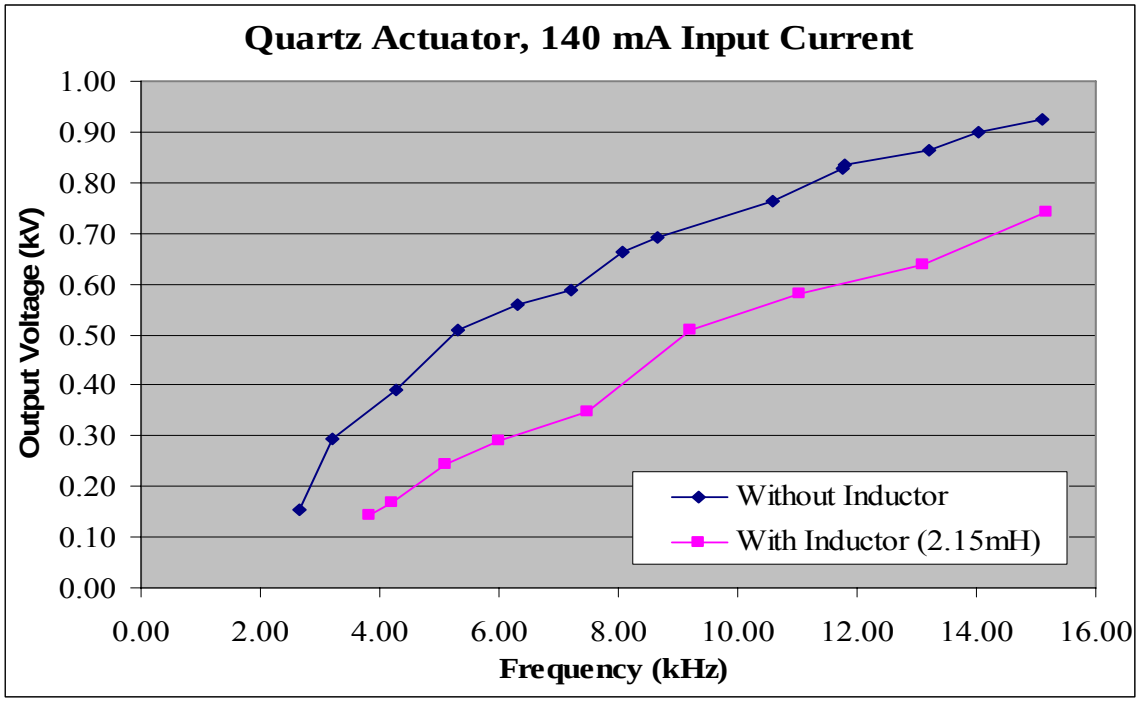

Figure 4.6. Quartz actuator data summary, 140 mA input current.

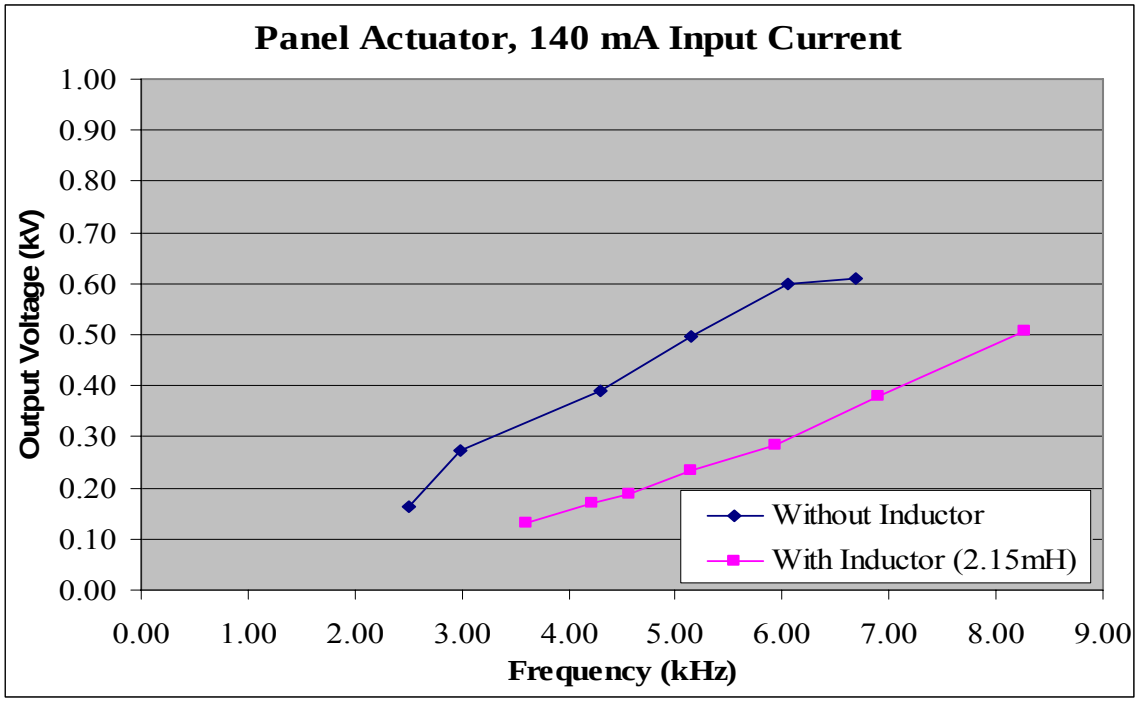

Figure 4.7. Panel actuator data summary, 140 mA input current.

value, and the lowest frequencies (and lowest output voltages) occurred when the secondary capacitance was set to maximum. It is evident that, in every case, as capacitance is added in the secondary to reduce system frequency, the output voltage declines. Addition of parallel inductance in the primary did not produce the expected frequency increase in the initial quartz actuator testing, but the undesired side-effect of output voltage reduction was observed, due to shunting of current away from the transformer primary. The panel actuator, because it has considerably more capacitance to begin with, developed lower output voltages and also operated over a much more limited frequency range. However, the addition of the auxiliary parallel inductor did improve the panel's frequency range to a slight extent.

Figures 4.8 and 4.9 illustrate the voltage waveform (Ch 4, green) measured across the entire switch, which is comprised of the MOSFET and the series diode together. The

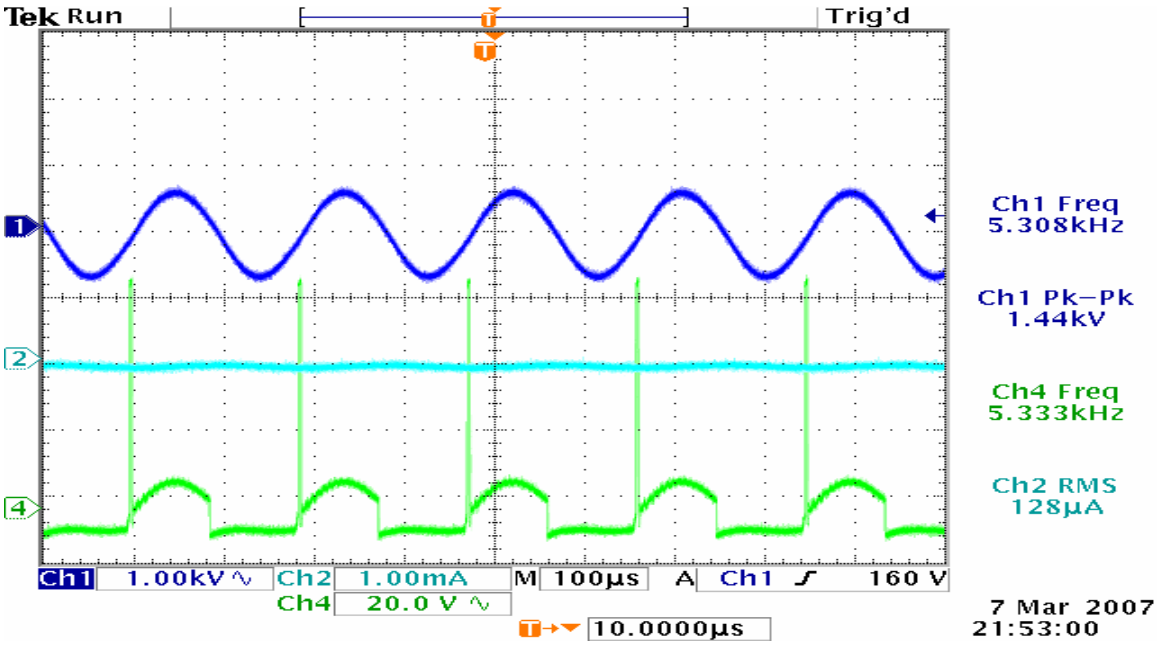

Figure 4.8. Switch waveform, optimum.

Ch1: output voltage (1 kV/div), Ch2: transformer secondary current (1 mA/div), Ch4: voltage across switch (20 V/div).

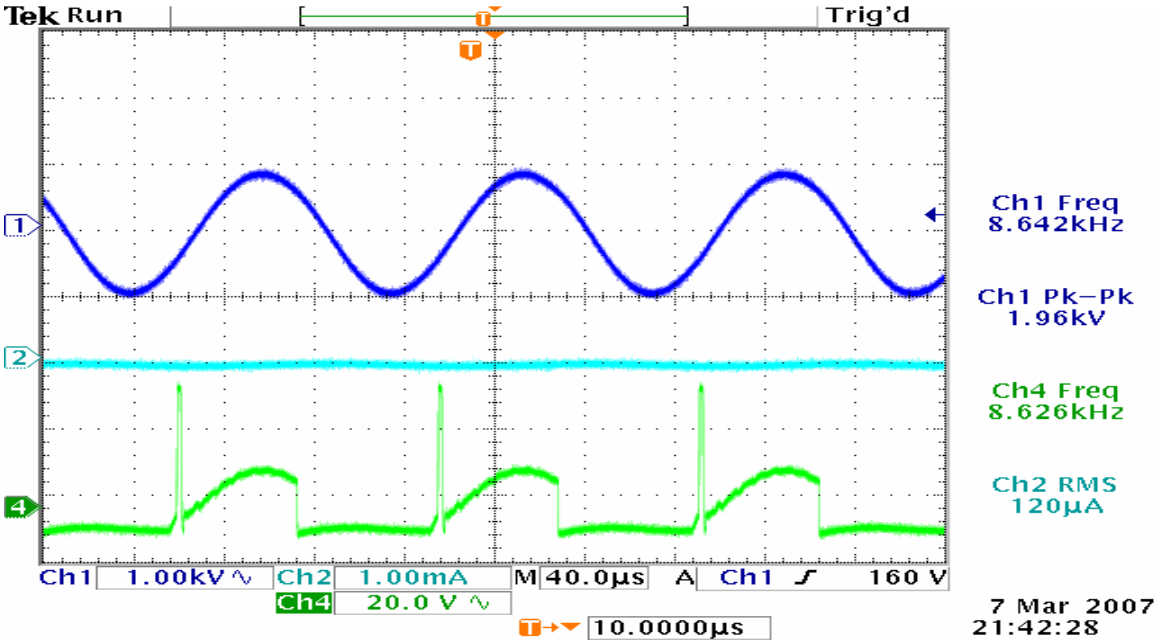

Figure 4.9. Switch waveform, non-optimum.

Ch1: output voltage (1 kV/div), Ch2: transformer secondary current (1 mA/div), Ch4: voltage across switch (20 V/div).

switching event is indicated by the sharp voltage spike, associated with the leakage inductance as it releases the energy stored in its magnetic field in response to the change in current. The switch waveform in Figure 4.8 is near-optimum, showing the symmetry associated with ideal timing as the voltage in the tank circuit is placed across the non-conducting switch, whereas in Figure 4.9 the switching event is slightly early, illustrating that the control circuit does not always drive the circuit exactly at resonant frequency. In fact, it is occasionally necessary to incrementally vary the timing capacitance associated with the control circuit in order to achieve operation at an optimum frequency as the secondary capacitance is varied. The UC3872 datasheet indicates that the switching event is actually triggered when the zero-detect feedback circuitry senses a value of 0.5 V, instead of exactly at 0 V, a feature which is incorporated into the integrated circuit design to allow for propagation delay associated with electronic circuitry.

4.4 Further Testing: 400 mA Input Current, No Plasma

Figures 4.10 and 4.11 summarize the resonant frequency and output voltage data for the two actuators operating with a total circuit input current of 400 mA, with no plasma generated. Once again, it is important to note that 400 mA is the total current supplied by the source, and that only half (or less) of that value passes through the transformer primary at any given instant. The data for each configuration are listed in Appendices E through H. Once again the same trends are evident: adding capacitance reduces the system frequency at the cost of decreased output voltage, and placing the auxiliary inductor in the circuit also reduces the output voltage. The quartz actuator, by virtue of its minimal starting capacitance, can operate over a wider frequency range, and in this

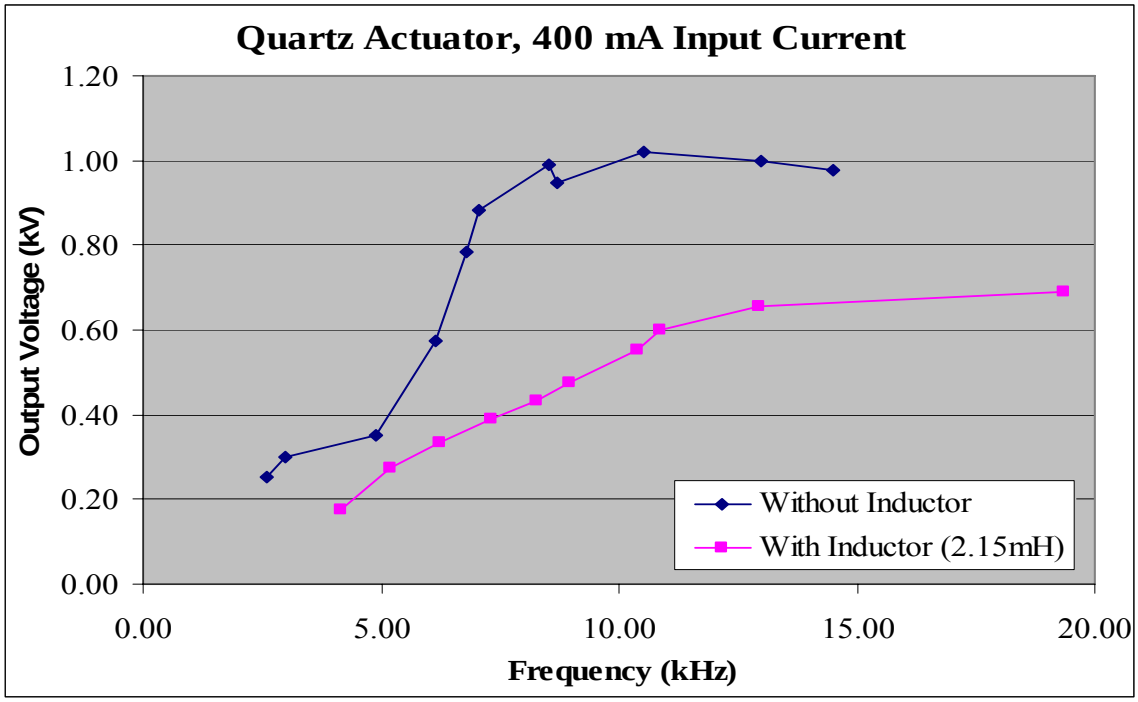

Figure 4.10. Quartz actuator data summary, 400 mA input current, no plasma generated.

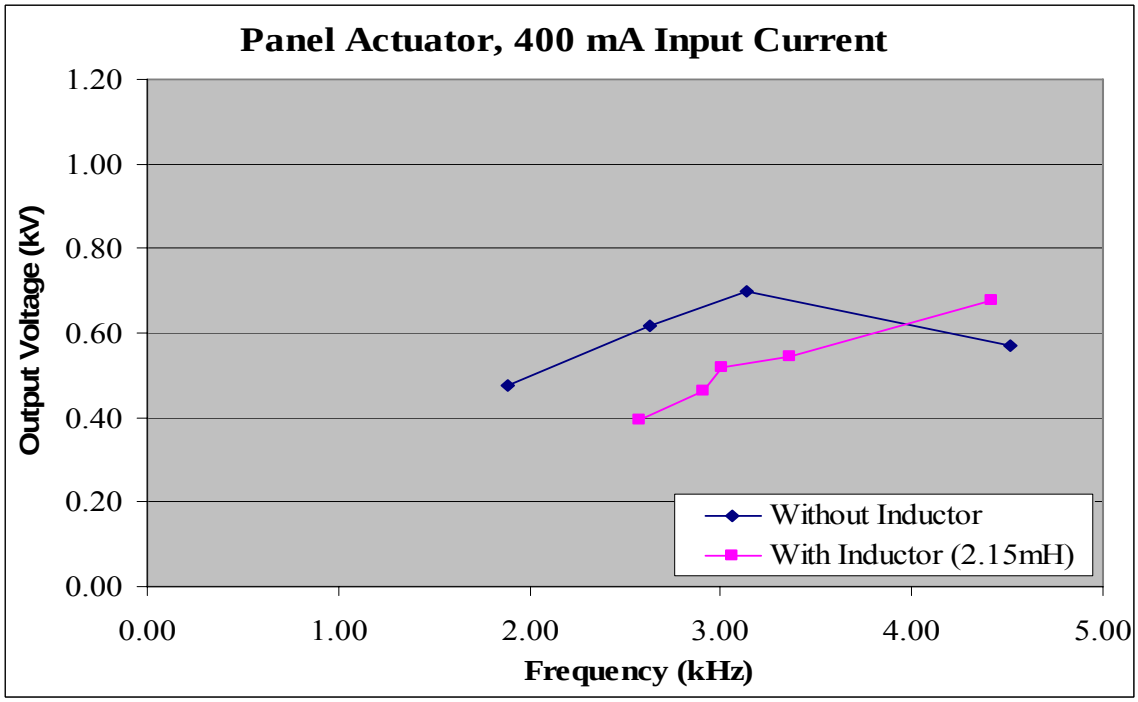

Figure 4.11. Panel actuator data summary, 400 mA input current, no plasma generated.

case reached a maximum frequency of 19 kHz with the addition of the auxiliary parallel inductor in the primary. The seemingly anomalous panel data can be explained by the fact that the data for each trial, with and without the auxiliary inductor, were collected on different dates, with slight differences in input current.

A recurring problem throughout testing was that of instability: the circuit operated normally for low power settings, but as input current was increased, the system became unstable and it was impossible to synchronize at any resonant frequency. Factors that may have caused this instability, and for which fixes were attempted, include faulty connections within the breadboard, vibration of the capacitor plates within the variable capacitor, poor impedance matching between secondary load and primary current source, and faulty switching components.

During unstable operation there was initially an audible noise emanating from the variable capacitors. Visual inspection and proper operation at lower currents indicated that there had not been a dielectric breakdown, and thus the noise was not due to arcing. It was suspected that the electrode plates might be vibrating, and so a few design adjustments were made to each capacitor. The bottom support plate was removed from the moving plate assembly, since it had the effect of holding the fixed plates suspended in air, allowing them to sag near their base connection. Additionally, a thin board was cut to fit over the plates and a brass weight was placed on top of this board, in an effort to press the plates down and prevent their vibration. These changes eliminated the noise coming from the capacitors and improved circuit operation somewhat. However, there remained a tendency towards instability as input current was increased. Figure 4.12 illustrates the waveforms of the circuit during unstable operation. The performance of the

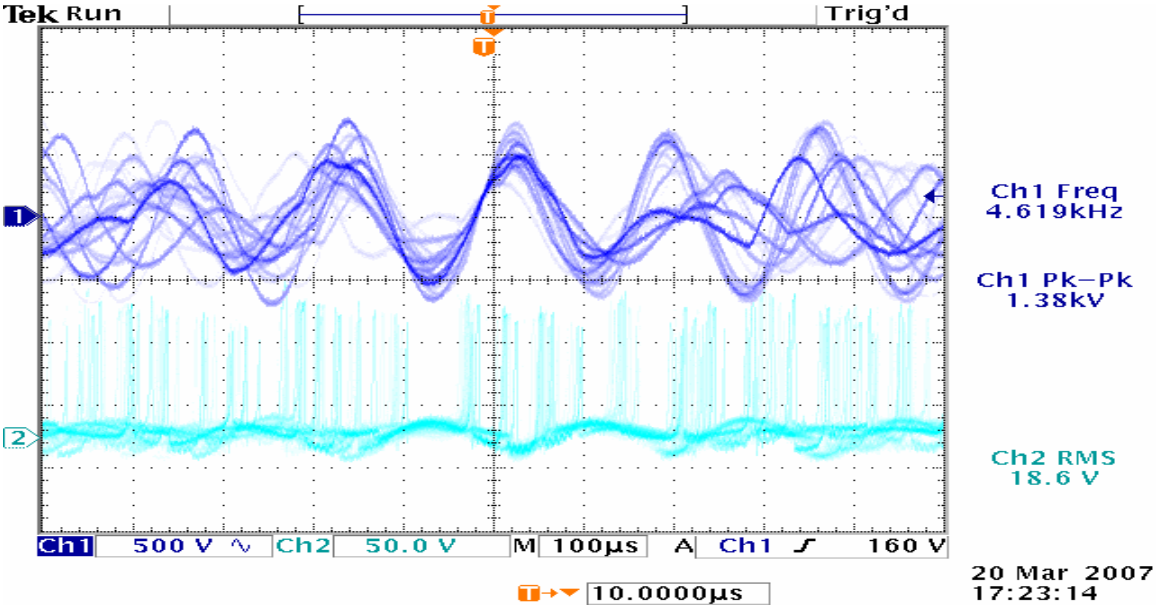

Figure 4.12. Unstable operation, a recurring problem.

Ch1: output voltage (500 V/div), Ch2: voltage across switch (50 V/div).

variable capacitors seemed to degrade over time, particularly the medium and large sizes with multiple electrodes, which suggested that the problem might be due to poor electrical contact between oxidizing aluminum surfaces.

4.5 Further Testing: 600 mA Input Current, First Plasma

It was suggested by Sirous Nourgostar, a fellow student in the Plasma Lab, that the instability preventing normal operation of the circuit might be due to poor impedance matching between the highly reactive load and the source. A method of impedance matching for plasma loads had been developed and described by Chen [27], a former student of Dr. Roth's, and the inductors he built were still available. One of these inductors, indicated as having a maximum value of 76 mH and a minimum value 3.2 mH (see Figure 4.13), was applied to the secondary circuit in parallel and resulted in no output oscillation whatsoever. However, when the impedance matching inductor was

Figure 4.13. Impedance matching inductor, built by Chen [27].

connected into the secondary circuit in series, the problem of instability was reduced and performance was significantly improved.

Although rated for 500 mA output, the Hewlett Packard Harrison 6102A DC power supply delivered 600 mA to the quartz actuator in combination with the series secondary impedance matching inductor and the auxiliary primary inductor for long enough to allow a complete survey of the frequency range attainable from maximum to minimum variable secondary capacitance. However, after only two measurements without the auxiliary inductor, the power supply was permanently damaged, along with the control IC and one of the MOSFETs. These tests were the first instances in which the output voltage reached values sufficient to generate a plasma discharge across the actuator. Plasma generation was first detected by the odor of ozone and then confirmed by turning out the

light in the laboratory to make the plasma visible. The collected data are listed in Appendices I and J, and is summarized in Figure 4.14. Once again, the data indicates that as capacitance increases in the secondary circuit, the frequency is decreased along with the output voltage, and the auxiliary inductor in the primary serves to increase the frequency range, as expected, but it also diverts energy from the transformer and thus the actuator load. While these tests represented a success, in that plasma was being generated, it was recognized that the circuit was not functioning correctly because the input current to the transformer primary was not in the form of a square wave, which was demonstrated as a characteristic of proper operation by Alonso [11].

4.6 Further Testing: Plasma Generation

As previously indicated, the Hewlett Packard Harrison 6102A DC power supply was the only available supply that operated in current mode. After its failure, two separate

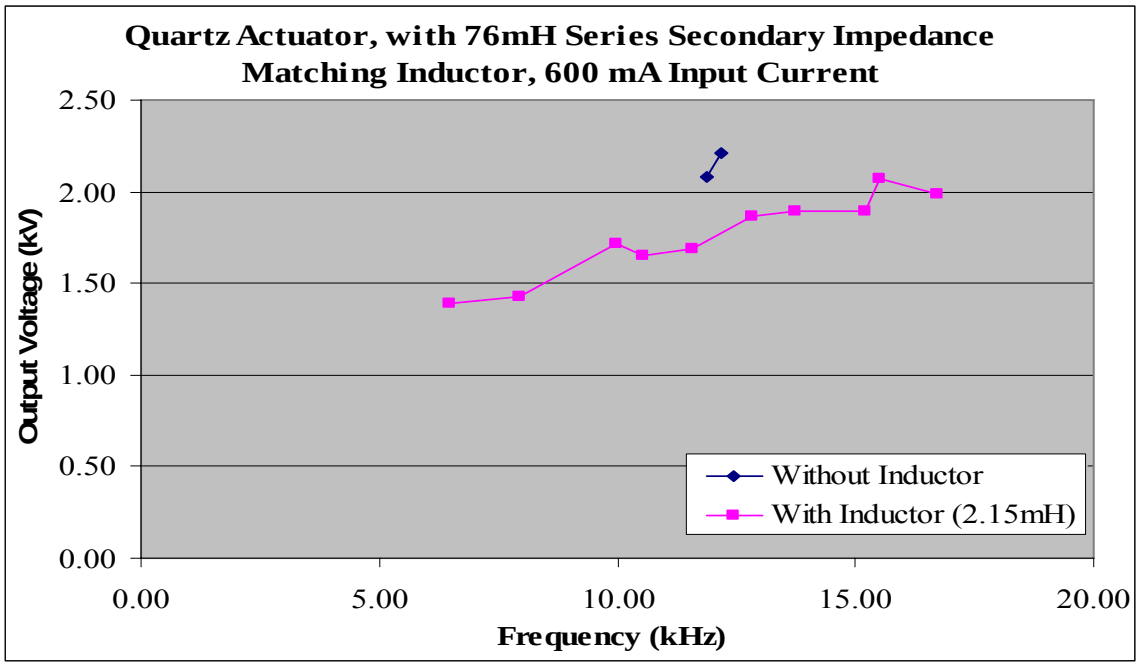

Figure 4.14. Quartz Actuator data summary, 600 mA input current.

supplies were required to provide a steady voltage for the gate drive circuitry and an adjustable current for the main tank circuit. As previously indicated, the Kepco CK40-0.8M and the Sorenson Q Nobatron QRC40-8 were used for these two functions, respectively. Although the Sorenson supply, rated for 8 A, was able to provide the current required by the oscillating circuit for full plasma generation, the output voltages attained during testing were limited due to its functioning in the voltage mode. The data presented represents circuit operation at the highest achievable power setting, at 40 VDC. The current drawn by the load in varied according to the total impedance presented to the Sorenson supply.

In addition to the power supplies, a MOSFET and the controller IC had to be replaced after the first tests during which plasma was generated. Inspection of the waveform data gathered during that test run led to the conclusion that the choke inductors were insufficient since the current was not a square wave as expected, so two 40 mH choke inductors were borrowed from Dr. Leon Tolbert. These changes greatly improved circuit operation, but an asymmetry was still present in the transformer primary current waveform. It was discovered that only one of the gate drive signals from the controller IC was functioning properly. The IC was replaced, but the same problem recurred. The circuit connections were verified, the order of power supply energization was modified, and new sample UC3872 IC's were acquired and tested, with no improvement. Since one of the gate signals from the defective IC was still operational it was split and passed through an inverter to provide the opposite switch gate signal, and thus proper operation of the system was restored.

The data gathered during plasma generation using the quartz actuator is presented in

Appendices K through N and summarized in Figures 4.15 and 4.16. Figure 4.15 illustrates the wide range of frequencies of operation attained by varying secondary capacitance and using various values of parallel auxiliary inductance in the primary circuit. Figure 4.16 illustrates that as secondary capacitance increases more current is required to charge it and maintain the output voltage levels needed for plasma generation.

During the quartz actuator tests both of the smallest variable capacitors, which had been constructed with only 4 sheets of BOPP dielectric, shorted and became unusable. The medium variable capacitor was used to finish gathering data, but that capacitor, like the large variable capacitor, tended toward unstable circuit operation. This unstable behavior was characterized by a sound emanating from within the capacitors at the secured ends where electrical connection was established, along with difficulty in achieving oscillation. Although it sounded like arcing due to dielectric breakdown, this seems unlikely since the sound originated at opposite ends of the capacitor, where there was no electrode overlap, and there was no evidence of any damage or arcing between opposite electrodes upon visual inspection.

The two smallest variable capacitors were not as susceptible to instability and never generated any such noise. The smallest capacitors consisted of only two electrodes, and connection to the exterior circuit was made directly using single brass tabs, whereas the medium and large capacitors had multiple electrode plates at each end, all requiring interconnection, which was made with aluminum tabs. It is suspected that the interconnecting tabs of aluminum did not provide sufficient contact and electrical connection, a condition that might have worsened over time due to oxidation of the aluminum surfaces. In such a case, as voltage in the secondary increased, the electric

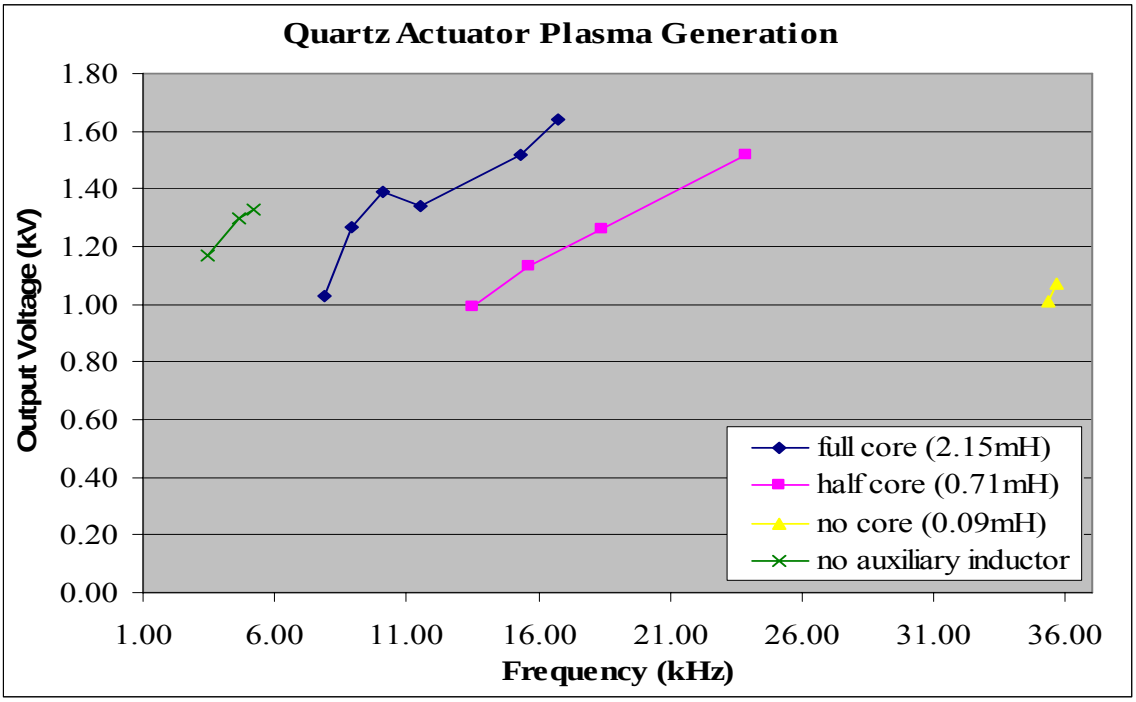

Figure 4.15. Quartz Actuator plasma generation, output voltage summary.

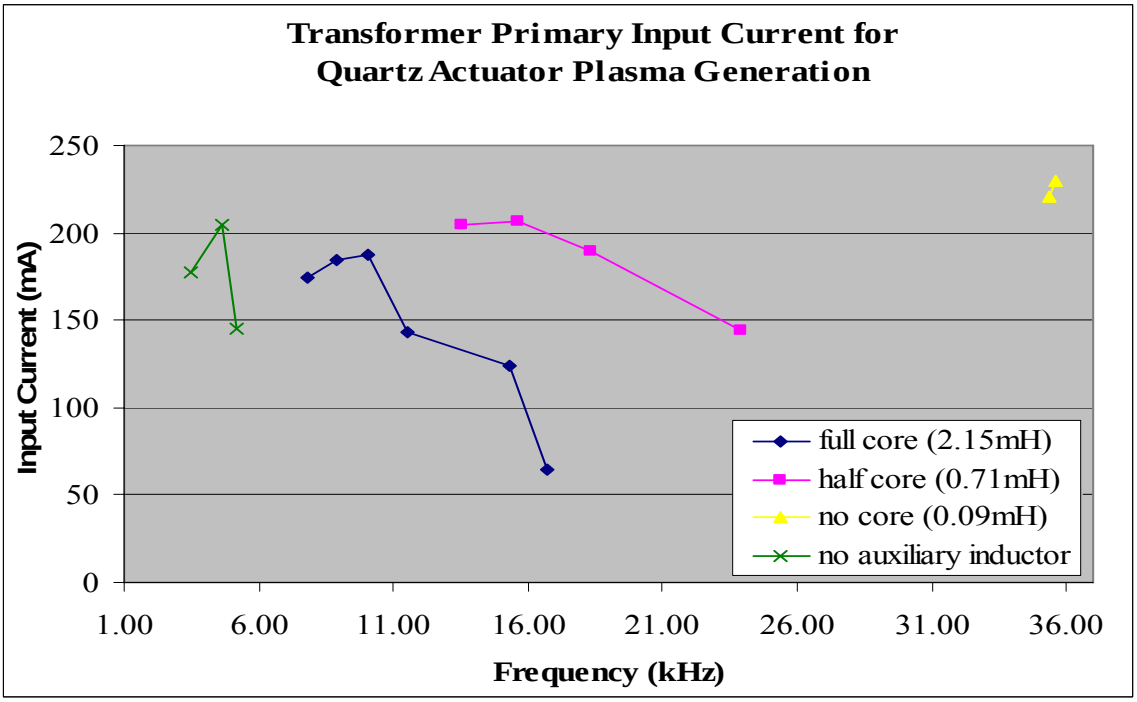

Figure 4.16. Quartz Actuator plasma generation, transformer primary current summary.

fields at the connecting strip edges might have intensified to such a degree that slight arcing may have occurred from the connecting strip edge to the main electrode plate face, which could produce audible as well as electrical noise. Figure 4.17 illustrates a design flaw in the multi-electrode capacitors that may be partially responsible for inadequate electrical connectivity. At the end of the moving electrode set for all of the variable capacitors, it was necessary to leave the connecting bolts slightly loosened to allow the plates to slide back and forth. This loose mechanical connection could serve to exacerbate the problem of electrical connection between electrodes.

Figure 4.18 is a picture of the quartz actuator during plasma generation. Figure 4.19 illustrates the waveform associated with plasma onset using the quartz actuator, which occurred in all cases when the output voltage reached approximately 1 kV. The voltage

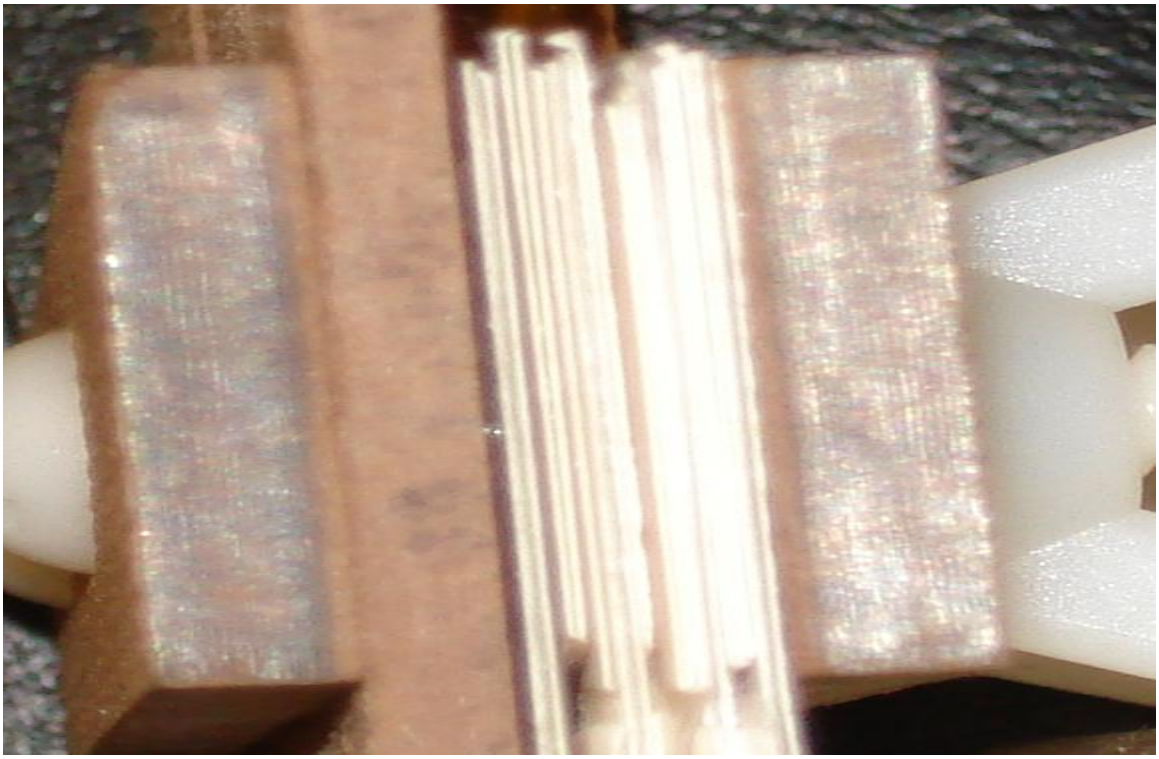

Figure 4.17.Loose mechanical connection, possible source of faulty electrical connection.

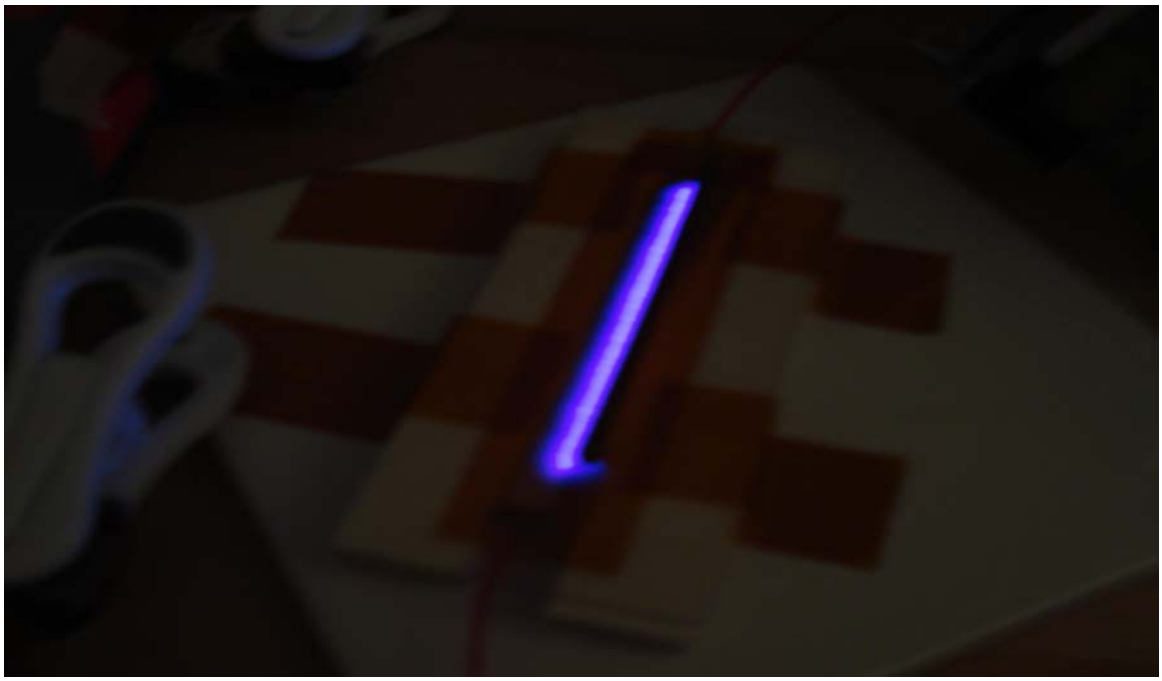

Figure 4.18.Quartz actuator plasma generation.

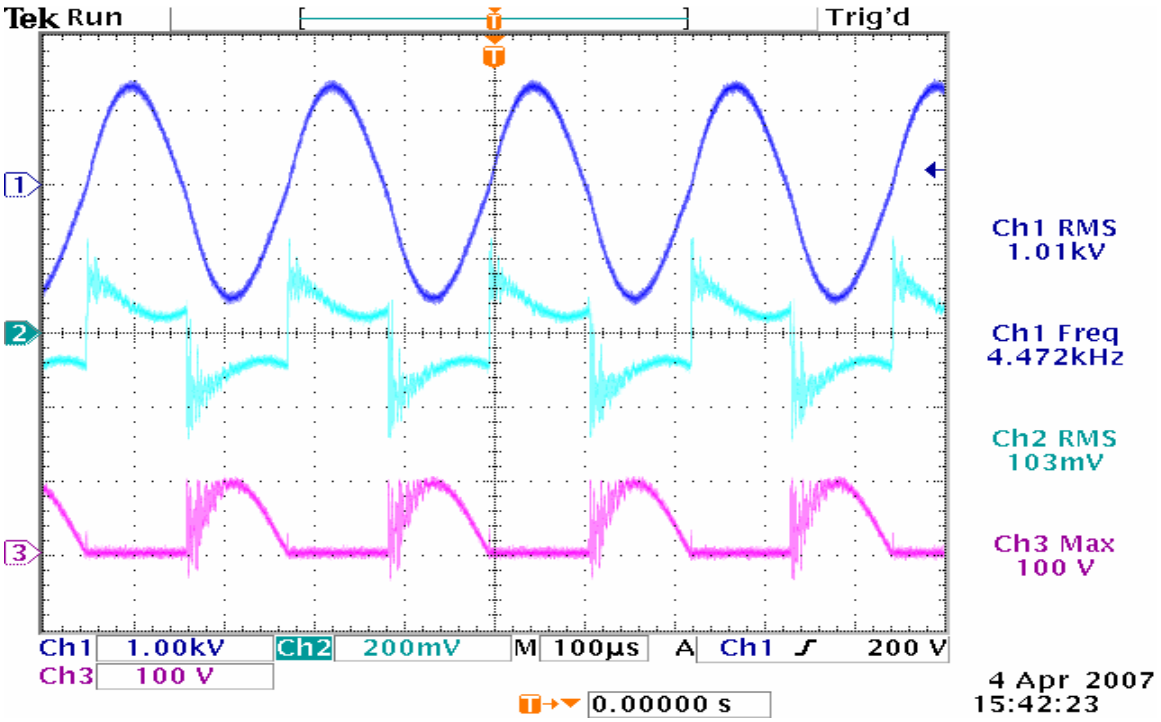

Figure 4.19.Quartz actuator plasma onset waveforms, 1.01 kV.

Ch1: output voltage (1 kV/div), Ch2: transformer primary current (200 mA/div), Ch4: voltage across switch (100 V/div).

spikes normally associated with plasma generation waveforms can be seen on the current (Ch 2) and switch voltage (Ch 3) waveforms. The waveforms associated with full plasma generation using the quartz actuator are illustrated in Figure 4.20. Once again, the current waveforms and the voltage across the switches bear typical noise/voltage spikes associated with plasma generation.

Due to the breakdown and degradation of the variable capacitors, a previously constructed high voltage capacitor made with plain polypropylene sheets was used for the panel actuator data series (see Figure 4.21). This capacitor has multiple electrodes that can be accessed individually, allowing variation of capacitance, but power must be turned off and the capacitor discharged for any change to be made. Testing of the panel made use of 2, 4, and then 6 electrodes of this capacitor, measured to have capacitance of 470 pF, 1.3 nF, and 2.2 nF respectively for each combination.

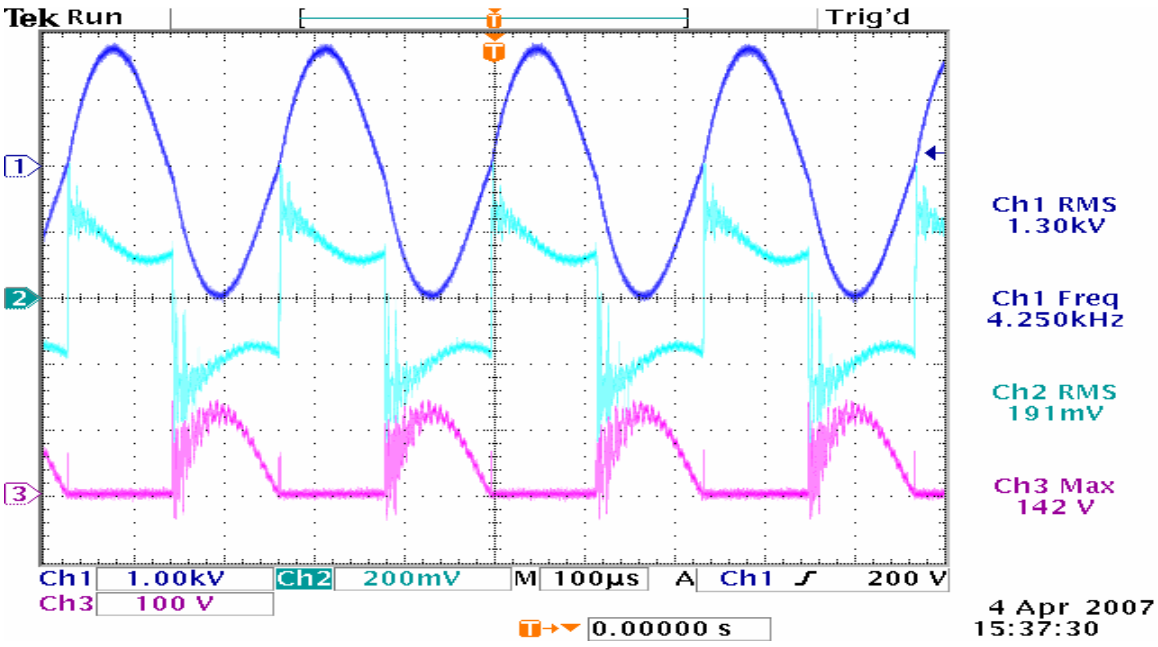

Figure 4.20.Quartz actuator full plasma waveforms, 1.30 kV.
Ch1: output voltage (1 kV/div), Ch2: transformer primary current (200 mA/div), Ch4: voltage across switch (100 V/div).

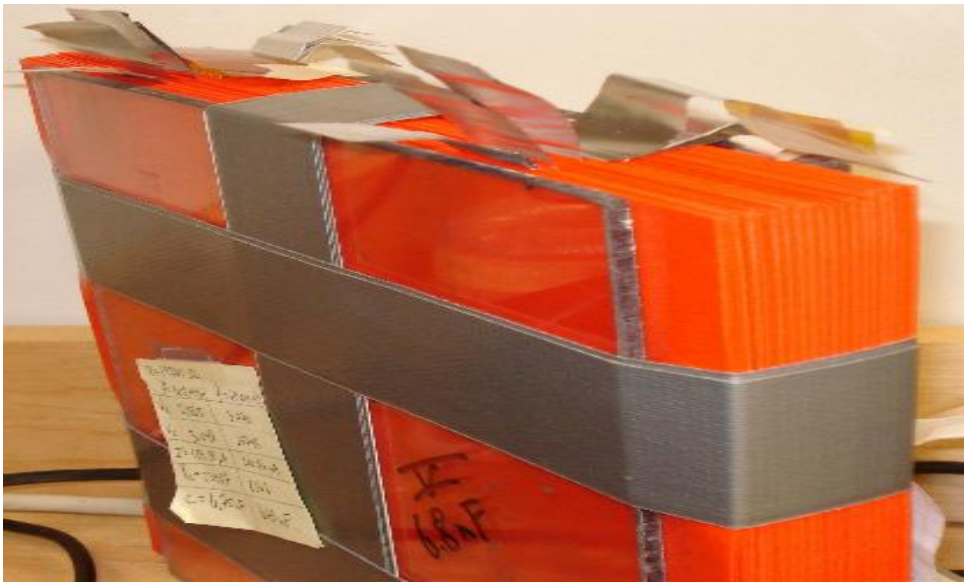

Figure 4.21.Alternate high voltage variable capacitor.

The data gathered during plasma generation using the panel actuator is listed in Appendices O through V and is summarized in Figures 4.22 through 4.25. Tests were conducted in an attempt to identify any trends associated with the inclusion of various series secondary impedance matching inductances, as had been used to stabilize circuit operation when plasma was generated for the first time. As previously noted, adding the matching inductor parallel in the secondary prevented any oscillation whatsoever. The transformer shrinks the apparent inductance value from secondary to primary by a factor of the turns ratio squared, which in parallel with the transformer primary results in a very small effective total resonating inductance, preventing oscillation at useful frequencies. However, adding the impedance matching inductor to the secondary in series did seem to have a slight stabilizing effect, possibly due to a balancing of total secondary reactance.

It is difficult to draw any conclusions from the data gathered during the panel actuator plasma generation tests, other than to confirm the trend of output voltage reduction as secondary capacitance is increased. The data sets in Figures 4.22 through 4.25 appear in

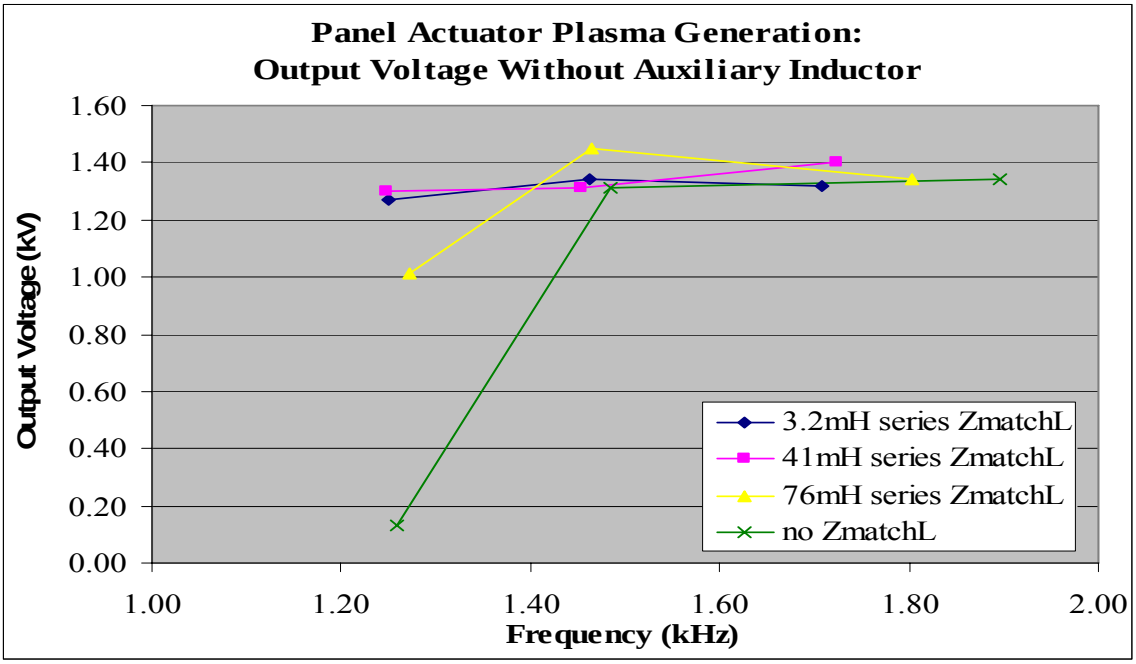

Figure 4.22.Panel Actuator plasma generation without Auxiliary Inductor, output voltage summary.

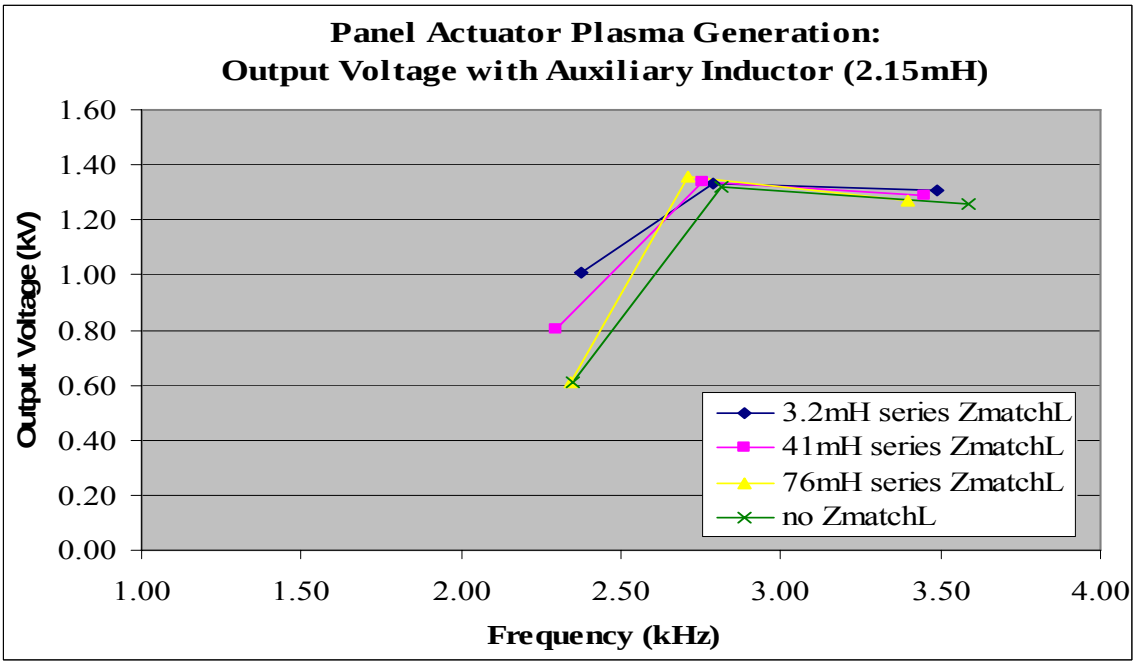

Figure 4.23.Panel Actuator plasma generation with Auxiliary Inductor, output voltage summary.

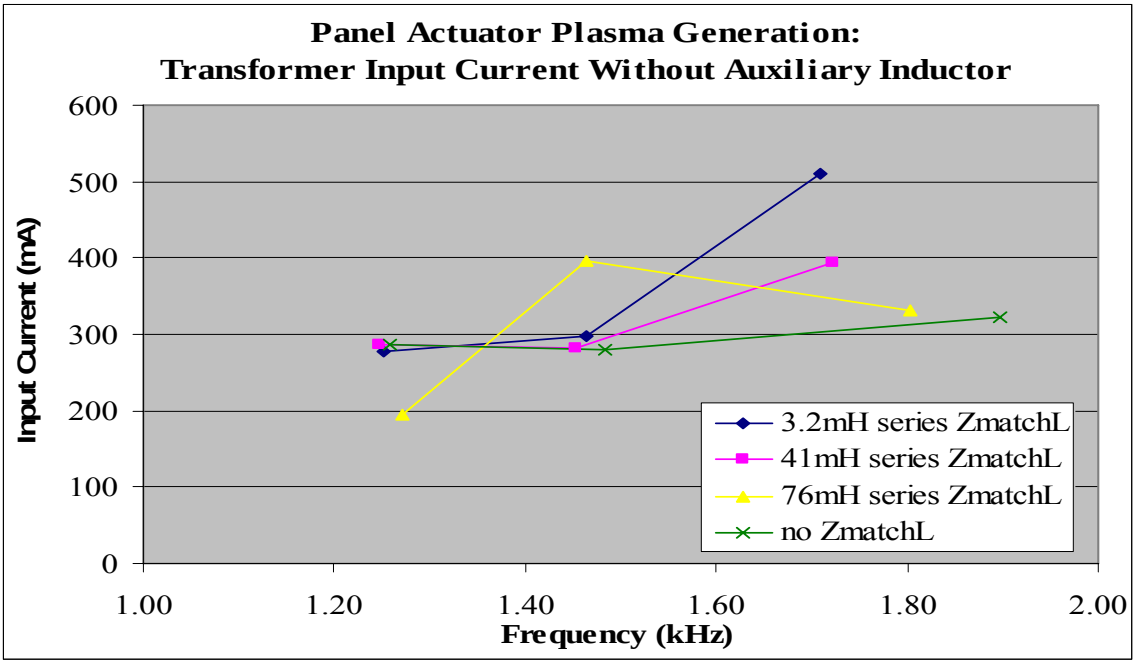

Figure 4.24.Panel Actuator plasma generation without Auxiliary Inductor, transformer primary current summary.

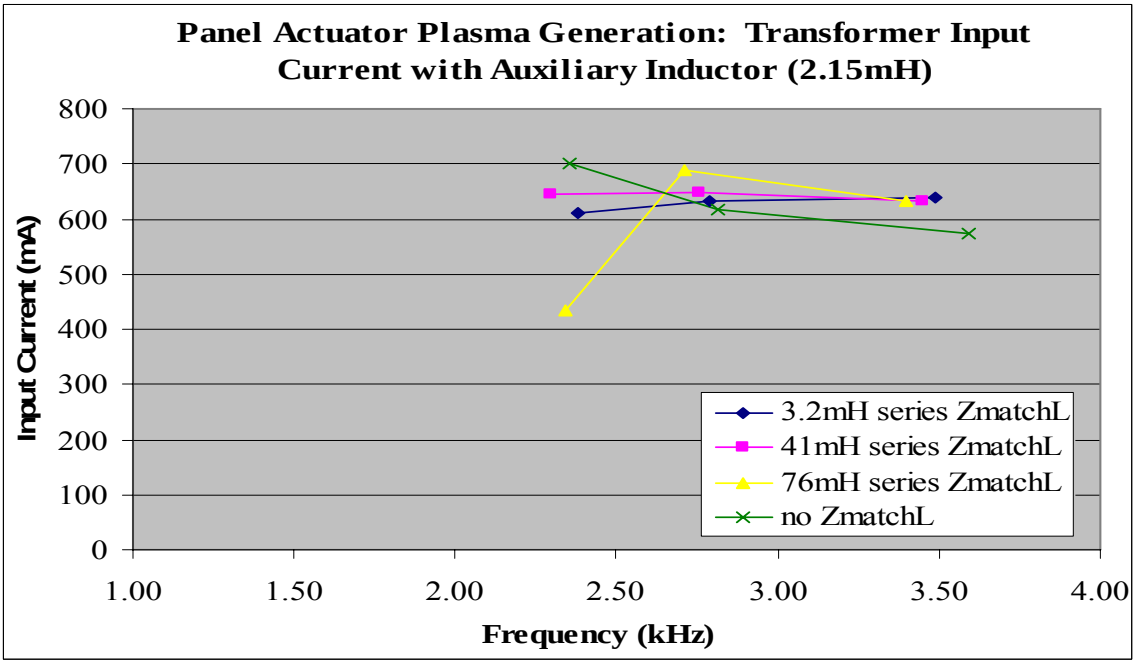

Figure 4.25.Panel Actuator plasma generation with Auxiliary Inductor, transformer primary current summary.

clusters at similar frequency values, with the highest frequency data points being associated with the 2 electrode secondary capacitor (470 pF) configuration and the lowest frequency data points associated with the 6 electrode secondary capacitor (2.2nF). The data presented in each case represent full plasma generation across the entire panel at the highest possible output from the Sorenson power supply, 40 VDC. Onset of plasma generation (see Figure 4.26) was accompanied by an audible hissing noise from the panel, a noticeable smell of ozone, and instability of operation attributable to fluctuations of capacitance associated with the plasma itself. The most notable feature of plasma onset with the panel actuator was the output voltage at which it occurred, between 700 V and 750 V in every instance.

Plasma onset was accompanied by significant instability of operation, likely due to capacitance fluctuations associated with the plasma. Attempts to operate the system with

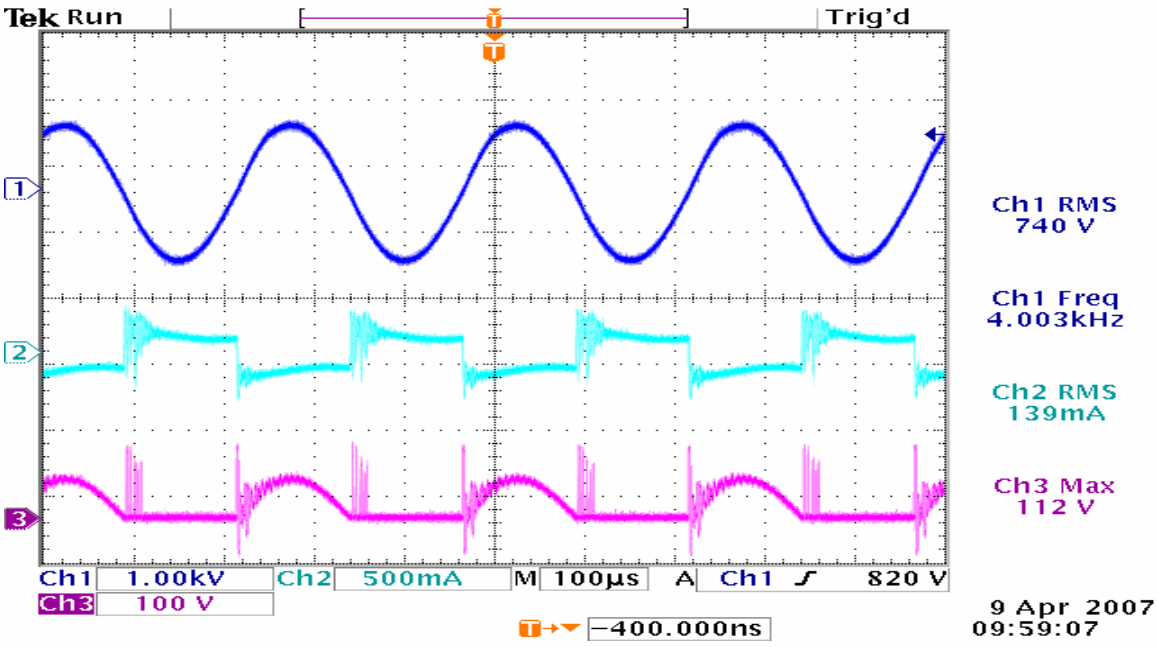

Figure 4.26.Panel actuator plasma onset waveforms, 740 V.

Ch1: output voltage (1 kV/div), Ch2: transformer primary current (500 mA/div), Ch4: voltage across switch (100 V/div).

no capacitor in the secondary were unsuccessful, likely due to these same capacitance fluctuations at plasma onset. Performance was improved when there was an additional capacitor added in the secondary. Increasing power beyond the point of onset resulted in some cases in re-stabilization as the plasma became uniform across the panel, due to a stabilization of the capacitance associated with the plasma. In other cases operation remained unstable, although plasma generation continued. Plasma coverage of the panel became uniform when the output voltage reached the 800 V to 850 V range. Figure 4.27 represents one of the most stable waveforms associated with full plasma generation across the panel actuator, and Figure 4.28 is a picture of the panel actuator when fully energized.

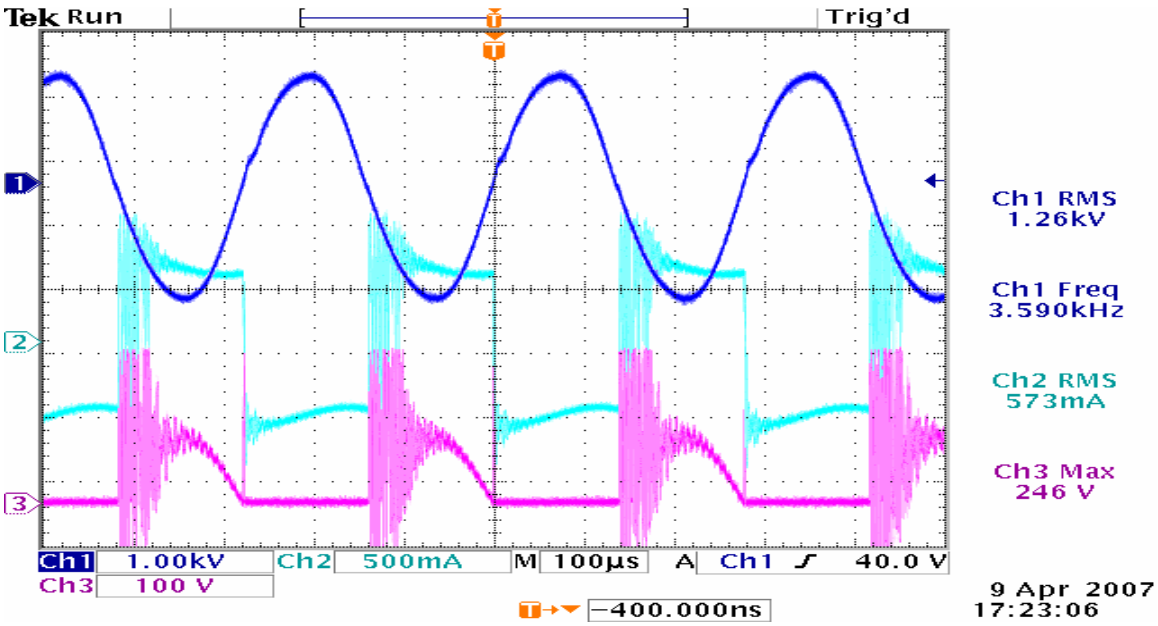

Figure 4.27.Panel actuator full plasma waveforms, 1.26 kV.

Ch1: output voltage (1 kV/div), Ch2: transformer primary current (500 mA/div), Ch4: voltage across switch (100 V/div).

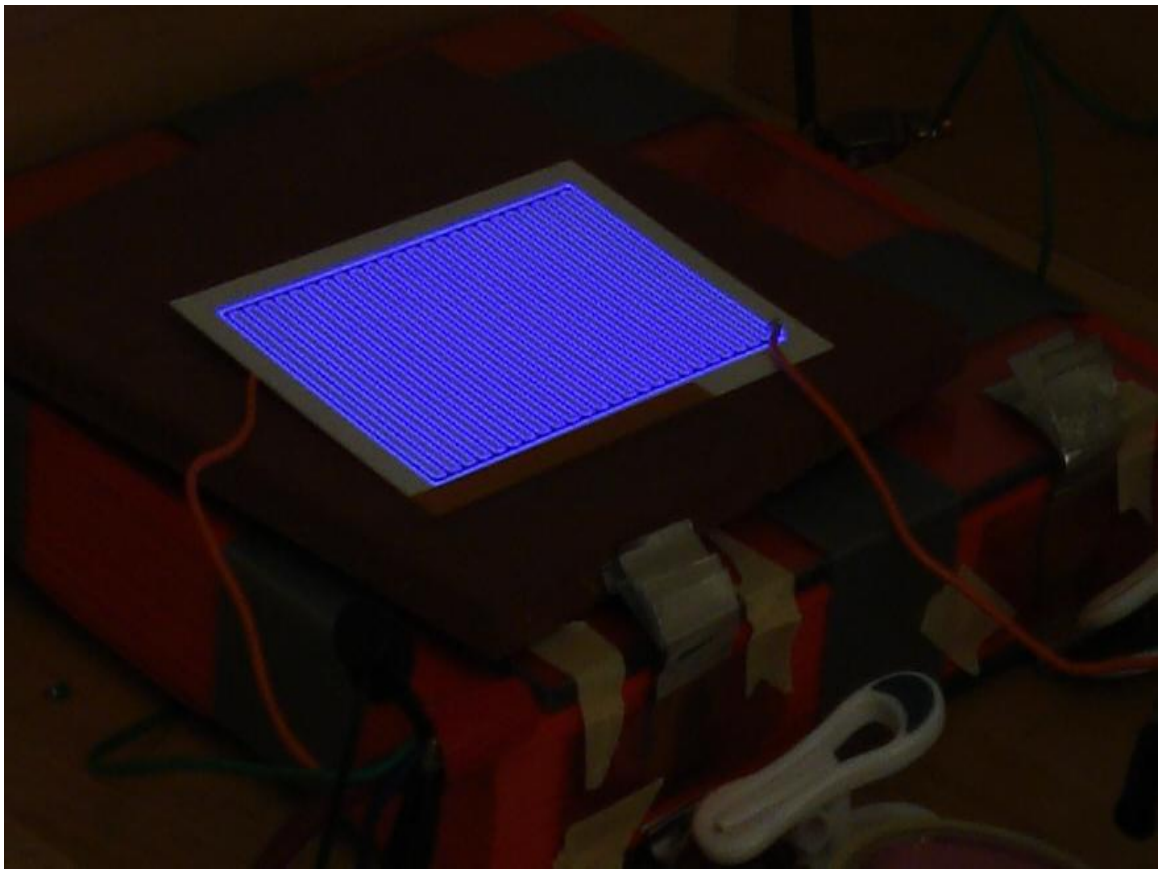

Figure 4.28.Panel actuator plasma generation.

5. Conclusions

Atmospheric plasmas are increasingly applied in industrial processes, and the uniform effect associated with the One Atmosphere Uniform Glow Discharge Plasma (OAUGDP®) is particularly useful in that it can provide energetic plasma and reactive species with minimal heating of workpieces. Additionally, the One Atmosphere Uniform Glow Discharge Plasma (OAUGDP®) can be generated efficiently at moderate voltages using audio frequencies and optimized actuators.

The goals of this thesis were achieved with respect to the range of frequency used to generate an atmospheric pressure plasma. The methods proposed to achieve this frequency variation were successfully demonstrated to be effective, although each had its particular drawbacks. The variable inductor was simple to construct and allowed operation at frequencies higher than that at which the transformer/plasma actuator system alone would oscillate. The greatest drawback associated with the variable inductor was that it diverted some power from the transformer primary and thus from the plasma load in the secondary. The variable capacitor, on the other hand, was very difficult and time-consuming to construct. It performed successfully in early testing, allowing operation at frequencies below that at which the transformer/plasma actuator system alone would oscillate. A significant drawback associated with the variable capacitor is that it requires increased system power input to maintain a given output voltage as the capacitance is increased. The greatest drawback of the variable capacitor was its faulty internal electrical connections, which resulted in unstable circuit operation. Some combination of the following might provide a solution to the problem of electrode interconnection: a

commercial paste to prevent oxidation of aluminum interconnections might be applied, or a conductive paste to provide good contact between surfaces might be applied, or brass interconnecting tabs might provide good electrical conduction without the problem of oxidation. Additionally, it is imperative that the means of mechanically securing the electrodes together as a set be separated from the means of moving the electrode set to and fro in relation to the fixed electrodes. This might be accomplished simply by applying an epoxy cement to secure the electrodes tightly together as a set.

Whereas the frequency goals of this thesis were successfully attained, the voltage goals were not. This was largely due the difficulty of operating available DC power supplies in current mode. Either a current mode power supply or a higher range of DC voltage supply might allow for further gains in output voltage. Another avenue for further exploration might be the use of an automotive battery as a power supply for the system. This would require additional components including an on/off switch, a current limiting fuse, and a variable ballast resistance in order to provide some control over the current supply. Although the output voltages attained with this system were low in comparison with the original goals, significant and useful plasma discharges were generated nonetheless.

The system examined herein, originally presented by Alonso, et al, [11], represents a significant reduction in the size and cost of power supplies for generating atmospheric plasma. The variable inductor and capacitor developed provide new tools for engineering and optimizing plasma generation systems based on the current-fed push-pull parallel resonant circuit topology.

REFERENCES

1. E. Sanchis-Kilders, J.M. Espi, J.A. Carrasco, D. Ramirez, A. Ferreres, and F. Badia, "New Application of an LLC Full Bridge Inverter Topology for Corona Generation in Plastic Industry," Applied Power Electronics Conference and Exposition, 2001 (APEC 2001), vol. 1, pp193 – 198, 4-8 March 2001. 0-7803-6618-2 IEEE, 2001.
2. Oleg Koudriavtsev, Shengpei Wang, and Mutsuo Nakaoka, "Power Supply For Silent Discharge Type Load," Industry Applications Conference, vol. 1, pp581 – 587, 8-12 October 2000.
3. O. Godoy-Cabrera, J.S. Benítez-Read, R. López-Callejas, and J. Pacheco-Sotelo, "A High Voltage Resonant Inverter for Dielectric Discharge Barrier Cell Plasma Applications," International Journal of Electronics, vol. 87, no. 3, pp 361-376, 2000.
4. J. Reece Roth, Jozef Rahel, Xin Dai, and Daniel M. Sherman, "The physics and phenomenology of One Atmosphere Uniform Glow Discharge Plasma (OAUGDP™) reactors for surface treatment applications," Journal of Physics D: Applied Physics, vol. 38, pp. 555-567, 2005.
5. J. Reece Roth, Industrial Plasma Engineering, Vol. I, Principles, Philadelphia: Institute of Physics Publishing, 1995. ISBN 0-7503-0318-2.
6. J. Reece Roth, Industrial Plasma Engineering, Vol. II, Applications to Nonthermal Plasma Processing, Philadelphia: Institute of Physics Publishing, 2001. ISBN 0-7503-0545-2.
7. Joel O. Pacheco-Sotelo, Ricardo Valdivia Barrientos, Marquidia Pacheco-Pacheco, José Fidel Ramos Flores, Miguel Angel Durán García, Jorge S. Benitez-Read, Rosendo Peña-Eguiluz, and Régulo López-Callejas, "A Universal Resonant Converter for Equilibrium and Nonequilibrium Plasma Discharges," IEEE Transactions on Plasma Science, vol. 32, pp. 2105-2112, October 2004.
8. S.D. Johnson, A.F. Witulski, and R.W. Erickson, "A Comparison of Resonant Topologies in High Voltage DC Applications," IEEE Transactions on Aerospace and Electronic Systems, vol. 24, Issue 3, pp. 263 – 274, May 1988.

9. M. Nakaoka, Y.J. Kim, H. Ogiwara, and H. Uemura, "Modern Digitally-Controlled Constant High-Frequency PWM Resonant DC-DC Converter Using Lumped Parasitic Reactive Circuit Components of High-Voltage Transformer & Feeding Cable and Its New Practical Application," Conference Record of the 1991 IEEE Industry Applications Society Annual Meeting, vol.1, pp. 1088 – 1097, 28 Sept. - 4 Oct. 1991.
10. Junming Sun, Mutsuo Nakaoka, and Hiroshi Takano, "High-Voltage Transformer Parasitic Resonant PWM DC-DC High-Power Converters and Their Performance Evaluations," Proceedings of the IEEE International Symposium on Industrial Electronics, 1997 (ISIE '97), vol. 2, pp 572 – 577, July 1997.
11. J.M. Alonso, J. García, A.J. Calleja, J. Ribas, and J. Cardesín, "Analysis, Design and Experimentation of a High Voltage Power Supply for Ozone Generation Based on the Current-Fed Parallel-Resonant Push-Pull Inverter," Conference Record of the 2004 IEEE Industry Applications Conference, vol.4, pp. 2687 – 2693, 3-7 Oct. 2004.
12. M. Teschke, D. Korzec, E.G. Finanțu-Dinu, J. Engemann, and R. Kennel, "Resonant, High Voltage, High Power Supply for Atmospheric Pressure Plasma Sources," 35th Annual Power Electronics Specialists Conference, vol.1, pp. 835 – 839, 20-25 June 2004.
13. Luigi Malesani, Paolo Mattavelli, Leopoldo Rossetto, Paolo Tenti, Walter Marin, and Alberto Pollmann, "Electronic Welder with High-Frequency Resonant Inverter," IEEE Transactions on Industry Applications, vol. 31, pp 273-279, March/April 1995.
14. Mokhtar Kamli, Shigehiro Yamamoto, and Minoru Abe, "A 50-150 kHz Half-Bridge Inverter for Induction Heating Applications," IEEE Transactions on Industrial Electronics, vol. 43, pp 163-172, February 1996.
15. J.M. Alonso, J. Cardesín, J.A. Martín-Ramos, J. García, and M. Rico-Secades, "Using Current-Fed Parallel-Resonant Inverters for Electro-Discharge Applications: A Case of Study," Nineteenth Annual IEEE Applied Power Electronics Conference and Exposition, vol. 1, pp. 109 – 115, 2004.
16. J. Marcos Alonso, Jesus Cardesín, Emilio Lopez Corominas, Manuel Rico-Secades, and Jorge García, "Low-Power High-Voltage High-Frequency Power Supply for Ozone Generation," IEEE Transactions on Industry Applications, vol. 40, pp 414-421, March/April 2004.

17. S. Potivejkul, V. Kinnares, and P. Rattanavichien, "Design of Ozone Generator using Solar Energy," 1998 IEEE Asia-Pacific Conference on Circuits and Systems, pp. 217 – 220, 24-27 Nov. 1998.
18. Huang Yushui, Wang Liqiao, Xiong Yu, and Zhang Zhongchao, "Load Resonant Type Power Supply of the Ozonizer Based on a Closed-loop Strategy," Nineteenth Annual IEEE Applied Power Electronics Conference and Exposition, vol. 3, pp. 1642 – 1646, 2004.
19. John L. Harrison, "A New Resonance Transformer," IEEE Transactions on Electron Devices, vol. ED-26, pp 1545-1549, October 1979.
20. R.M. Ness, S.G.E. Pronko, J.R. Cooper, and E.Y. Chu, "Resonance Transformer Power Conditioners," IEEE Conference Record of the 1990 Nineteenth Power Modulator Symposium, pp. 38-43, 26-28 June 1990.
21. S.D. Johnson, A.F. Witulski, and R.W. Erickson, "A Comparison of Resonant Topologies in High Voltage DC Applications," IEEE Transactions on Aerospace and Electronic Systems, vol. 24, Issue 3, pp263 – 274, May 1988.
22. S. Ben-Yaakov and M.M. Peretz, "A self-adjusting sinusoidal power source suitable for driving capacitive loads," IEEE Transactions on Power Electronics, vol. 21, Issue 4, pp. 890 – 898, July 2006.
23. Mor Mordechai Peretz and Sam Ben-Yaakov, "Analysis of the Current-Fed Push-Pull Parallel Resonant Inverter Implemented with Unidirectional Switches," IEEE 36th Conference on Power Electronics Specialists, pp. 880 – 884, 11-14 Sept. 2005.
24. Marian Kazimierczuk and Dariusz Czarkowski, Resonant Power Converters, New York: John Wiley and Sons, 1995.
25. Unitrode Datasheet, UC3872 Resonant Lamp Ballast Controller, 1999.
26. Resonant System Components, Resonant Magnetics v002.DOC, page 2, Plasma Technics, Inc., Racine, WI., 2004. http://www.plasmatechnics.com/Resonant%20Magnetics%20v002.pdf.
27. Z. Chen, "Impedance matching for one atmosphere uniform glow discharge plasma (OAUGDP) reactors," IEEE Trans. Plasma Sci., vol. 30, pp. 1922-1930, October 2002.
28. B. Babani, Coil Design and Construction Manual, London: Bernard Babani (publishing) LTD, 1960. ISBN 0-85934-050-3

29. Bureau of Naval Personnel, Basic Electricity, New York: Dover Publications, Inc., 1970. ISBN 0-486-20973-3
30. Product Specification Document K_FB_0802-05_Q_Product_specification.doc, Rev.: 29.01.07, KOPAFILM MET, published by KOPAFILM Elektrofolien, 2007. http://www.spo-kopafilm.de/downloads/kopaspec.pdf.
31. Paper Thickness Chart, Case Paper Company, Inc., New York, http://casepaper.com/pdfs/CasePaper_AverageCaliper.pdf.
32. Dielectric Constant, Strength, & Loss Tangent Table, RF Cafe, 2006. http://www.rfcafe.com/references/electrical/dielectric_constants_strengths.htm.
33. FerroxCube Application and Information Document, Soft Ferrites and Accessories, 2004. http://www.ferroxcube.com/appl/info/HB2005.pdf.

APPENDICES

Appendix A: Low Power (140mA) Data: Quartz Actuator, without Auxiliary Inductor

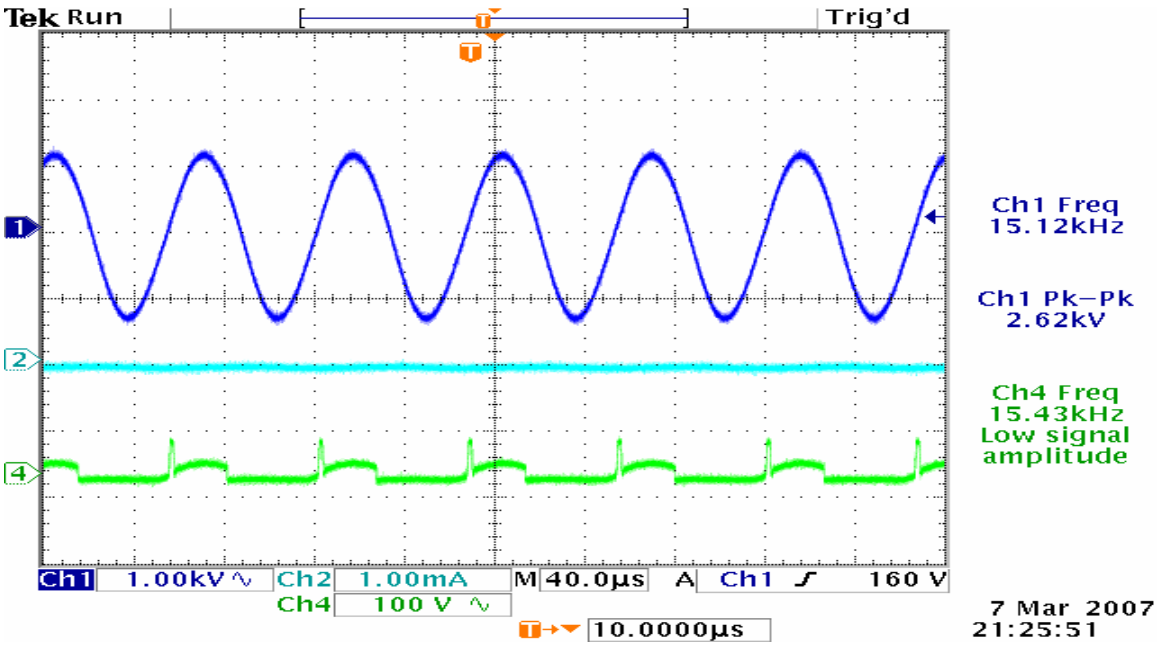

Figure A.1. Quartz Actuator, 140 mA input current, w/out Aux. Inductor, 15 kHz. Ch1: output voltage (1 kV/div), Ch2: transformer secondary current (1 mA/div), Ch4: voltage across switch (100 V/div).

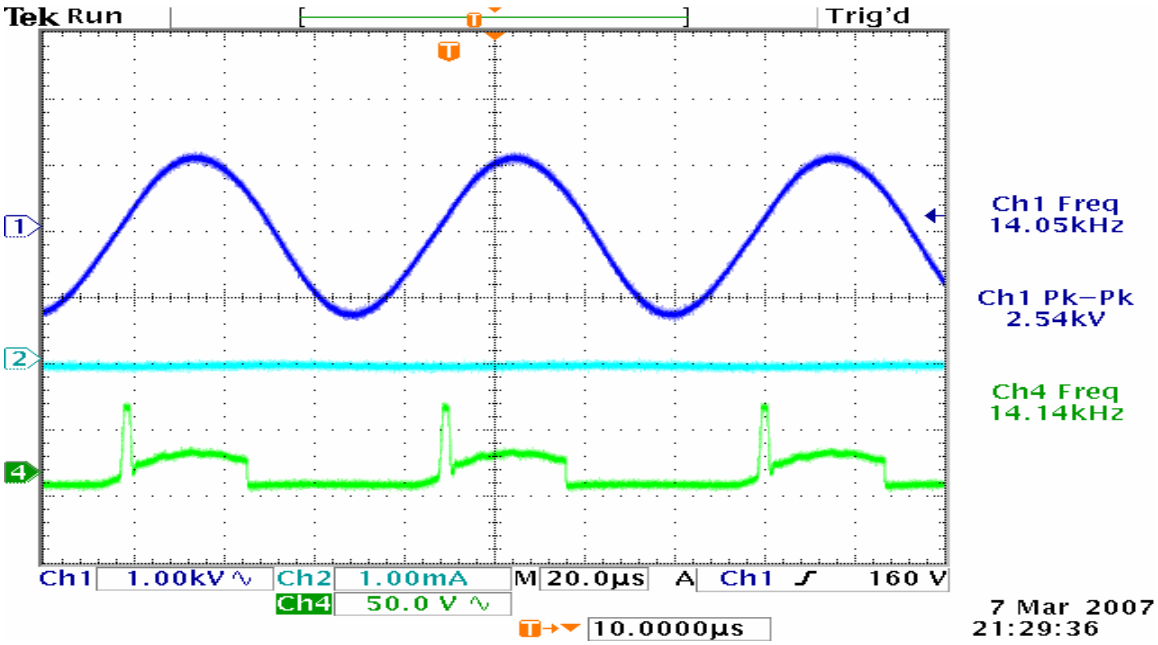

Figure A.2. Quartz Actuator, 140 mA input current, w/out Aux. Inductor, 14 kHz.
Ch1: output voltage (1 kV/div), Ch2: transformer secondary current (1 mA/div),
Ch4: voltage across switch (50 V/div).

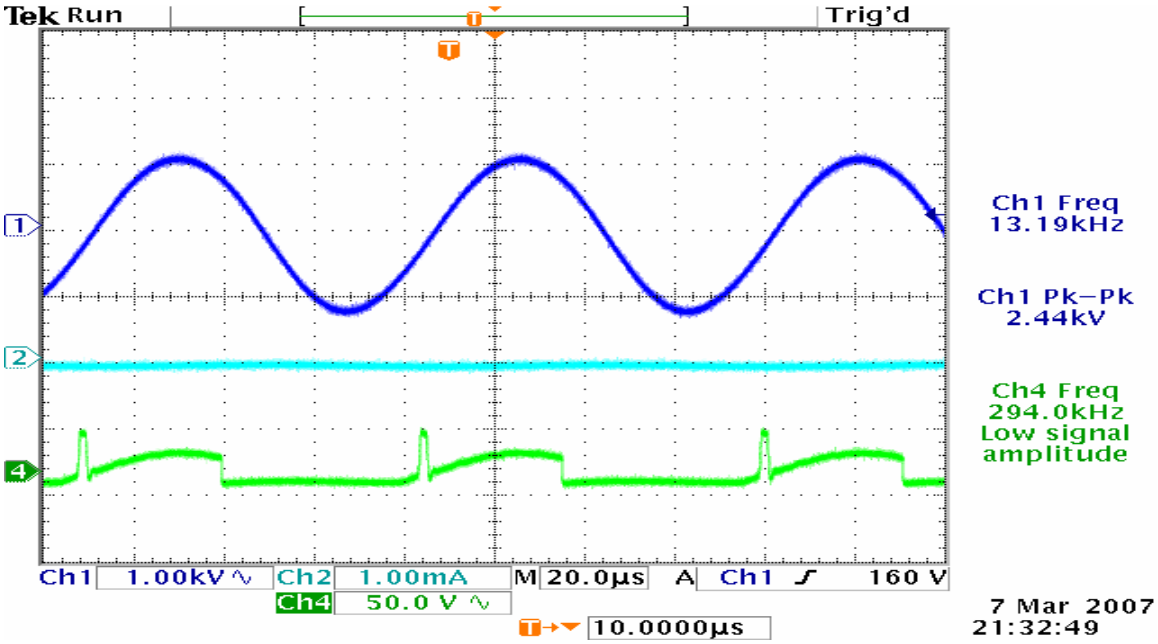

Figure A.3. Quartz Actuator, 140 mA input current, w/out Aux. Inductor, 13.2 kHz.
Ch1: output voltage (1 kV/div), Ch2: transformer secondary current (1 mA/div),
Ch4: voltage across switch (50 V/div).

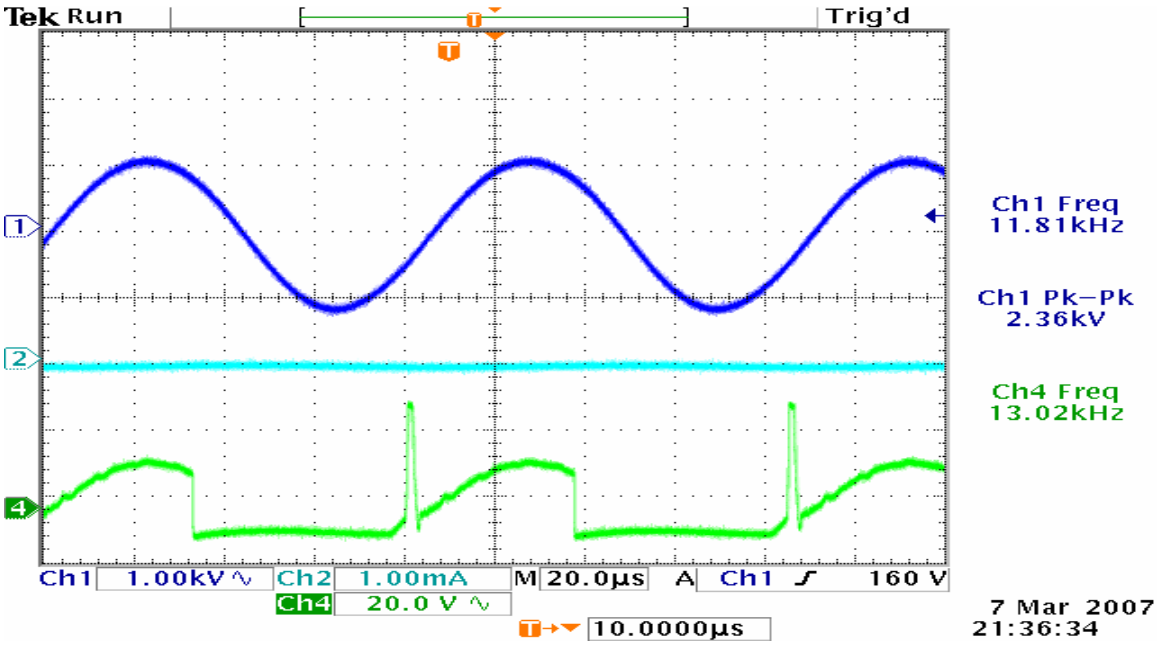

Figure A.4. Quartz Actuator, 140 mA input current, w/out Aux. Inductor, 11.8 kHz.
Ch1: output voltage (1 kV/div), Ch2: transformer secondary current (1 mA/div),
Ch4: voltage across switch (20 V/div).

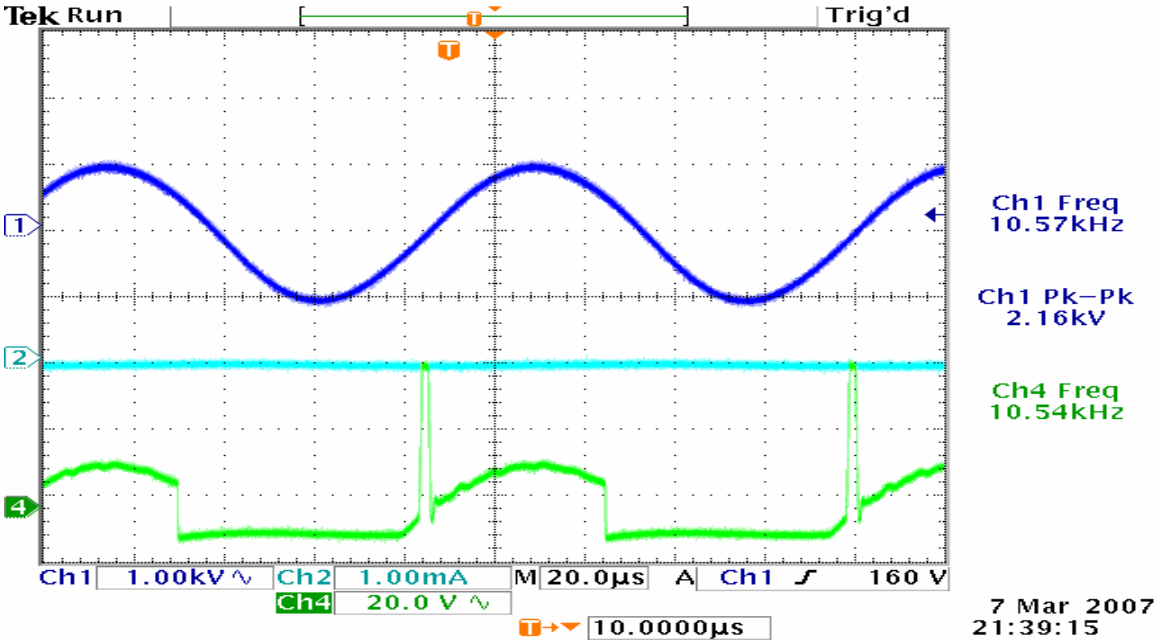

Figure A.5. Quartz Actuator, 140 mA input current, w/out Aux. Inductor, 10.6 kHz.
Ch1: output voltage (1 kV/div), Ch2: transformer secondary current (1 mA/div),
Ch4: voltage across switch (20 V/div).

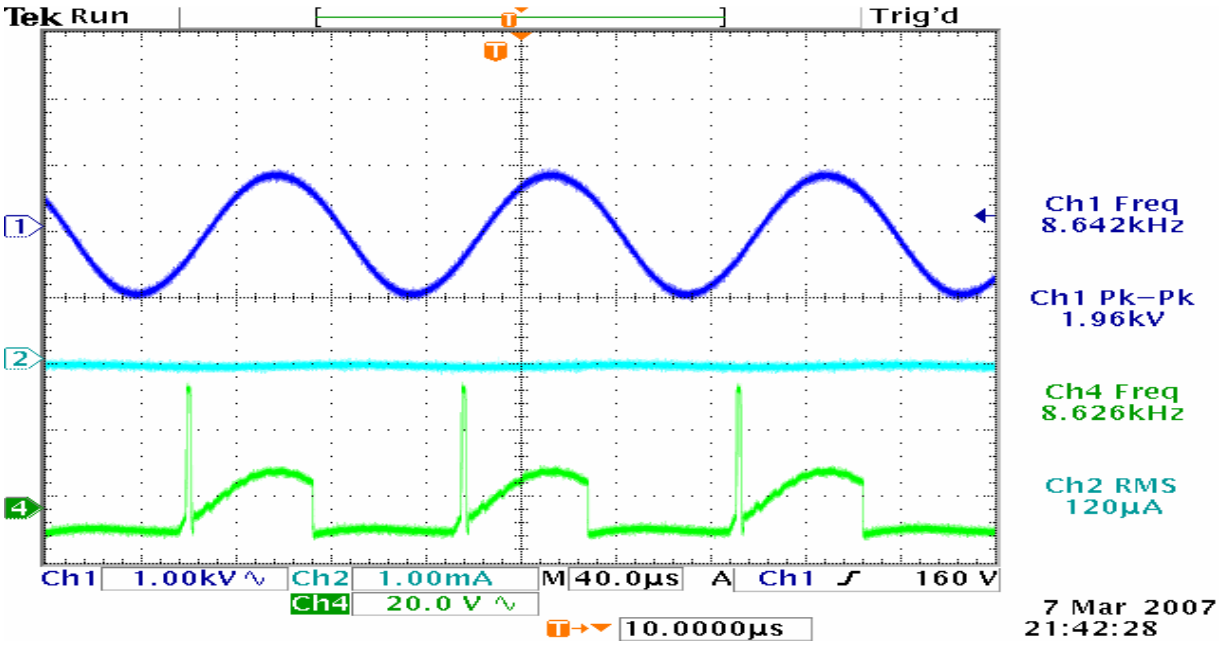

Figure A.6. Quartz Actuator, 140 mA input current, w/out Aux. Inductor, 8.6 kHz.
Ch1: output voltage (1 kV/div), Ch2: transformer secondary current (1 mA/div),
Ch4: voltage across switch (20 V/div).

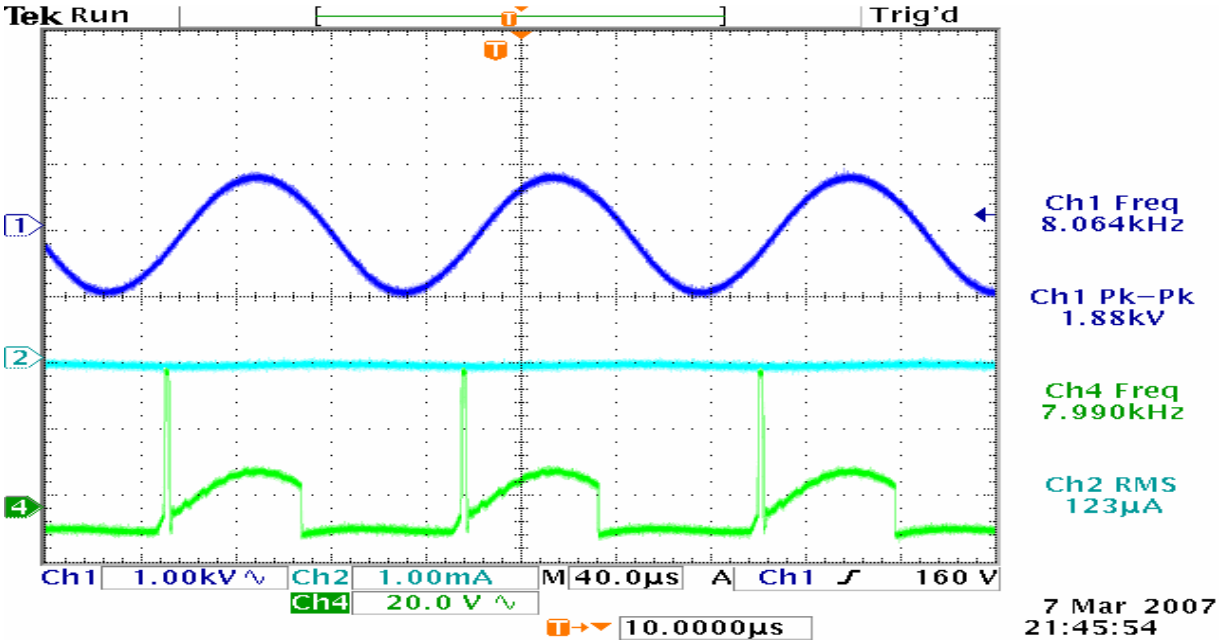

Figure A.7. Quartz Actuator, 140 mA input current, w/out Aux. Inductor, 8.1 kHz.
Ch1: output voltage (1 kV/div), Ch2: transformer secondary current (1 mA/div),
Ch4: voltage across switch (20 V/div).

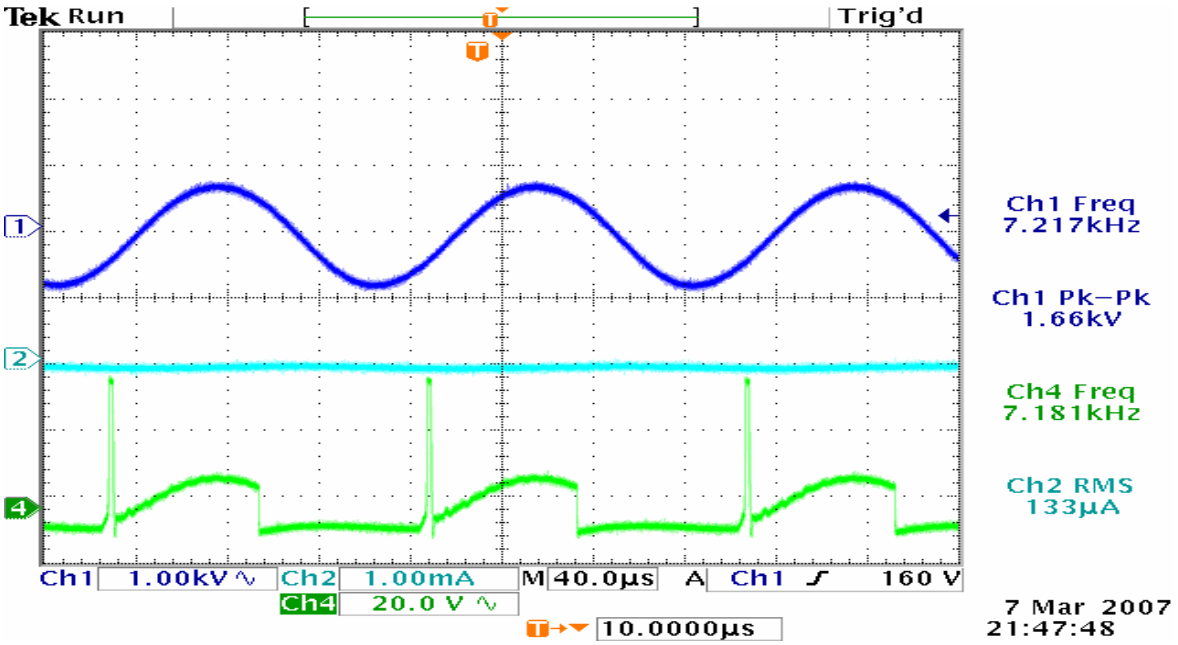

Figure A.8. Quartz Actuator, 140 mA input current, w/out Aux. Inductor, 7.2 kHz.
Ch1: output voltage (1 kV/div), Ch2: transformer secondary current (1 mA/div),
Ch4: voltage across switch (20 V/div).

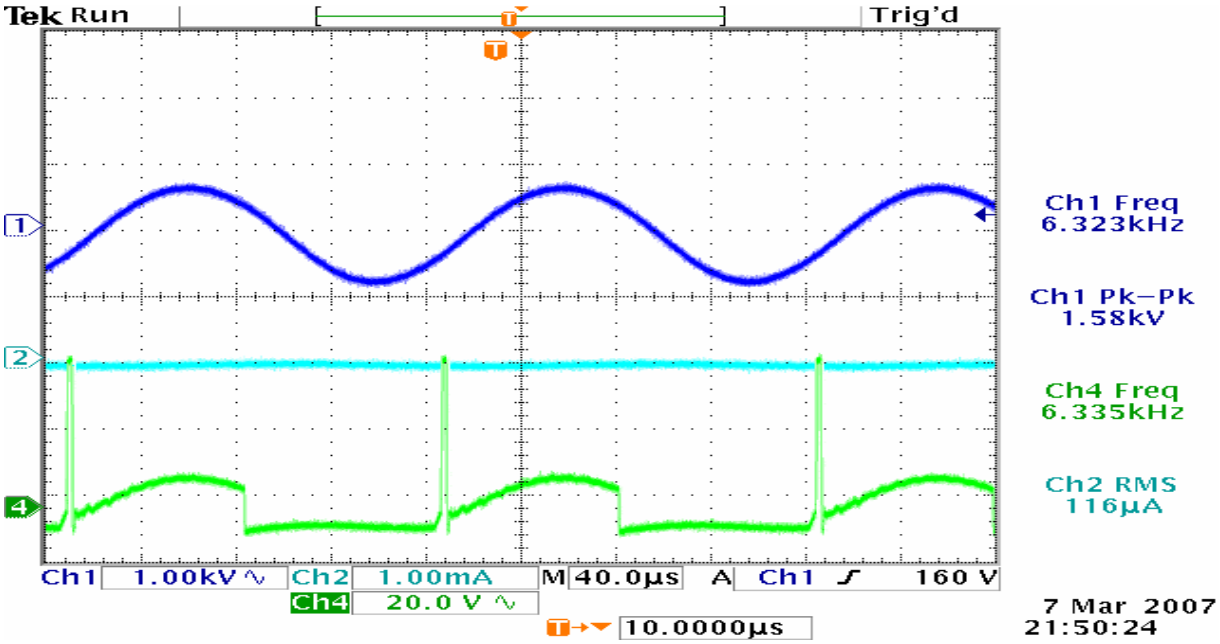

Figure A.9. Quartz Actuator, 140 mA input current, w/out Aux. Inductor, 6.3 kHz.
Ch1: output voltage (1 kV/div), Ch2: transformer secondary current (1 mA/div),
Ch4: voltage across switch (20 V/div).

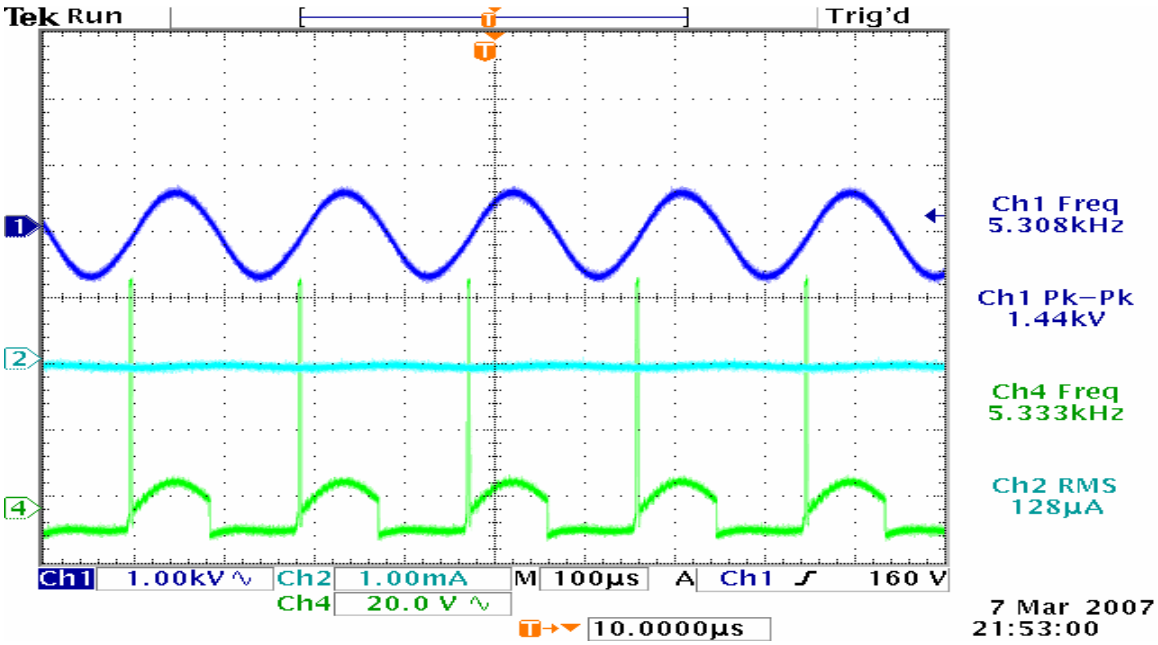

Figure A.10. Quartz Actuator, 140 mA input current, w/out Aux. Inductor, 5.3 kHz.
Ch1: output voltage (1 kV/div), Ch2: transformer secondary current (1 mA/div),
Ch4: voltage across switch (20 V/div).

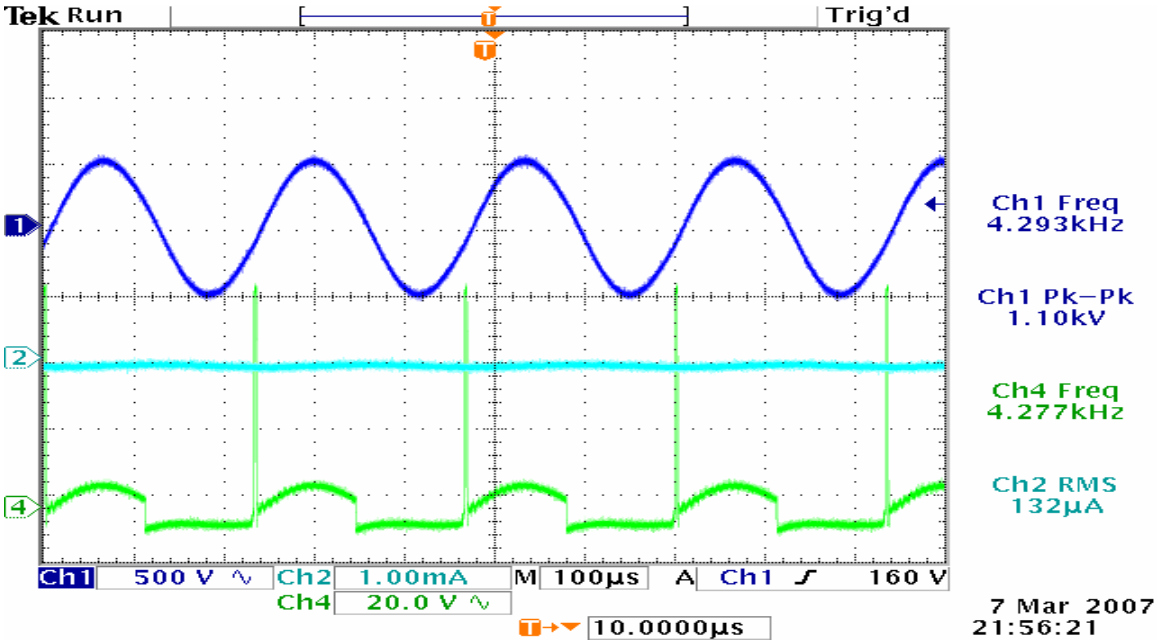

Figure A.11. Quartz Actuator, 140 mA input current, w/out Aux. Inductor, 4.3 kHz.
Ch1: output voltage (500 V/div), Ch2: transformer secondary current (1 mA/div),
Ch4: voltage across switch (20 V/div).

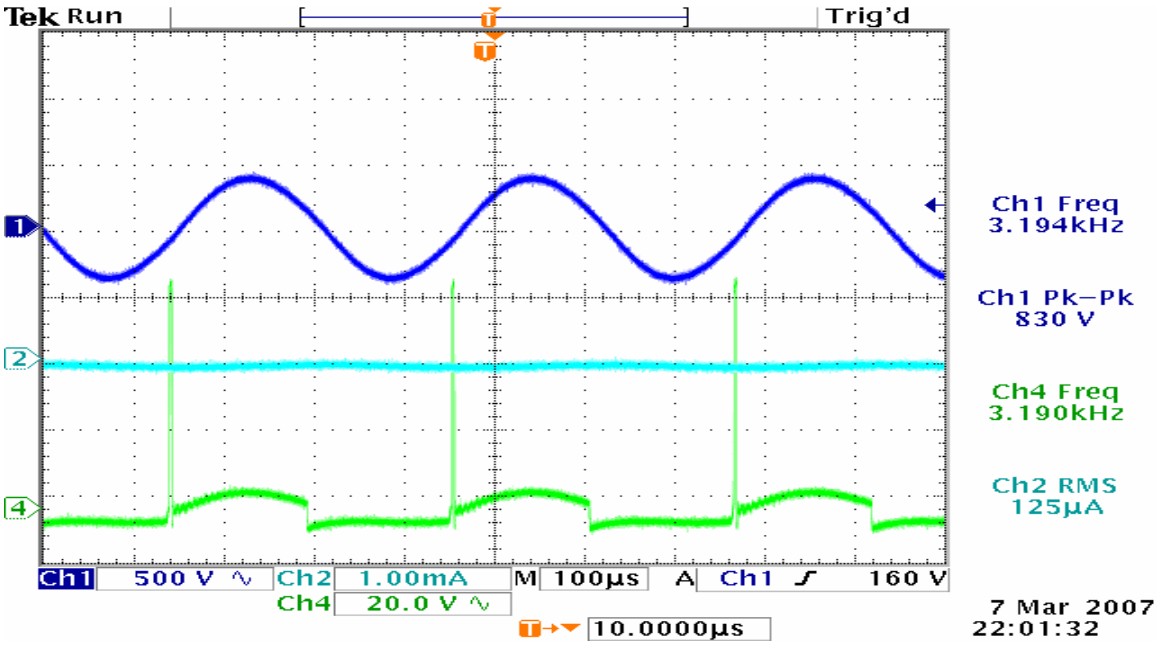

Figure A.12. Quartz Actuator, 140 mA input current, w/out Aux. Inductor, 3.2 kHz.
Ch1: output voltage (500 V/div), Ch2: transformer secondary current (1 mA/div),
Ch4: voltage across switch (20 V/div).

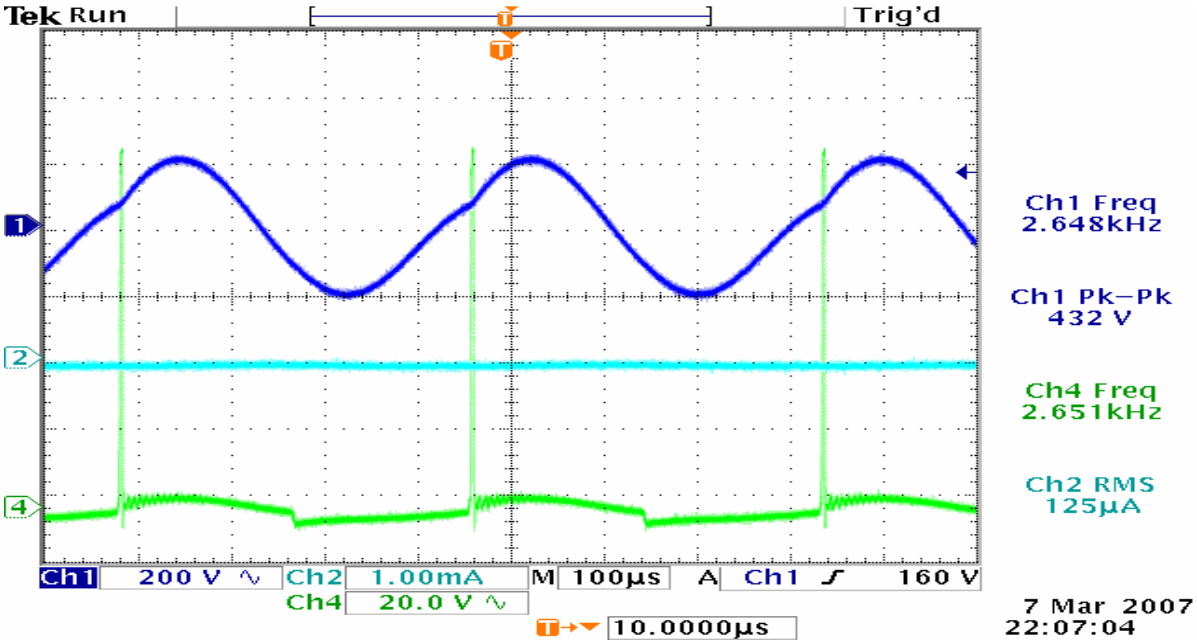

Figure A.13. Quartz Actuator, 140 mA input current, w/out Aux. Inductor, 2.6 kHz.
Ch1: output voltage (200 V/div), Ch2: transformer secondary current (1 mA/div),
Ch4: voltage across switch (20 V/div).

Appendix B: Low Power (140mA) Data: Quartz Actuator, with 2.15mH parallel primary Auxiliary Inductor

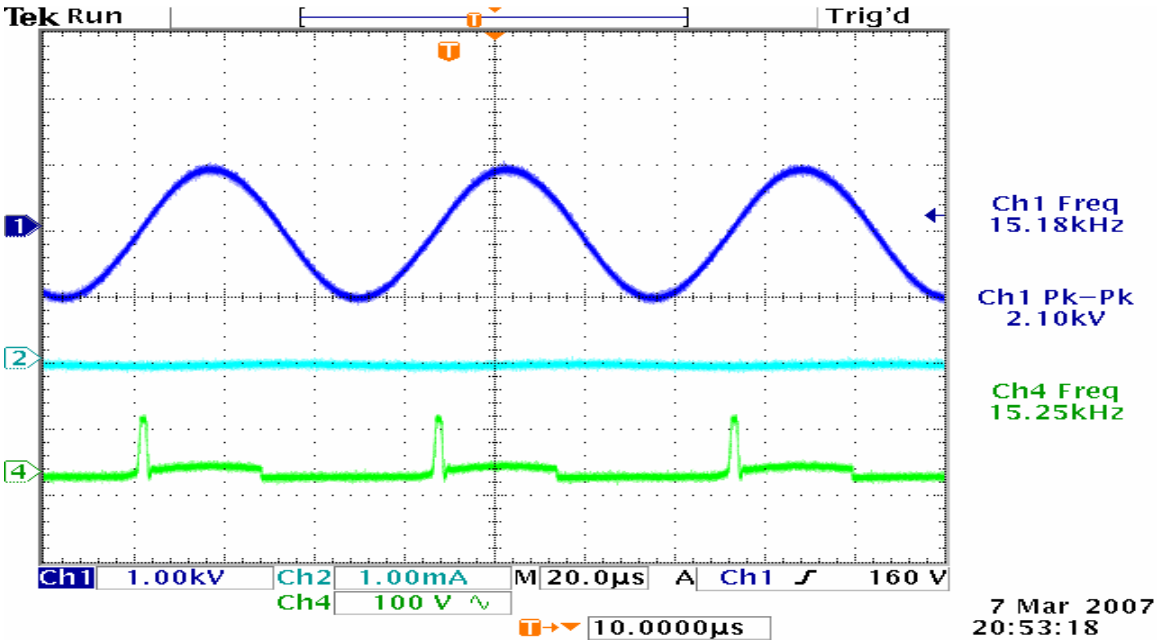

Figure B.1. Quartz Actuator, 140 mA input current, with Aux. Inductor, 15.2 kHz. Ch1: output voltage (1 kV/div), Ch2: transformer secondary current (1 mA/div), Ch4: voltage across switch (100 V/div).

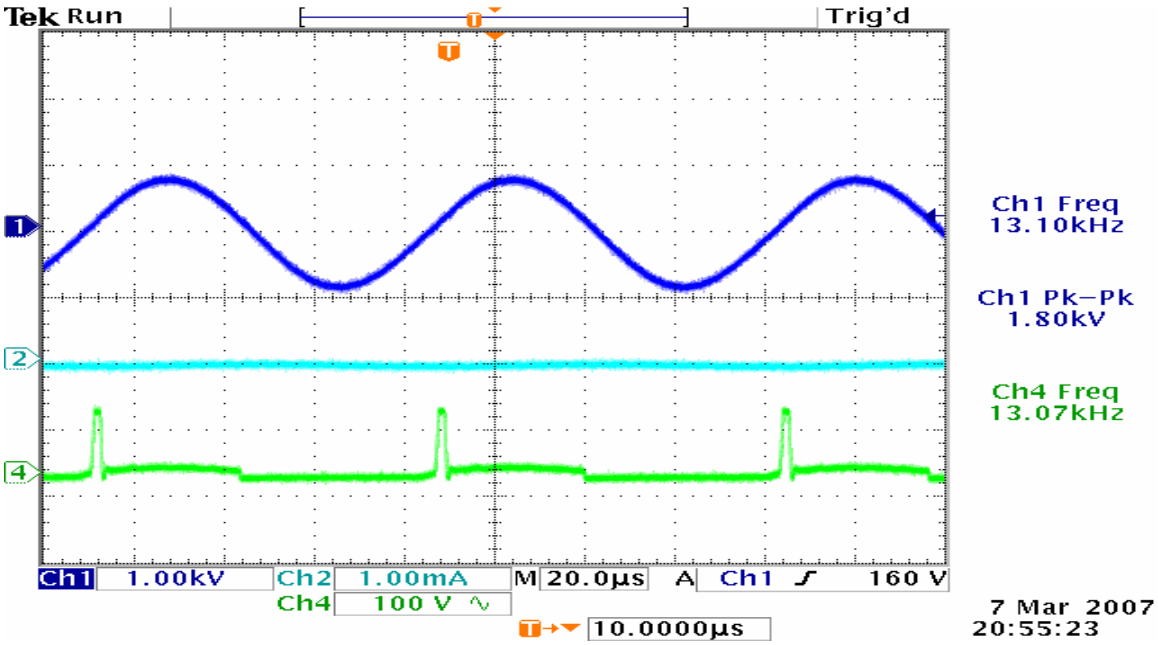

Figure B.2. Quartz Actuator, 140 mA input current, with Aux. Inductor, 13.1 kHz.
Ch1: output voltage (1 kV/div), Ch2: transformer secondary current (1 mA/div),
Ch4: voltage across switch (100 V/div).

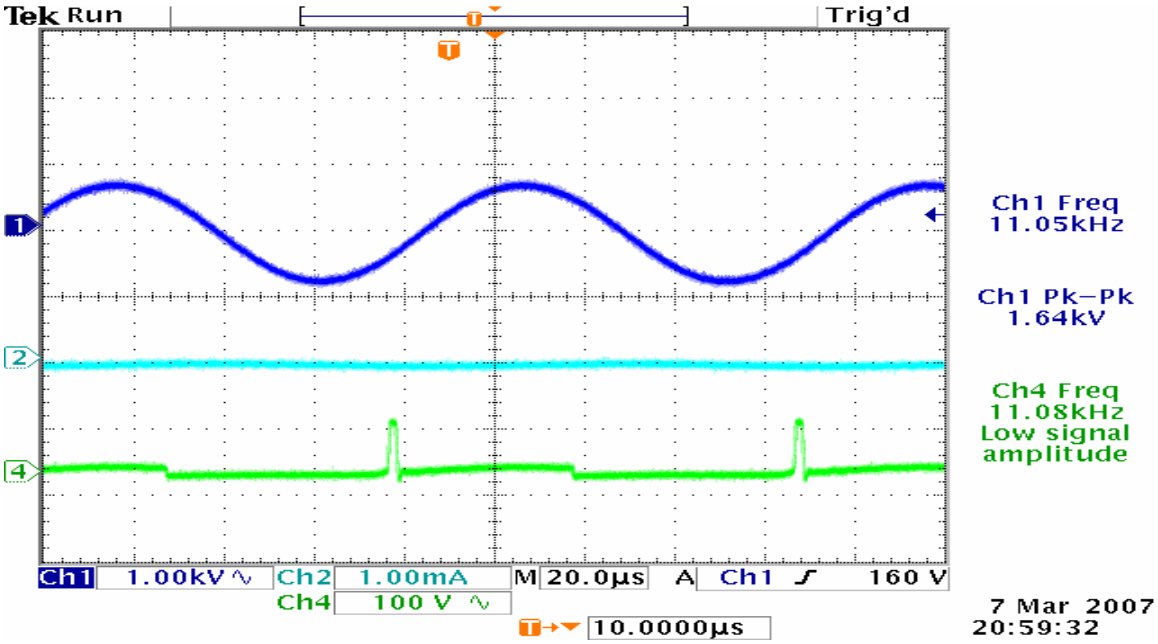

Figure B.3. Quartz Actuator, 140 mA input current, with Aux. Inductor, 11 kHz.
Ch1: output voltage (1 kV/div), Ch2: transformer secondary current (1 mA/div),
Ch4: voltage across switch (100 V/div).

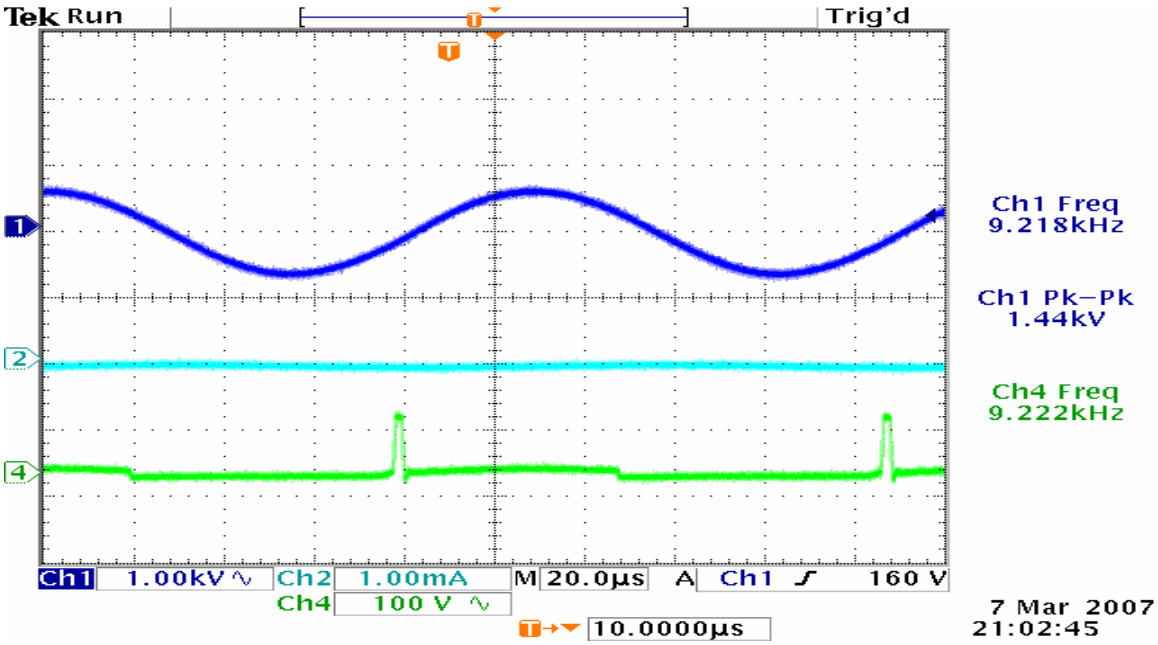

Figure B.4. Quartz Actuator, 140 mA input current, with Aux. Inductor, 9.2 kHz.
Ch1: output voltage (1 kV/div), Ch2: transformer secondary current (1 mA/div),
Ch4: voltage across switch (100 V/div).

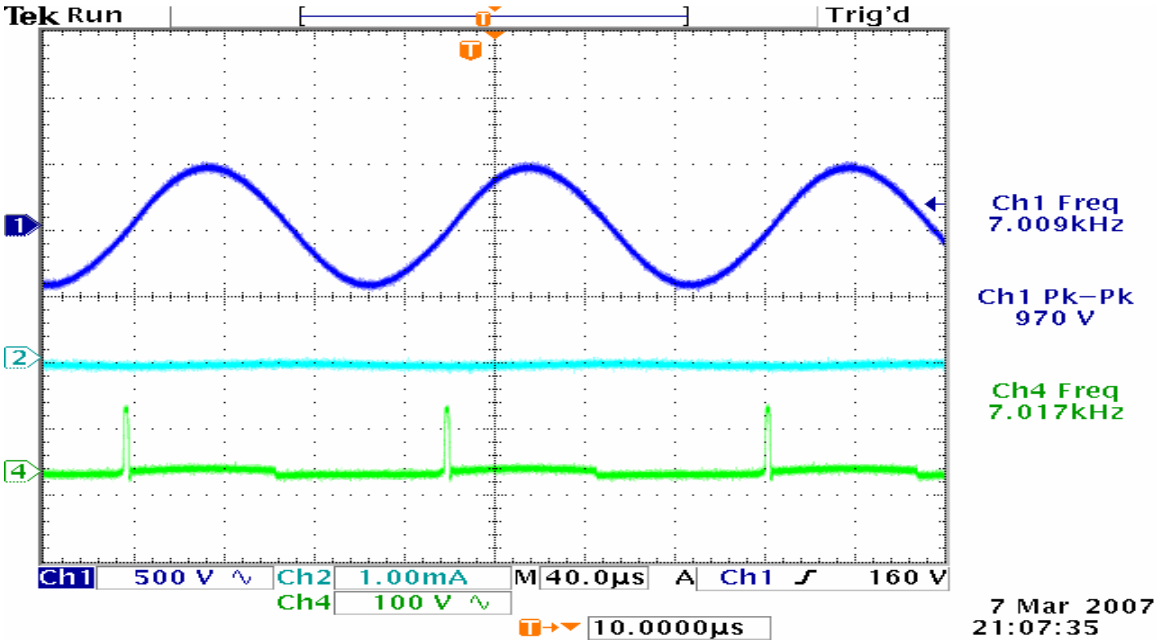

Figure B.5. Quartz Actuator, 140 mA input current, with Aux. Inductor, 7 kHz.
Ch1: output voltage (500 V/div), Ch2: transformer secondary current (1 mA/div),
Ch4: voltage across switch (100 V/div).

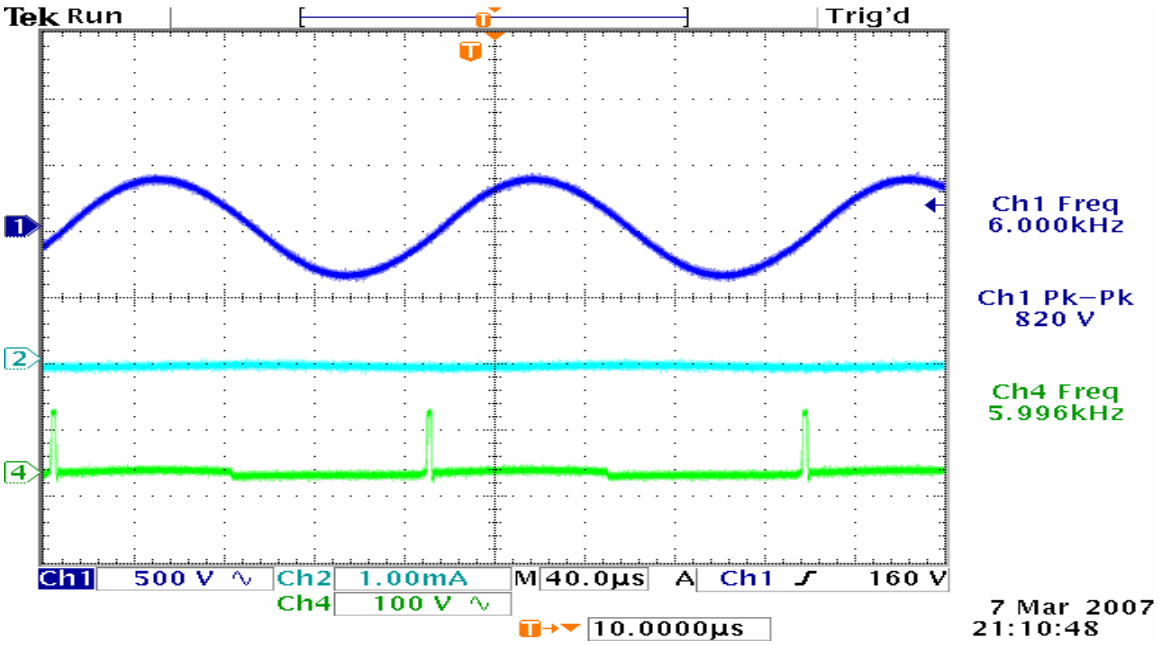

Figure B.6. Quartz Actuator, 140 mA input current, with Aux. Inductor, 6 kHz.
Ch1: output voltage (500 V/div), Ch2: transformer secondary current (1 mA/div),
Ch4: voltage across switch (100 V/div).

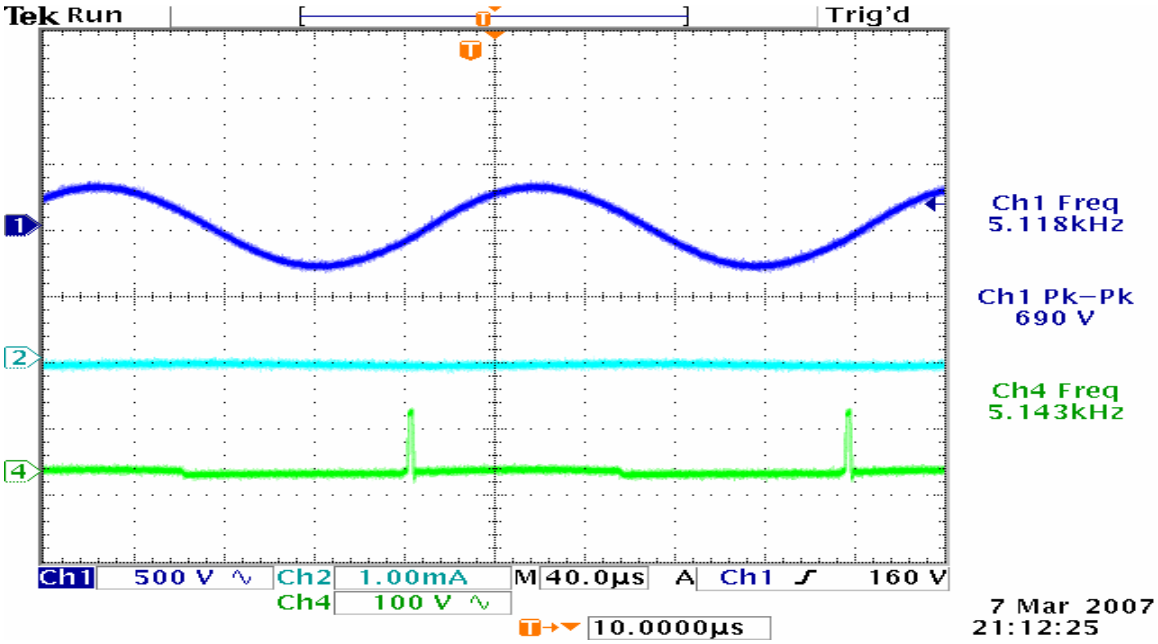

Figure B.7. Quartz Actuator, 140 mA input current, with Aux. Inductor, 5.1 kHz.
Ch1: output voltage (500 V/div), Ch2: transformer secondary current (1 mA/div),
Ch4: voltage across switch (100 V/div).

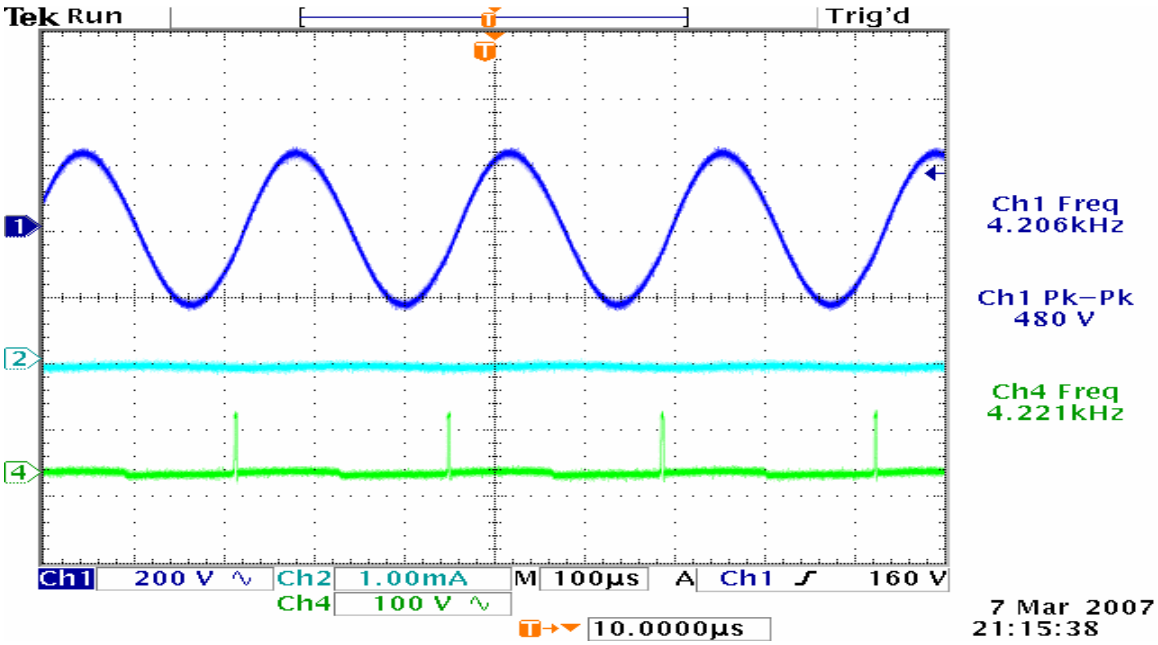

Figure B.8. Quartz Actuator, 140 mA input current, with Aux. Inductor, 4.2 kHz.
Ch1: output voltage (200 V/div), Ch2: transformer secondary current (1 mA/div),
Ch4: voltage across switch (100 V/div).

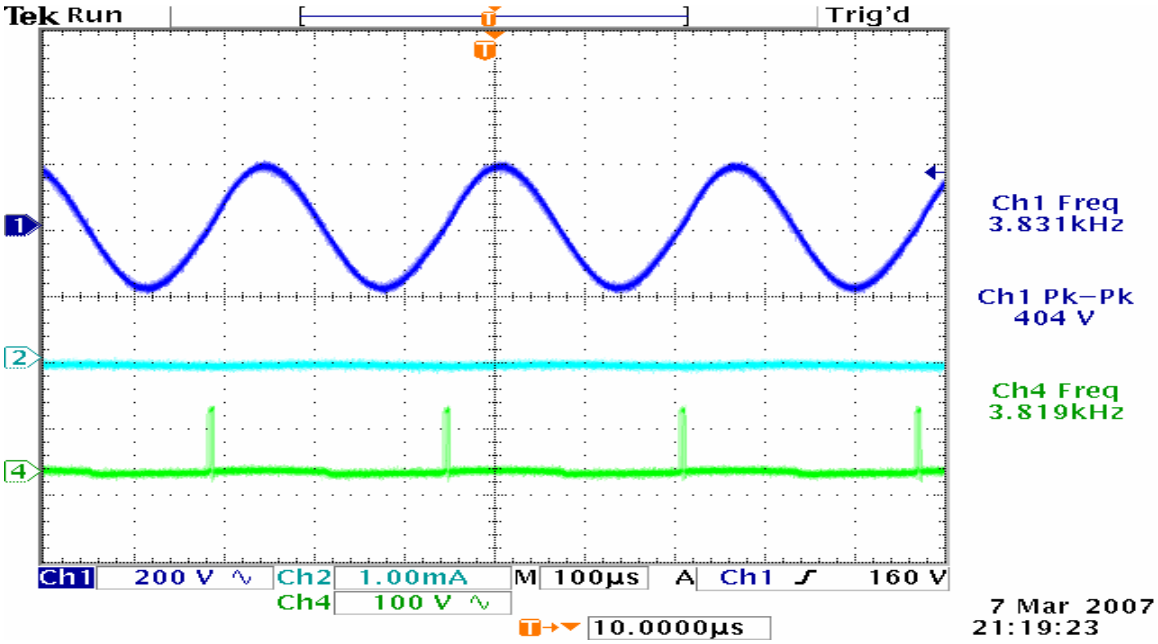

Figure B.9. Quartz Actuator, 140 mA input current, with Aux. Inductor, 3.8 kHz.
Ch1: output voltage (200 V/div), Ch2: transformer secondary current (1 mA/div),
Ch4: voltage across switch (100 V/div).

Appendix C: Low Power (140mA) Data: Panel Actuator, without Auxiliary Inductor

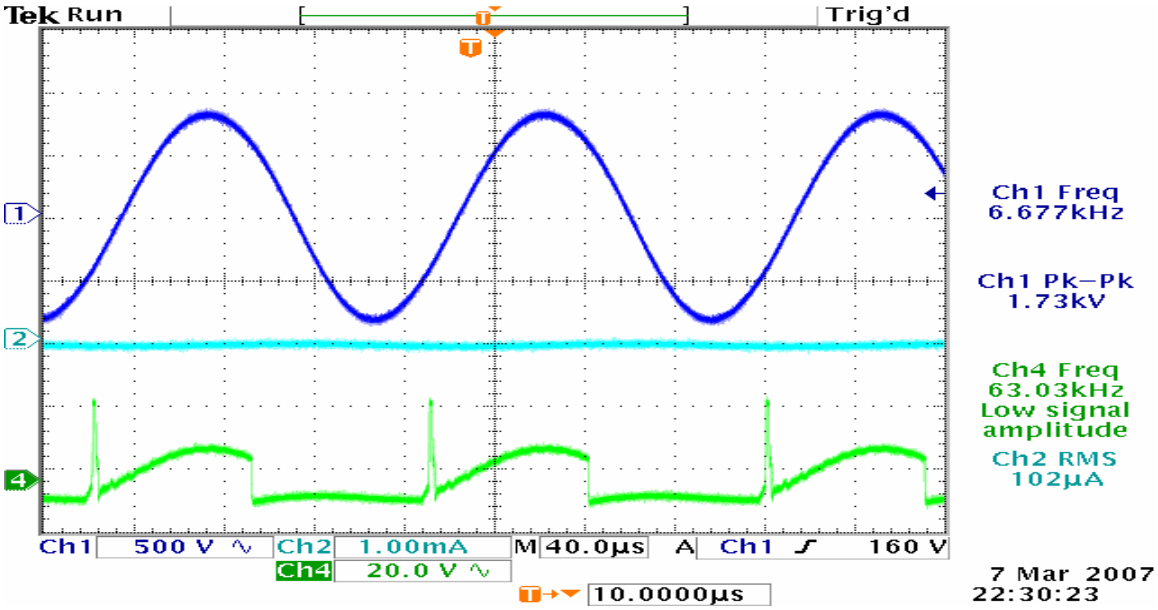

Figure C.1. Panel Actuator, 140 mA input current, w/out Aux. Inductor, 6.7 kHz. Ch1: output voltage (500 V/div), Ch2: transformer secondary current (1 mA/div), Ch4: voltage across switch (20 V/div).

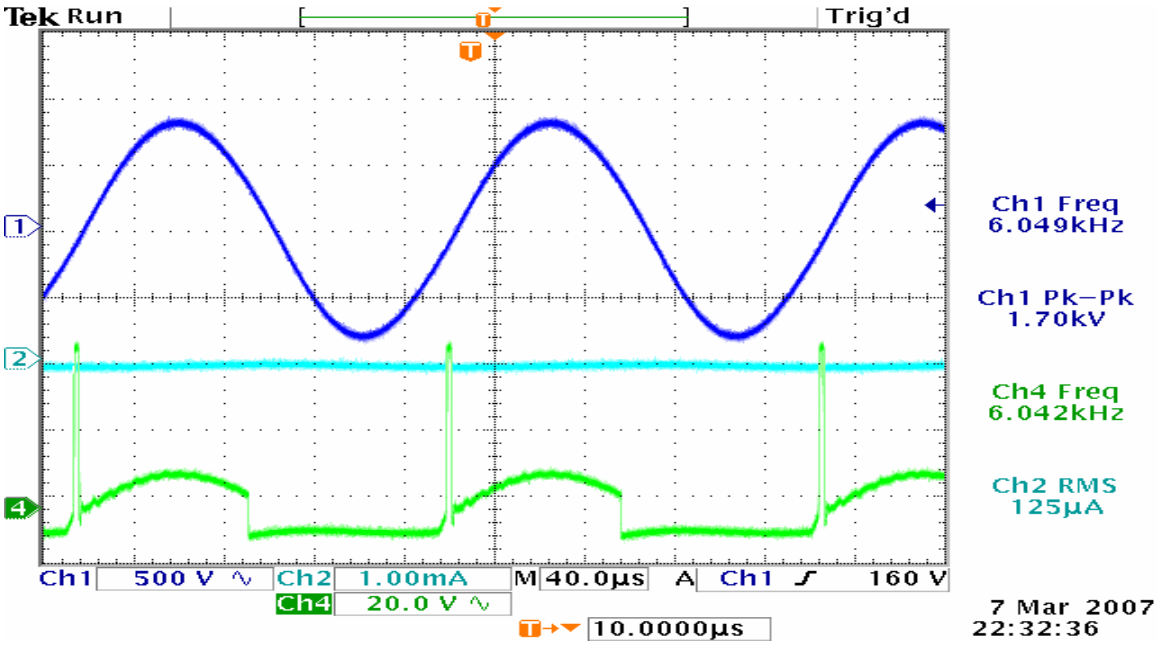

Figure C.2. Panel Actuator, 140 mA input current, w/out Aux. Inductor, 6 kHz.
Ch1: output voltage (500 V/div), Ch2: transformer secondary current (1 mA/div),
Ch4: voltage across switch (20 V/div).

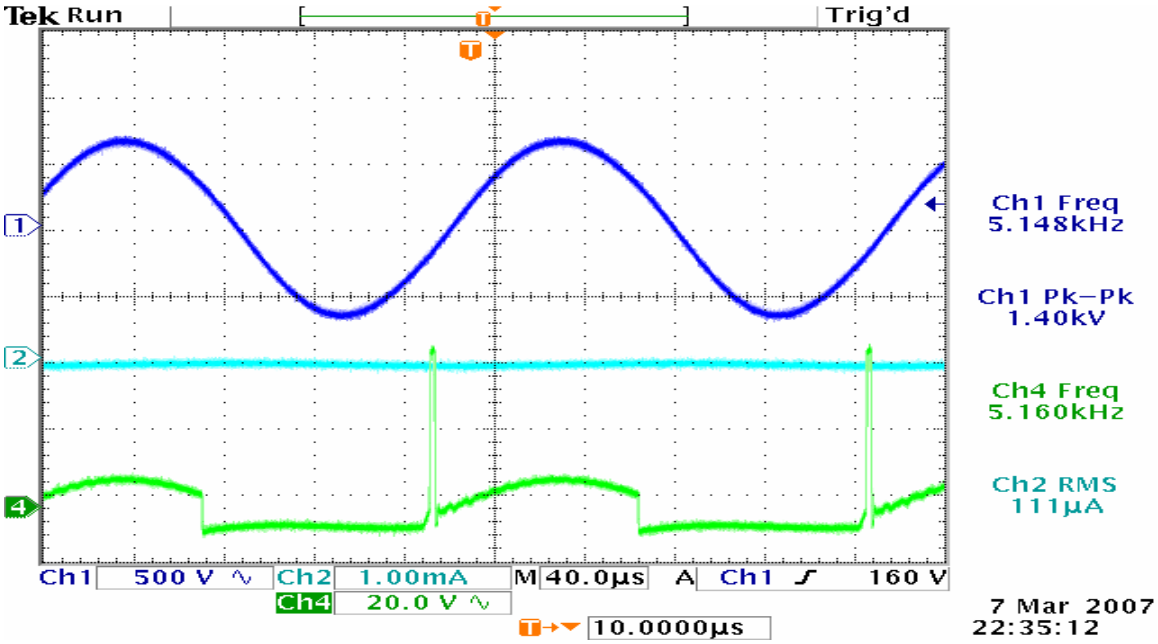

Figure C.3. Panel Actuator, 140 mA input current, w/out Aux. Inductor, 5.1 kHz.
Ch1: output voltage (500 V/div), Ch2: transformer secondary current (1 mA/div),
Ch4: voltage across switch (20 V/div).

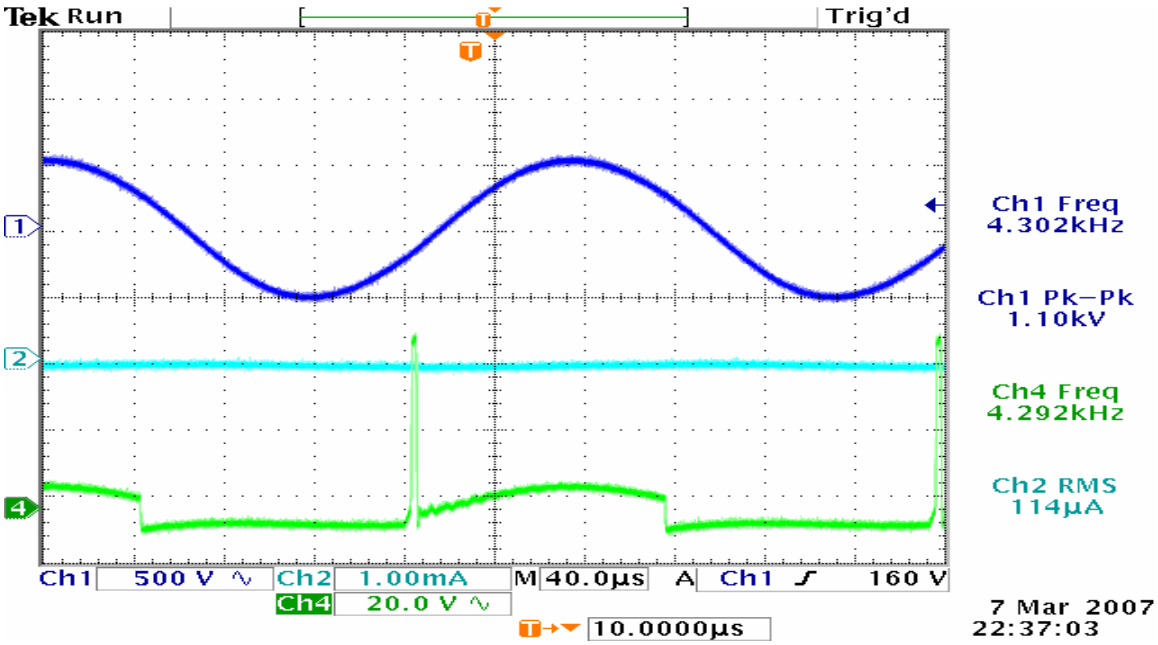

Figure C.4. Panel Actuator, 140 mA input current, w/out Aux. Inductor, 4.3 kHz.
Ch1: output voltage (500 V/div), Ch2: transformer secondary current (1 mA/div),
Ch4: voltage across switch (20 V/div).

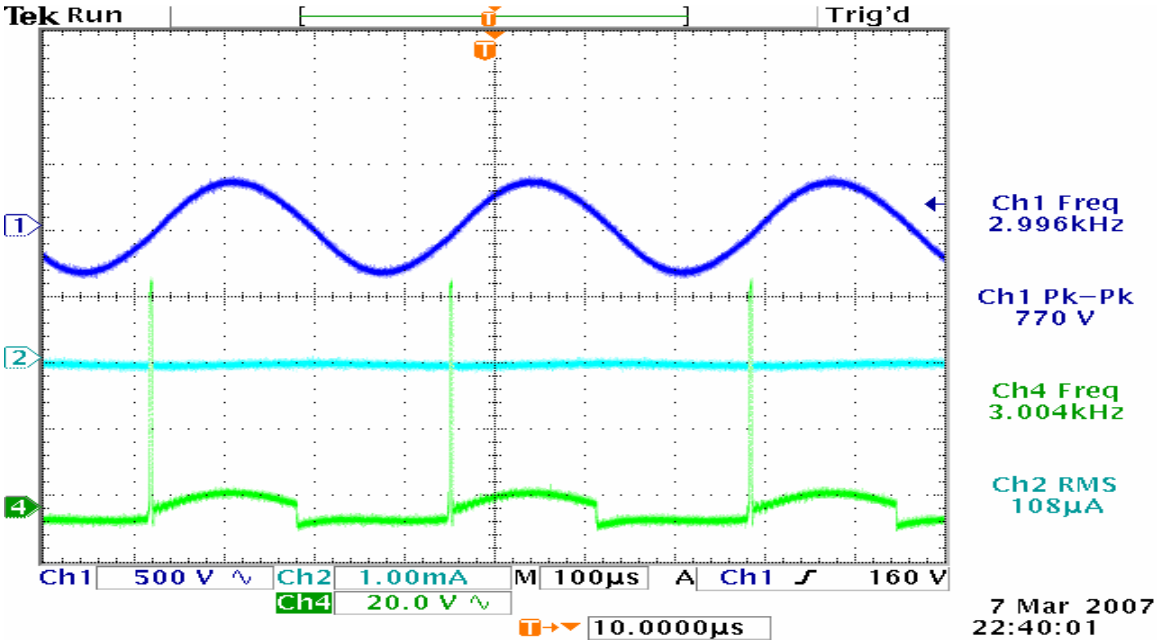

Figure C.5. Panel Actuator, 140 mA input current, w/out Aux. Inductor, 3 kHz.
Ch1: output voltage (500 V/div), Ch2: transformer secondary current (1 mA/div),
Ch4: voltage across switch (20 V/div).

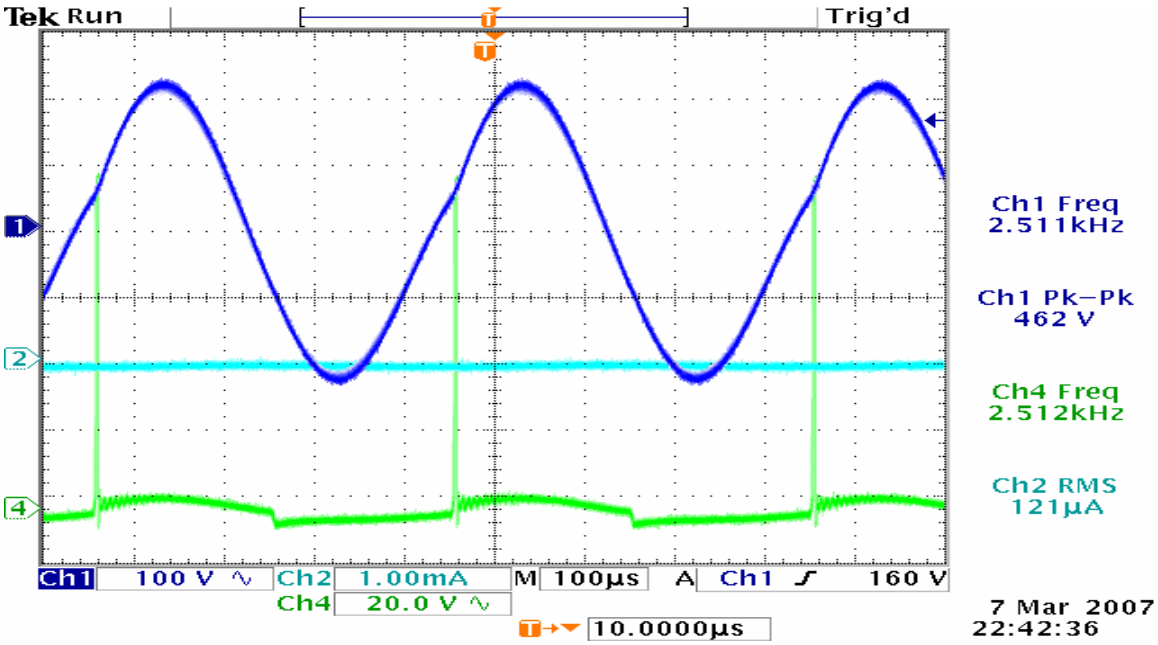

Figure C.6. Panel Actuator, 140 mA input current, w/out Aux. Inductor, 2.5 kHz. Ch1: output voltage (100 V/div), Ch2: transformer secondary current (1 mA/div), Ch4: voltage across switch (20 V/div).

Appendix D: Low Power (140mA) Data: Panel Actuator, with 2.15mH parallel primary Auxiliary Inductor

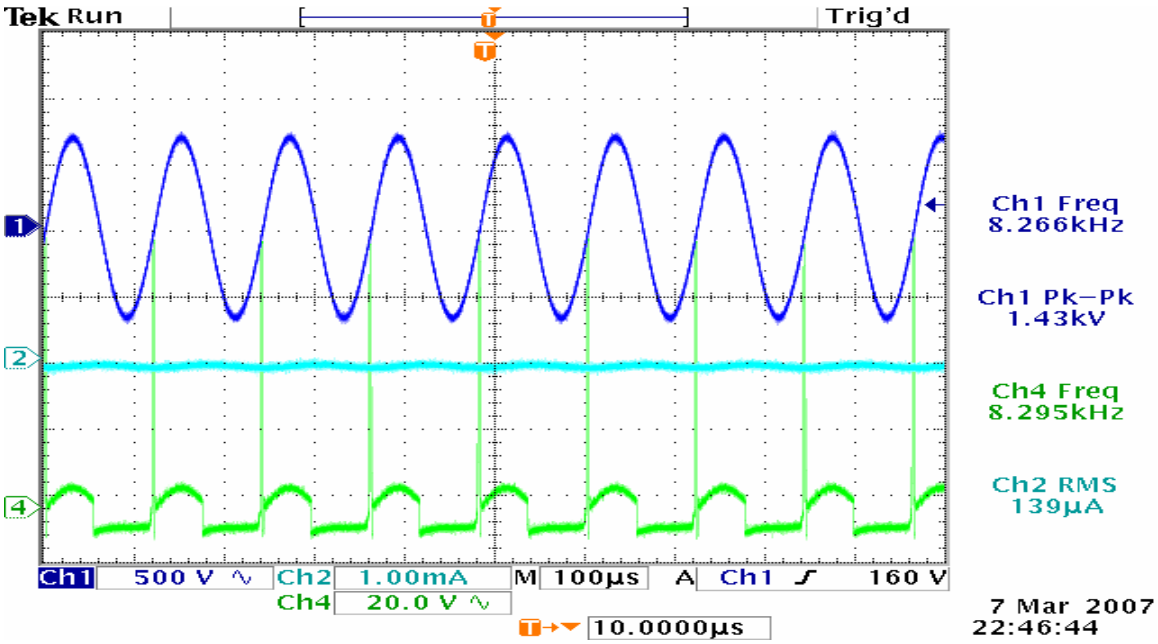

Figure D.1. Panel Actuator, 140 mA input current, with Aux. Inductor, 8.3 kHz.
Ch1: output voltage (500 V/div), Ch2: transformer secondary current (1 mA/div), Ch4: voltage across switch (20 V/div).

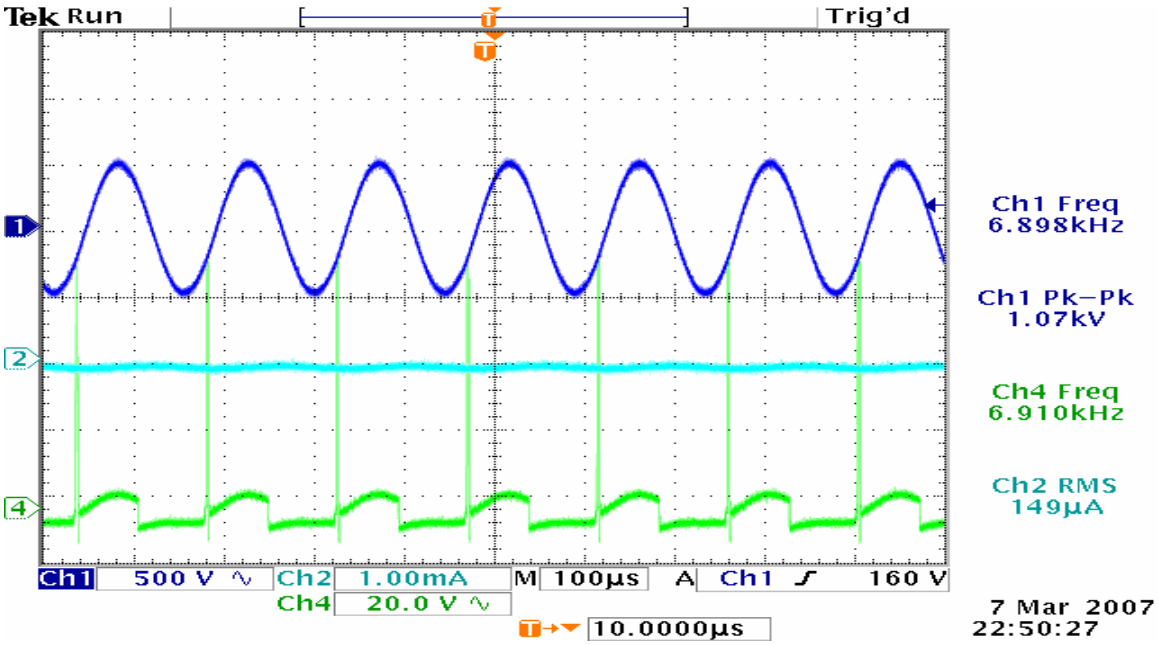

Figure D.2. Panel Actuator, 140 mA input current, with Aux. Inductor, 6.9 kHz.
Ch1: output voltage (500 V/div), Ch2: transformer secondary current (1 mA/div),
Ch4: voltage across switch (20 V/div).

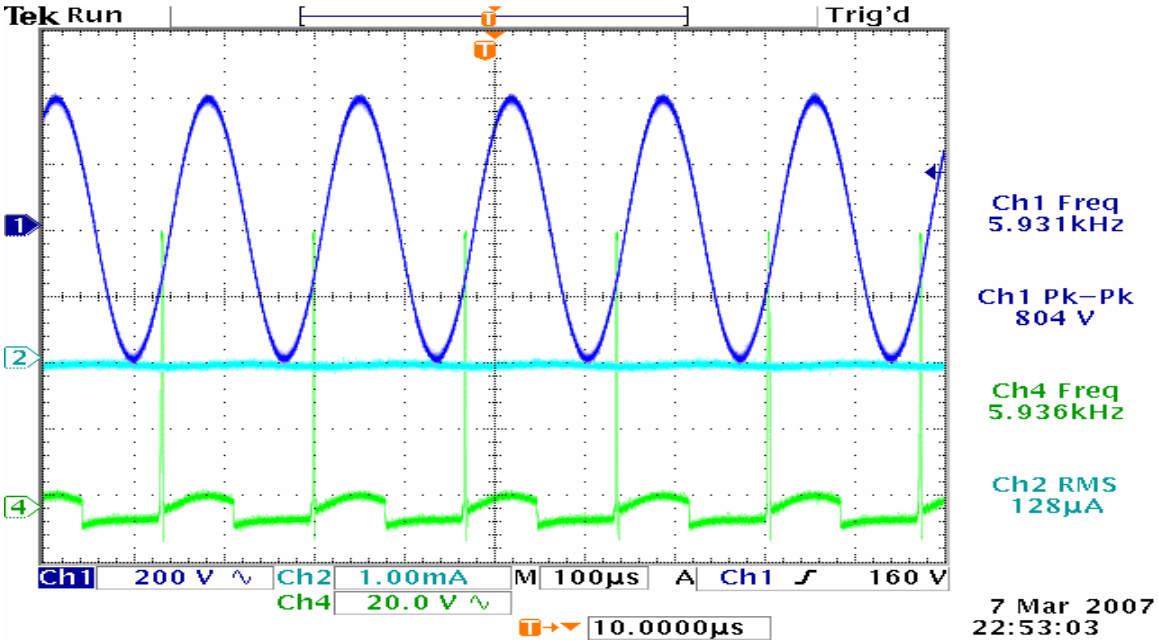

Figure D.3. Panel Actuator, 140 mA input current, with Aux. Inductor, 5.9 kHz.
Ch1: output voltage (200 V/div), Ch2: transformer secondary current (1 mA/div),
Ch4: voltage across switch (20 V/div).

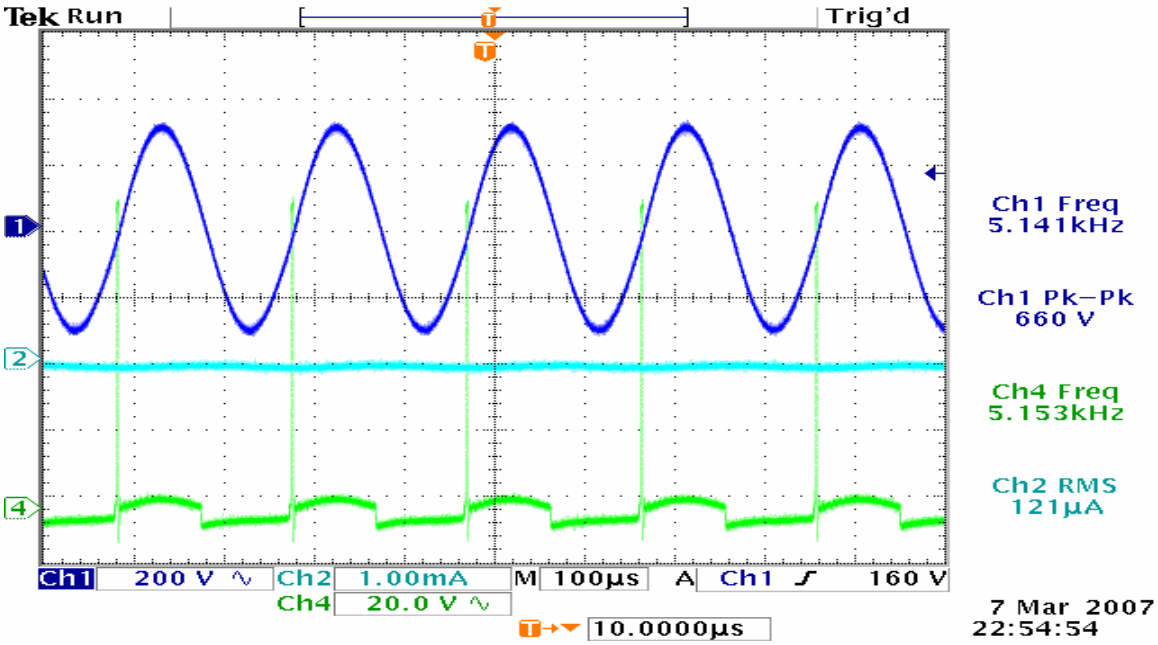

Figure D.4. Panel Actuator, 140 mA input current, with Aux. Inductor, 5.1 kHz.
Ch1: output voltage (200 V/div), Ch2: transformer secondary current (1 mA/div),
Ch4: voltage across switch (20 V/div).

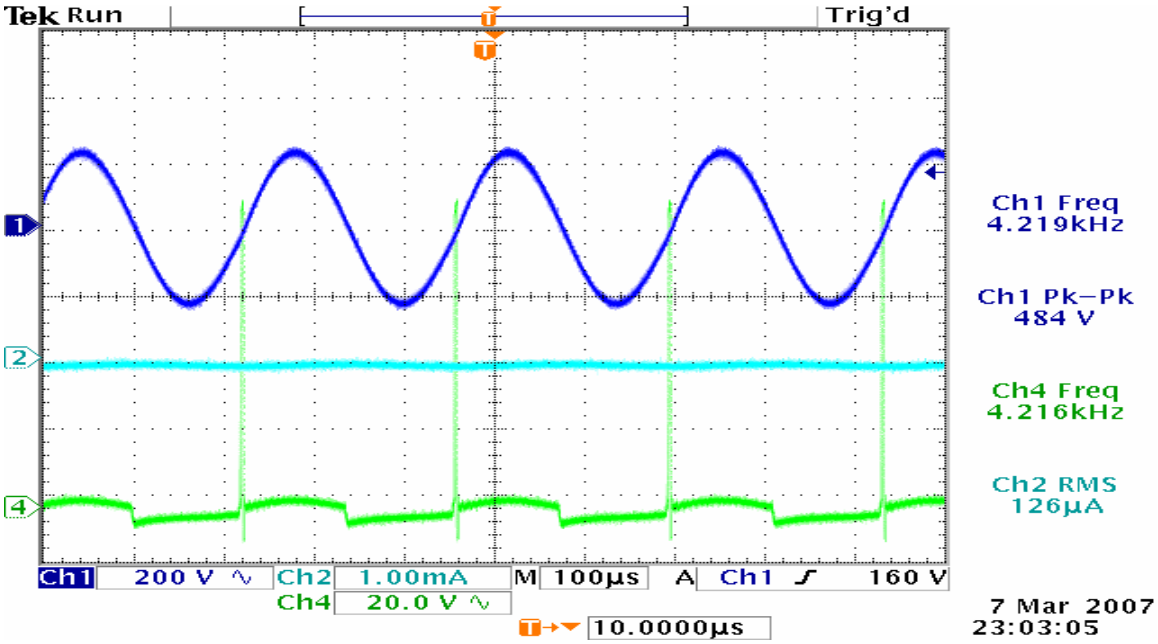

Figure D.5. Panel Actuator, 140 mA input current, with Aux. Inductor, 4.2 kHz.
Ch1: output voltage (200 V/div), Ch2: transformer secondary current (1 mA/div),
Ch4: voltage across switch (20 V/div).

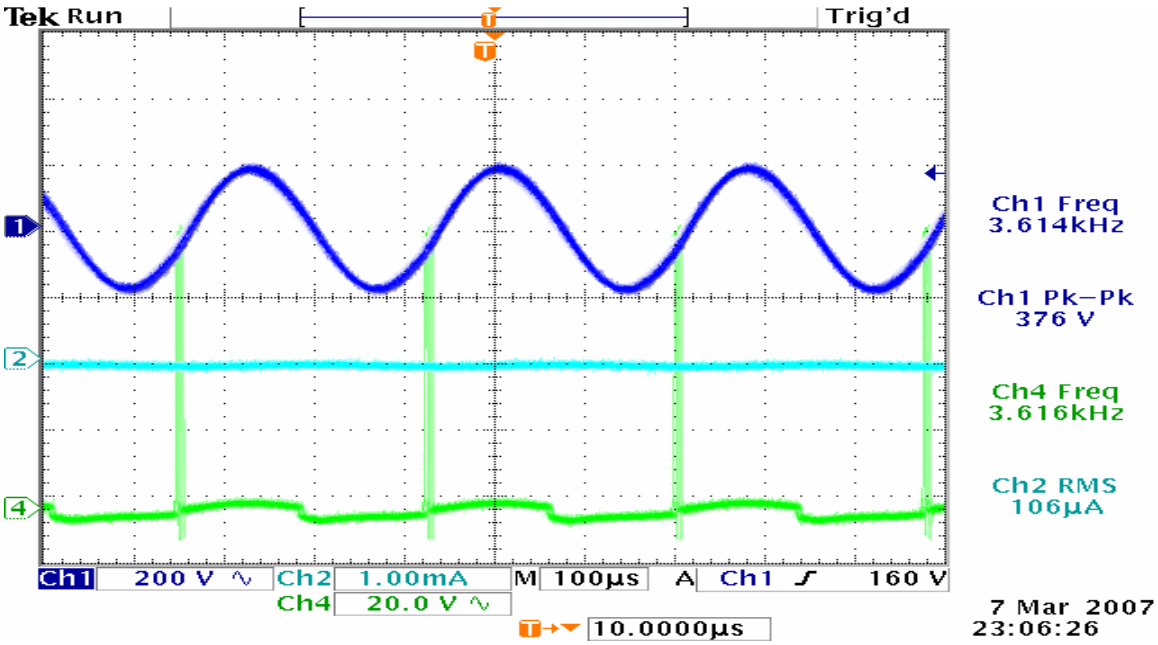

Figure D.6. Panel Actuator, 140 mA input current, with Aux. Inductor, 3.6 kHz.
Ch1: output voltage (200 V/div), Ch2: transformer secondary current (1 mA/div), Ch4: voltage across switch (20 V/div).

Appendix E: Low Power (400mA) Data: Quartz Actuator, without Auxiliary Inductor

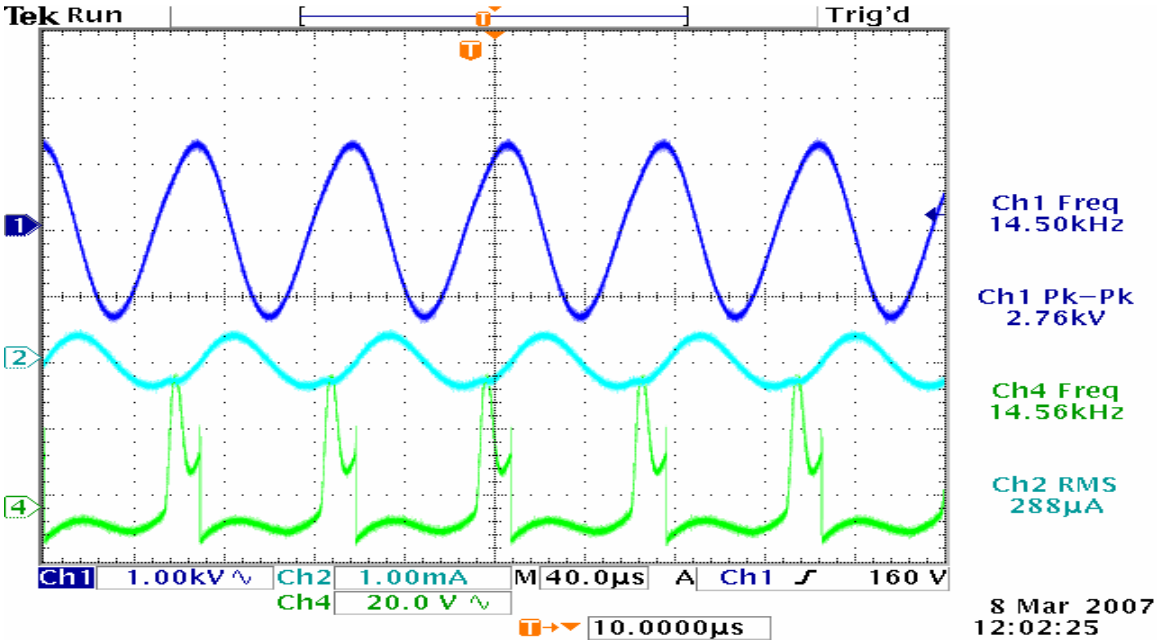

Figure E.1. Quartz Actuator, 400 mA input current, w/out Aux. Inductor, 14.5 kHz. Ch1: output voltage (1 kV/div), Ch2: transformer primary current (1 mA/div), Ch4: voltage across switch (20 V/div).

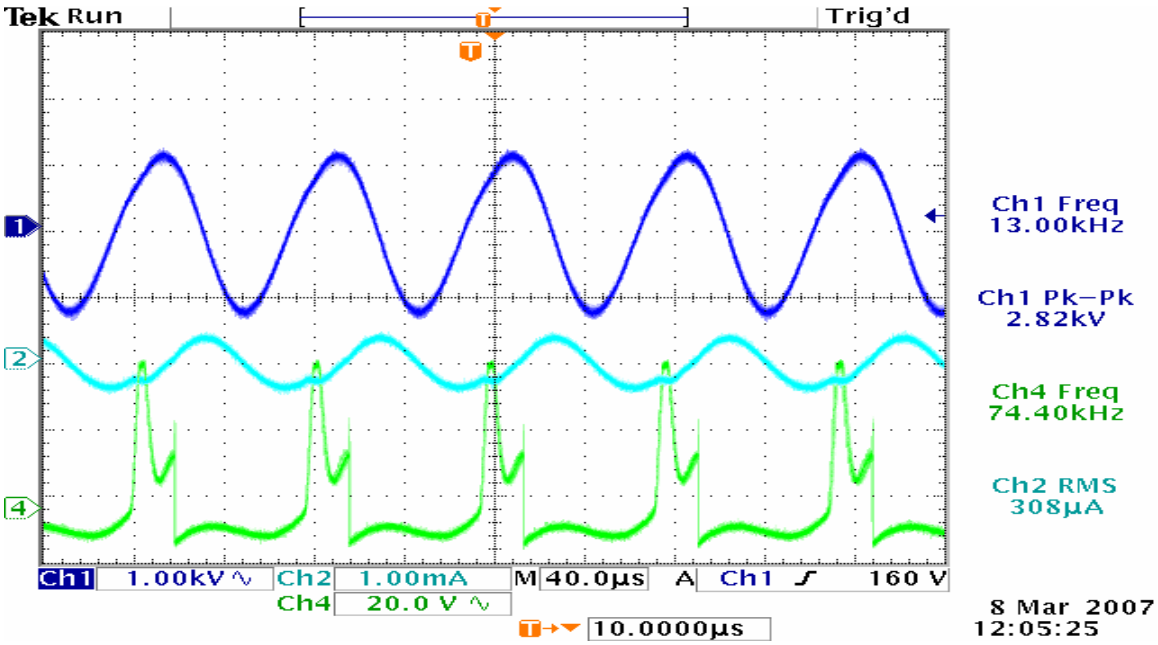

Figure E.2. Quartz Actuator, 400 mA input current, w/out Aux. Inductor, 13 kHz.
Ch1: output voltage (1 kV/div), Ch2: transformer primary current (1 mA/div),
Ch4: voltage across switch (20 V/div).

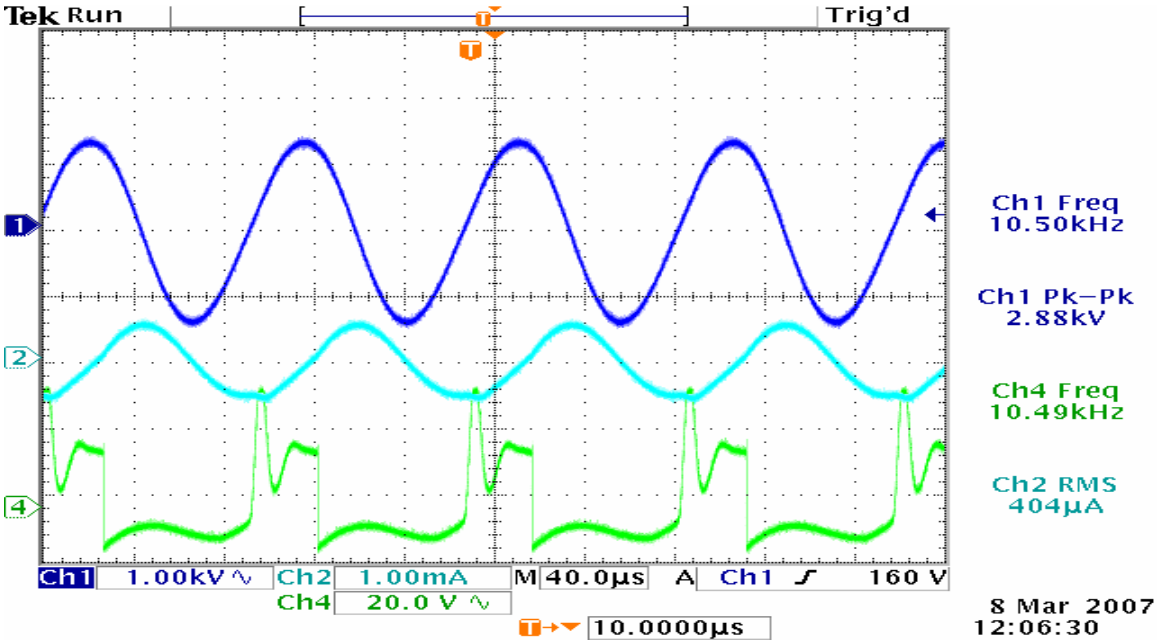

Figure E.3. Quartz Actuator, 400 mA input current, w/out Aux. Inductor, 10.5 kHz.
Ch1: output voltage (1 kV/div), Ch2: transformer primary current (1 mA/div),
Ch4: voltage across switch (20 V/div).

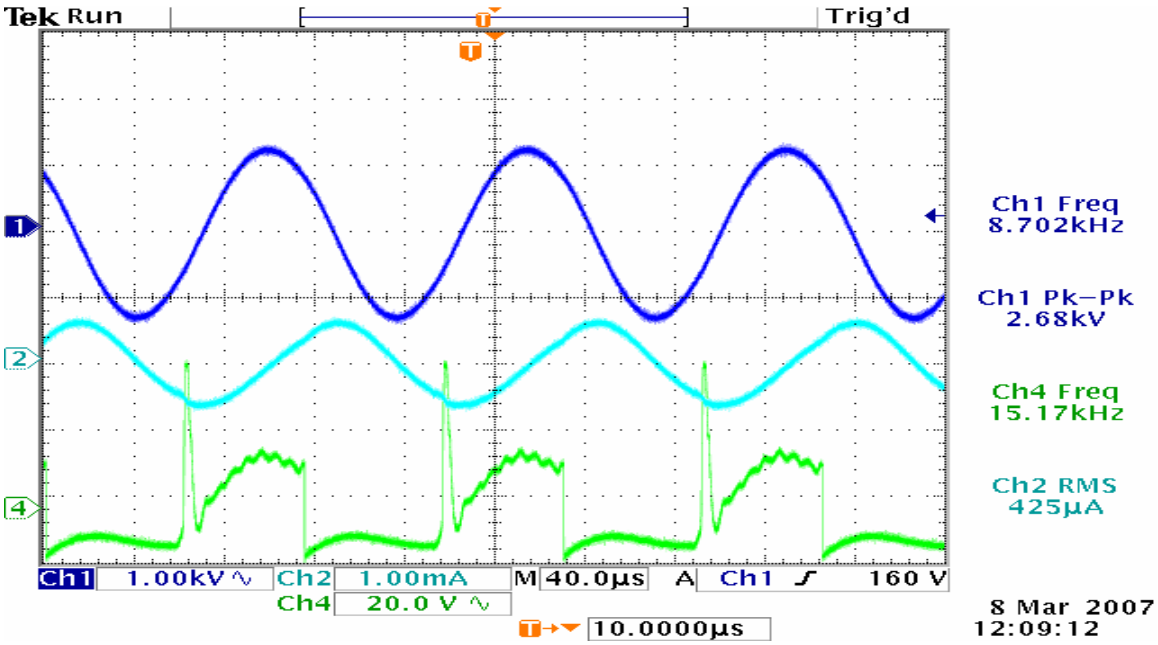

Figure E.4. Quartz Actuator, 400 mA input current, w/out Aux. Inductor, 8.7 kHz.
Ch1: output voltage (1 kV/div), Ch2: transformer primary current (1 mA/div),
Ch4: voltage across switch (20 V/div).

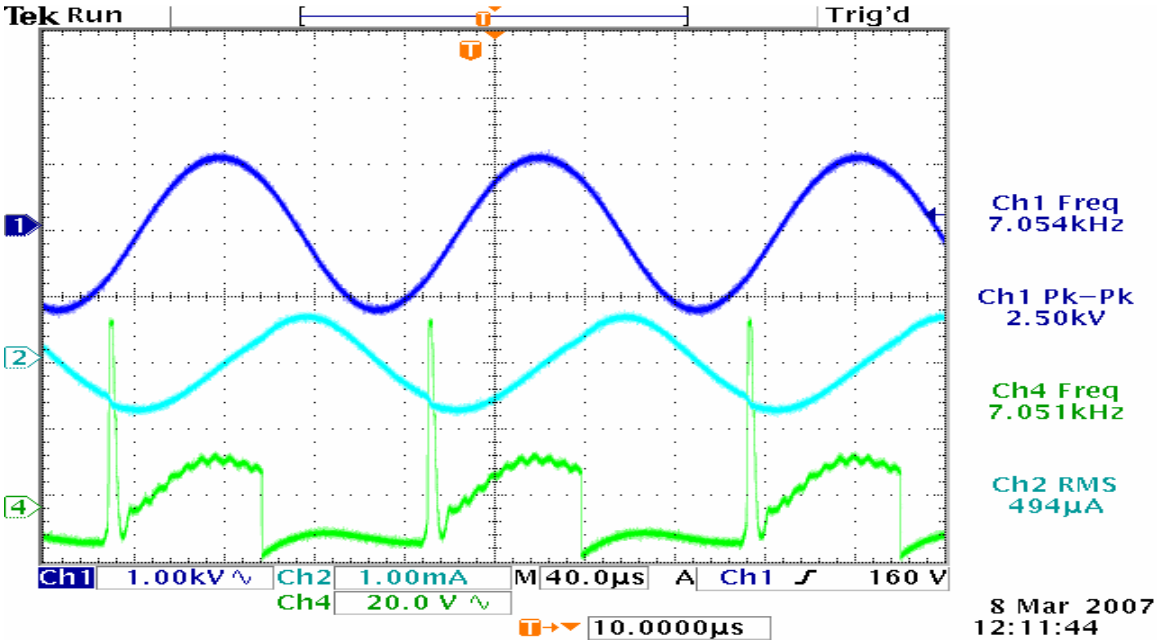

Figure E.5. Quartz Actuator, 400 mA input current, w/out Aux. Inductor, 7.1 kHz.
Ch1: output voltage (1 kV/div), Ch2: transformer primary current (1 mA/div),
Ch4: voltage across switch (20 V/div).

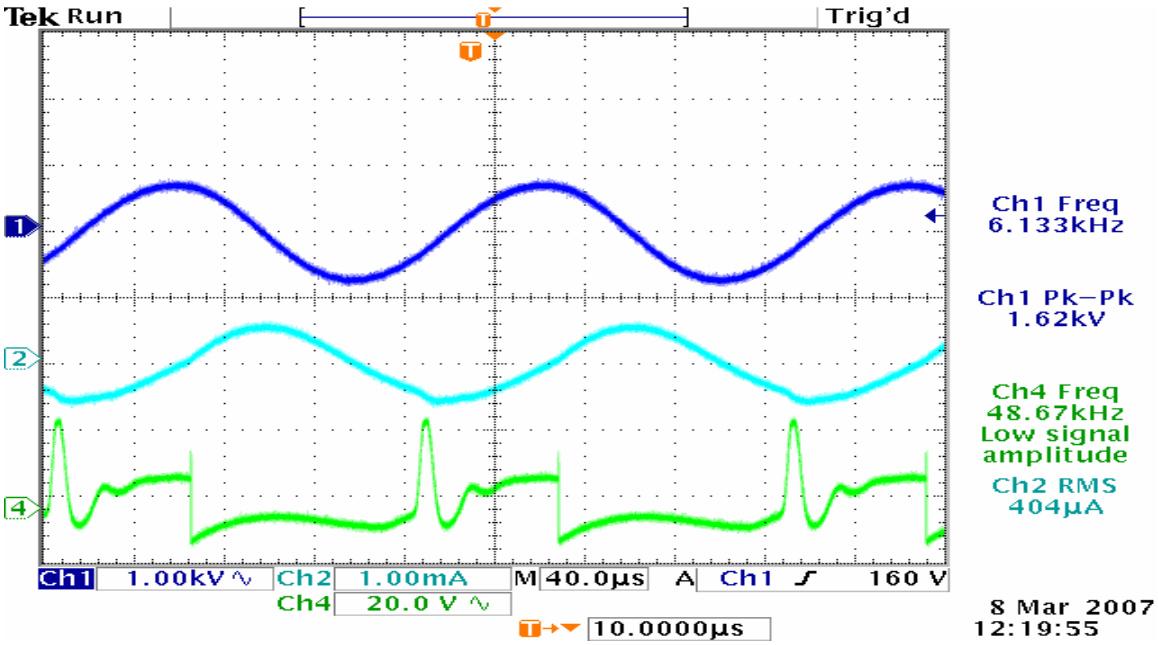

Figure E.6. Quartz Actuator, 400 mA input current, w/out Aux. Inductor, 6.1 kHz.
Ch1: output voltage (1 kV/div), Ch2: transformer primary current (1 mA/div),
Ch4: voltage across switch (20 V/div).

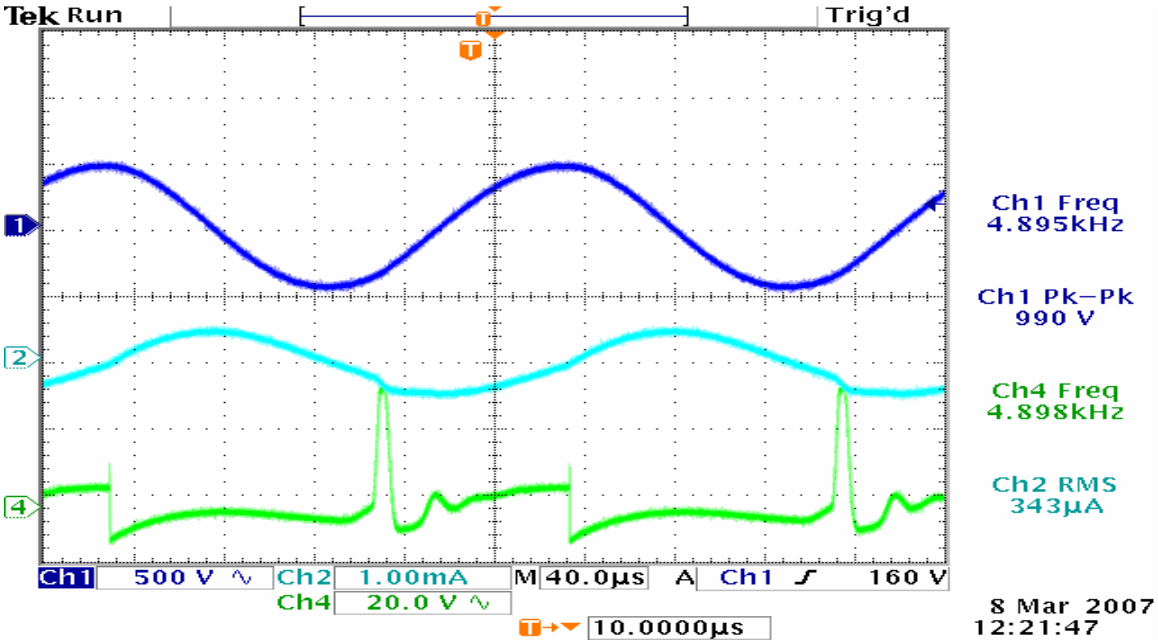

Figure E.7. Quartz Actuator, 400 mA input current, w/out Aux. Inductor, 4.9 kHz.
Ch1: output voltage (500 V/div), Ch2: transformer primary current (1 mA/div),
Ch4: voltage across switch (20 V/div).

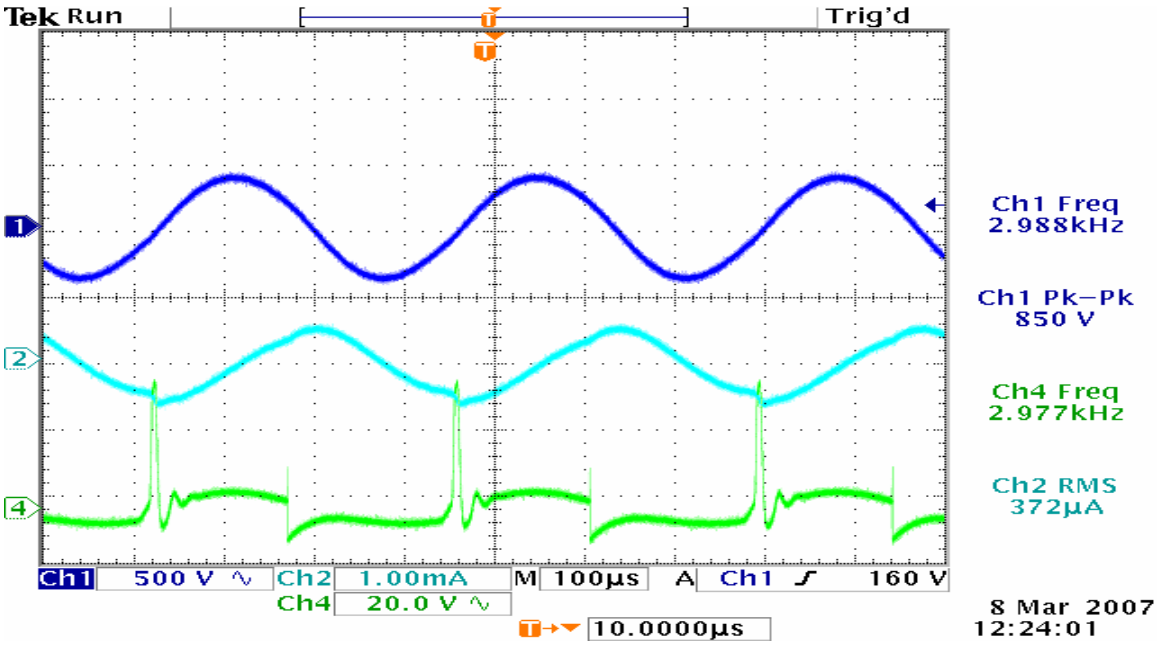

Figure E.8. Quartz Actuator, 400 mA input current, w/out Aux. Inductor, 3 kHz.
Ch1: output voltage (500 V/div), Ch2: transformer primary current (1 mA/div),
Ch4: voltage across switch (20 V/div).

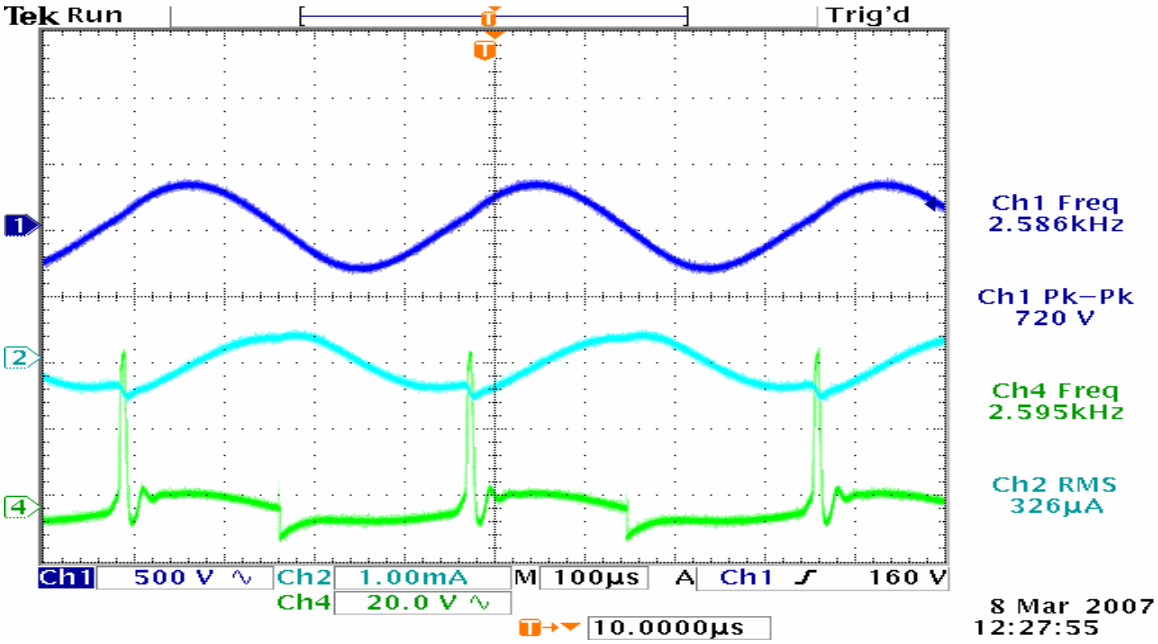

Figure E.9. Quartz Actuator, 400 mA input current, w/out Aux. Inductor, 2.6 kHz.
Ch1: output voltage (500 V/div), Ch2: transformer primary current (1 mA/div),
Ch4: voltage across switch (20 V/div).

Appendix F: Low Power (400mA) Data: Quartz Actuator, with 2.15mH parallel primary Auxiliary Inductor

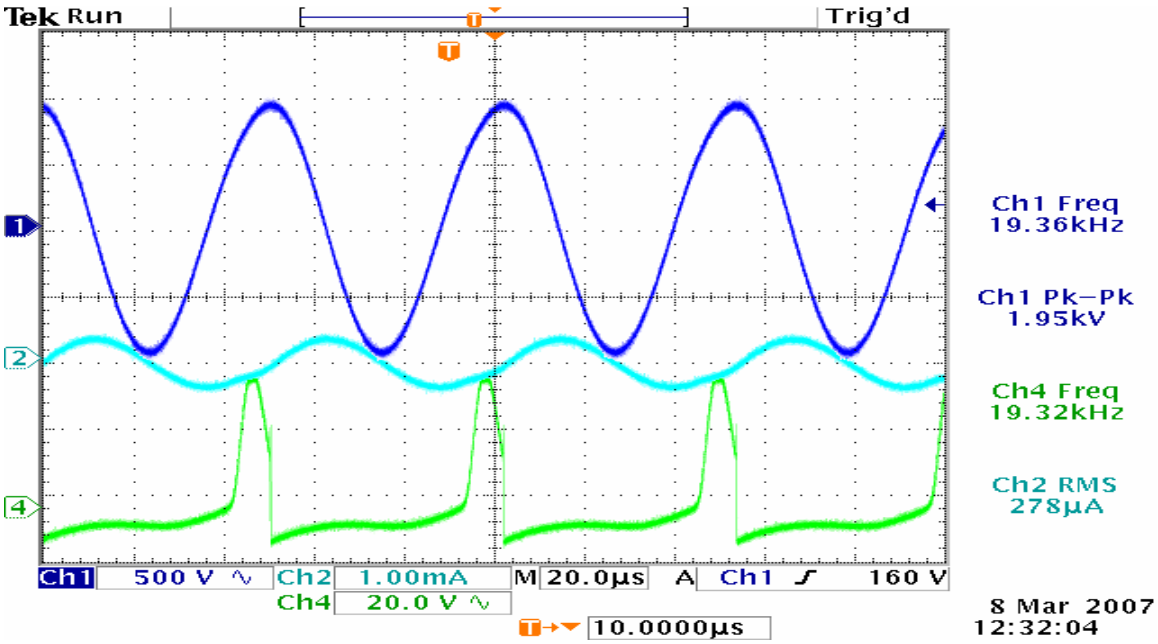

Figure F.1. Quartz Actuator, 400 mA input current, with Aux. Inductor, 19.4 kHz.
Ch1: output voltage (500 V/div), Ch2: transformer primary current (1 mA/div),
Ch4: voltage across switch (20 V/div).

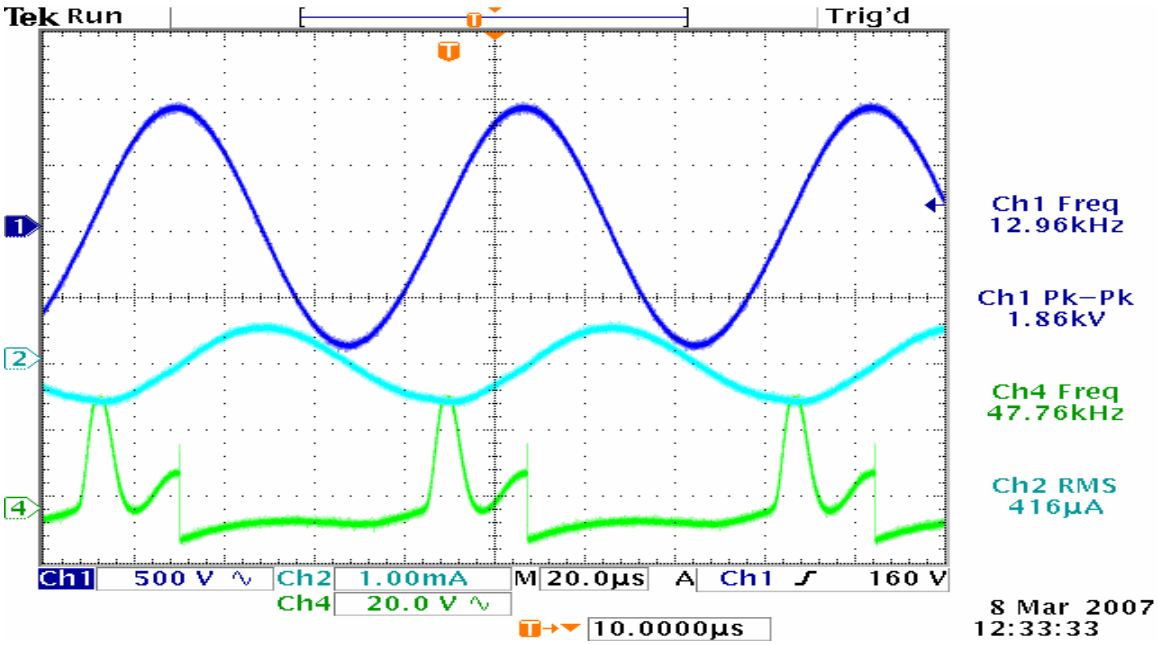

Figure F.2. Quartz Actuator, 400 mA input current, with Aux. Inductor, 13 kHz.
Ch1: output voltage (500 V/div), Ch2: transformer primary current (1 mA/div),
Ch4: voltage across switch (20 V/div).

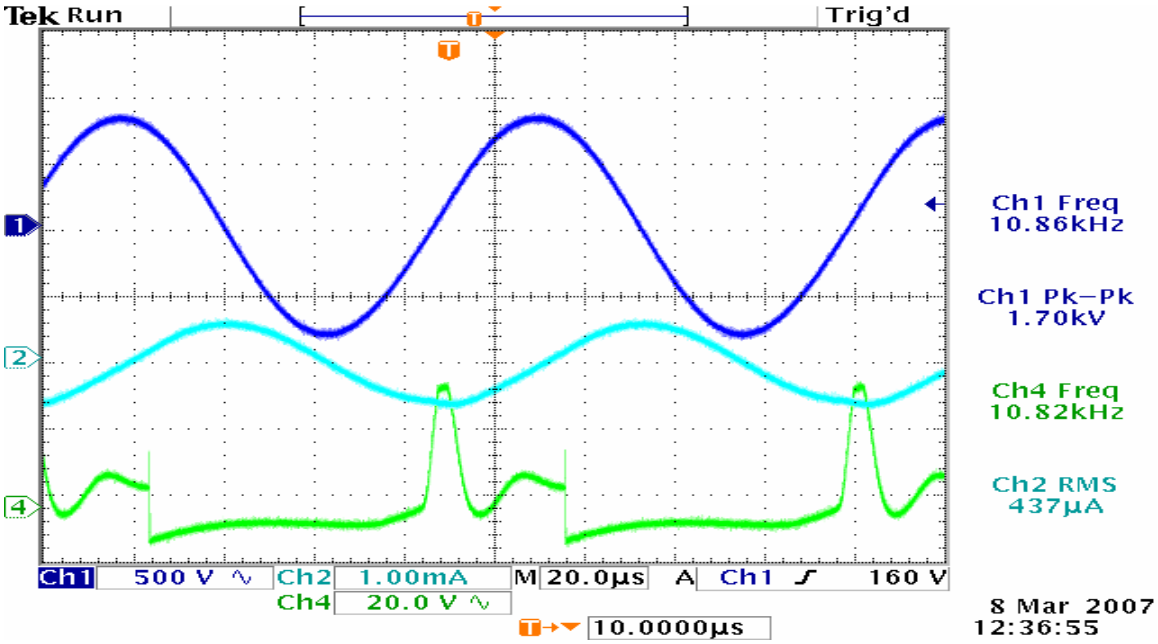

Figure F.3. Quartz Actuator, 400 mA input current, with Aux. Inductor, 10.9 kHz.
Ch1: output voltage (500 V/div), Ch2: transformer primary current (1 mA/div),
Ch4: voltage across switch (20 V/div).

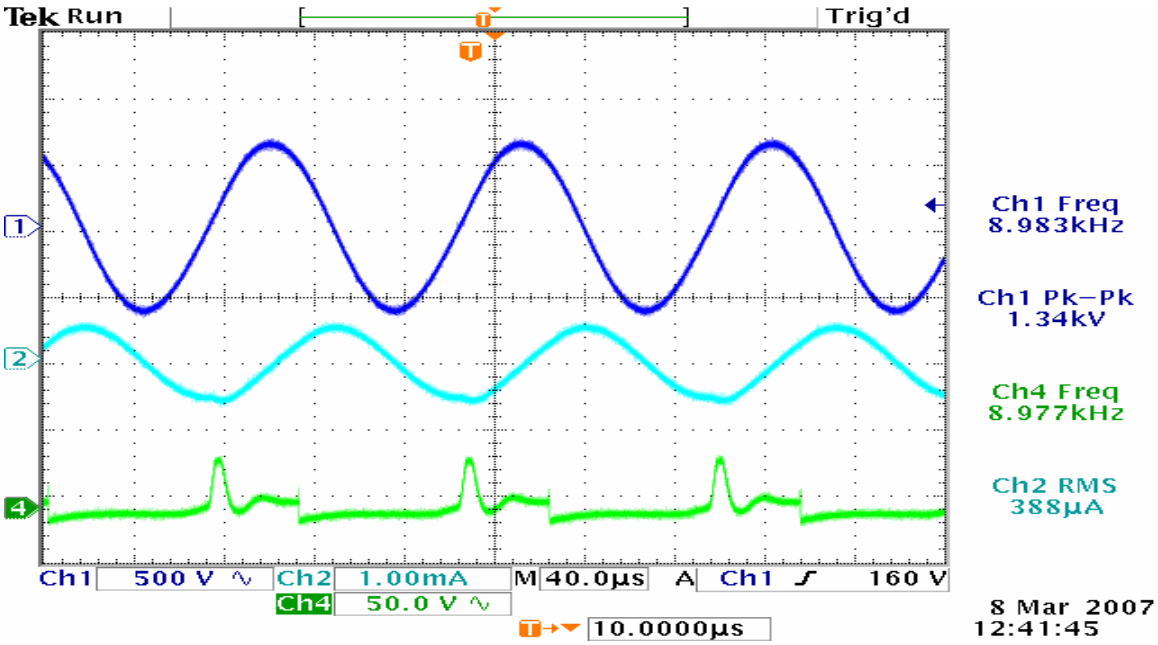

Figure F.4. Quartz Actuator, 400 mA input current, with Aux. Inductor, 9 kHz.
Ch1: output voltage (500 V/div), Ch2: transformer primary current (1 mA/div),
Ch4: voltage across switch (50 V/div).

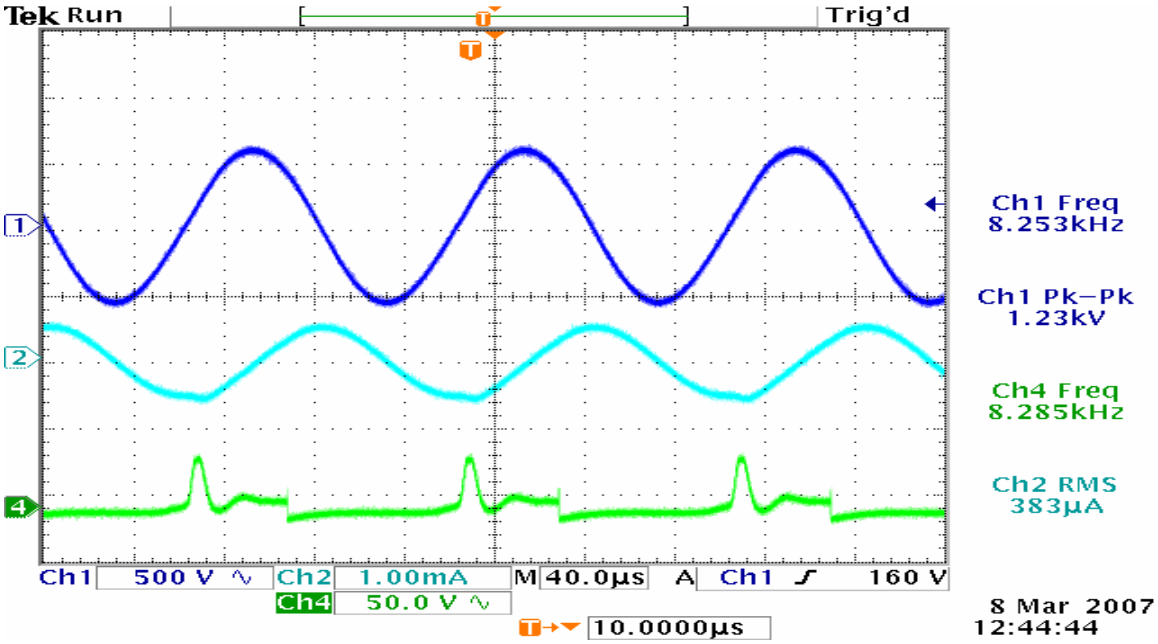

Figure F.5. Quartz Actuator, 400 mA input current, with Aux. Inductor, 8.3 kHz.
Ch1: output voltage (500 V/div), Ch2: transformer primary current (1 mA/div),
Ch4: voltage across switch (50 V/div).

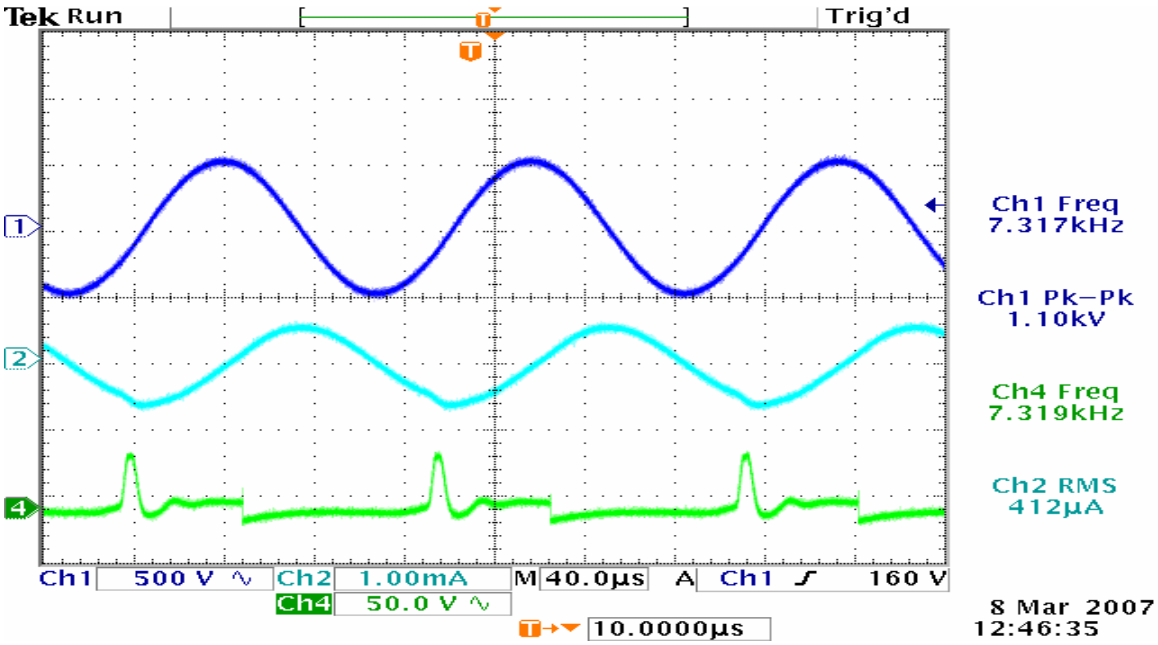

Figure F.6. Quartz Actuator, 400 mA input current, with Aux. Inductor, 7.3 kHz.
Ch1: output voltage (500 V/div), Ch2: transformer primary current (1 mA/div),
Ch4: voltage across switch (50 V/div).

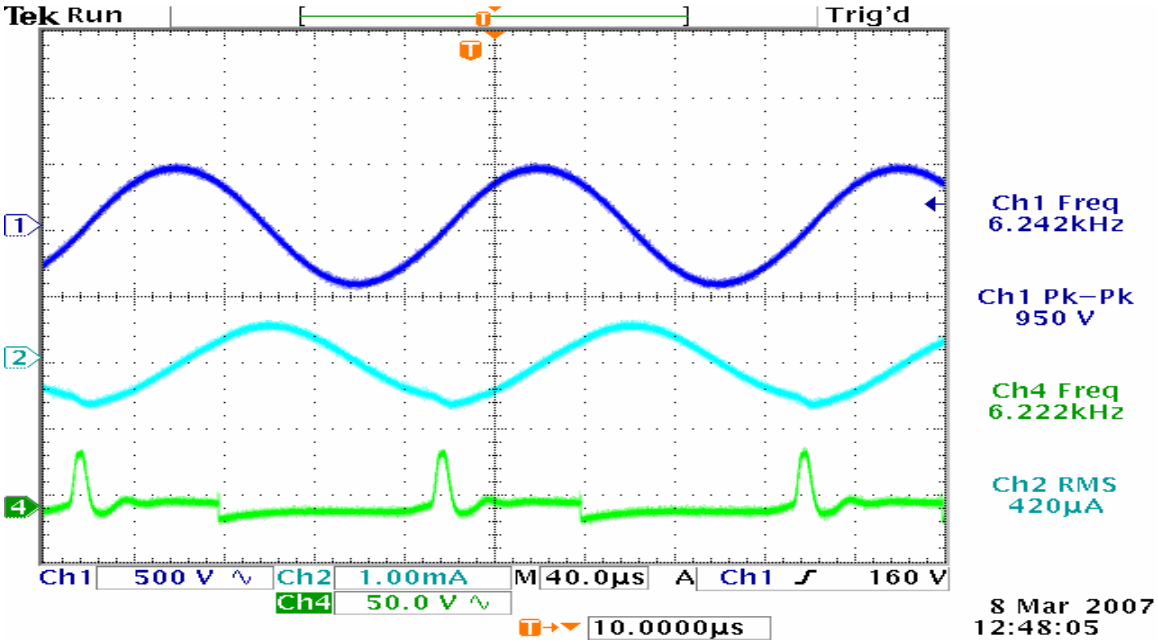

Figure F.7. Quartz Actuator, 400 mA input current, with Aux. Inductor, 6.2 kHz.
Ch1: output voltage (500 V/div), Ch2: transformer primary current (1 mA/div),
Ch4: voltage across switch (50 V/div).

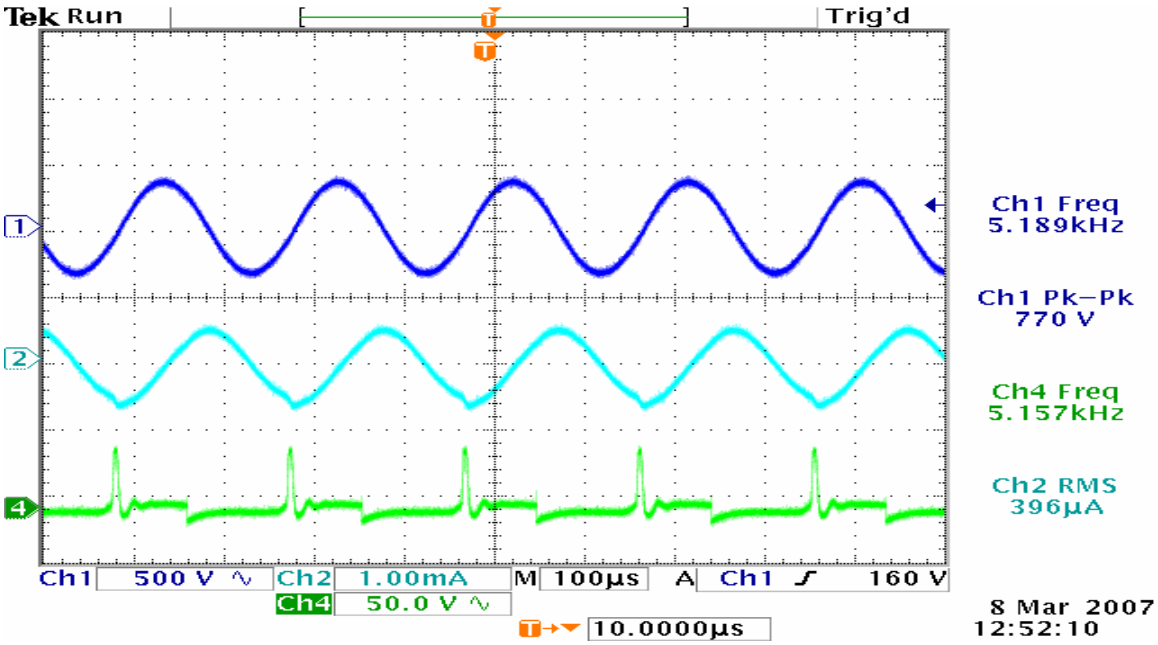

Figure F.8. Quartz Actuator, 400 mA input current, with Aux. Inductor, 5.2 kHz.
Ch1: output voltage (500 V/div), Ch2: transformer primary current (1 mA/div),
Ch4: voltage across switch (50 V/div).

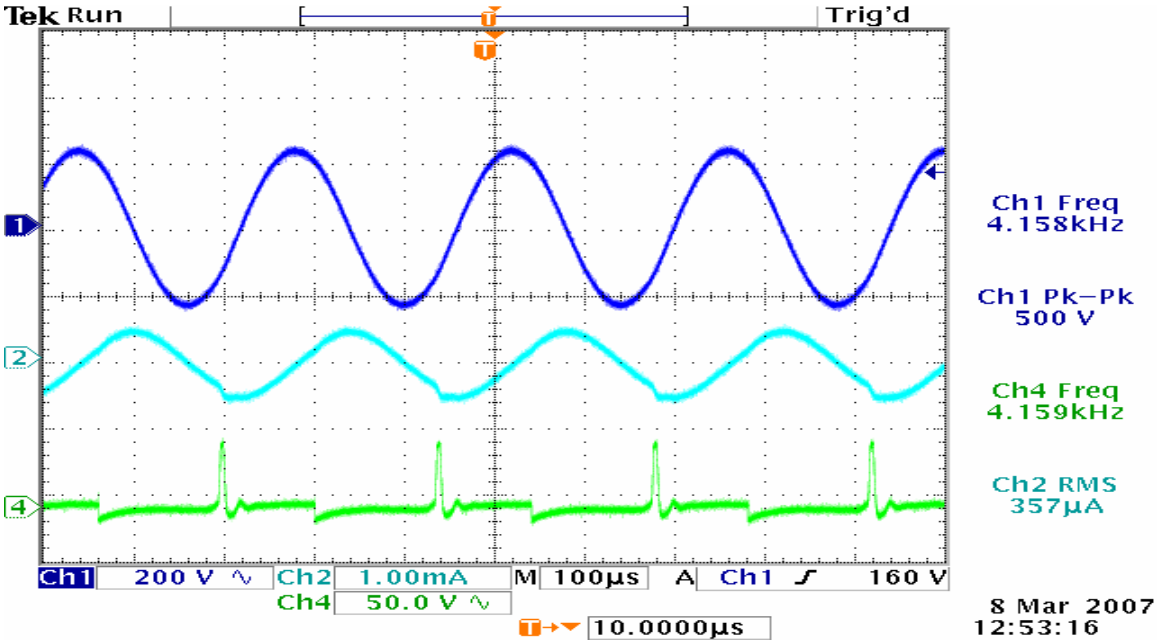

Figure F.9. Quartz Actuator, 400 mA input current, with Aux. Inductor, 4.2 kHz.
Ch1: output voltage (200 V/div), Ch2: transformer primary current (1 mA/div),
Ch4: voltage across switch (50 V/div).

Appendix G: Low Power (400mA) Data: Panel Actuator, without Auxiliary Inductor

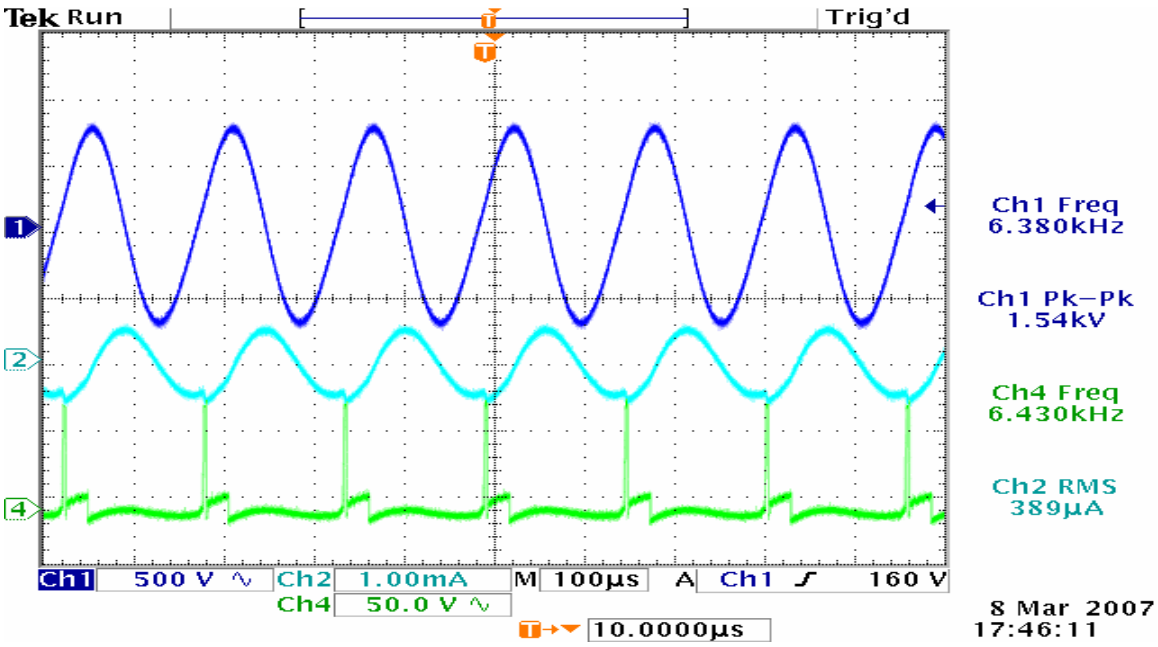

Figure G.1. Panel Actuator, 400 mA input current, w/out Aux. Inductor, 6.4 kHz.
Ch1: output voltage (500 V/div), Ch2: transformer primary current (1 mA/div),
Ch4: voltage across switch (50 V/div).

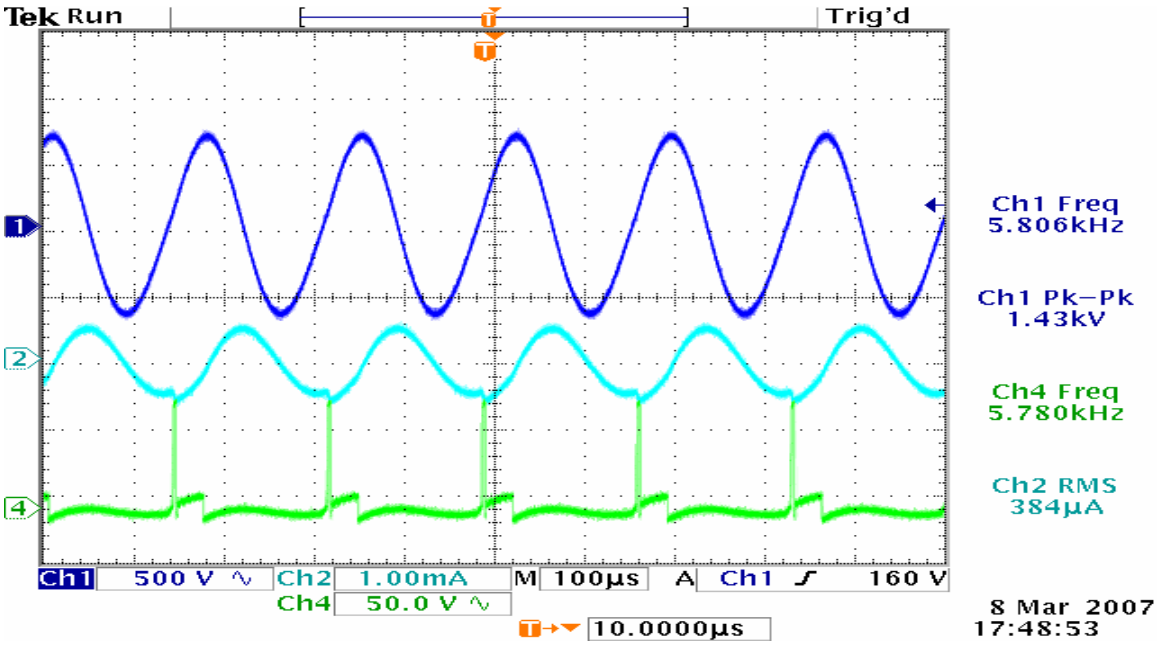

Figure G.2. Panel Actuator, 400 mA input current, w/out Aux. Inductor, 5.8 kHz.
Ch1: output voltage (500 V/div), Ch2: transformer primary current (1 mA/div),
Ch4: voltage across switch (50 V/div).

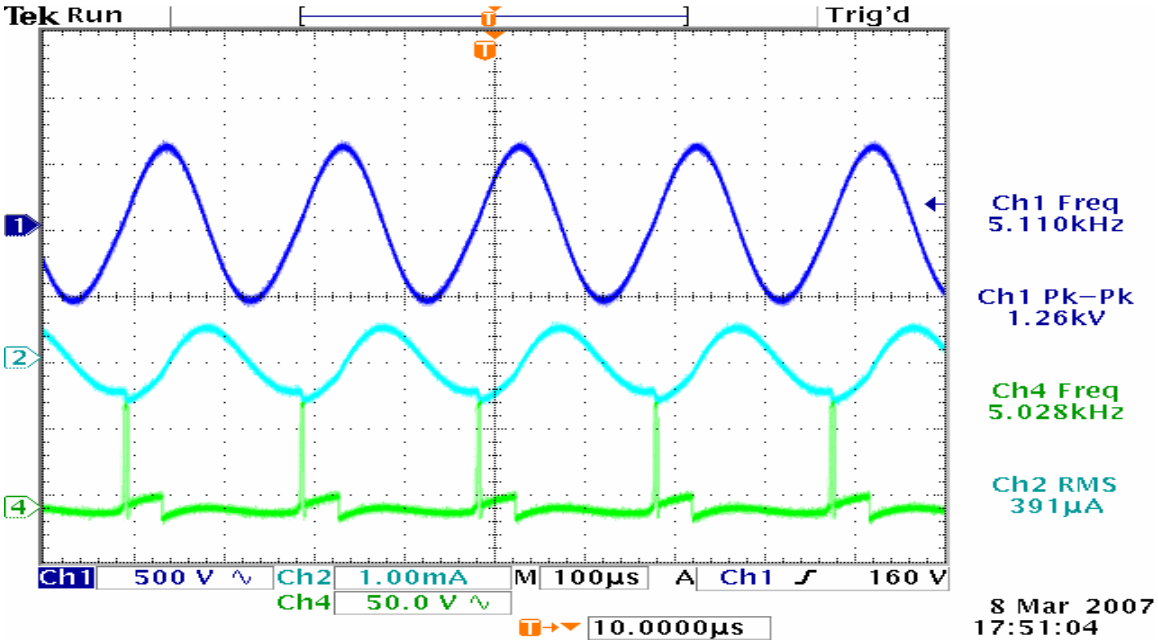

Figure G.3. Panel Actuator, 400 mA input current, w/out Aux. Inductor, 5.1 kHz.
Ch1: output voltage (500 V/div), Ch2: transformer primary current (1 mA/div),
Ch4: voltage across switch (50 V/div).

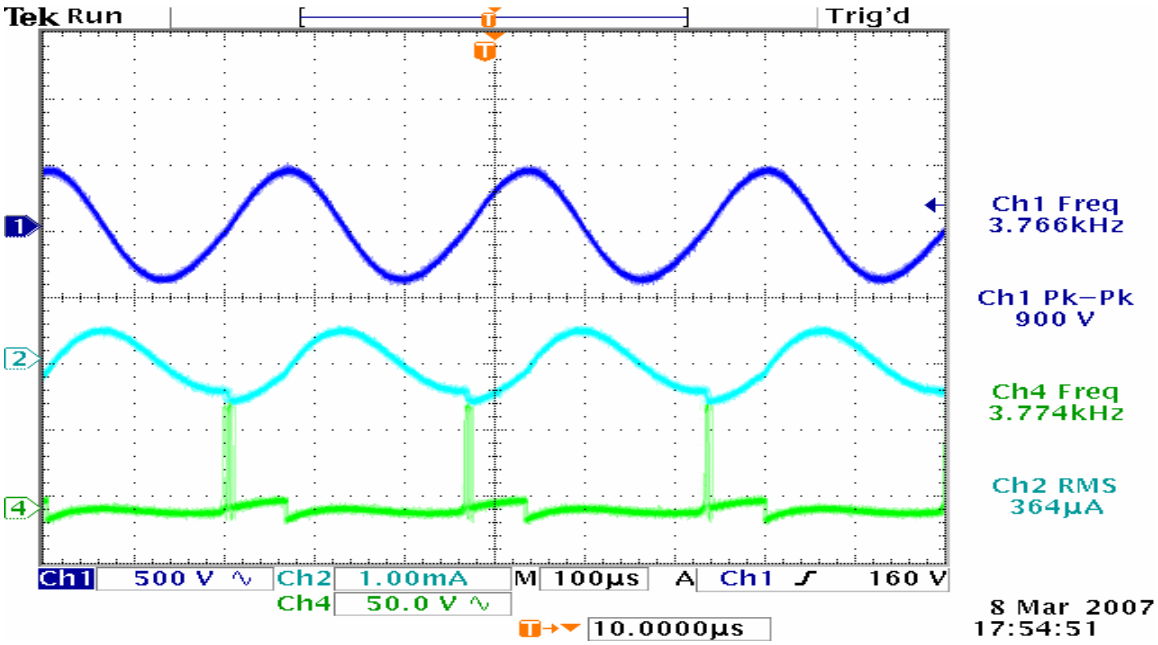

Figure G.4. Panel Actuator, 400 mA input current, w/out Aux. Inductor, 3.8 kHz.
Ch1: output voltage (500 V/div), Ch2: transformer primary current (1 mA/div),
Ch4: voltage across switch (50 V/div).

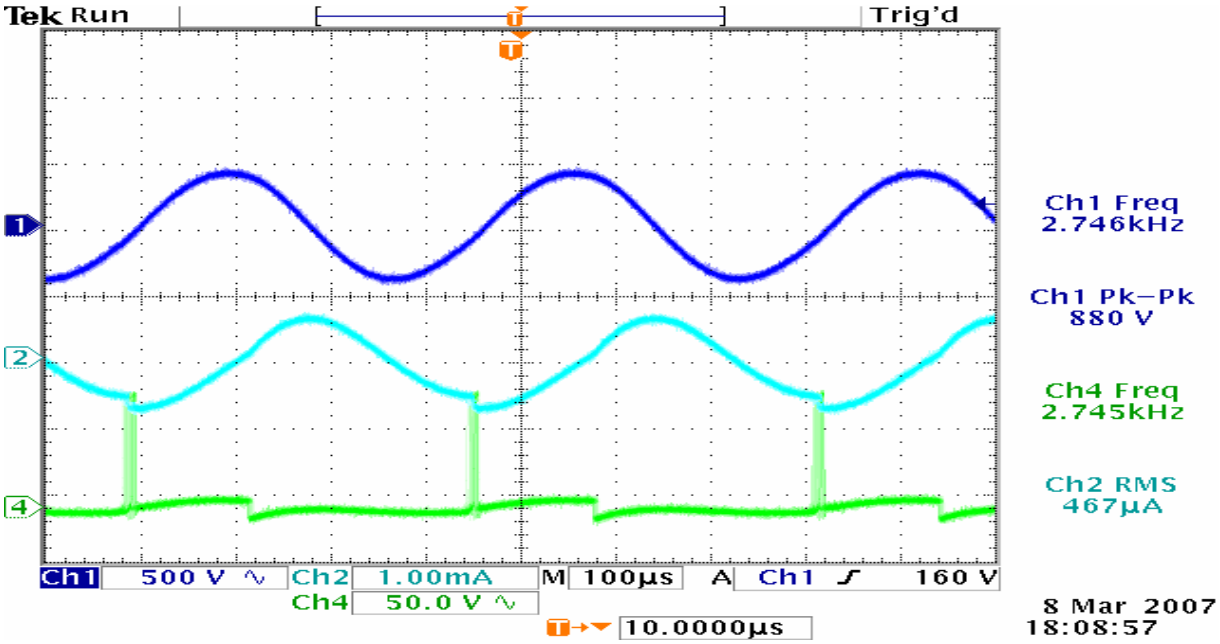

Figure G.5. Panel Actuator, 400 mA input current, w/out Aux. Inductor, 2.7 kHz.
Ch1: output voltage (500 V/div), Ch2: transformer primary current (1 mA/div),
Ch4: voltage across switch (50 V/div).

Appendix H: Low Power (400mA) Data: Panel Actuator, with 2.15mH parallel primary Auxiliary Inductor

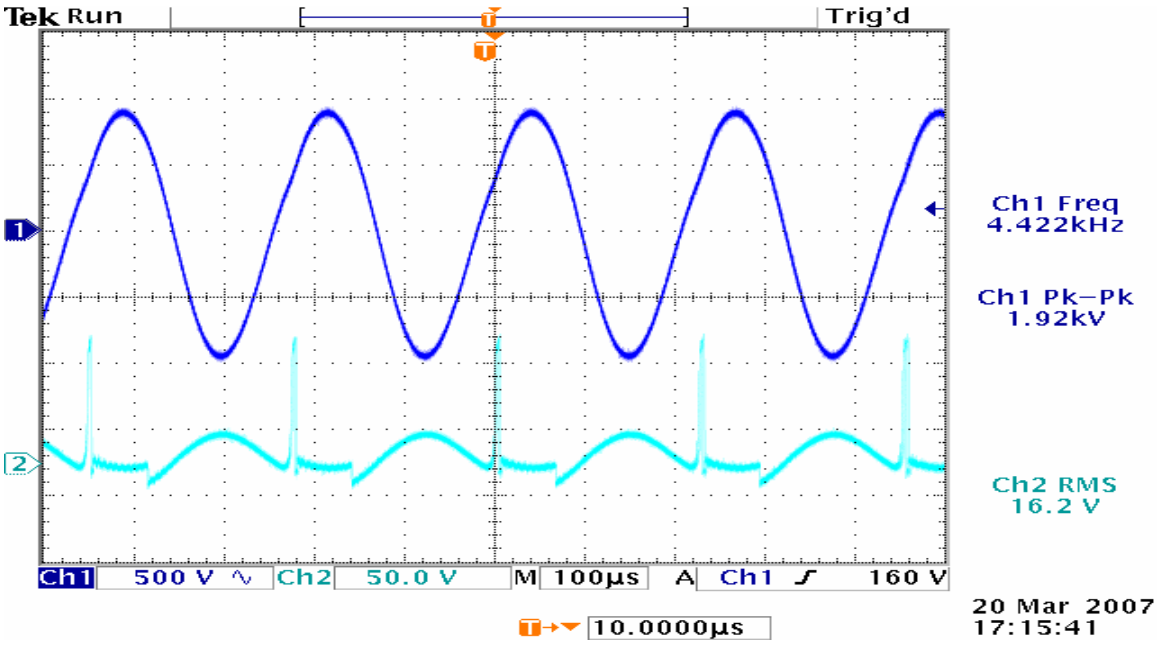

Figure H.1. Panel Actuator, 400 mA input current, with Aux. Inductor, 4.4 kHz.
Ch1: output voltage (500 V/div), Ch2: voltage across switch (50 V/div).

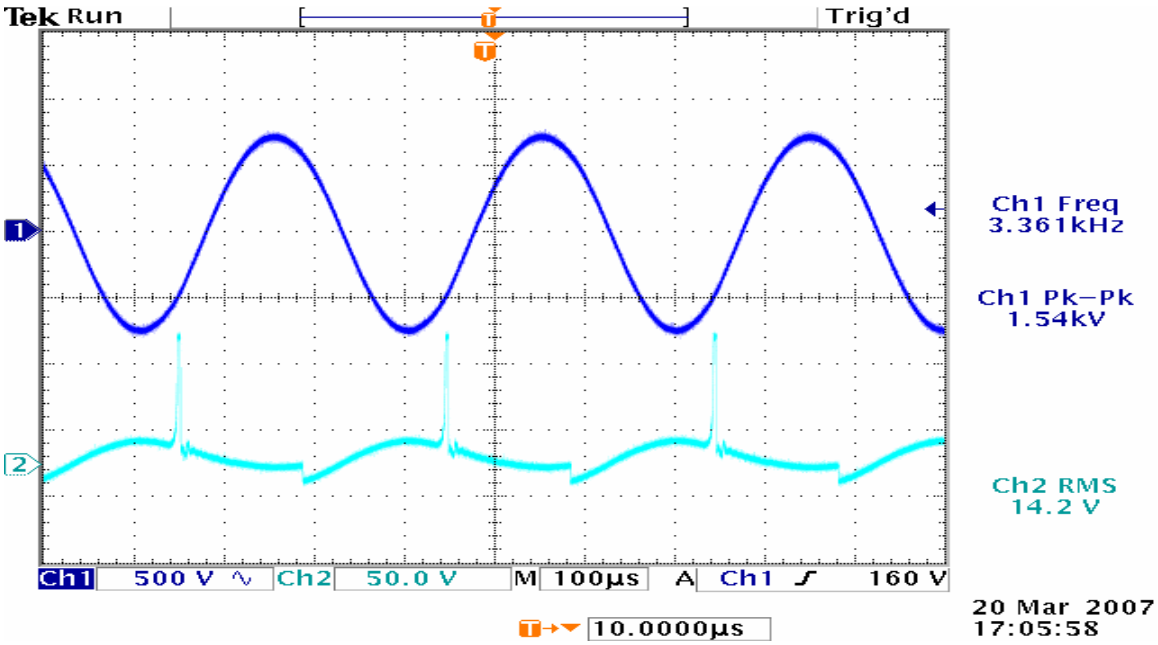

Figure H.2. Panel Actuator, 400 mA input current, with Aux. Inductor, 3.4 kHz.
Ch1: output voltage (500 V/div), Ch2: voltage across switch (50 V/div).

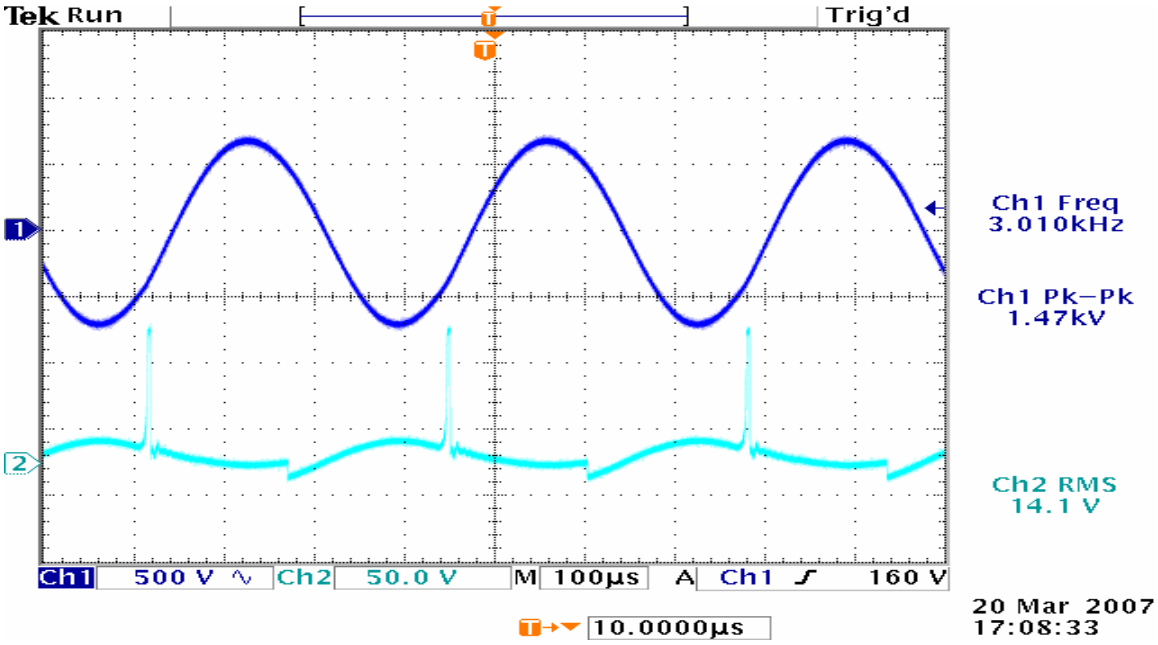

Figure H.3. Panel Actuator, 400 mA input current, with Aux. Inductor, 3 kHz.
Ch1: output voltage (500 V/div), Ch2: voltage across switch (50 V/div).

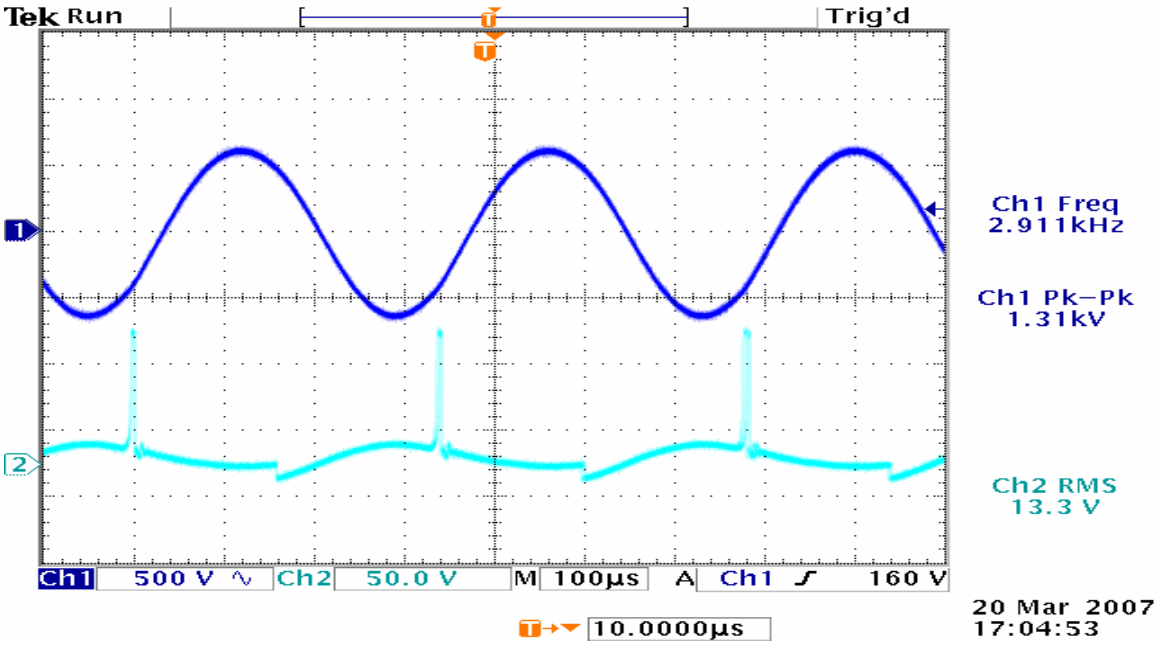

Figure H.4. Panel Actuator, 400 mA input current, with Aux. Inductor, 2.9 kHz.
Ch1: output voltage (500 V/div), Ch2: voltage across switch (50 V/div).

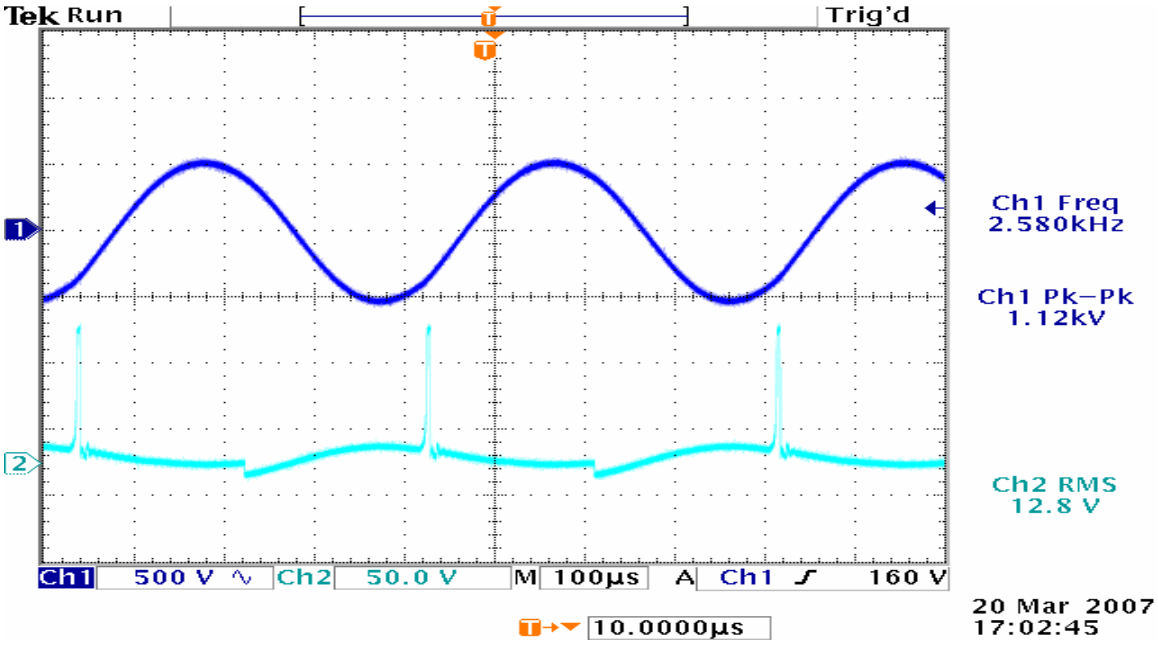

Figure H.5. Panel Actuator, 400 mA input current, with Aux. Inductor, 2.6 kHz.
Ch1: output voltage (500 V/div), Ch2: voltage across switch (50 V/div).

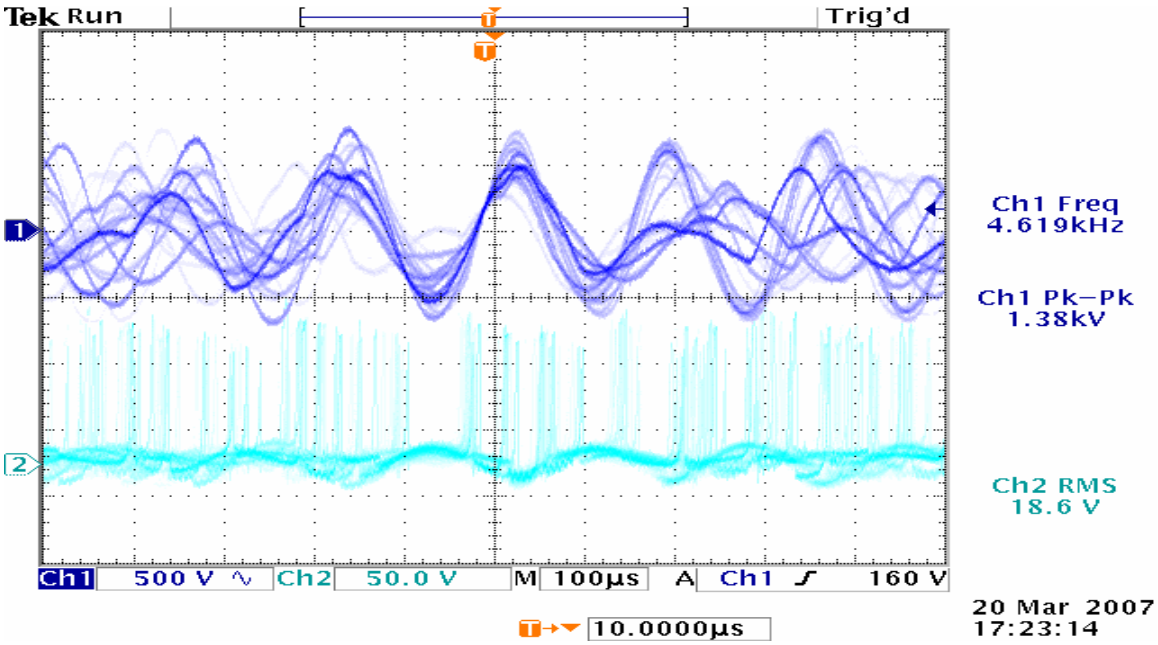

Figure H.6. Panel Actuator, 400 mA input current, with Aux. Inductor, unstable.
Ch1: output voltage (500 V/div), Ch2: voltage across switch (50 V/div).

Appendix I: Medium Power (600mA) Data: Quartz Actuator, without Auxiliary Inductor, with 76mH series secondary Impedance Matching Inductor

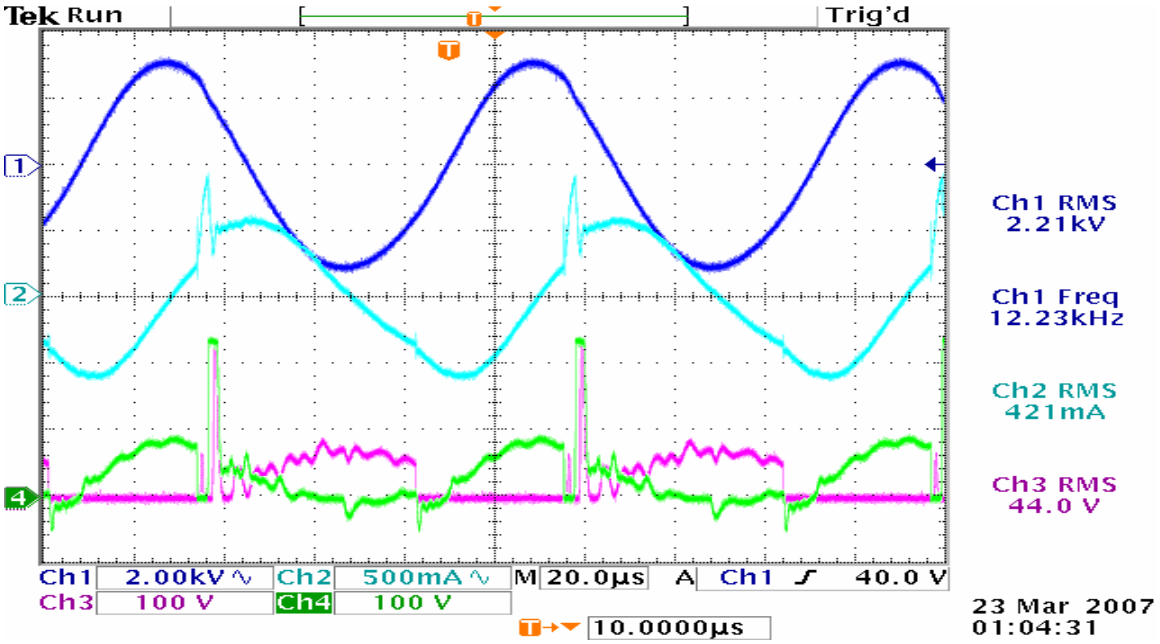

Figure I.1. Quartz Actuator, 600 mA input current, w/out Aux. Inductor, with Impedance-Matching Inductor in series in secondary, 12.2 kHz.
Ch1: output voltage (2 kV/div), Ch2: transformer primary current (500 mA/div), Ch3 and Ch4: voltage across each switch (100 V/div).

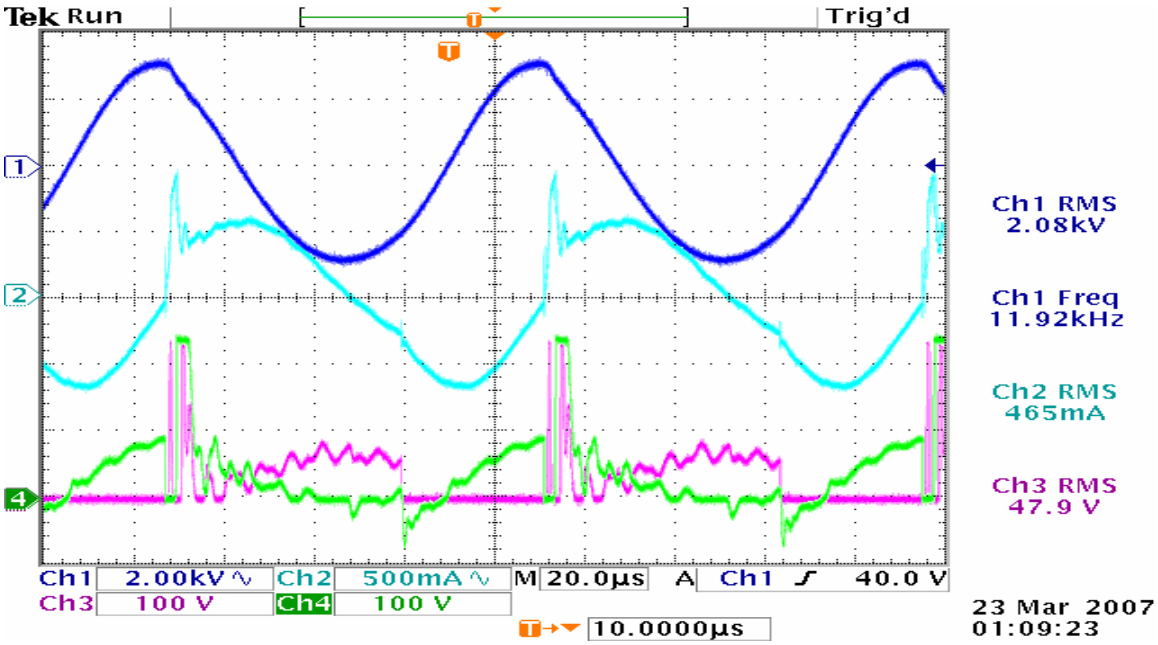

Figure I.2. Quartz Actuator, 600 mA input current, w/out Aux. Inductor, with Impedance-Matching Inductor in series in secondary, 11.9 kHz.

Ch1: output voltage (2 kV/div), Ch2: transformer primary current (500 mA/div), Ch3 and Ch4: voltage across each switch (100 V/div).

Appendix J: Medium Power (600mA) Data: Quartz Actuator, with 2.15mH parallel primary Auxiliary Inductor, with 76mH series secondary Impedance Matching Inductor

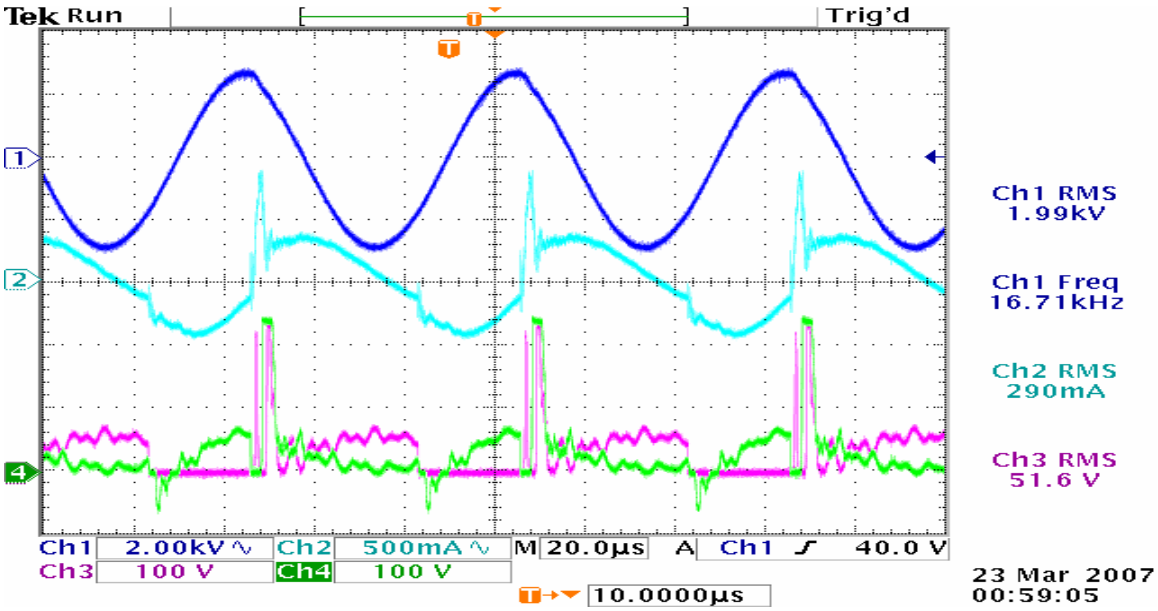

Figure J.1. Quartz Actuator, 600 mA input current, with Aux. Inductor, with Impedance-Matching Inductor in series in secondary, 16.7 kHz.
Ch1: output voltage (2 kV/div), Ch2: transformer primary current (500 mA/div), Ch3 and Ch4: voltage across each switch (100 V/div).

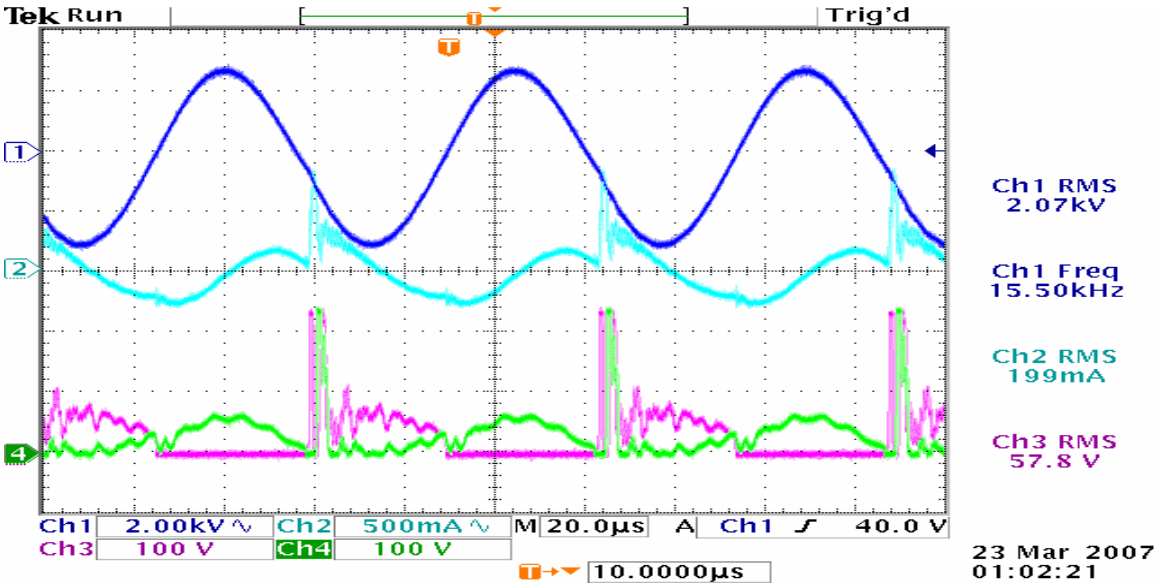

Figure J.2. Quartz Actuator, 600 mA input current, with Aux. Inductor, with Impedance-Matching Inductor in series in secondary, 15.5 kHz.

Ch1: output voltage (2 kV/div), Ch2: transformer primary current (500 mA/div), Ch3 and Ch4: voltage across each switch (100 V/div).

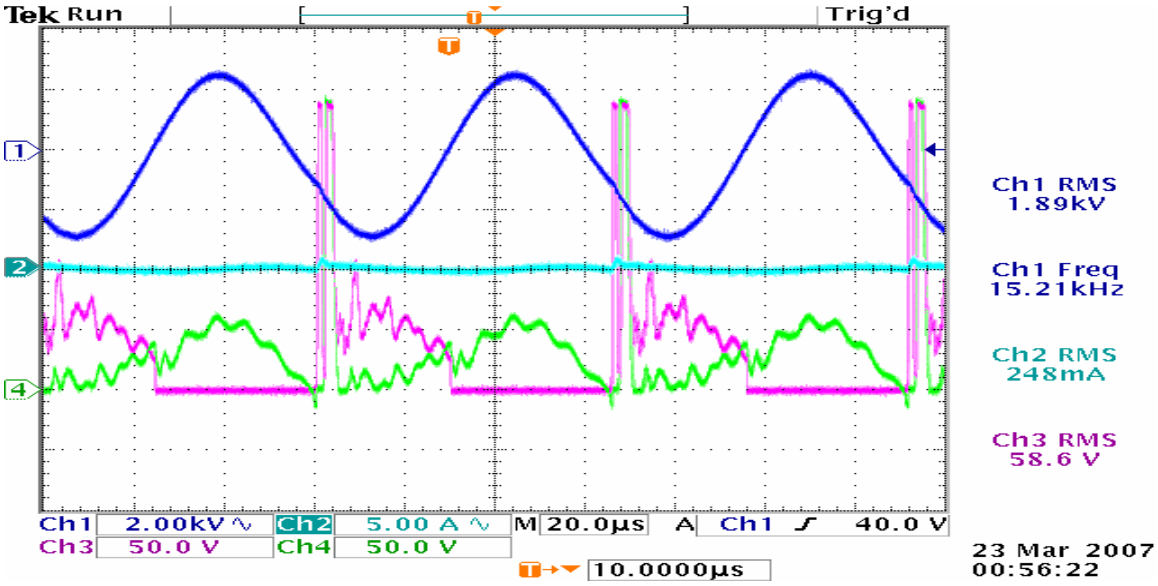

Figure J.3. Quartz Actuator, 600 mA input current, with Aux. Inductor, with Impedance-Matching Inductor in series in secondary, 15.2 kHz.

Ch1: output voltage (2 kV/div), Ch2: transformer primary current (5 A/div), Ch3 and Ch4: voltage across each switch (50 V/div).

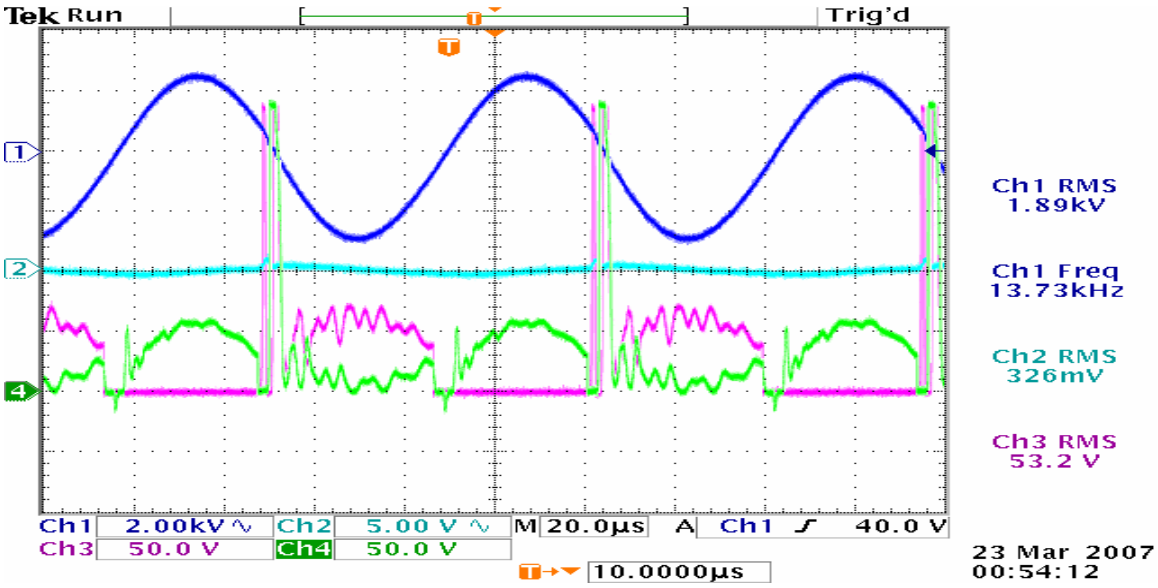

Figure J.4. Quartz Actuator, 600 mA input current, with Aux. Inductor, with Impedance-Matching Inductor in series in secondary, 13.7 kHz.

Ch1: output voltage (2 kV/div), Ch2: transformer primary current (5 A/div), Ch3 and Ch4: voltage across each switch (50 V/div).

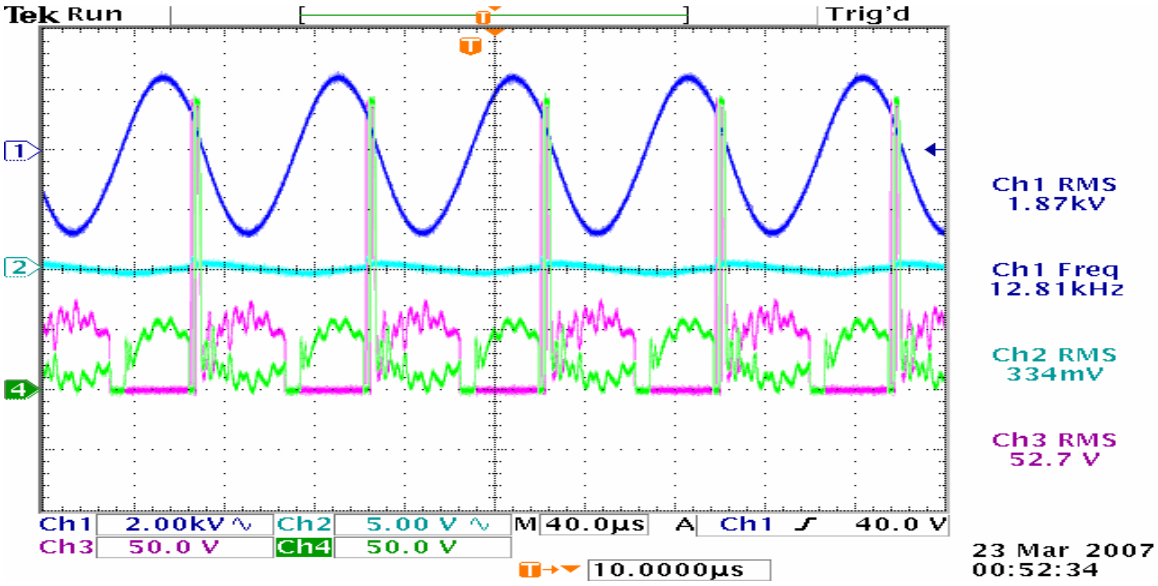

Figure J.5. Quartz Actuator, 600 mA input current, with Aux. Inductor, with Impedance-Matching Inductor in series in secondary, 12.8 kHz.

Ch1: output voltage (2 kV/div), Ch2: transformer primary current (5 A/div), Ch3 and Ch4: voltage across each switch (50 V/div).

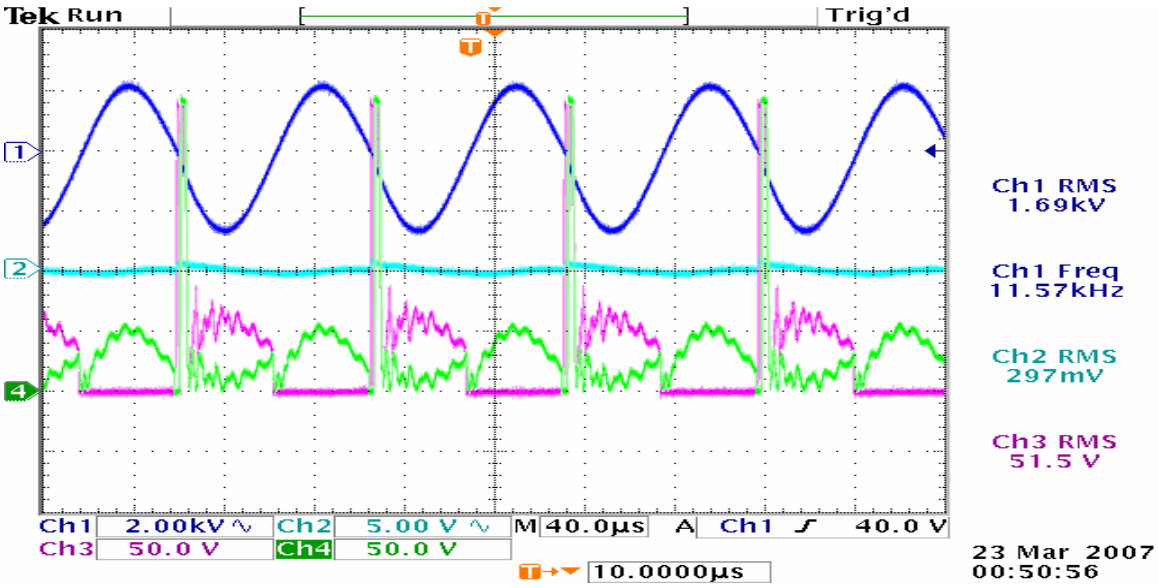

Figure J.6. Quartz Actuator, 600 mA input current, with Aux. Inductor, with Impedance-Matching Inductor in series in secondary, 11.6 kHz.

Ch1: output voltage (2 kV/div), Ch2: transformer primary current (5 A/div), Ch3 and Ch4: voltage across each switch (50 V/div).

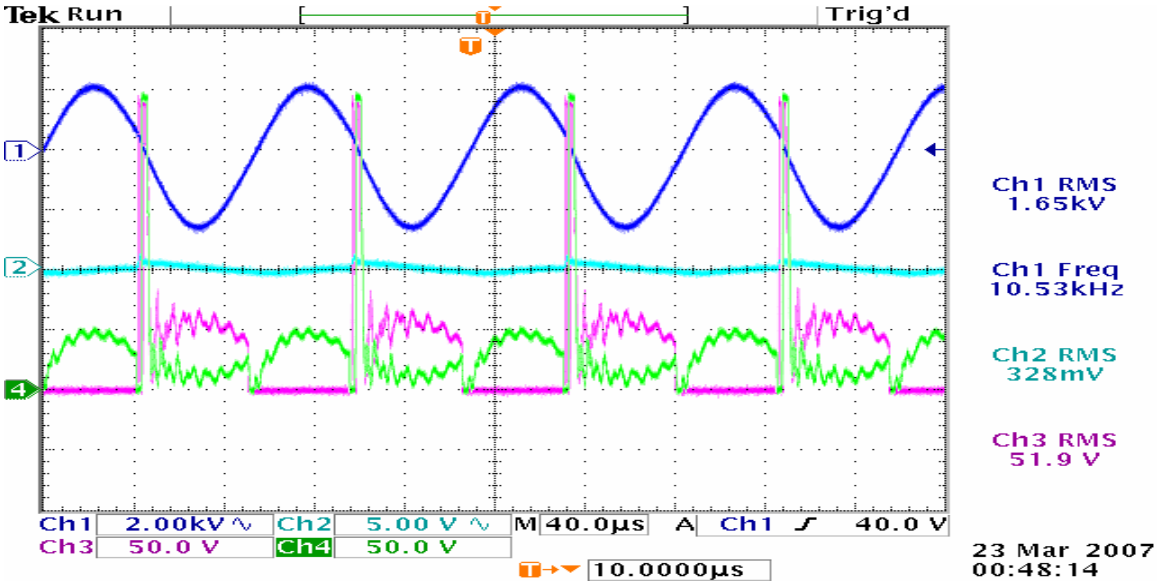

Figure J.7. Quartz Actuator, 600 mA input current, with Aux. Inductor, with Impedance-Matching Inductor in series in secondary, 10.5 kHz.

Ch1: output voltage (2 kV/div), Ch2: transformer primary current (5 A/div), Ch3 and Ch4: voltage across each switch (50 V/div).

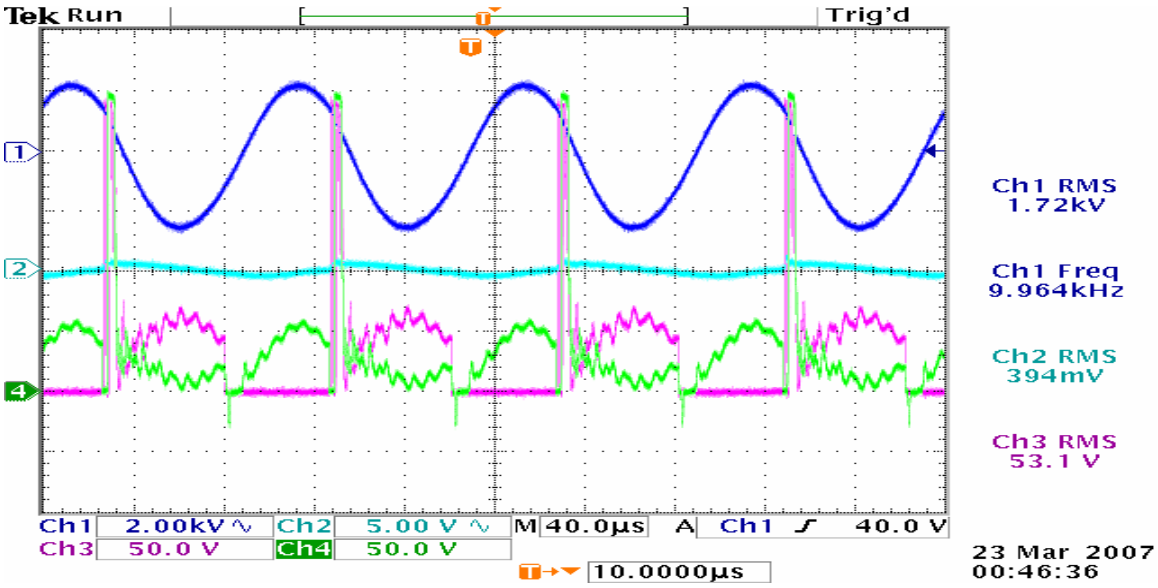

Figure J.8. Quartz Actuator, 600 mA input current, with Aux. Inductor, with Impedance-Matching Inductor in series in secondary, 10 kHz.

Ch1: output voltage (2 kV/div), Ch2: transformer primary current (5 A/div), Ch3 and Ch4: voltage across each switch (50 V/div).

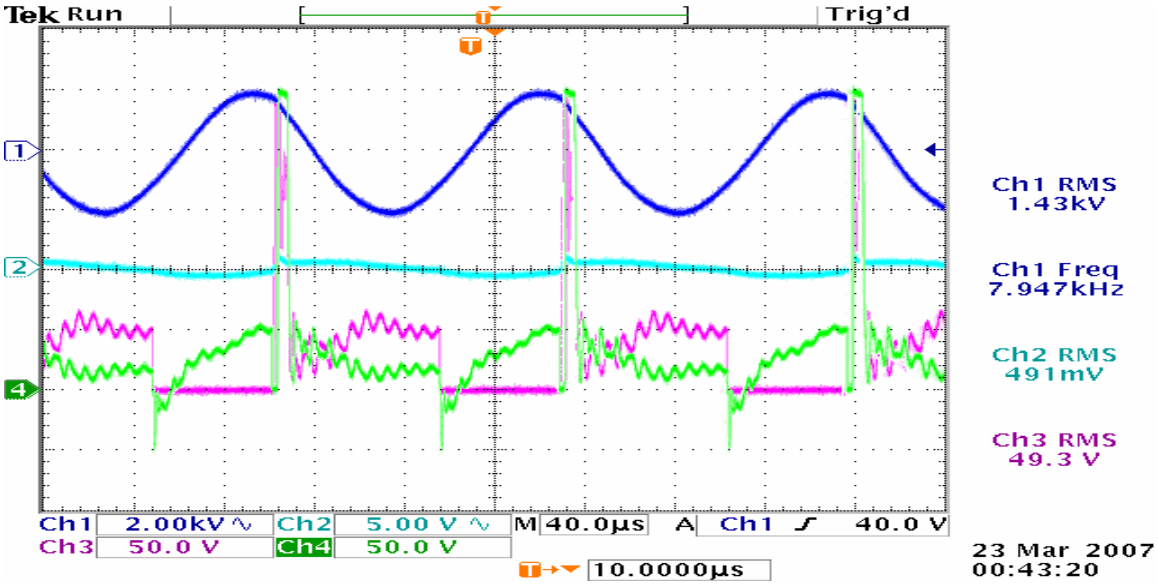

Figure J.9. Quartz Actuator, 600 mA input current, with Aux. Inductor, with Impedance-Matching Inductor in series in secondary, 7.9 kHz.

Ch1: output voltage (2 kV/div), Ch2: transformer primary current (5 A/div), Ch3 and Ch4: voltage across each switch (50 V/div).

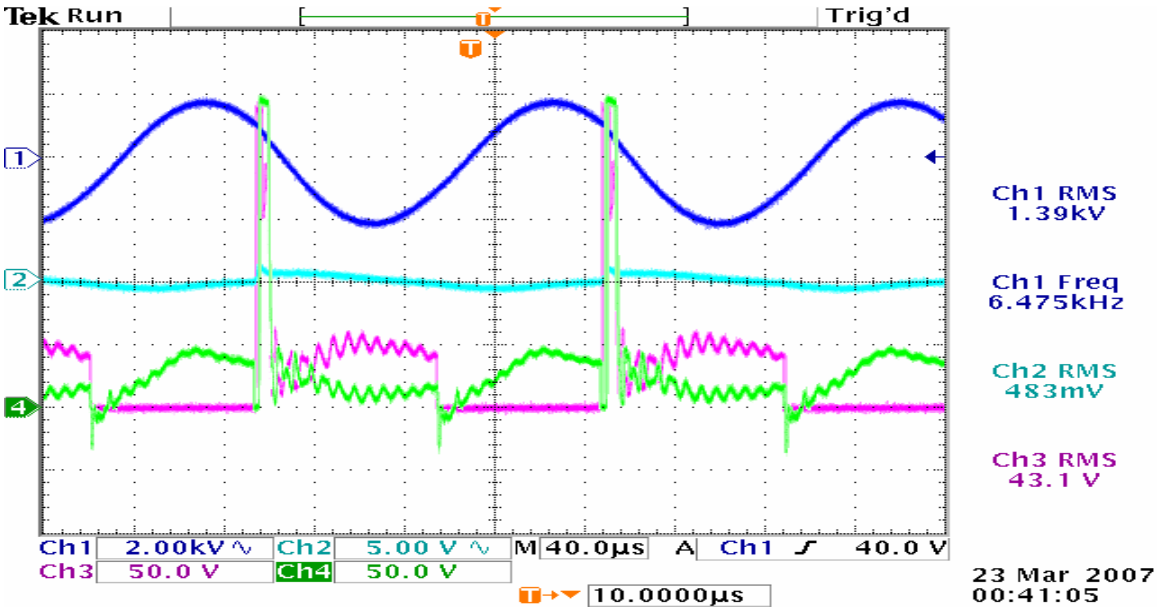

Figure J.10. Quartz Actuator, 600 mA input current, with Aux. Inductor, with Impedance-Matching Inductor in series in secondary, 6.5 kHz.

Ch1: output voltage (2 kV/div), Ch2: transformer primary current (5 A/div), Ch3 and Ch4: voltage across each switch (50 V/div).

Appendix K: Further Testing: Quartz Actuator Plasma Generation, without Auxiliary Inductor

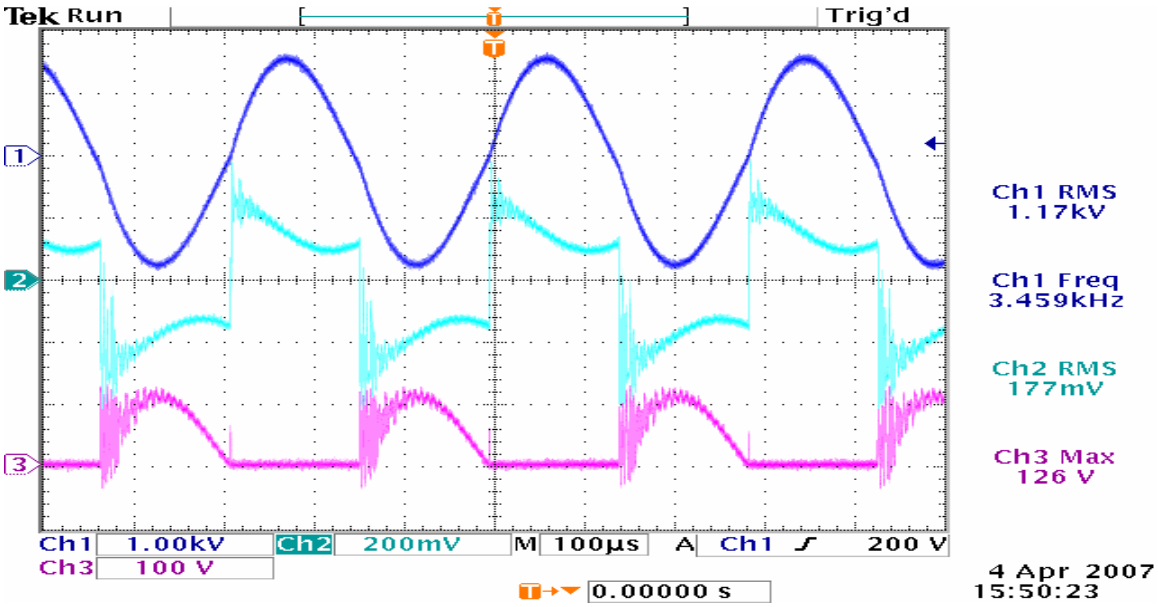

Figure K.1. Quartz Actuator Plasma Generation, w/out Aux. Inductor, 3.5 kHz.
Ch1: output voltage (1 kV/div), Ch2: transformer primary current (200 mA/div),
Ch3: voltage across switch (100 V/div).

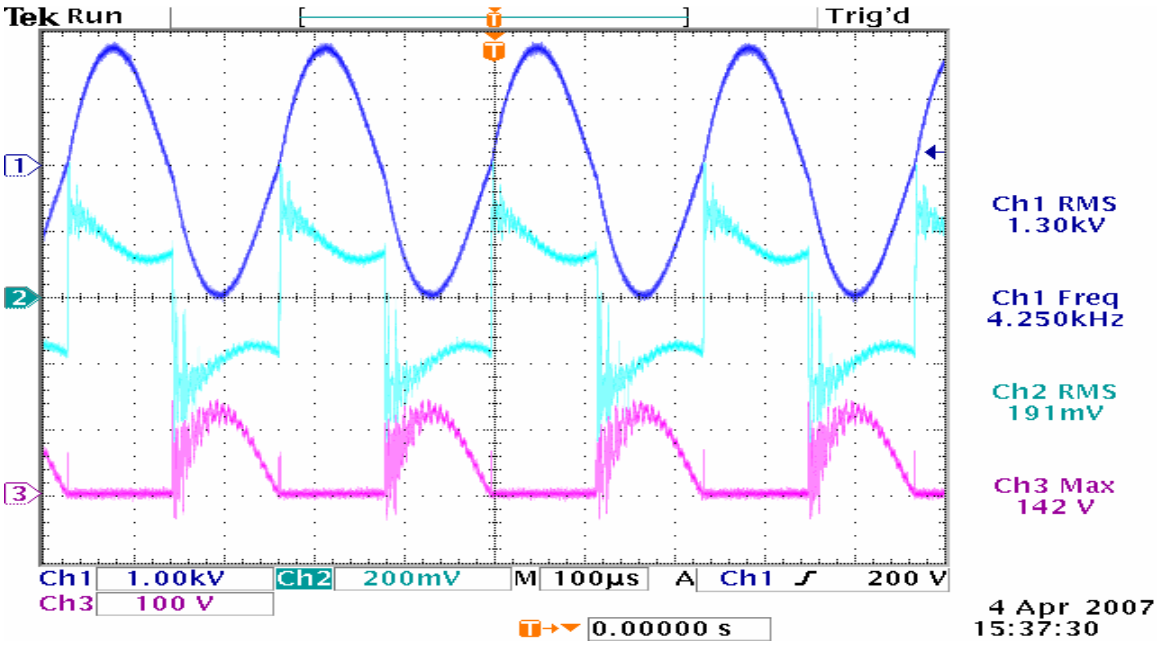

Figure K.2. Quartz Actuator Plasma Generation, w/out Aux. Inductor, 4.3 kHz.
Ch1: output voltage (1 kV/div), Ch2: transformer primary current (200 mA/div),
Ch3: voltage across switch (100 V/div).

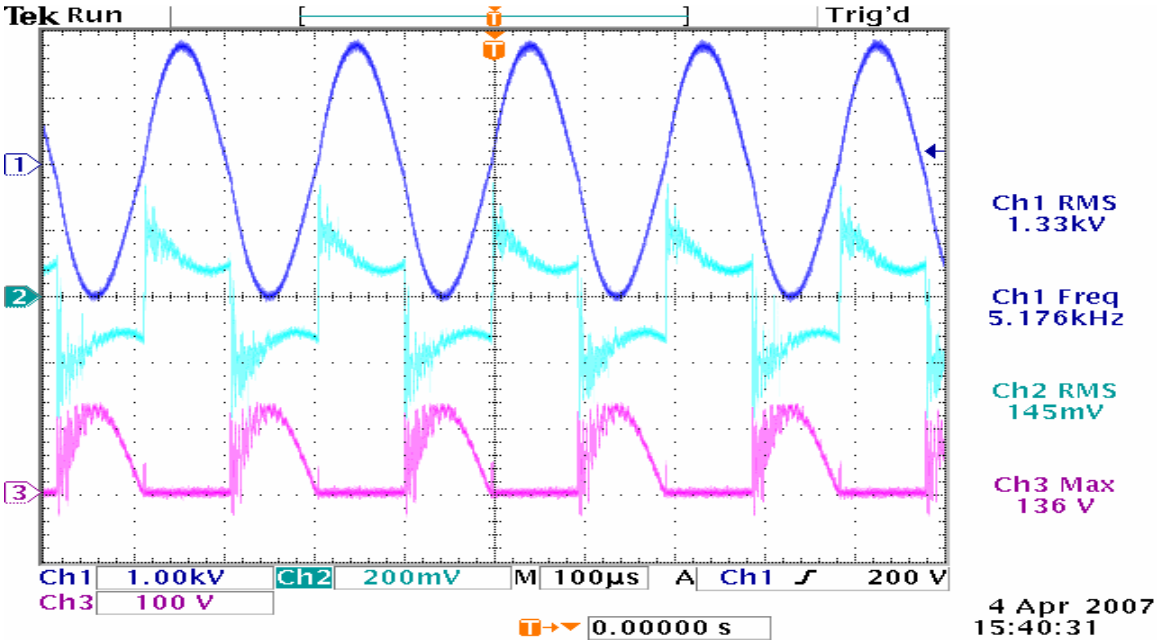

Figure K.3. Quartz Actuator Plasma Generation, w/out Aux. Inductor, 5.2 kHz.
Ch1: output voltage (1 kV/div), Ch2: transformer primary current (200 mA/div),
Ch3: voltage across switch (100 V/div).

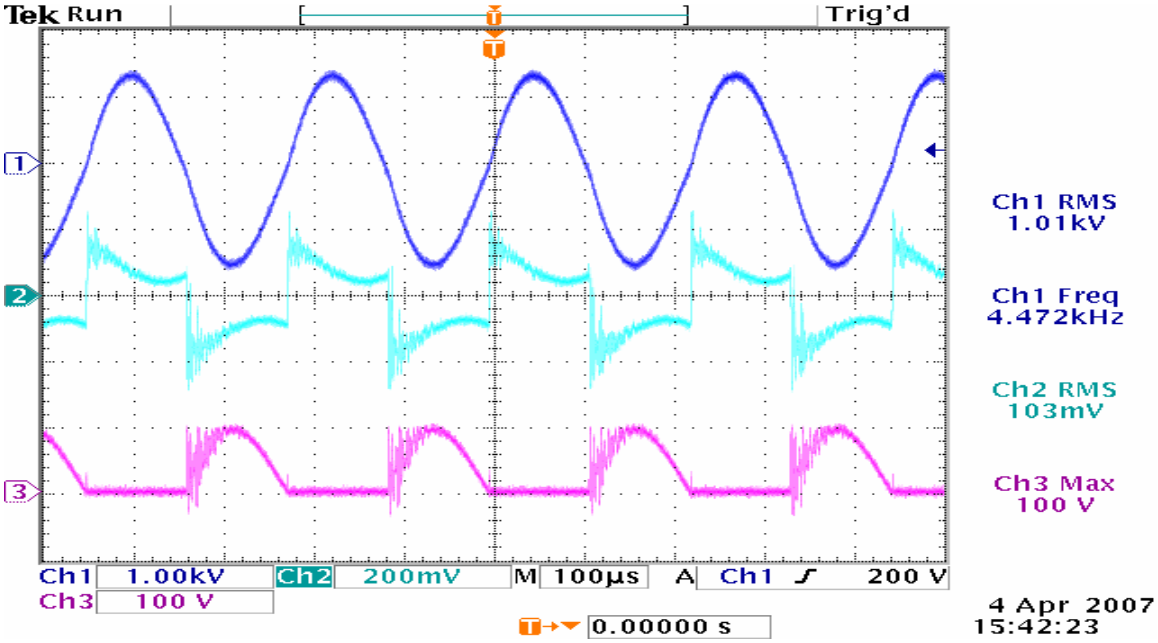

Figure K.4. Quartz Actuator Plasma Onset, w/out Aux. Inductor, 4.5 kHz.
Ch1: output voltage (1 kV/div), Ch2: transformer primary current (200 mA/div), Ch3: voltage across switch (100 V/div).

Appendix L: Further Testing: Quartz Actuator Plasma Generation, with parallel primary Auxiliary Inductor, Full Core Inserted (2.15 mH)

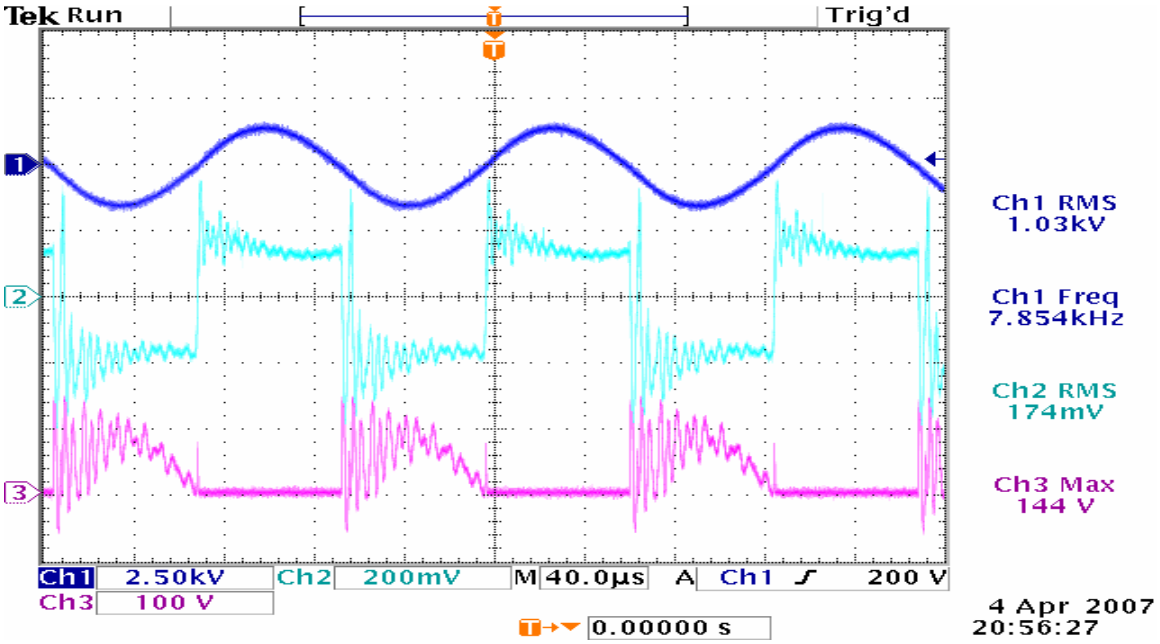

Figure L.1. Quartz Actuator Plasma Generation, with Aux. Inductor (2.15mH), 7.9 kHz. Ch1: output voltage (2.5 kV/div), Ch2: transformer primary current (200 mA/div), Ch3: voltage across switch (100 V/div).

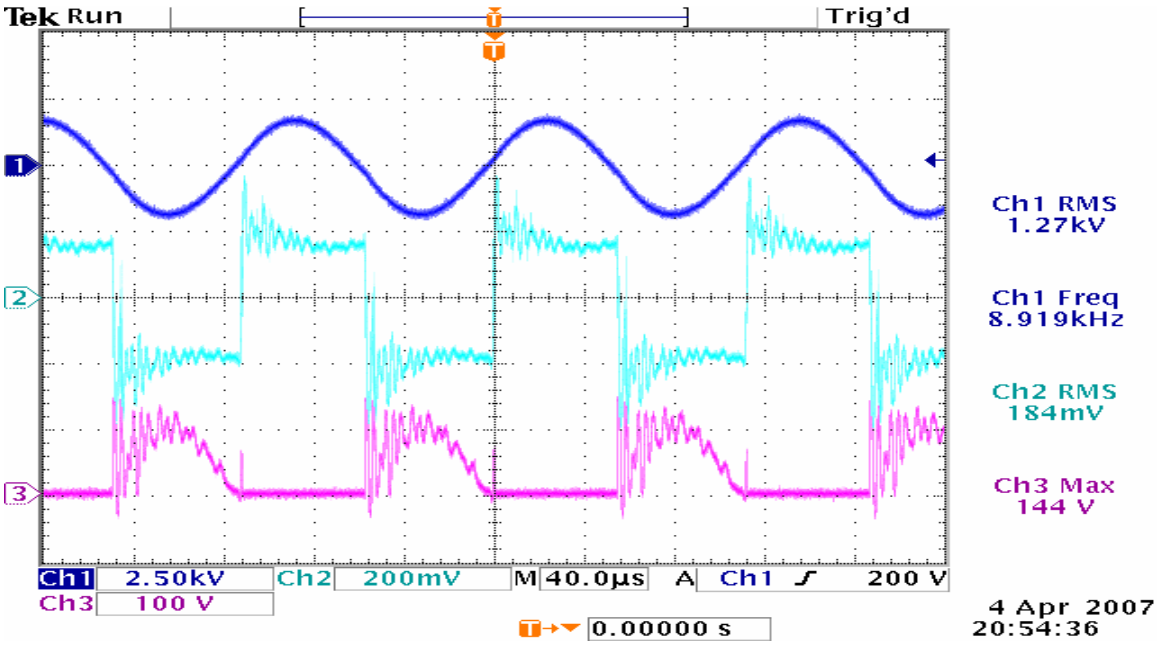

Figure L.2. Quartz Actuator Plasma Generation, with Aux. Inductor (2.15mH), 8.9 kHz. Ch1: output voltage (2.5 kV/div), Ch2: transformer primary current (200 mA/div), Ch3: voltage across switch (100 V/div).

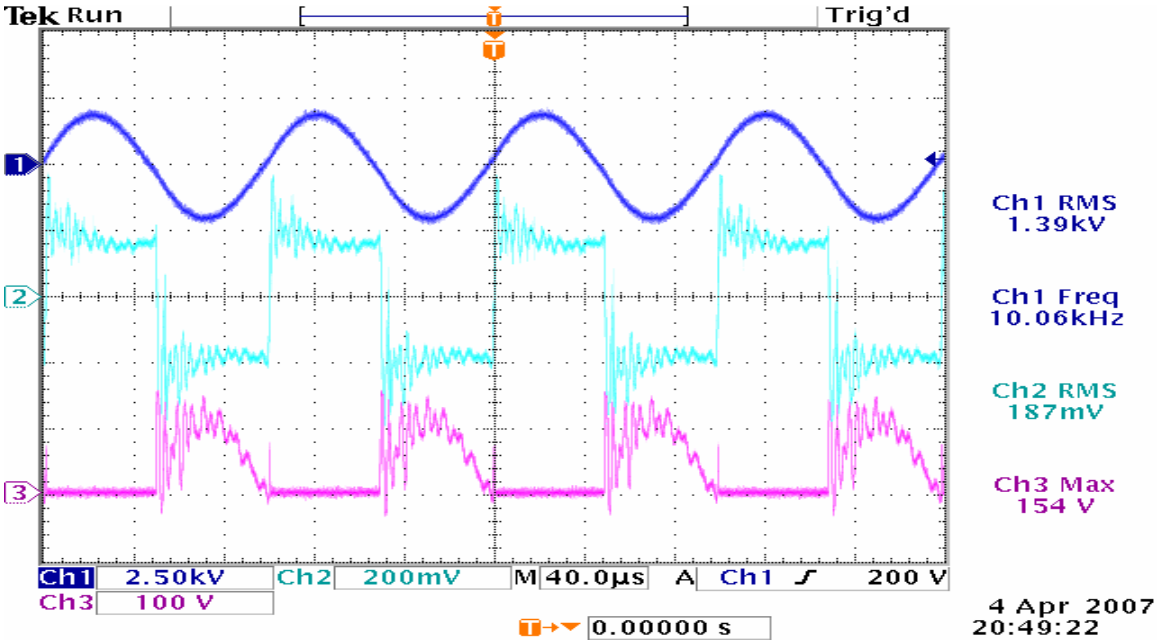

Figure L.3. Quartz Actuator Plasma Generation, with Aux. Inductor (2.15mH), 10 kHz. Ch1: output voltage (2.5 kV/div), Ch2: transformer primary current (200 mA/div), Ch3: voltage across switch (100 V/div).

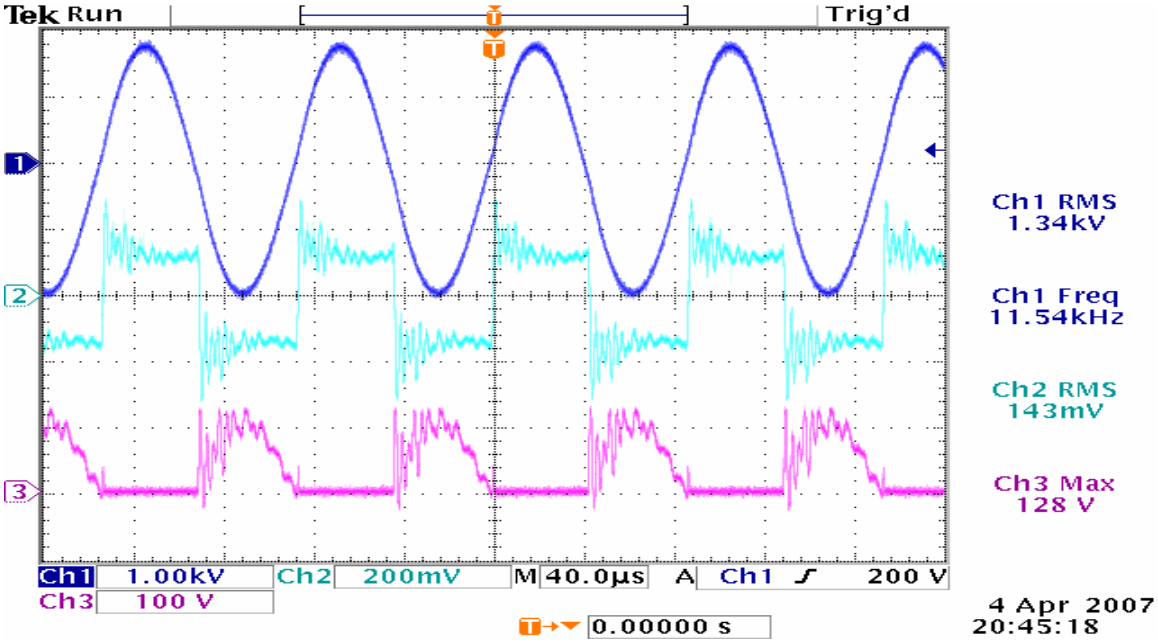

Figure L.4. Quartz Actuator Plasma Generation, with Aux. Inductor (2.15mH), 11.5 kHz. Ch1: output voltage (1 kV/div), Ch2: transformer primary current (200 mA/div), Ch3: voltage across switch (100 V/div).

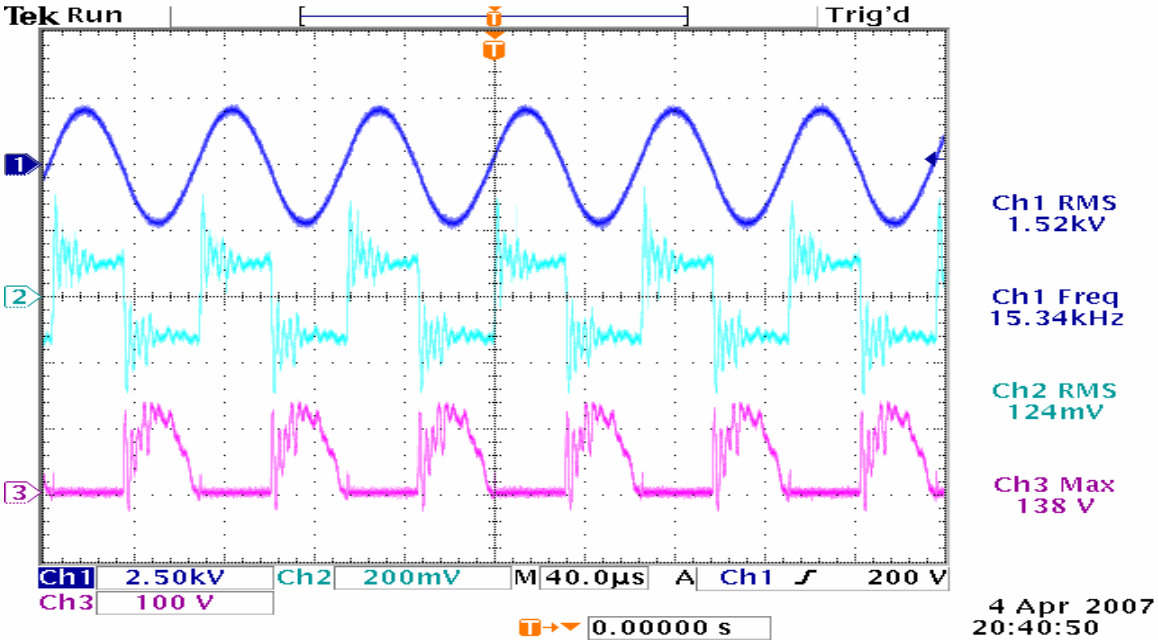

Figure L.5. Quartz Actuator Plasma Generation, with Aux. Inductor (2.15mH), 15.3 kHz. Ch1: output voltage (2.5 kV/div), Ch2: transformer primary current (200 mA/div), Ch3: voltage across switch (100 V/div).

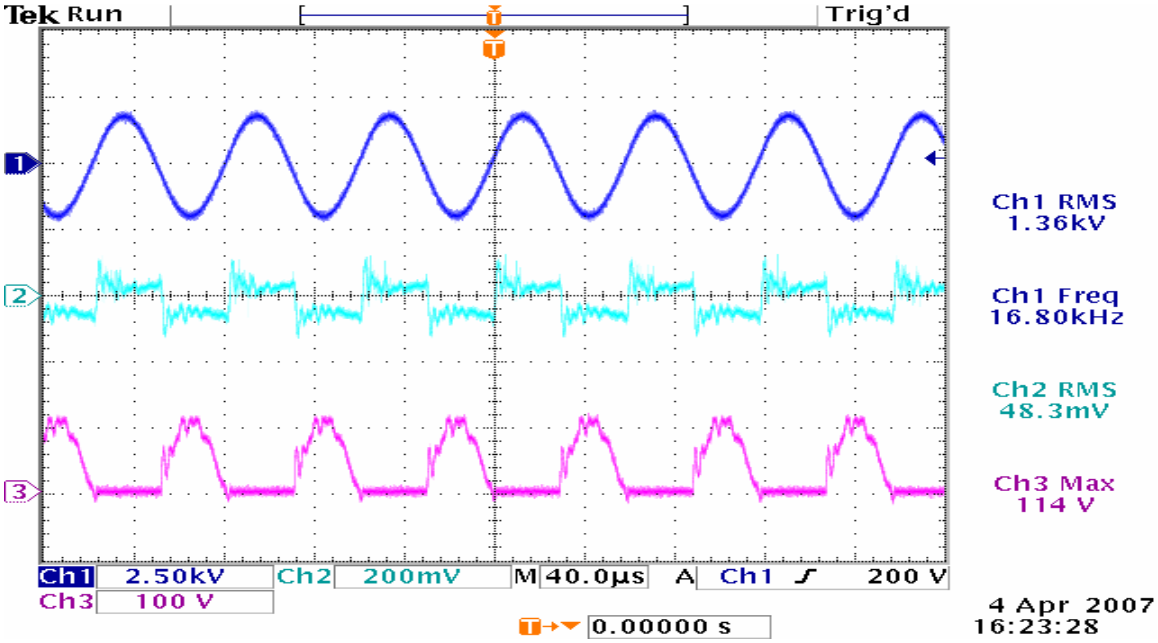

Figure L.6. Quartz Actuator Plasma Generation, with Aux. Inductor (2.15mH), 16.8 kHz. Ch1: output voltage (2.5 kV/div), Ch2: transformer primary current (200 mA/div), Ch3: voltage across switch (100 V/div).

Appendix M: Further Testing: Quartz Actuator Plasma Generation, with parallel primary Auxiliary Inductor, Half Core Inserted (0.71 mH)

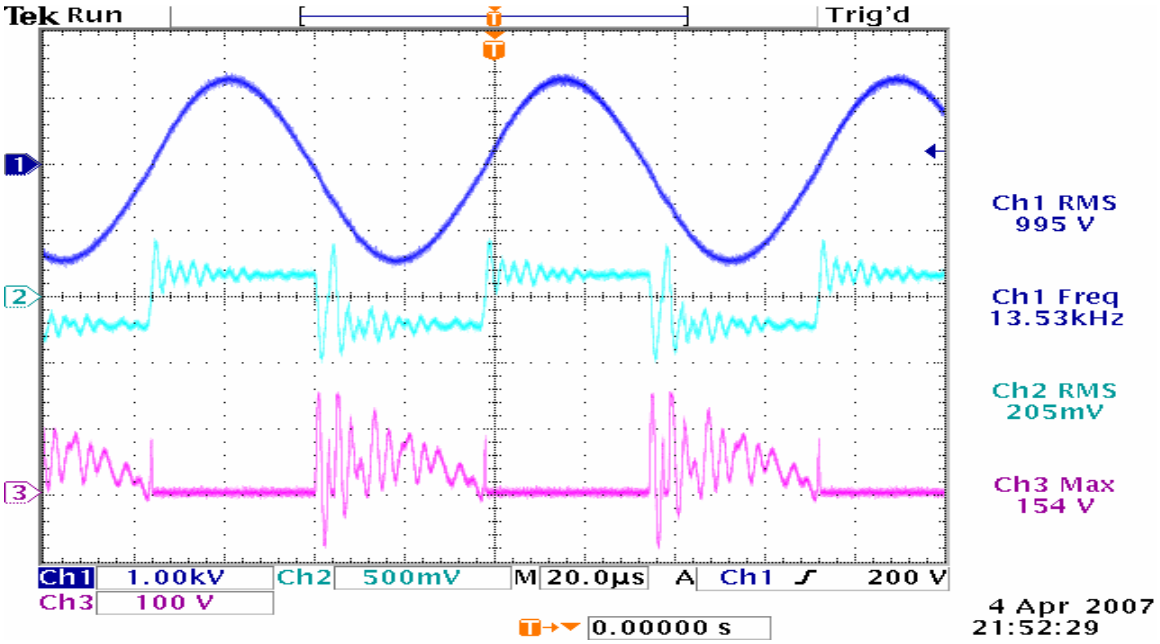

Figure M.1. Quartz Actuator Plasma Generation, with Aux. Inductor (0.71mH), 13.5kHz. Ch1: output voltage (1 kV/div), Ch2: transformer primary current (500 mA/div), Ch3: voltage across switch (100 V/div).

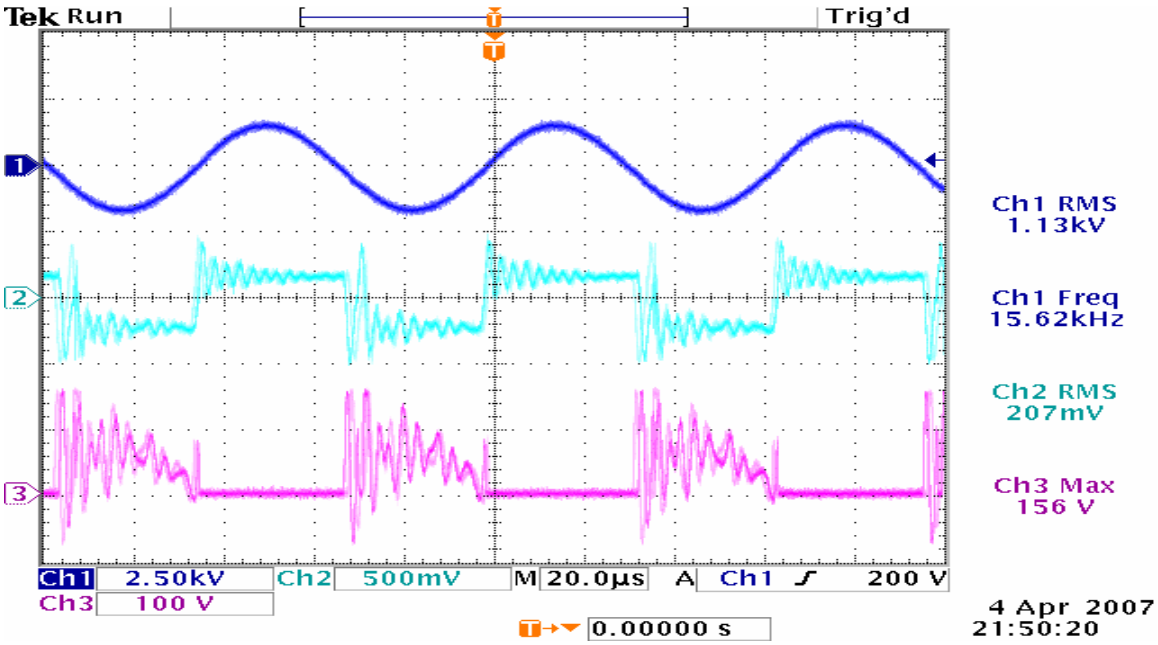

Figure M.2. Quartz Actuator Plasma Generation, with Aux. Inductor (0.71mH), 15.6kHz. Ch1: output voltage (2.5 kV/div), Ch2: transformer primary current (500 mA/div), Ch3: voltage across switch (100 V/div).

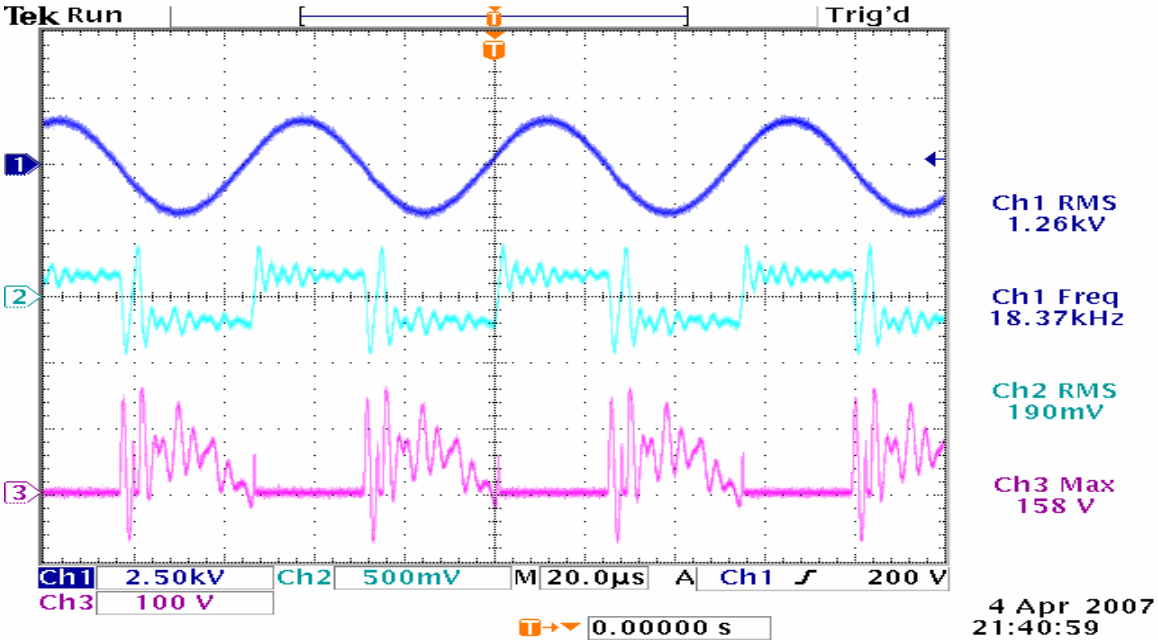

Figure M.3. Quartz Actuator Plasma Generation, with Aux. Inductor (0.71mH), 18.4kHz. Ch1: output voltage (2.5 kV/div), Ch2: transformer primary current (500 mA/div), Ch3: voltage across switch (100 V/div).

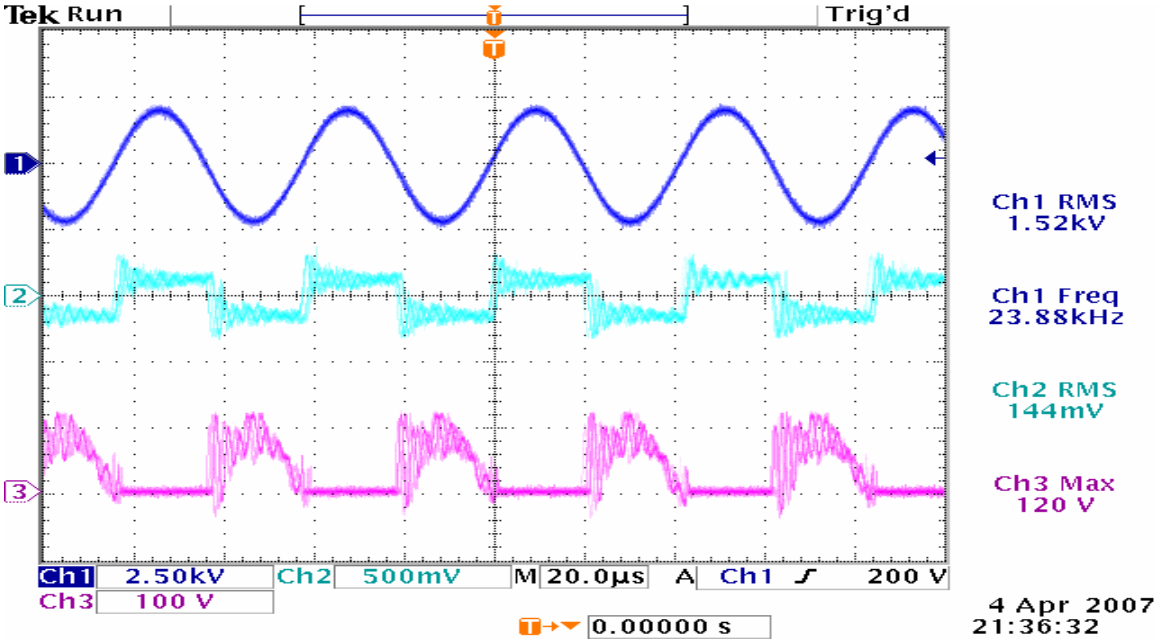

Figure M.4. Quartz Actuator Plasma Generation, with Aux. Inductor (0.71mH), 23.9kHz. Ch1: output voltage (2.5 kV/div), Ch2: transformer primary current (500 mA/div), Ch3: voltage across switch (100 V/div).

Appendix N: Further Testing: Quartz Actuator Plasma Generation, with parallel primary Auxiliary Inductor, No Core Inserted (0.09 mH)

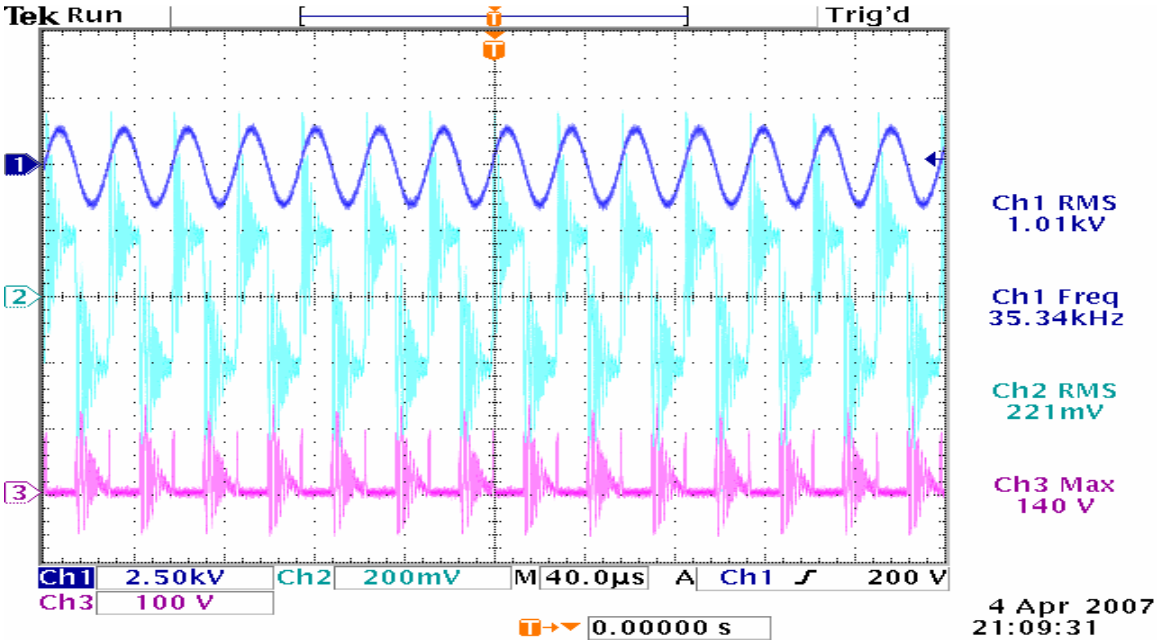

Figure N.1. Quartz Actuator Plasma Generation, with Aux. Inductor (0.09mH), 35.3kHz. Ch1: output voltage (2.5 kV/div), Ch2: transformer primary current (200 mA/div), Ch3: voltage across switch (100 V/div).

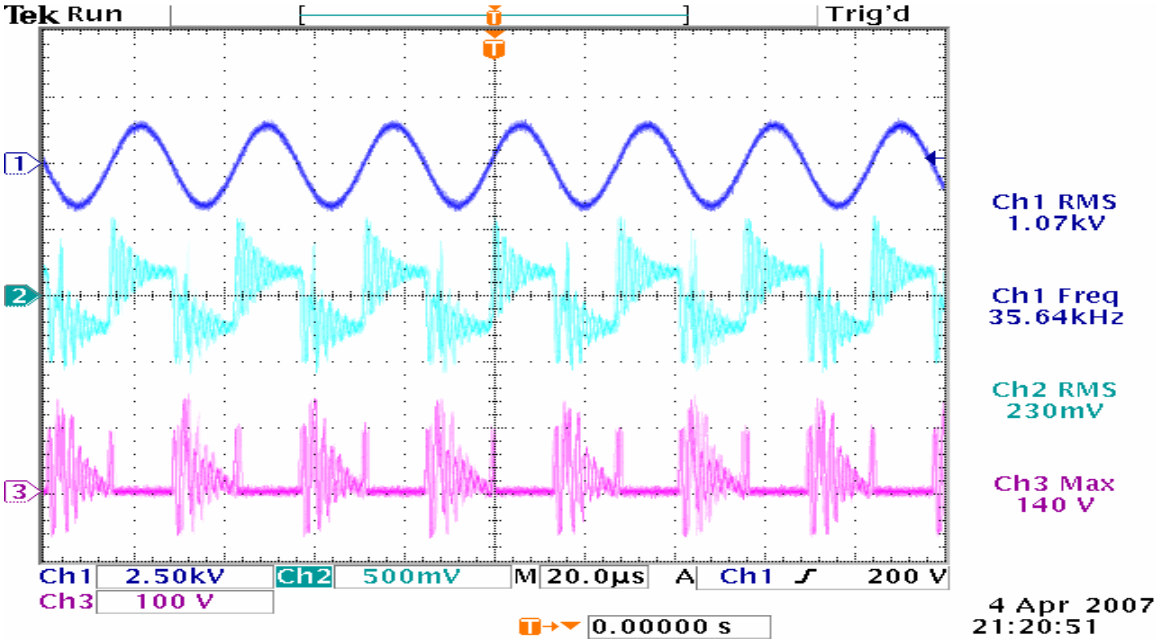

Figure N.2. Quartz Actuator Plasma Generation, with Aux. Inductor (0.09mH), 35.6kHz. Ch1: output voltage (2.5 kV/div), Ch2: transformer primary current (500 mA/div), Ch3: voltage across switch (100 V/div).

Appendix O: Further Testing: Panel Actuator Plasma Generation, without Auxiliary Inductor, without Impedance Matching Inductor

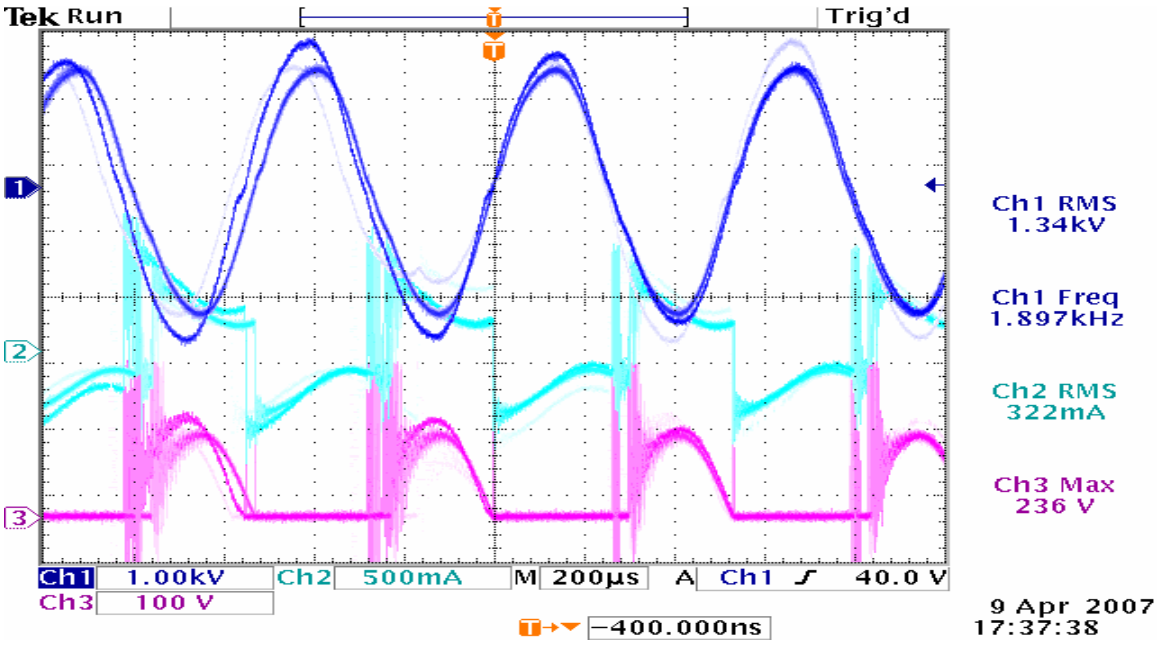

Figure O.1. Panel Actuator Plasma Generation, w/out Auxiliary Inductor, w/out Impedance Matching Inductor, 1.9 kHz.
Ch1: output voltage (1 kV/div), Ch2: transformer primary current (500 mA/div), Ch3: voltage across switch (100 V/div).

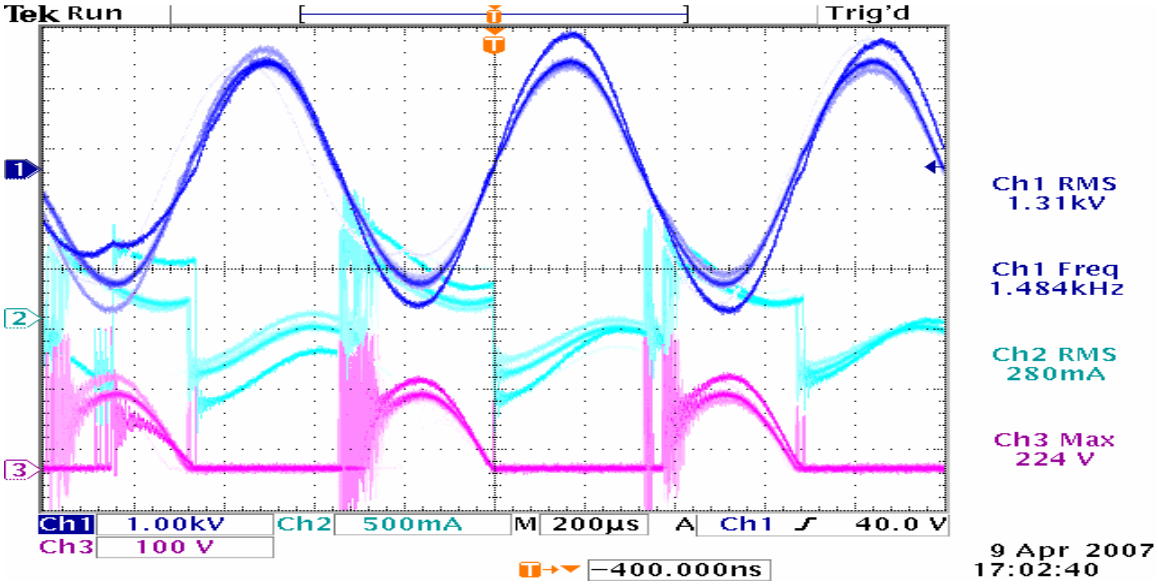

Figure O.2. Panel Actuator Plasma Generation, w/out Auxiliary Inductor, w/out Impedance Matching Inductor, 1.48 kHz.

Ch1: output voltage (1 kV/div), Ch2: transformer primary current (500 mA/div), Ch3: voltage across switch (100 V/div).

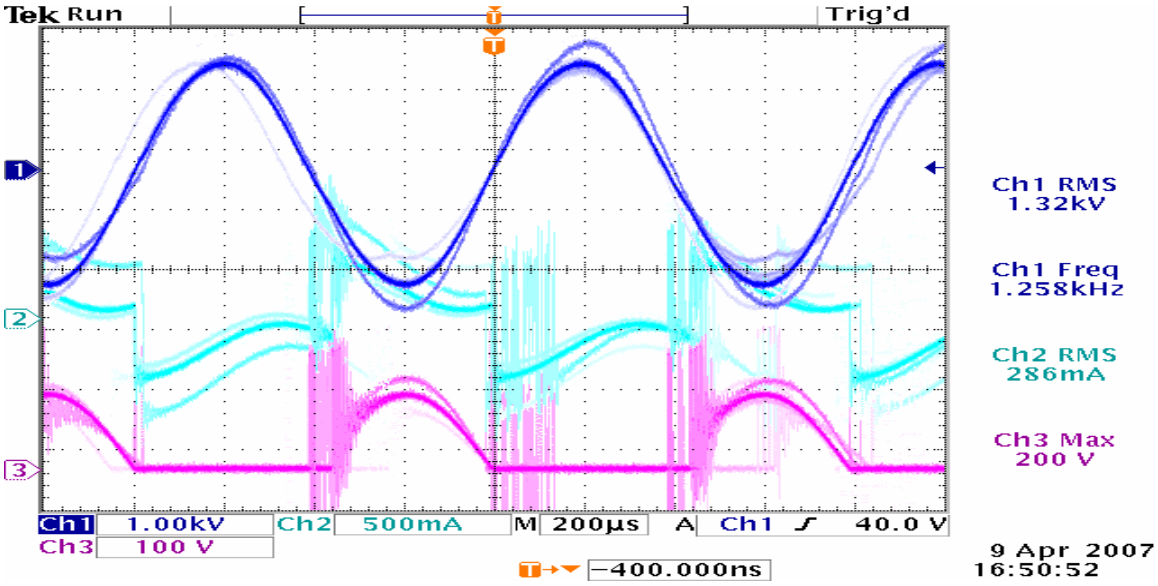

Figure O.3. Panel Actuator Plasma Generation, w/out Auxiliary Inductor, w/out Impedance Matching Inductor, 1.26 kHz.

Ch1: output voltage (1 kV/div), Ch2: transformer primary current (500 mA/div), Ch3: voltage across switch (100 V/div).

Appendix P: Further Testing: Panel Actuator Plasma Generation, without Auxiliary Inductor, with 3.2mH series secondary Impedance Matching Inductor

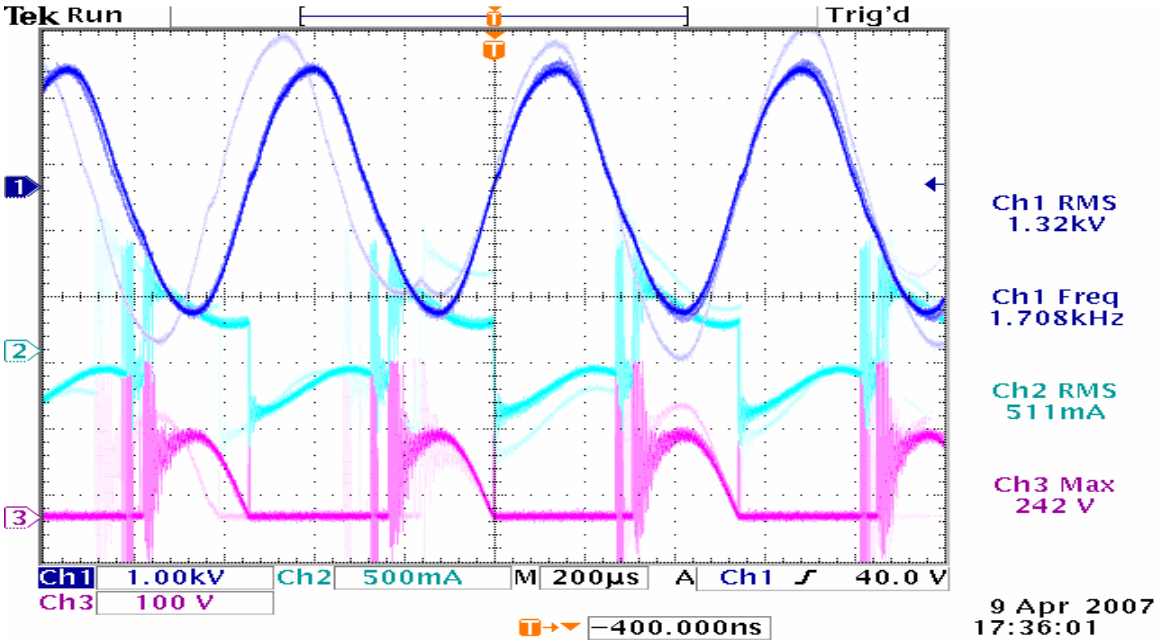

Figure P.1. Panel Actuator Plasma Generation, w/out Auxiliary Inductor, with 3.2mH series secondary Impedance Matching Inductor, 1.71 kHz.
Ch1: output voltage (1 kV/div), Ch2: transformer primary current (500 mA/div),
Ch3: voltage across switch (100 V/div).

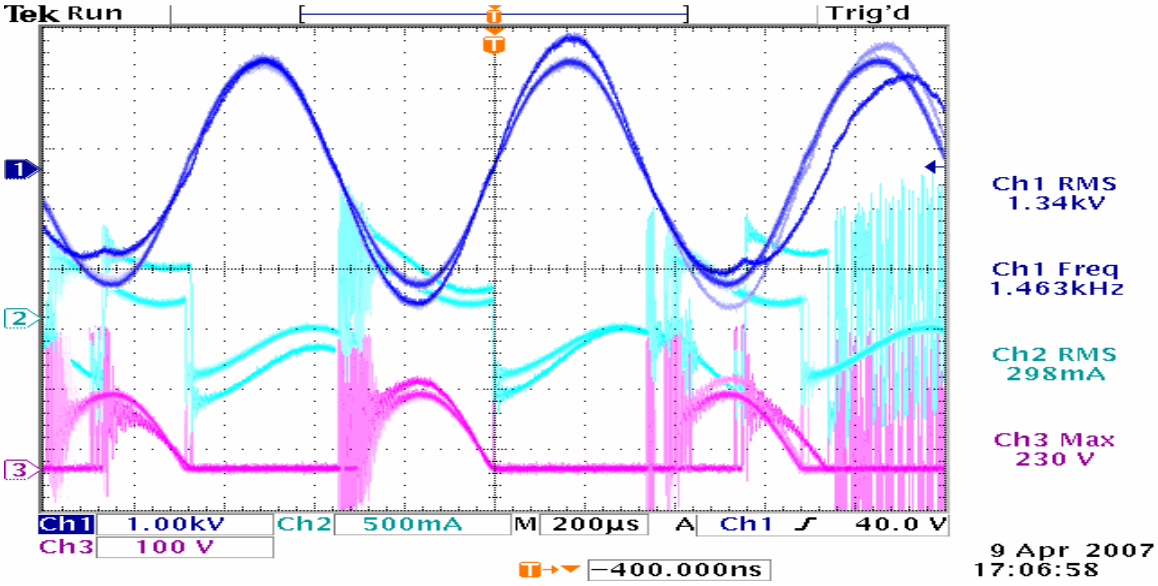

Figure P.2. Panel Actuator Plasma Generation, w/out Auxiliary Inductor, with 3.2mH series secondary Impedance Matching Inductor, 1.46 kHz.

Ch1: output voltage (1 kV/div), Ch2: transformer primary current (500 mA/div), Ch3: voltage across switch (100 V/div).

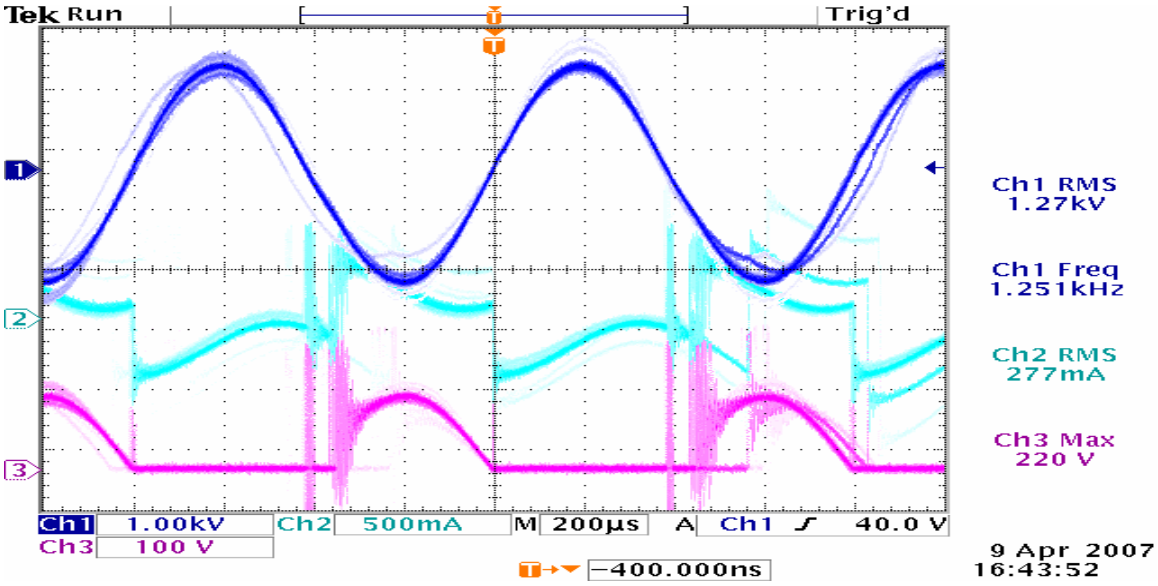

Figure P.3. Panel Actuator Plasma Generation, w/out Auxiliary Inductor, with 3.2mH series secondary Impedance Matching Inductor, 1.25 kHz.

Ch1: output voltage (1 kV/div), Ch2: transformer primary current (500 mA/div), Ch3: voltage across switch (100 V/div).

Appendix Q: Further Testing: Panel Actuator Plasma Generation, without Auxiliary Inductor, with 41mH series secondary Impedance Matching Inductor

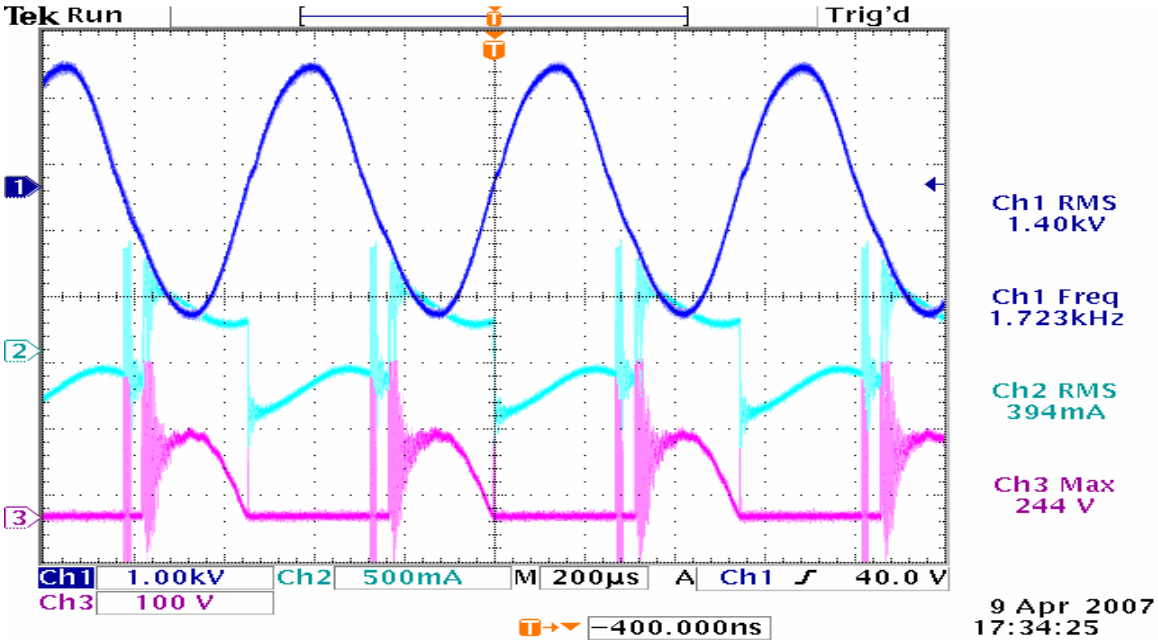

Figure Q.1. Panel Actuator Plasma Generation, w/out Auxiliary Inductor, with 41mH series secondary Impedance Matching Inductor, 1.72 kHz.
Ch1: output voltage (1 kV/div), Ch2: transformer primary current (500 mA/div), Ch3: voltage across switch (100 V/div).

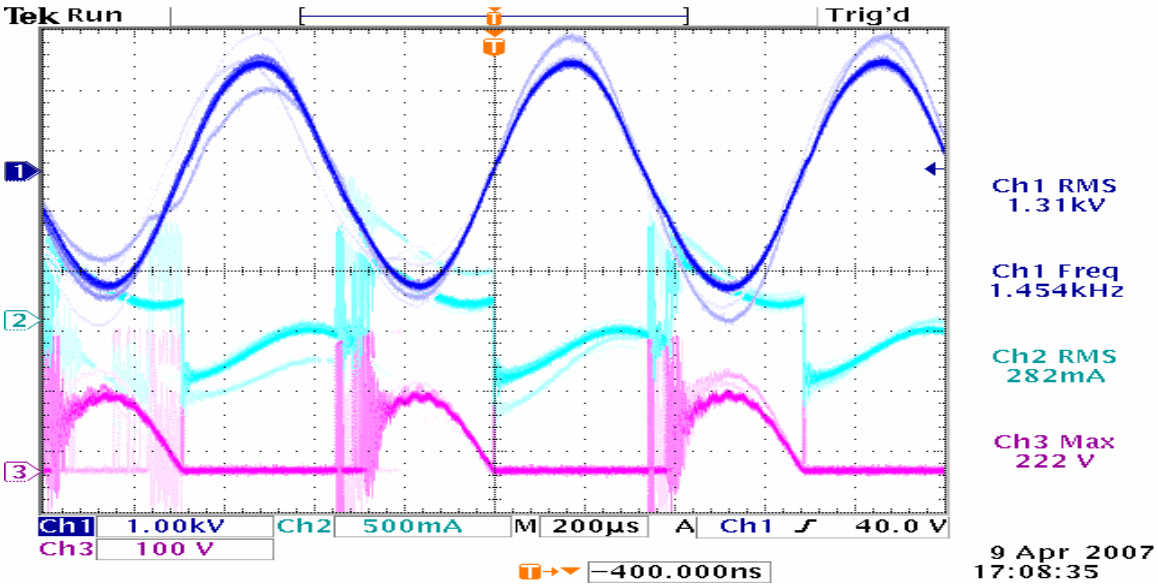

Figure Q.2. Panel Actuator Plasma Generation, w/out Auxiliary Inductor, with 41mH series secondary Impedance Matching Inductor, 1.45 kHz.
Ch1: output voltage (1 kV/div), Ch2: transformer primary current (500 mA/div), Ch3: voltage across switch (100 V/div).

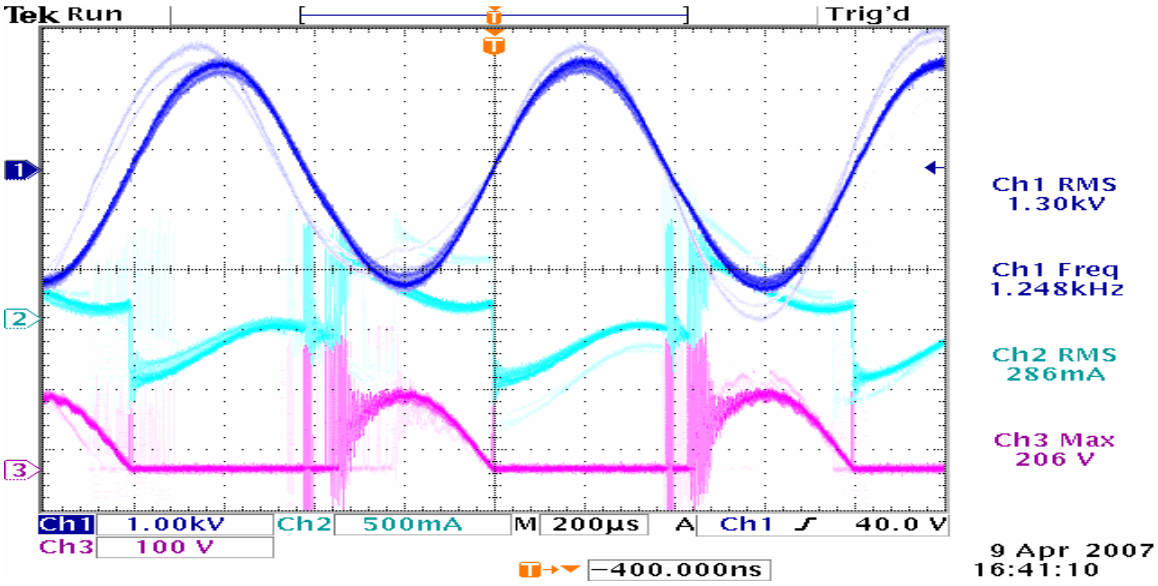

Figure Q.3. Panel Actuator Plasma Generation, w/out Auxiliary Inductor, with 41mH series secondary Impedance Matching Inductor, 1.25 kHz.
Ch1: output voltage (1 kV/div), Ch2: transformer primary current (500 mA/div), Ch3: voltage across switch (100 V/div).

Appendix R: Further Testing: Panel Actuator Plasma Generation, without Auxiliary Inductor, with 76mH series secondary Impedance Matching Inductor

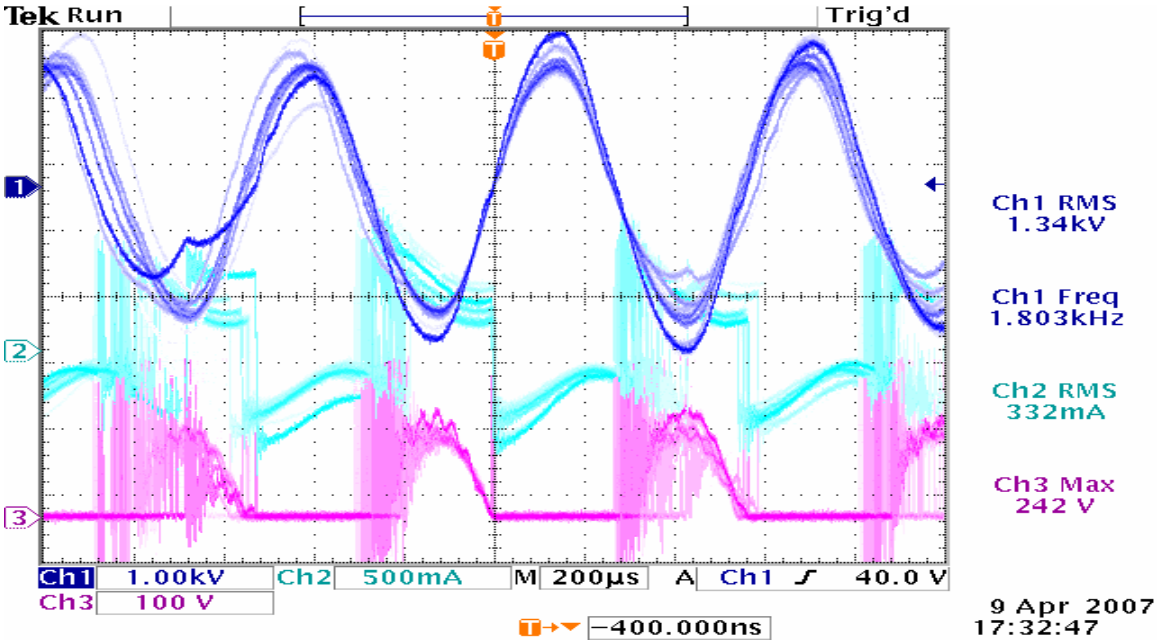

Figure R.1. Panel Actuator Plasma Generation, w/out Auxiliary Inductor, with 76mH series secondary Impedance Matching Inductor, 1.80 kHz.
Ch1: output voltage (1 kV/div), Ch2: transformer primary current (500 mA/div), Ch3: voltage across switch (100 V/div).

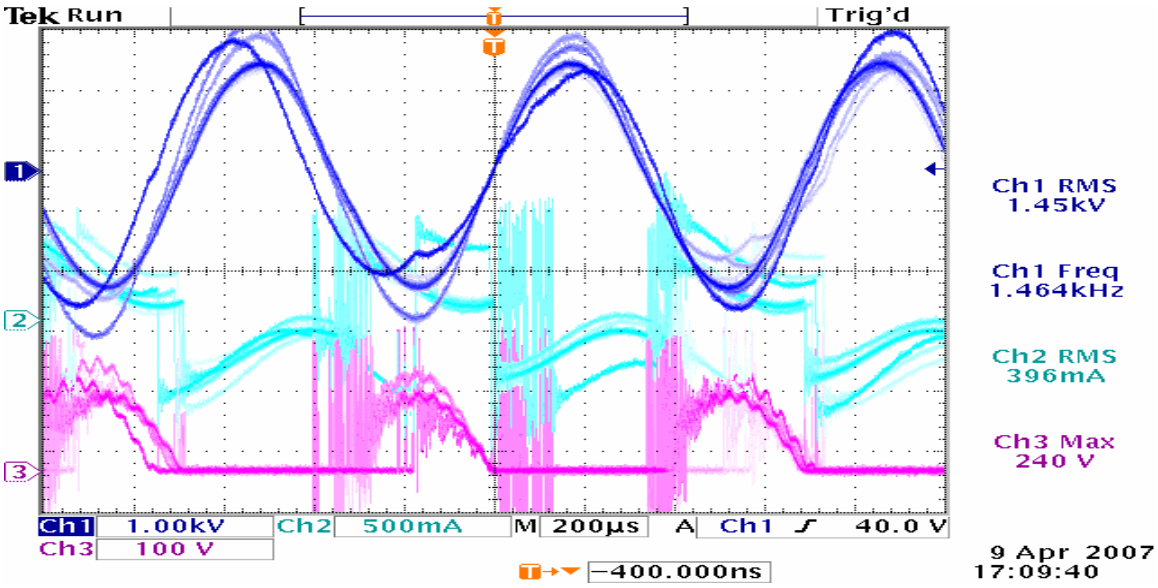

Figure R.2. Panel Actuator Plasma Generation, w/out Auxiliary Inductor, with 76mH series secondary Impedance Matching Inductor, 1.46 kHz.
Ch1: output voltage (1 kV/div), Ch2: transformer primary current (500 mA/div), Ch3: voltage across switch (100 V/div).

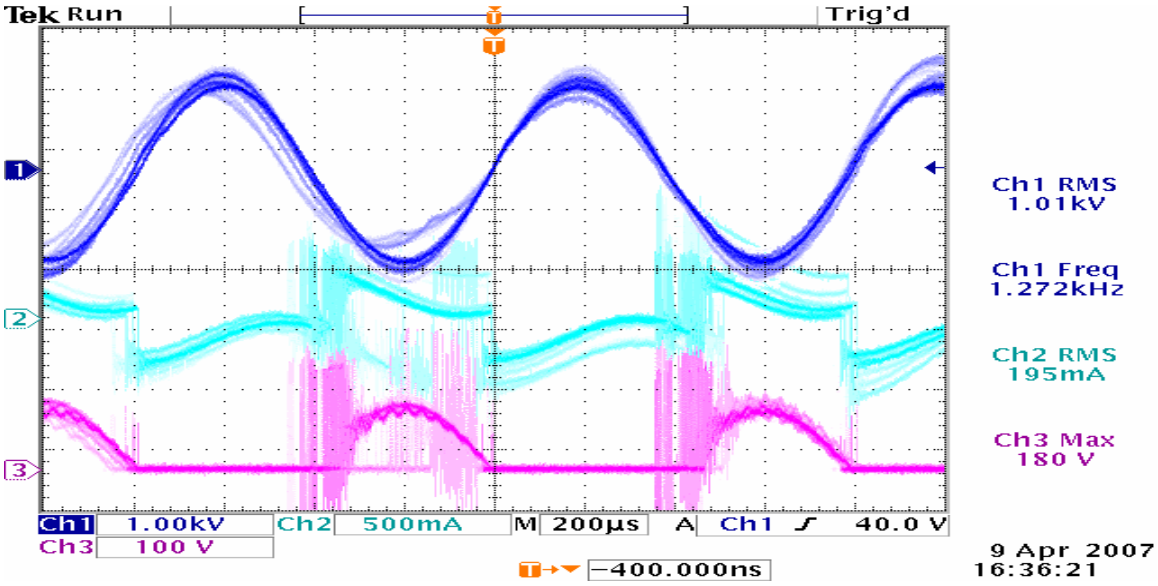

Figure R.3. Panel Actuator Plasma Generation, w/out Auxiliary Inductor, with 76mH series secondary Impedance Matching Inductor, 1.27 kHz.
Ch1: output voltage (1 kV/div), Ch2: transformer primary current (500 mA/div), Ch3: voltage across switch (100 V/div).

Appendix S: Further Testing: Panel Actuator Plasma Generation, with 2.15mH parallel primary Auxiliary Inductor, without Impedance Matching Inductor

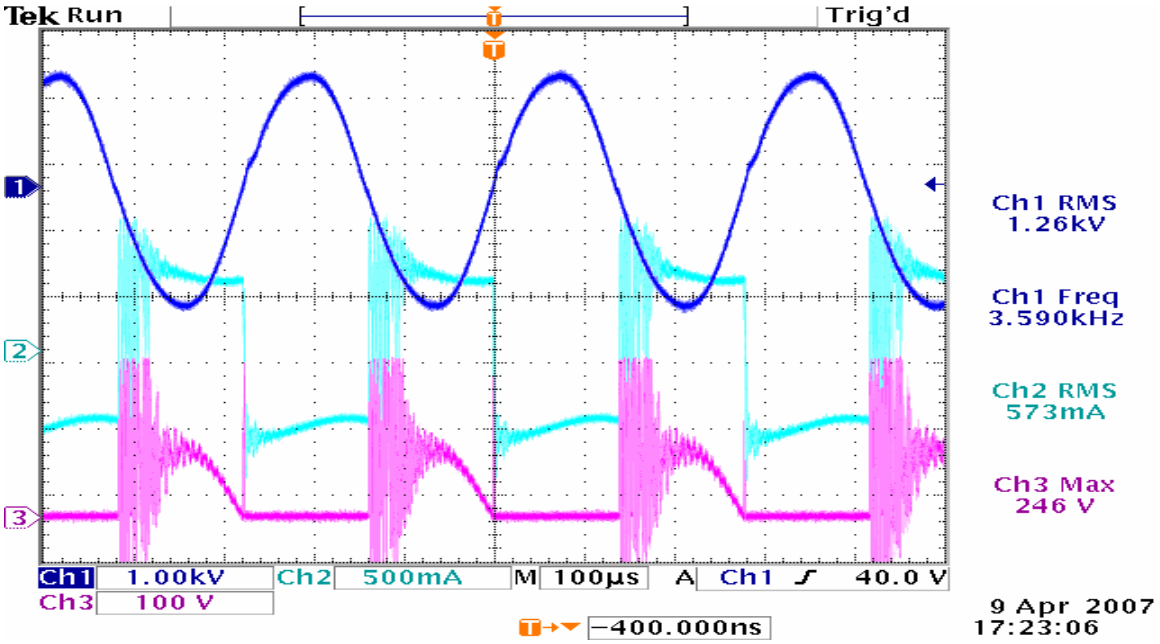

Figure S.1. Panel Actuator Plasma Generation, with 2.15mH parallel primary Auxiliary Inductor, w/out Impedance Matching Inductor, 3.59 kHz.
Ch1: output voltage (1 kV/div), Ch2: transformer primary current (500 mA/div), Ch3: voltage across switch (100 V/div).

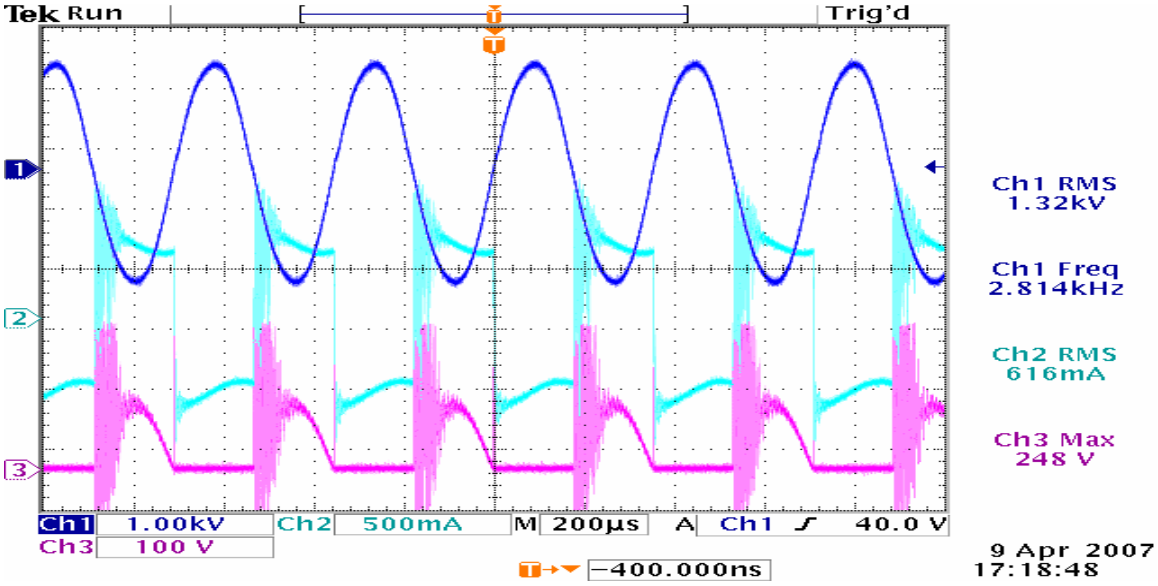

Figure S.2. Panel Actuator Plasma Generation, with 2.15mH parallel primary Auxiliary Inductor, w/out Impedance Matching Inductor, 2.81 kHz.

Ch1: output voltage (1 kV/div), Ch2: transformer primary current (500 mA/div), Ch3: voltage across switch (100 V/div).

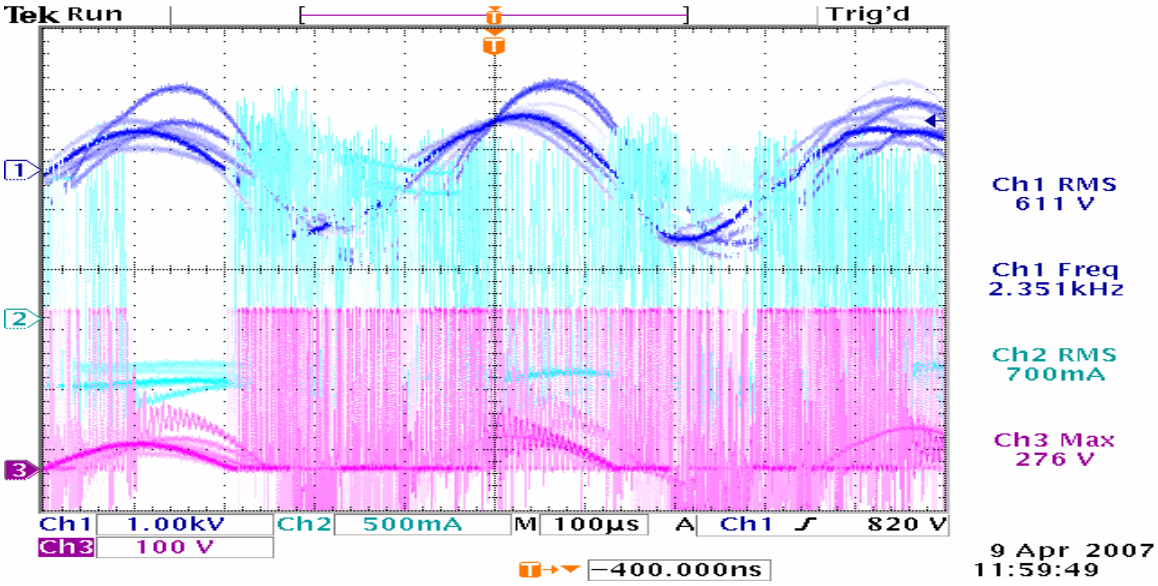

Figure S.3. Panel Actuator Plasma Generation, with 2.15mH parallel primary Auxiliary Inductor, w/out Impedance Matching Inductor, 2.35 kHz.

Ch1: output voltage (1 kV/div), Ch2: transformer primary current (500 mA/div), Ch3: voltage across switch (100 V/div).

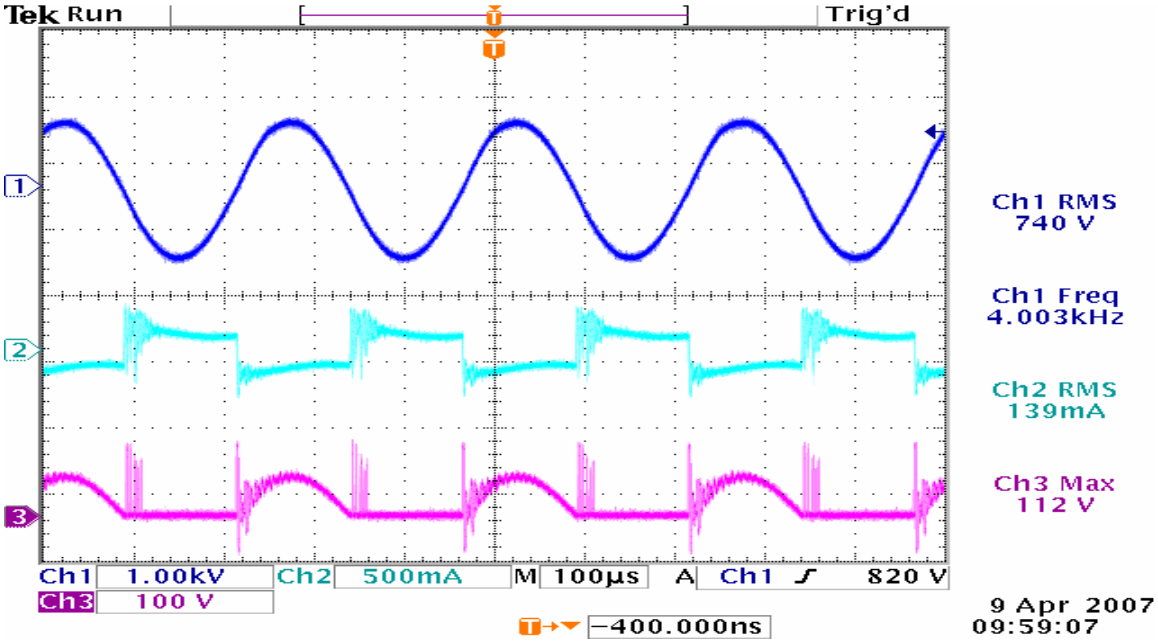

Figure S.4. Panel Actuator Plasma Onset, with 2.15mH parallel primary Auxiliary Inductor, w/out Impedance Matching Inductor, 4 kHz.

Ch1: output voltage (1 kV/div), Ch2: transformer primary current (500 mA/div), Ch3: voltage across switch (100 V/div).

Appendix T: Further Testing: Panel Actuator Plasma Generation, with 2.15mH parallel primary Auxiliary Inductor, with 3.2mH series secondary Impedance Matching Inductor

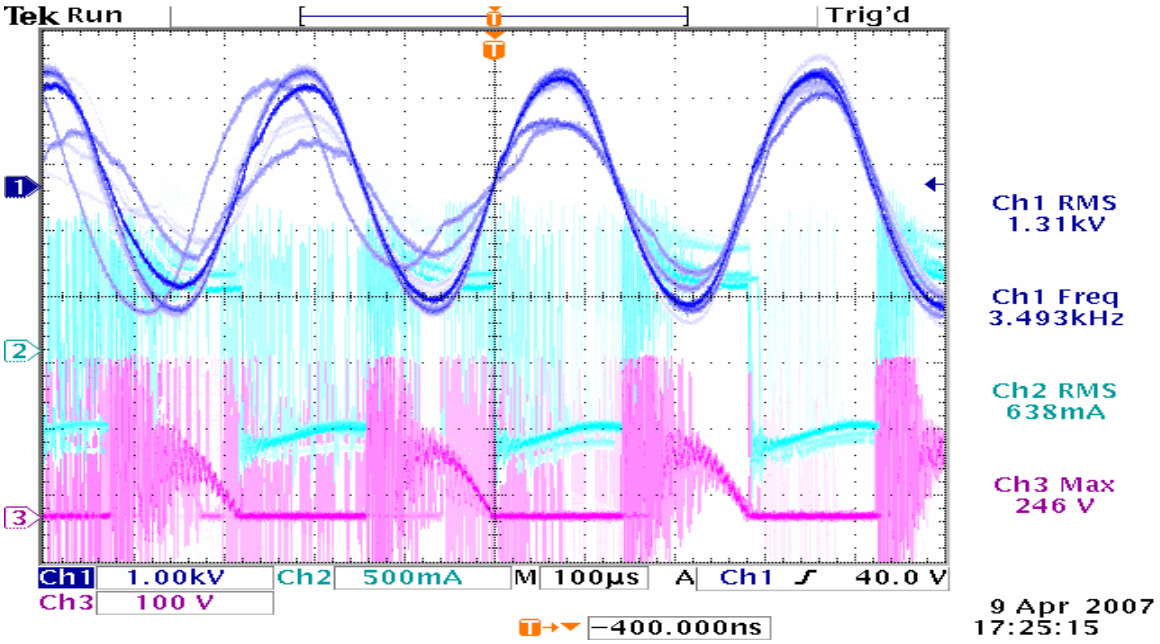

Figure T.1. Panel Actuator Plasma Generation, with 2.15mH parallel primary Auxiliary Inductor, with 3.2mH series secondary Impedance Matching Inductor, 3.49 kHz. Ch1: output voltage (1 kV/div), Ch2: transformer primary current (500 mA/div), Ch3: voltage across switch (100 V/div).

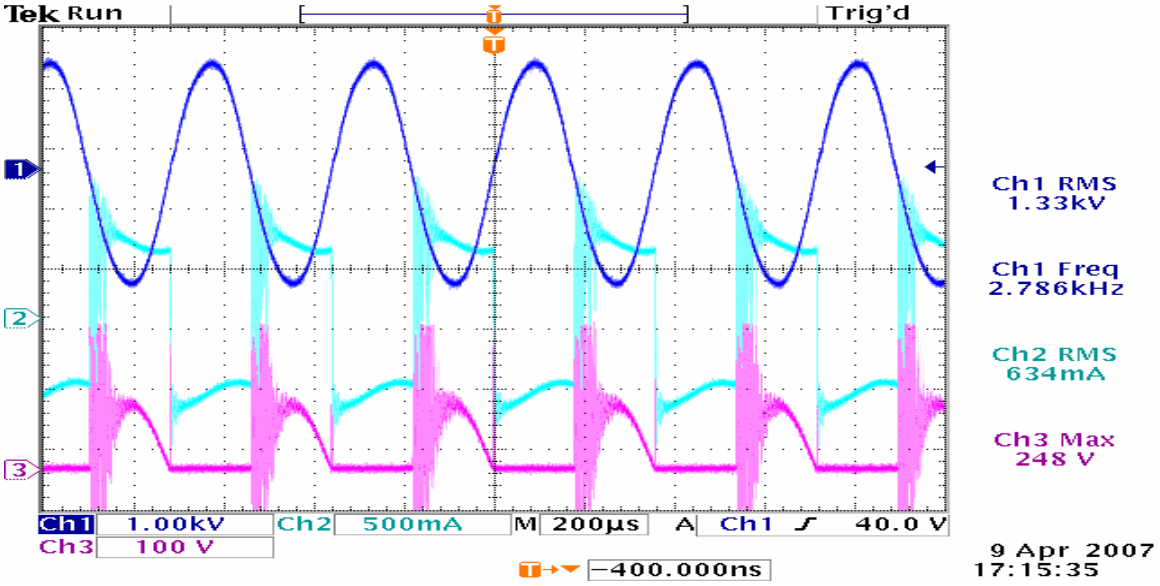

Figure T.2. Panel Actuator Plasma Generation, with 2.15mH parallel primary Auxiliary Inductor, with 3.2mH series secondary Impedance Matching Inductor, 2.79kHz. Ch1: output voltage (1 kV/div), Ch2: transformer primary current (500 mA/div), Ch3: voltage across switch (100 V/div).

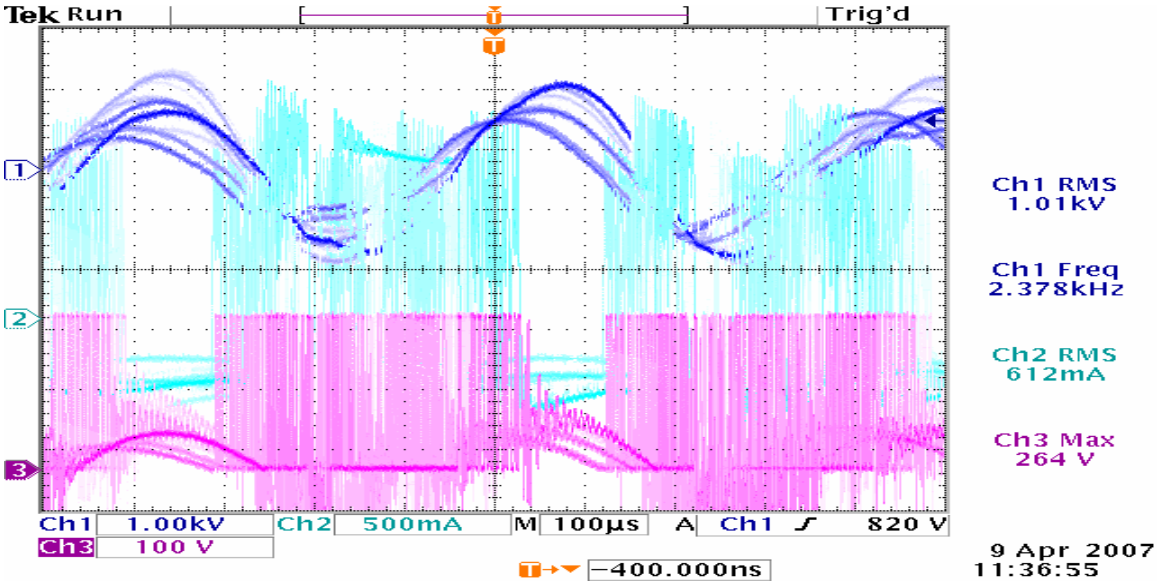

Figure T.3. Panel Actuator Plasma Generation, with 2.15mH parallel primary Auxiliary Inductor, with 3.2mH series secondary Impedance Matching Inductor, 2.38 kHz. Ch1: output voltage (1 kV/div), Ch2: transformer primary current (500 mA/div), Ch3: voltage across switch (100 V/div).

Appendix U: Further Testing: Panel Actuator Plasma Generation, with 2.15mH parallel primary Auxiliary Inductor, with 41mH series secondary Impedance Matching Inductor

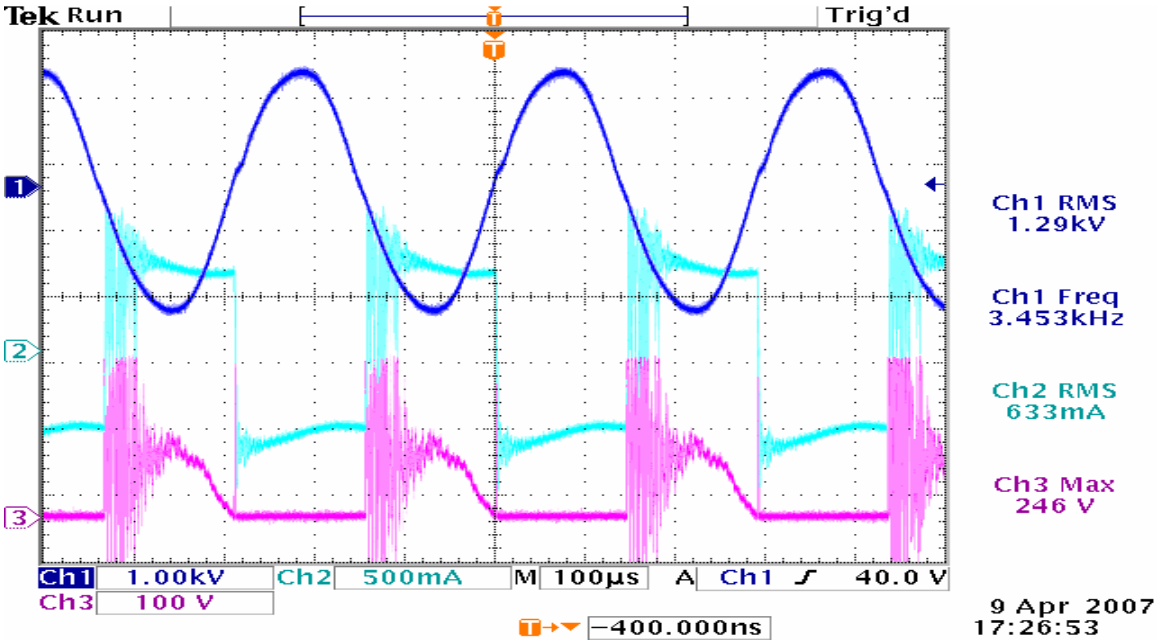

Figure U.1. Panel Actuator Plasma Generation, with 2.15mH parallel primary Auxiliary Inductor, with 41mH series secondary Impedance Matching Inductor, 3.45 kHz. Ch1: output voltage (1 kV/div), Ch2: transformer primary current (500 mA/div), Ch3: voltage across switch (100 V/div).

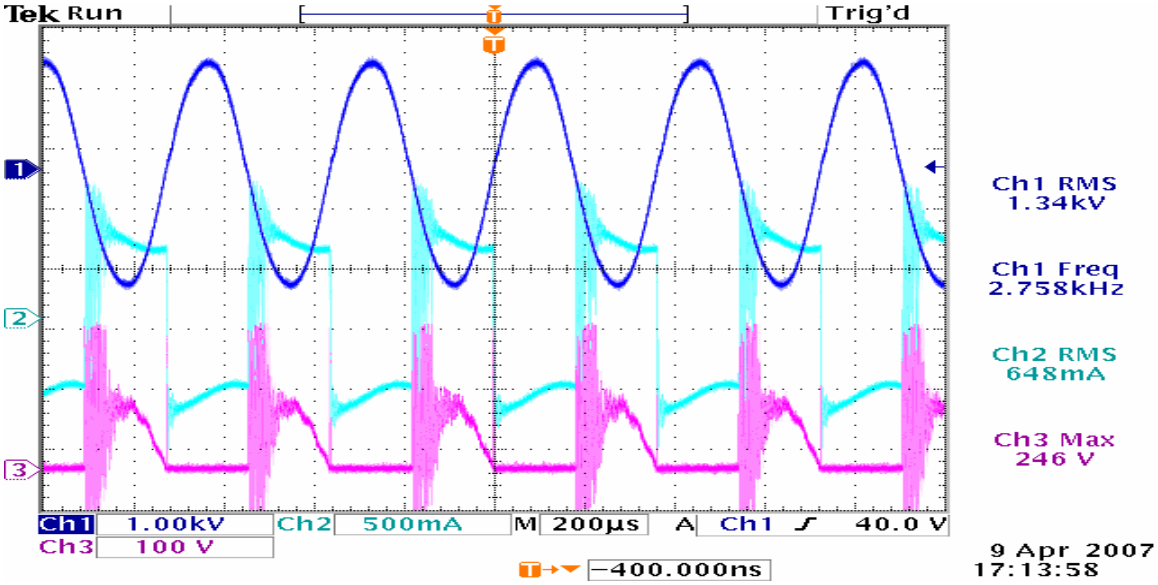

Figure U.2. Panel Actuator Plasma Generation, with 2.15mH parallel primary Auxiliary Inductor, with 41mH series secondary Impedance Matching Inductor, 2.76 kHz. Ch1: output voltage (1 kV/div), Ch2: transformer primary current (500 mA/div), Ch3: voltage across switch (100 V/div).

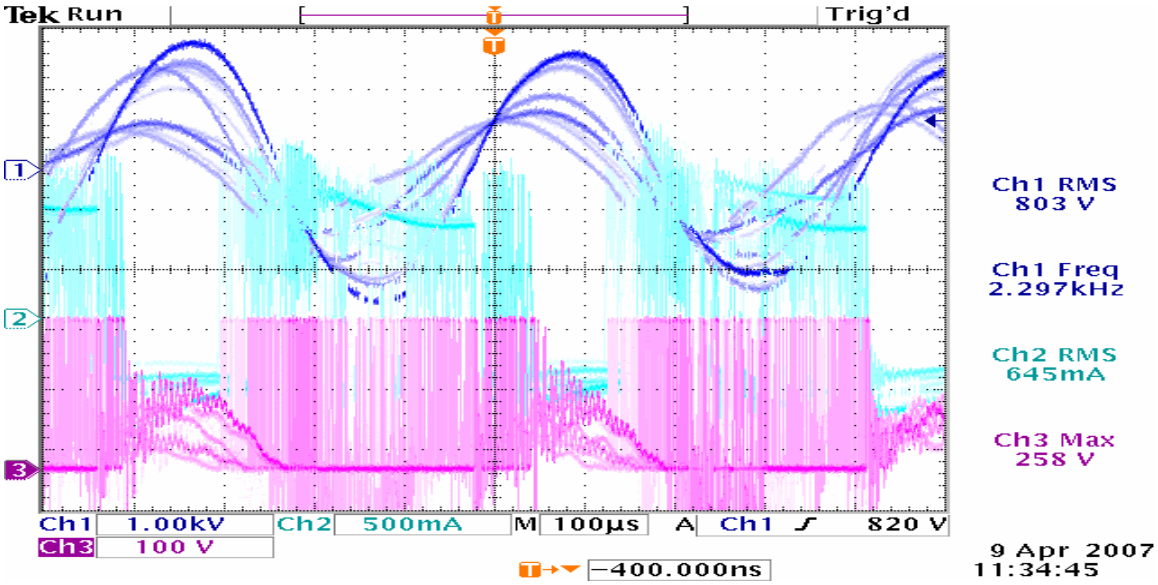

Figure U.3. Panel Actuator Plasma Generation, with 2.15mH parallel primary Auxiliary Inductor, with 41mH series secondary Impedance Matching Inductor, 2.3kHz. Ch1: output voltage (1 kV/div), Ch2: transformer primary current (500 mA/div), Ch3: voltage across switch (100 V/div).

Appendix V: Further Testing: Panel Actuator Plasma Generation, with 2.15mH parallel primary Auxiliary Inductor, with 76mH series secondary Impedance Matching Inductor

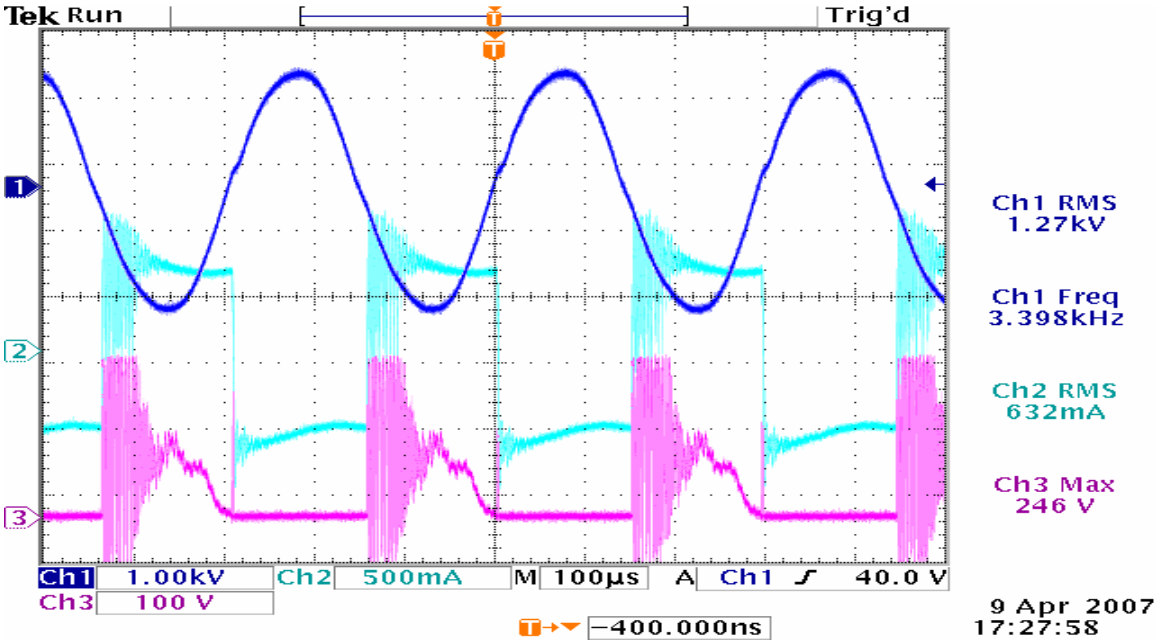

Figure V.1. Panel Actuator Plasma Generation, with 2.15mH parallel primary Auxiliary Inductor, with 76mH series secondary Impedance Matching Inductor, 3.4 kHz. Ch1: output voltage (1 kV/div), Ch2: transformer primary current (500 mA/div), Ch3: voltage across switch (100 V/div).

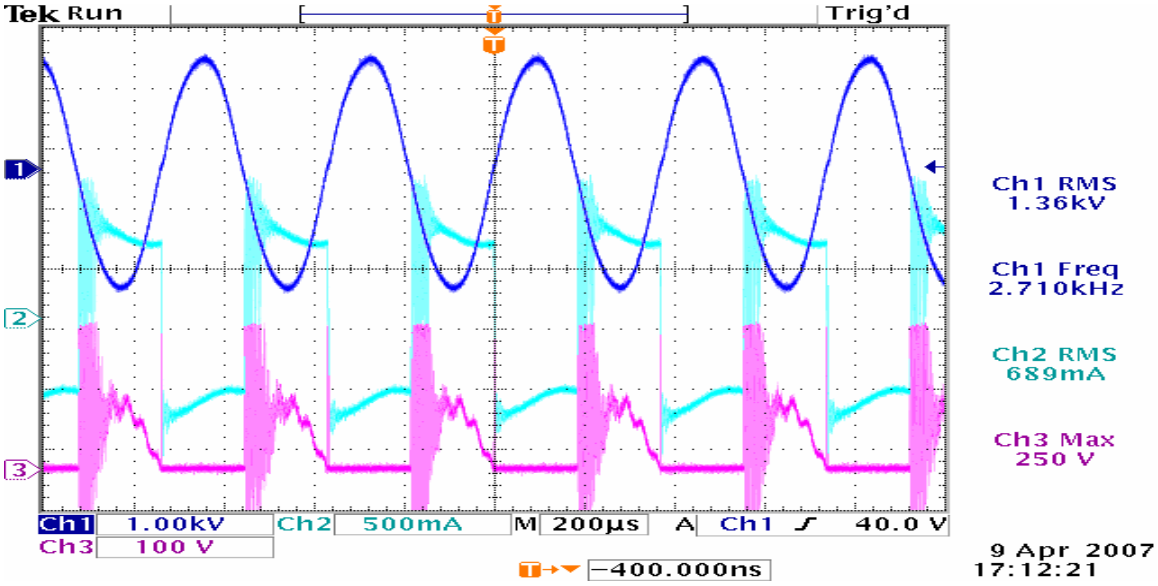

Figure V.2. Panel Actuator Plasma Generation, with 2.15mH parallel primary Auxiliary Inductor, with 76mH series secondary Impedance Matching Inductor, 2.71 kHz. Ch1: output voltage (1 kV/div), Ch2: transformer primary current (500 mA/div), Ch3: voltage across switch (100 V/div).

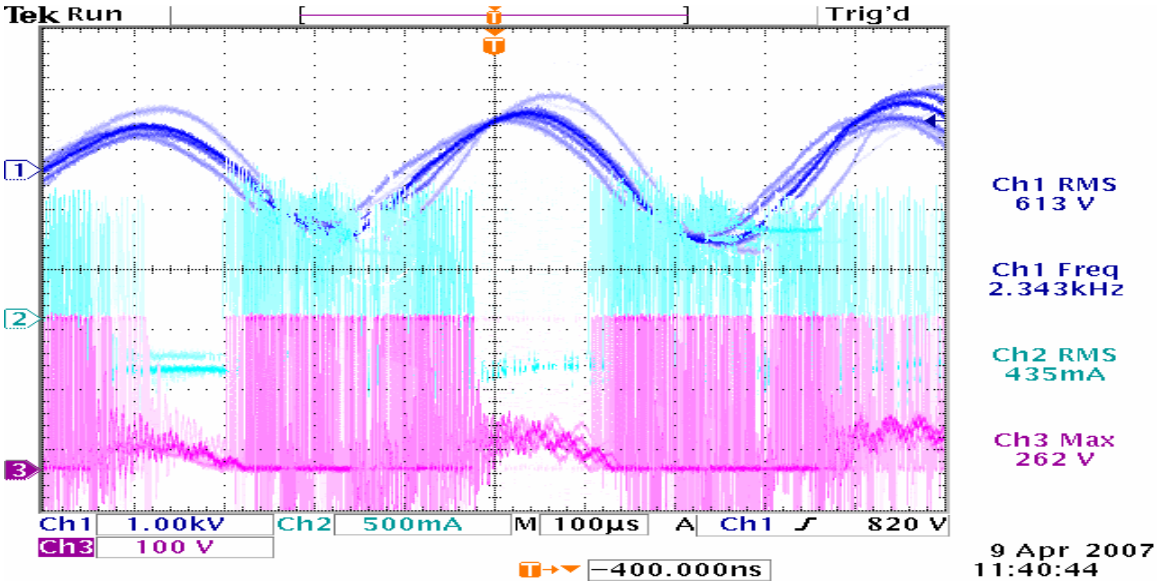

Figure V.3. Panel Actuator Plasma Generation, with 2.15mH parallel primary Auxiliary Inductor, with 76mH series secondary Impedance Matching Inductor, 2.34 kHz. Ch1: output voltage (1 kV/div), Ch2: transformer primary current (500 mA/div), Ch3: voltage across switch (100 V/div).

VITA

Jo Calvez was born in Opelika, Alabama in 1968. From the age of two he grew up in Clemson, South Carolina, and then later moved to Powdersville, South Carolina, where he attended Wren High School, graduating in 1986. Jo attended Clemson University, earning a bachelor of science degree in secondary education (science teaching) in 1992. He then taught science at Landrum High School in Landrum, South Carolina before enrolling in the electronics engineering technology program at Spartanburg Technical College in Spartanburg, South Carolina, from which he graduated with an associate's degree in 1996. After working as a technician in a manufacturing environment for several years, he was cast as an extra (red coat corps) in Mel Gibson's "The Patriot," so he went off to play "Hollywood" in the remote pastures of Chester County, South Carolina in late summer of 1999. When his movie career ended in December 1999, Jo returned to his home in Greenville, South Carolina, where he bought a few extra jugs of fresh water and sighted in his BB gun in preparation for the impending Y2K disaster. In January 2000 he returned to teaching, this time at a private technical college in Greenville, South Carolina. During that time he read a book about industrial plasma engineering, which re-ignited his perennial thirst for higher learning and led him to re-enroll at Clemson University, where he earned a second bachelor of science degree, in electrical engineering, in 2004. Jo then attended the University of Tennessee, Knoxville as a graduate student in electrical engineering, focusing on plasma studies, working as a graduate teaching assistant in the Engage Engineering Fundamentals program, and finishing his coursework and earning a master's degree in electrical engineering in 2007.